Biocrude production from biomass and mixed plastics via hydrothermal liquefaction for fuel and chemicals

by

Tawsif Rahman

A dissertation submitted to the Graduate Faculty of
Auburn University
in partial fulfillment of the
requirements for the Degree of
Doctor of Philosophy

Auburn, Alabama
December 10, 2022

Keywords: Hydrothermal liquefaction, Biomass, Plastic, Biocrude, Reaction environment, Red mud

Approved by

Sushil Adhikari, Chair, Professor of Biosystems Engineering
Brian Via, Professor of Biosystems Engineering
Maria Auad, Professor of Chemical Engineering
Brendan Higgins, Associate Professor of Biosystems Engineering

Abstract

Hydrothermal liquefaction (HTL) is a promising technology to convert organic feedstocks into value-added fuel precursors known as biocrude, solids (hydrochar), and gaseous byproducts. The HTL process can efficiently break down mixed feedstocks, such as waste, into valuable chemicals. The current study has investigated the HTL conversion of three waste materials:municipal sewage sludge,waste plastics,forest residue and an algae strain. This research applied various gaseous environment beside traditional inert gas with red mud (an iron-rich industrial waste) catalyst to enhance the biocrude production with improved quality.

The municipal sewage sludge from the wastewater plant was the first feedstock of this study. This study applied ethylene gas and pretreated red mud as reaction environment and catalyst, respectively, to induce the stability in produced biocrude. With respect to the oxidation state, three modified red mud catalysts were prepared by calcination at 575°C (CRM), and reduction at 500°C (RRM500) and 700°C (RRM700). The HTL treatment of sludge was highly influenced by ethylene without any catalyst and produced 41.6 wt.% biocrude yields. The viscosity of the ethylene-derived biocrudes showed lower variances compared to biocrudes from an inert atmosphere. The RRM500 lowered the acidity by 14%, while the RRM700 minimized the viscosity by 47% compared to non-catalytic-inert biocrude samples. The reduced nitrogen content found the mutual effect of RRM500-ethylene in the biocrude. This study showed the potential of ethylene gas in improved biocrude production via catalytic HTL treatment.

The second study explored the effects of ethylene, reducing, and oxidative gases to compare the influences of reaction ambiances over HTL conversion. This work utilized the "*Tetraselmis* sp." algae strain as feedstock and two forms of RM catalysts: RM reduced at 500°C (RRM500) and nickel-supported RM (Ni/RM). The goal was to compare the catalytic activities of RRM500 and Ni/RM under four different reaction atmospheres for algae HTL conversion.The nickel metal on red mud (Ni/RM) catalyst maximized biocrude yield (37 wt.%) in an ethylene environment, generated the lowest total acid number (14 mgKOH/g) under inert atmosphere, and lowered sulfur (33-66%) and oxygen (18-30%) from biocrude products irrespective of environments. The RRM500 catalyst increased carbon content under the reducing environment and minimized the heavy metal and phosphorus transfer from the feedstock to biocrude in studied ambiances. Among the reaction environments, the reducing atmosphere optimized carbon content (54.3wt.%) and calorific value (28 MJ/kg) with minimum oxygen amount (27wt.%) in biocrudes without any catalyst.

The household waste plastic mix was the third feedstock to evaluate the efficacy of HTL technology for waste plastic treatment. The chosen plastics were polyethylene terephthalate (PET), high-density polyethylene (HDPE), low-density polyethylene (LDPE), polypropylene (PP), and polystyrene (PS). The reduced red mud at 500°C (RRM500) was utilized as a catalyst for its proven efficiency in sludge and algae liquefaction. Before mixing, each plastic material was studied individually as control experiments. Without any catalyst, the HDPE generated the maximum crude yield of 76 wt.%, whereas the PET produced mainly solid (80wt.%) and gaseous products. The biocrude yield production from non-catalytic plastic conversion followed this trend: HDPE>PS>PP>LDPE. The mixed plastic feedstock produced approximately 22 wt.% of crudes and comparatively high solid residue of 35wt.%. The RRM500 catalyst generally suppressed the

biocrude and solid formation from individual plastic feedstock but effectively reduced viscosity and acidity. After depolymerization, HDPE mainly decomposed into straight-chain alkanes, while PP and PS-derived crudes were composed of aromatic-cyclic compounds. The catalyst promoted straight-chain alkanes in LDPE biocrudes. Almost 36-92% of the plastic-derived oil had gasoline boiling range compounds. The HTL conversion of plastics could be a promising route for mixed plastic waste treatment with valuable fuel range chemical production.

This study's fourth objective was to increase HTL biocrude production from lignocellulosic biomass (southern yellow pine). The Pine saw dust was liquified via HTL process using water and water-ethanol mixture at 250,300 and 350℃ reaction temperatures. Iron (Fe) (at zero-valent oxidation state) was used as a catalyst in the HTL system to enhance the catalytic activity. The biocrude yield was enhanced by increased ethanol concentration in a water-ethanol medium, and the pine HTL produced the maximum biocrude yield of 34wt.% at 300℃ temperature within 1:1(wt./wt.) water-ethanol mixture. The higher reaction temperature in pure water promoted biocrude yield without a catalyst. The highest biocrude yield from the water was 18wt.% at 350℃. The iron catalyst performed the best at 300℃ reaction temperature within the water and resulted in 27wt.% biocrude yield. Moreover, the catalyst improved the biocrude quality by lowering oxygen content and acidity. The pine-derived biocrudes were mainly composed of phenolic and acids. The ethanol neutralized the acids by an esterification reaction. The catalyst accelerated the esterification process. Overall this research has proved the potential of individual waste-based feedstock for liquid fuel production. The research findings will be beneficiary to mitigate waste materials by energy production.

Keywords: Hydrothermal liquefaction, Biomass, Plastic, Biocrude, Reaction environment, Red mud

Acknowledgments

First, I would like to thank my Ph.D. advisor, Dr. Sushil Adhikari, from the deepest corner of my heart. It is literally a matter of great luck to have him as a Ph.D. supervisor. The continuous communication and guidance from Dr. Adhikari made me mature in my academic as well as personal life. Thank you, Dr. Adhikari, for everything you have done for me. I am grateful to have suggestions and guidance from my Ph.D. committee members: Dr. Maria Auad, Dr. Brian Via, and Dr. Brendan Higgins. Special thanks to Dr. Dengjun Wang for serving as a University Reader on my Ph.D. Committee.

I acknowledge the help and support from all past and present members of Dr. Adhikari's research group. I would like to thank Vivek Patil, Nikhil Jain, and Sanjeev KC for introducing me to the Biological Engineering Research Laboratory, equipment, and life in Auburn. I appreciate the support and help from fellow lab mates: Sanjita Wasti, Temitope Damilotun Soneye, Poulami Roy, Ashish Bhattarai, Manish Sakhakarmy, Haley Mason, Rachel Day, Dale Hartmann, Ayden Kemp and many more. Special thanks to Temitope Damilotun Soneye for introducing me to the hydrothermal liquefaction process. I will always remember the help and support from Poulami Roy. We started working as colleagues, and then close collaboration in research work with mutual study hours has turned us into close friends. I would like to show my deep gratitude to Dr. Hossein Jahromi for providing valuable suggestions and support throughout my Ph.D. study. The collaboration with Poulami Roy and Dr. Jahromi has resulted in several research publications. Thank you both of you for such great teamwork. Special thanks to Dr. Pixiang Wang and Dr. Bijoy Biswas for their advice, help, and suggestions in my research work.

I am honored to be part of the Biosystems Engineering Department at Auburn University. I would like to thank all the faculty members for the amazing classes, seminars, and social events. Especially, I will remember the amazing communications from our Department Head, Dr. Oladiran Fasina. The seminar sessions by Dr. Yi Wang were a great opportunity to learn the research of other students as well as faculty from different departments and scientific backgrounds. The e-portfolio course of Dr. Brendan Higgins was my first experience with an online portfolio. I am thankful to have continuous technical support from James Johnson, Bobby Bradford, Bobby Epling, and Caroline Whiting during my four and half year long Ph.D. journey. Without their help, my research projects would not have been completed. Special thanks to Bionca King for performing all the documentation and administrative work. I would like to thank all the graduate and undergraduate students I have met in my Ph.D. journey at Auburn University. Special thanks to Hemendra Kumar, Bijoy Takhellambam, Ritesh Karki, Peetika Kaur, and Ana Gabriela Itokazu for making my student life more memorable and colorful.

I would like to acknowledge the financial support for my research from the Alabama Department of Economic and Community Affairs (ADECA-1ARDEF22 02), National Science Foundation (Award No.:2119809), and Alabama Agricultural Experiment Station and the Hatch program (ALA014-1-19068) of the National Institute of Food and Agriculture, U.S. Department of Agriculture (USDA).

Finally, and most importantly, profound gratitude for my mom and siblings, who continuously supported me from home to continue my studies thousands of miles away from home.

Table of Contents

List of Tables

List of Figures

List of Abbreviations

HTL	Hydrothermal Liquefaction
RM	Red Mud
CRM	Calcined Red Mud
RRM500	Reduced Red Mud at 500℃
RRM700	Reduced Red Mud at 700℃
DCM	Dichloromethane
TGA	Thermogravimetric Analysis
TAN	Total Acid Number
FTIR	Fourier-Transform Infrared Spectroscopy
NMR	Nuclear Magnetic Resonance Spectroscopy
GC-MS	Gas Chromatography Mass Spectrometry
BET	Brunauer-Emmett-Teller
XRD	X-ray Diffraction
TOC	Total Organic Carbon
TN	Total Nitrogen
COD	Chemical Oxygen Demand
RRM	Reduced Red Mud at 500℃
Ni/RM	Red Mud Supported Nickel Catalyst
MEOH	Methanol
PET	Polyethylene Terephthalate

HDPE	High Density Polyethylene
LDPE	Low Density Polyethylene
PP	Polypropylene
PS	Polystyrene
PM	Plastic Mixture
ESI-MS	Electrospray Ionization Mass Spectrometry

Chapter 1

Introduction

1.1 Background

Due to the uneven distribution of natural resources; global population growth, dependence on fossil-based fuels, and depletion of fossil energy resources have created an energy crisis worldwide [1].For the past few decades, 80% of the total global energy has come from petroleum-based resources [2]. Dependency on fossil fuels for the fulfillment of energy demand has resulted in vast amounts of greenhouse gases (CO_2, CH_4, NO_2) in nature which are putting nonreversible effects on climate, including climate change, rise in sea level, loss of biodiversity with consequential effects on our society and economy [3]. According to the United States Environmental Protection Agency (US EPA), the transportation sector accounts for about 27% of the total U.S. GHG emissions, the largest contributor among different sectors. The GHG emissions decreased by 13% during the COVID-19 pandemic due to travel restrictions but are expected to reach the pre-pandemic emission level in 2022 [4]. Moreover, the ongoing political crisis between Russia and Ukraine, with subsequent international sanctions against Russia, has raised the price of petroleum fuel at an unprecedented rate [5]. The ever-increasing demand and the negative environmental impact of fossil fuels have led to a continuous global effort to search for eco-friendly and alternative energy sources. Bioenergy covering two-thirds of global renewable energy consumption, can significantly combat climate change with effective energy transition from fossil fuel to renewable energy sources [6]. The abundant biomass is a renewable resource and is considered carbon neutral as the CO_2 released during combustion or other conversion processes will be re-captured by the regrowth of the biomass through photosynthesis [7,8]. The biomass-

derived biofuels is a promising bioenergy source to replace traditional fossil fuel. This fuel is renewable in nature as it is produced from abundant organic materials of nature and is reported to produce less GHGs than traditional petroleum fuel. Moreover, the production and utilization of biofuel can reduce the high fossil fuel demand and mitigate the dependency on petroleum-rich countries [9]. Recently, the electrification of ground transport has become a critical factor in the global energy market. For the marine and aviation sectors, liquid fossil fuels are still the primary energy source, where biofuels can reduce carbon emissions [10]. Since the early 1980s, the production and consumption of biofuels in the United States have gradually increased. The U.S. government has adopted policies and programs favoring biofuels to reduce the dependency on petroleum-based transportation fuel. Due to the COVID-19 pandemic, there was a decline in biofuel demand which recovered in 2021 to pre-pandemic levels [11]. According to the U.S. Energy Information Administration (EIA), the total production of biofuel was 17.5 billion gallons, where 16.8 billion gallons were consumed, and 0.8 billion gallons were exported [12]. Biofuels can be utilized by blending with petroleum fuel or in their pure form [13]. However, the cost of biofuel production, along with downstream processing costs, could be twice the cost of commercial fuels. On the other hand, the greenhouse gas emission from biofuel could be as low as 15% of fossil fuel emissions [14]. Thus, biofuel can offset harmful emissions and can offer a sustainable solution to the energy crisis.

1.2 Hydrothermal liquefaction

Biofuels is a broad term for liquid, solid, and gaseous fuels produced from bio-based materials. Though biofuels are mostly used as liquid fuel in the transportation sector, they can either be used as liquid or gaseous forms for power generation or heating purposes [12]. Various biofuel production methods include biological, chemical, and physical conversion processes [15]. The

biological methods for biomass conversion are time-consuming, and biofuel yield is comparatively low [16,17]. On the other hand, thermochemical conversion technologies, such as direct combustion, gasification, torrefaction, pyrolysis, and hydrothermal liquefaction (HTL), can decompose feedstocks into syngas, biocrude (oil), and solid fuels. Due to the moisture content of the biomass, a pre-drying treatment of the feedstock is required before the combustion, gasification, and pyrolysis conversion process [18,19]. Moreover, the excessive moisture content adds transportation as well as energy cost for drying. It was found that almost half of the total energy requirements for biofuel production can be consumed by distillation and drying steps [20]. The HTL is the only thermochemical conversion route that uses a water medium during the conversion reaction; thus, the energy-sensitive drying treatment can be avoided [21]. The HTL process breaks down organic feedstocks into liquid fuel by hot compressed water at moderate temperatures (250–400 ◦C) and pressures (10–35 MPa) [22]. Pyrolysis and HTL are two major thermochemical routes for liquid biofuel production. Though HTL biofuel yield was reported to be lower than the pyrolysis process, the calorific value of HTL biofuel was much higher because of low oxygen content [23]. The concept of biomass decomposition in hot water with an alkali catalyst for oil extraction was first reported in the 1920s [24]. The unique features of the HTL include less tar yield with increased energy proficiency compared to other thermochemical processes [22]. When biomass is decomposed under high pressure and temperature, the produced liquid biofuel is known as “biocrude” [25]. The biocrude obtained from HTL has increased energy density with improved thermal and storage stabilities compared to biofuels from other biomass conversion techniques [26]. Moreover, the HTL biocrude can be processed to obtain different fuel fractions from the distillation process [27]. Despite the numerous advantages of HTL of biomass, very few labs- and pilot- scales plants exist worldwide [28]. During 1960-1970, the U.S. Bureau

of Mines Pittsburgh Energy Research Center (PERC) successfully produced oil-like substances by catalytic reaction between various biomass materials (wood municipal solid waste and cattle manure) and carbon monoxide under moderate temperature and high pressure. The Arab oil embargo of the 1970s drove the U.S. government to implement the research outcome of PERC into a commercial size plant known as Albany Biomass Liquefaction Experimental Facility. The wood dust was used as feedstock in the Albany facility. Wood was blended with recycled oil, water, and sodium carbonate as a catalyst and then pumped as slurry to a pressurized reactor at approximately 350℃ temperature for 20-60 minutes [29]. Later, Shell adopted the similar HTL procedure of the Albany setup without catalyst or carbon monoxide gases which raised the oxygen content of the oil. This process was scaled up to a 10 kg/h dry biomass feed pilot plant and operated for a 500 h design run in 2004 [30]. For research purposes, the small (10–1000 ml) batch-type autoclave stirred reactors are widely used to liquefy various feedstock with process optimization [21]. For a commercial setup, continuous HTL reactor systems offer superior process efficiency and economic feasibility through advanced process control and feed system [32,33].

The HTL process uses high pressure and temperature with solvent (mostly water) to form a highly reactive environment. Biomass includes a wide range of materials with varying compositions of carbohydrates, lignin, proteins, and lipids. Therefore, the reaction mechanisms of biomass decomposition are complicated [34]. The HTL process mechanism is classified into two feedstock types: lignocellulose biomass (dry feedstock) and algal biomass (wet feedstock). It is widely accepted that the HTL process breaks down biomass into small reactive compounds that depolymerize to form biocrude, water-soluble chemicals, solid residue, and gas. The four significant reactions that take place during HTL conversion include a) decomposition of biomass into water-soluble monomers, b) transformation of monomer by dehydration, deamination, and

decarboxylation reaction, c) rearrangement of reactive fractions into water-insoluble biocrude, d) polymerizing into char for the longer reaction[33]. Figure 1.1 shows the schematic overview of the HTL reaction pathway, adopted from Gollakota et al.[35].

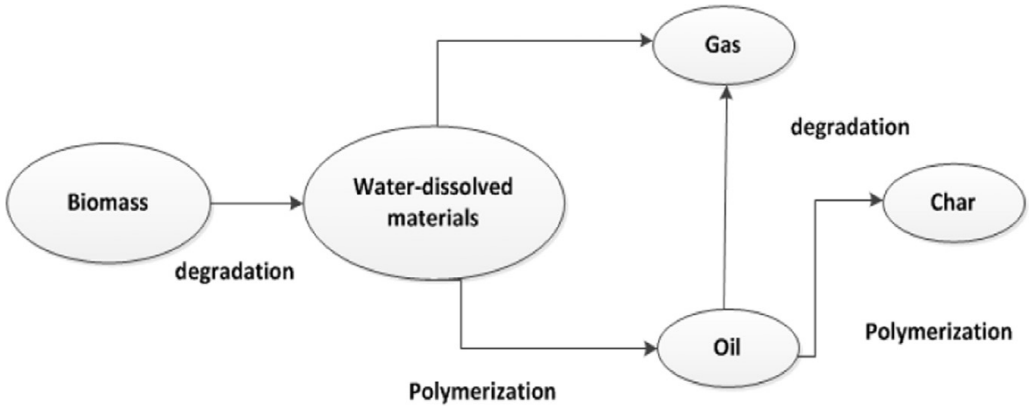

Figure 1.1: Reaction pathway of hydrothermal liquefaction

The hydrothermal liquefaction procedure aims to convert biomass to biocrude that can be upgraded to the whole distillate range of petroleum-derived fuel products. The HTL process is capable of recovering more than 70% of the feedstock carbon content, and the crude product of this process has lower oxygen and moisture content with increased higher heating value, thus requiring less upgrading treatment, which reduces both the fixed and operative costs of handling equipment and storage compared to other biomass conversion mechanism [36]. In addition, the solid by-products of the HTL process can be utilized as fertilizer, and aqueous products can be reused in the HTL process or for other purposes, such as algae growth medium. However, the high-pressure system increases the installation cost of the HTL unit and raises safety concerns about the HTL operation [35].

1.3 Process parameters of HTL

The main HTL process parameters that primarily influence the HTL process are the reaction temperature, the residence time, the use and type of catalyst, the reaction medium (solvent), the reaction environment, and the biomass-solvent ratio[31]. The increasing reaction temperature facilitated biocrude formation up to a specific temperature limit, and beyond that limit, no notable change in biocrude yield was observed [31,37,38]. The residence time of HTL indicates the period at which the maximum temperature is maintained for HTL reaction [28,31]. Increasing residence time positively affects biocrude yield and properties until it reaches the threshold limit [39]. The threshold limit of residence time depends on feedstock type, composition, types of catalysts, and HTL operating conditions [40]. The catalyst mainly repeals the char formation by reducing the polymerization reactions of HTL intermediates, subsequently augmenting biocrude yield with lower solid residue yield [31]. The “alkali” catalyst has been considered the most common in HTL depolymerization[27]. The HTL studies were mainly performed under an inert atmosphere (N_2); other gases, such as CO_2, O_2, and H_2, were also introduced to the HTL system [41]. The effect of solvents depends on feedstocks and operating parameters [28]. Water is widely used in the HTL depolymerization process, although alcohols such as methanol and ethanol can be more effective solvents. During the HTL process, feedstock to water ratio plays a vital role as the wet feedstock is generally processed through HTL [28]. It was found that using cosolvents could significantly raise the biocrude yield compared to a single solvent [31]. The abovementioned parameters have been extensively studied. Feedstock-specific studies are required to evaluate the true potential of the HTL process.

1.4 HTL feedstocks

Biomass is one of the major renewable energy sources and can play a key role in sustainable energy systems [34]. It is mainly derived from trees, crops, algae, and organic wastes such as municipal sludge and kitchen waste [42]. The thermochemical process, such as HTL, transforms biomass(feedstock) into liquid fuels and other value-added products by using the property of hot pressurized water [27,33]. The composition and production of HTL biocrude products largely depend on feedstock composition [33]. The HTL conversion of macroalgae, microalgae, forestry residues, agricultural residues, manure, bacteria, yeast, food waste, and sludge has been investigated [43]. This broad range of biomass feedstocks can be classified into two major groups: dry feedstocks and wet feedstocks, where the major difference is the pre-drying treatment of the feedstock. Dry feedstocks generally represent wood and other lignocellulose biomass composed of hemicellulose, cellulose, and lignin constituents. On the contrary, algae are recognized as wet feedstock built with lipids, proteins, and carbohydrates. The HTL decomposition of wood was reported to have only 20–30% biocrude yield, whereas the yields from algae range from 40-45% [31]. However, scaling up biocrude production from algae requires overcoming the challenges of cultivation and logistics issues [44].

Recently, the use of residual biomass and waste materials as HTL feedstock has drawn significant attention from the research community. Waste to energy is considered a promising alternative for waste disposal, reducing the waste volume while producing heat, electricity, or transportation fuel[45]. Annually, almost 18 billion metric tons of carbon are disposed of as waste materials throughout the world which can be utilized by the HTL process [46]. Widely available forest residues or wood-processing industrial wastes have been extensively studied using HTL, but commercial production was hindered by low biocrude production[31]. The HTL conversion of

agricultural and municipal wastes such as sewage sludge from wastewater treatment plants, swine manure, human waste, kitchen waste, and waste plastics has already been studied for biocrude production [47-51]. The average HTL biocrude from these wet waste depolymerization varied from 35–45% [31]. The HTL treatments of secondary pulp/paper sludge produced 20–45 wt.% water soluble and 15–25 wt.% water insoluble biocrude products [38]. The HTL conversion of bioethanol fermentation residues of reed and corn stover decomposed into lignin and various organic acids (levulinic acid, acetic acid, propionic acid and formic acid) [52]. Besides value addition, the HTL process can successfully eliminate the pathogens of waste feedstock and can concentrate heavy metals from waste in a single HTL product(solid char) [51,53]. The waste material generally has low bulk density which makes transportation costly and mixing water does not help much to create pumpable homogenous slurry because of significant density difference. The use of organic solvents has some advantages over water in making pumpable slurry.The co-liquefaction of shredded waste with algae can also be a feasible option to valorize the waste materials[33].

1.5 Research objectives

The main goal of this research is to explore and document the HTL treatment over four specific feedstocks with and without catalysts in different reaction parameters. The selected feedstocks and catalysts have become an issue in the waste management sector. The overall objective of this work is to valorize waste materials as feedstock as well as catalysts for hydrothermal liquefaction (HTL) with improved biocrude products. To achieve this goal, reaction environment, catalyst, reaction temperature and mixed reaction mediums were varied in HTL process.

Objective 1: Hydrothermal liquefaction of municipal sewage sludge

In this study, the municipal sewage sludge was decomposed using the HTL process at 350℃ for 1 hour, under ethylene and nitrogen(inert) reaction environments using red mud catalyst to evaluate the effects on biocrude and other byproducts. The detail of this study is provided in Chapter 2.

Objective 2: Influence of red mud catalyst and reaction atmosphere on hydrothermal liquefaction of algae

This study explored the effects of reaction environments of inert (N_2), ethylene (C_2H_4), reducing ($10\%H_2/90\%N_2$), and oxidizing ($10\%O_2/90\%N_2$) on biocrude production from "*Tetraselmis* sp." algae strain using HTL process in the presence of reduced red mud (RRM) and nickel-supported red mud (Ni/RM) catalysts. The reaction temperature was fixed at 275℃ for 1 hour reaction time. The methodology of the proposed work and its results are discussed in Chapter 3.

Objective 3: Depolymerization of household plastic waste via catalytic hydrothermal liquefaction

In this work, the mixture of five prominent plastic polymers, such as polyethylene terephthalate (PET), high-density polyethylene (HDPE), low-density polyethylene (LDPE), polypropylene (PP), and polystyrene (PS), were depolymerized using HTL process with and without reduced red mud (RM) catalyst. The reaction temperature was approximately 430℃ with 2 hours of residence time. The detailed experimental procedure and outcome of the study are discussed in Chapter 4.

Objective 4: Hydrothermal liquefaction of southern yellow pine

In this study, pine sawdust was liquefied using water and water-ethanol mixtures as solvents at 250, 300, and 350℃ reaction temperatures in the presence of the metallic iron (Fe) catalyst. The

catalyst was changed from red mud, to increase biocrude yield from lignecellulosic biomass. Varying ethanol concentration was studied to observe the effect on biocrude production and properties. The details of this objective are provided in Chapter 5.

The overall conclusions of this dissertation, with recommendations for future work, are discussed in Chapter 6.

1.6 References

[1] E.D. Coyle, R.A. Simmons, Understanding the Global Energy Crisis, Purdue University Press, 2014. https://library.oapen.org/handle/20.500.12657/30124 (accessed October 10, 2022).

[2] Fossil Fuels | EESI, (n.d.). https://www.eesi.org/topics/fossil-fuels/description (accessed October 25, 2022).

[3] R.E. Gullison, P.C. Frumhoff, J.G. Canadell, C.B. Field, D.C. Nepstad, K. Hayhoe, R. Avissar, L.M. Curran, P. Friedlingstein, C.D. Jones, C. Nobre, Tropical Forests and Climate Policy, Science. 316 (2007) 985–986. https://doi.org/10.1126/science.1136163.

[4] O. US EPA, Sources of Greenhouse Gas Emissions, (2015). https://www.epa.gov/ghgemissions/sources-greenhouse-gas-emissions (accessed October 10, 2022).

[5] Oil price rises again as buyers shun Russian crude, BBC News. (2022). https://www.bbc.com/news/business-60584798 (accessed October 10, 2022).

[6] Bioenergy for the Transition: Ensuring Sustainability and Overcoming Barriers, /Publications/2022/Aug/Bioenergy-for-the-Transition. (n.d.). https://www.irena.org/publications/2022/Aug/Bioenergy-for-the-Transition (accessed October 10, 2022).

[7] B.M. Jenkins, L.L. Baxter, T.R. Miles, T.R. Miles, Combustion properties of biomass, Fuel Processing Technology. 54 (1998) 17–46. https://doi.org/10.1016/S0378-3820(97)00059-3.

[8] P. McKendry, Energy production from biomass (part 1): overview of biomass, Bioresource Technology. 83 (2002) 37–46. https://doi.org/10.1016/S0960-8524(01)00118-3.

[9] O. US EPA, Economics of Biofuels, (2014). https://www.epa.gov/environmental-economics/economics-biofuels (accessed October 10, 2022).

[10] Electrification and the bioeconomy: three sides to the story, (2019). https://www.sei.org/publications/electrification-bioeconomy-three-sides-to-the-story/ (accessed November 19, 2022).

[11] Renewable Energy Market Update 2022, (2022) 29.

[12] Biofuels explained - U.S. Energy Information Administration (EIA), (n.d.). https://www.eia.gov/energyexplained/biofuels/ (accessed October 10, 2022).

[13] T. Mizik, G. Gyarmati, Economic and Sustainability of Biodiesel Production—A Systematic Literature Review, Clean Technologies. 3 (2021) 19–36. https://doi.org/10.3390/cleantechnol3010002.

[14] K.F. Tzanetis, J.A. Posada, A. Ramirez, Analysis of biomass hydrothermal liquefaction and biocrude-oil upgrading for renewable jet fuel production: The impact of reaction conditions on production costs and GHG emissions performance, Renewable Energy. 113 (2017) 1388–1398. https://doi.org/10.1016/j.renene.2017.06.104.

[15] N. Hajilary, M. Rezakazemi, S. Shirazian, Biofuel types and membrane separation, Environ Chem Lett. 17 (2019) 1–18. https://doi.org/10.1007/s10311-018-0777-9.

[16] H.B. Goyal, D. Seal, R.C. Saxena, Bio-fuels from thermochemical conversion of renewable resources: A review, Renewable and Sustainable Energy Reviews. 12 (2008) 504–517. https://doi.org/10.1016/j.rser.2006.07.014.

[17] S.N. Naik, V.V. Goud, P.K. Rout, A.K. Dalai, Production of first and second generation biofuels: A comprehensive review, Renewable and Sustainable Energy Reviews. 14 (2010) 578–597. https://doi.org/10.1016/j.rser.2009.10.003.

[18] G.W. Huber, S. Iborra, A. Corma, Synthesis of Transportation Fuels from Biomass: Chemistry, Catalysts, and Engineering, Chem. Rev. 106 (2006) 4044–4098. https://doi.org/10.1021/cr068360d.

[19] G.W. Huber, J.A. Dumesic, An overview of aqueous-phase catalytic processes for production of hydrogen and alkanes in a biorefinery, Catalysis Today. 111 (2006) 119–132. https://doi.org/10.1016/j.cattod.2005.10.010.

[20] A.A. Peterson, F. Vogel, R.P. Lachance, M. Fröling, J. Michael J. Antal, J.W. Tester, Thermochemical biofuel production in hydrothermal media: A review of sub- and supercritical water technologies, Energy Environ. Sci. 1 (2008) 32–65. https://doi.org/10.1039/B810100K.

[21] J. Yang, Q. (Sophia) He, L. Yang, A review on hydrothermal co-liquefaction of biomass, Applied Energy. 250 (2019) 926–945. https://doi.org/10.1016/j.apenergy.2019.05.033.

[22] D. Castello, T.H. Pedersen, L.A. Rosendahl, Continuous Hydrothermal Liquefaction of Biomass: A Critical Review, Energies. 11 (2018) 3165. https://doi.org/10.3390/en11113165.

[23] C. Hognon, F. Delrue, J. Texier, M. Grateau, S. Thiery, H. Miller, A. Roubaud, Comparison of pyrolysis and hydrothermal liquefaction of Chlamydomonas reinhardtii. Growth studies on the recovered hydrothermal aqueous phase, Biomass and Bioenergy. 73 (2015) 23–31. https://doi.org/10.1016/j.biombioe.2014.11.025.

[24] E. Berl, Production of Oil from Plant Material, Science. 99 (1944) 309–312. https://doi.org/10.1126/science.99.2573.309.

[25] Bio-crude | Task 34, (n.d.). https://task34.ieabioenergy.com/bio-crude/ (accessed October 10, 2022).

[26] P. Duan, B. Wang, Y. Xu, Catalytic hydrothermal upgrading of crude bio-oils produced from different thermo-chemical conversion routes of microalgae, Bioresource Technology. 186 (2015) 58–66. https://doi.org/10.1016/j.biortech.2015.03.050.

[27] D.C. Elliott, P. Biller, A.B. Ross, A.J. Schmidt, S.B. Jones, Hydrothermal liquefaction of biomass: Developments from batch to continuous process, Bioresource Technology. 178 (2015) 147–156. https://doi.org/10.1016/j.biortech.2014.09.132.

[28] R.K. Mishra, V. kumar, P. Kumar, K. Mohanty, Hydrothermal liquefaction of biomass for bio-crude production: A review on feedstocks, chemical compositions, operating parameters, reaction kinetics, techno-economic study, and life cycle assessment, Fuel. 316 (2022) 123377. https://doi.org/10.1016/j.fuel.2022.123377.

[29] T.E. Lindemuth, Investigations of the PERC Process for Biomass Liquefaction at the Department of Energy, Albany, Oregon Experimental Facility, in: Solid Wastes and Residues, American Chemical Society, 1978: pp. 371–391. https://doi.org/10.1021/bk-1978-0076.ch019.

[30] D.C. Elliott, Historical Developments in Hydroprocessing Bio-oils, Energy Fuels. 21 (2007) 1792–1815. https://doi.org/10.1021/ef070044u.

[31] A. Dimitriadis, S. Bezergianni, Hydrothermal liquefaction of various biomass and waste feedstocks for biocrude production: A state of the art review, Renewable and Sustainable Energy Reviews. 68 (2017) 113–125. https://doi.org/10.1016/j.rser.2016.09.120.

[32] C. Jazrawi, P. Biller, A.B. Ross, A. Montoya, T. Maschmeyer, B.S. Haynes, Pilot plant testing of continuous hydrothermal liquefaction of microalgae, Algal Research. 2 (2013) 268–277. https://doi.org/10.1016/j.algal.2013.04.006.

[33] R. Ghadge, N. Nagwani, N. Saxena, S. Dasgupta, A. Sapre, Design and scale-up challenges in hydrothermal liquefaction process for biocrude production and its upgradation, Energy Conversion and Management: X. 14 (2022) 100223. https://doi.org/10.1016/j.ecmx.2022.100223.

[34] S.S. Toor, L. Rosendahl, A. Rudolf, Hydrothermal liquefaction of biomass: A review of subcritical water technologies, Energy. 36 (2011) 2328–2342. https://doi.org/10.1016/j.energy.2011.03.013.

[35] A.R.K. Gollakota, N. Kishore, S. Gu, A review on hydrothermal liquefaction of biomass, Renewable and Sustainable Energy Reviews. 81 (2018) 1378–1392. https://doi.org/10.1016/j.rser.2017.05.178.

[36] S. Bensaid, R. Conti, D. Fino, Direct liquefaction of ligno-cellulosic residues for liquid fuel production, Fuel. 94 (2012) 324–332. https://doi.org/10.1016/j.fuel.2011.11.053.

[37] P. Sun, M. Heng, S. Sun, J. Chen, Direct liquefaction of paulownia in hot compressed water: Influence of catalysts, Energy. 35 (2010) 5421–5429. https://doi.org/10.1016/j.energy.2010.07.005.

[38] C. Xu, J. Lancaster, Conversion of secondary pulp/paper sludge powder to liquid oil products for energy recovery by direct liquefaction in hot-compressed water, Water Research. 42 (2008) 1571–1582. https://doi.org/10.1016/j.watres.2007.11.007.

[39] R. Li, B. Li, T. Yang, Y. Xie, Liquefaction of rice stalk in sub- and supercritical ethanol, Journal of Fuel Chemistry and Technology. 41 (2013) 1459–1465. https://doi.org/10.1016/S1872-5813(14)60006-2.

[40] L. Ye, J. Zhang, J. Zhao, S. Tu, Liquefaction of bamboo shoot shell for the production of polyols, Bioresource Technology. 153 (2014) 147–153. https://doi.org/10.1016/j.biortech.2013.11.070.

[41] W. Peng, C. Wu, S. Wu, Y. Wu, J. Gao, The Effects of Reaction Atmosphere on Composition, Oxygen Distribution, and Heating Value of Products from the Hydrothermal Liquefaction of Corn Stalk, Energy Sources, Part A: Recovery, Utilization, and Environmental Effects. 36 (2014) 347–356. https://doi.org/10.1080/15567036.2010.540636.

[42] J. Akhtar, N.A.S. Amin, A review on process conditions for optimum bio-oil yield in hydrothermal liquefaction of biomass, Renewable and Sustainable Energy Reviews. 15 (2011) 1615–1624. https://doi.org/10.1016/j.rser.2010.11.054.

[43] J. Ni, L. Qian, Y. Wang, B. Zhang, H. Gu, Y. Hu, Q. Wang, A review on fast hydrothermal liquefaction of biomass, Fuel. 327 (2022) 125135. https://doi.org/10.1016/j.fuel.2022.125135.

[44] D.R. Georgianna, S.P. Mayfield, Exploiting diversity and synthetic biology for the production of algal biofuels, Nature. 488 (2012) 329–335. https://doi.org/10.1038/nature11479.

[45] O. Okoligwe, T. Radu, M.C. Leaper, J.L. Wagner, Characterization of municipal solid waste residues for hydrothermal liquefaction into liquid transportation fuels, Waste Management. 140 (2022) 133–142. https://doi.org/10.1016/j.wasman.2022.01.026.

[46] C.S. Marxsen, Potential world garbage and waste carbon sequestration, Environmental Science & Policy. 4 (2001) 293–300. https://doi.org/10.1016/S1462-9011(01)00035-1.

[47] Y. Zhai, H. Chen, B. Xu, B. Xiang, Z. Chen, C. Li, G. Zeng, Influence of sewage sludge-based activated carbon and temperature on the liquefaction of sewage sludge: Yield and composition of bio-oil, immobilization and risk assessment of heavy metals, Bioresource Technology. 159 (2014) 72–79. https://doi.org/10.1016/j.biortech.2014.02.049.

[48] A. Gollakota, P.E. Savage, Hydrothermal Liquefaction of Model Food Waste Biomolecules and Ternary Mixtures under Isothermal and Fast Conditions, ACS Sustainable Chem. Eng. 6 (2018) 9018–9027. https://doi.org/10.1021/acssuschemeng.8b01368.

[49] P.T. Williams, E. Slaney, Analysis of products from the pyrolysis and liquefaction of single plastics and waste plastic mixtures, Resources, Conservation and Recycling. 51 (2007) 754–769. https://doi.org/10.1016/j.resconrec.2006.12.002.

[50] S. Xiu, A. Shahbazi, V. Shirley, D. Cheng, Hydrothermal pyrolysis of swine manure to bio-oil: Effects of operating parameters on products yield and characterization of bio-oil, Journal of Analytical and Applied Pyrolysis. 88 (2010) 73–79. https://doi.org/10.1016/j.jaap.2010.02.011.

[51] J. Lu, J. Zhang, Z. Zhu, Y. Zhang, Y. Zhao, R. Li, J. Watson, B. Li, Z. Liu, Simultaneous production of biocrude oil and recovery of nutrients and metals from human feces via hydrothermal liquefaction, Energy Conversion and Management. 134 (2017) 340–346. https://doi.org/10.1016/j.enconman.2016.12.052.

[52] J. Lu, X. Li, R. Yang, J. Zhao, Y. Liu, Y. Qu, Liquefaction of fermentation residue of reed- and corn stover-pretreated with liquid hot water in the presence of ethanol with aluminum chloride as the catalyst, Chemical Engineering Journal. 247 (2014) 142–151. https://doi.org/10.1016/j.cej.2014.02.094.

[53] H. Li, J. Lu, Y. Zhang, Z. Liu, Hydrothermal liquefaction of typical livestock manures in China: Biocrude oil production and migration of heavy metals, Journal of Analytical and Applied Pyrolysis. 135 (2018) 133–140. https://doi.org/10.1016/j.jaap.2018.09.010.

Chapter 2

Hydrothermal liquefaction of municipal sewage sludge

Abstract

In this study, ethylene and nitrogen(inert) reaction environments were applied into the hydrothermal liquefaction (HTL) process of municipal sewage sludge with red mud catalyst to evaluate the effects on biocrude and other byproducts. Red mud in three oxidation states was used: red mud calcined at 575°C (CRM), reduced at 500°C (RRM500), and 700°C (RRM700). The RRM500 lowered the acidity by 14%; whereas, the RRM700 minimized the viscosity by 47% comparing to non-catalytic-inert biocrude samples. The ethylene ambiance successfully maximized the biocrude yield by 41.6 wt.% without any catalyst. The viscosity of the biocrudes produced under ethylene environment, showed lower differences compared to nitrogen environment. The RRM500-ethylene reaction efficiently reduced the nitrogen content in the biocrude by 14%. These results suggested that the ethylene atmosphere has the potential for improved biocrude production during catalytic HTL treatment.

Keywords: Municipal sewage sludge, hydrothermal liquefaction, red mud, ethylene, biocrude oil

2.1 Introduction

Municipal sewage sludge is a nutrient-rich byproduct of the wastewater treatment process. In 2019, 4.75 million dry metric tons of municipal sewage sludge were generated alone in the U.S. Among the produced municipal sewage sludge, only 51% was applied to the land for both agricultural and non-agricultural purposes, whereas the rest was disposed of through incineration (16%), landfilling (22%), and other management practices (10%) [2]. The availability, high volatile content, and high calorific value make the municipal sewage sludge a promising feedstock for renewable energy

production. However, the high moisture content of municipal sewage sludge is the greatest barrier for the thermal conversion pathways. The heat consumed during the drying of feedstock can significantly affect the conversion efficiency [3]. Only for hydrothermal liquefaction (HTL) process, the extensive water content of municipal sewage sludge can play the key role since this thermochemical process uses water as the reaction medium and catalyst at 280-400ºC temperature under high pressure (10-2 5MPa) [4,5]. The product distribution of the HTL process includes biocrude, aqueous phase, gaseous and solid products. Water loading and density of the slurry can affect the liquefaction outcomes[6]. From the previous studies of HTL using municipal sewage sludge, the biocrude yield varies from 10 to 48 wt.% [7,8]. Recently the researchers have adopted different strategies to improve the biocrude quality and production from municipal sewage sludge. The HTL of secondary municipal sewage sludge at different temperatures (260–350 °C) was studied by Xu et al. to understand the variation in yields and compositions of different products (gases, biocrude and solids). It was found out that the increasing temperature improved the biocrude quality and the gas yield with reduced water-soluble substance yield, the solid yield, and the total organic carbon content in the aqueous phase [9]. Fan et al. used two different phases of sludge from water treatment plant (with and without lipid) to maximize valorization. This integrated approach of lipid extraction and HTL treatment enhanced biocrude from 21.26 to 29.29 wt.% compared with the HTL of untreated sludge at optimized temperature[10]. The sub-supercritical conditions were applied to non-catalytic and catalytic (K_2CO_3) HTL reactions of secondary municipal sewage sludge where the effects of catalysts were more distinguished than the temperature [11]. The wastewater derived microalgal biomass and sewage treatment plant sludge was blended for HTL treatment to solve the inconsistent supply of algal feedstock. The maximum biocrude yield of this co-liquefaction study was higher than the individual HTL highest

yield of algae or sludge [12]. Different pretreatments on the HTL of dewatered sludge such as subcritical water pretreatment, cetyl trimethyl ammonium bromide pretreatment, fatty alcohol polyoxyethylene ether pretreatment, and microwave pretreatment were reported. The subcritical water pretreatment reduced nitrogen content, cetyl trimethyl ammonium bromide pretreatment increased calorific value, fatty alcohol polyoxyethylene ether pretreatment brought a change in chemical composition, and microwave pretreatment enhanced the yield of biocrude products [13,14]. Liu et al. have explored the effects of inorganic (HCl, HNO_3, and H_2SO_4) and organic (HCOOH, CH_3COOH, and HOOCCOOH) acid pretreatments on HTL of municipal secondary sludge. Overall, the acid pretreatments enhanced biocrude yield with upgraded properties [15]. These pretreatments raise the overall cost of the HTL process. Introducing waste material-based additives or catalysts in the municipal sewage sludge liquefaction systems might offer a more economical approach making the process sustainable in the long run. The Pacific Northwest National Laboratory (PNNL) of the U.S. Department of Energy has done extensive studies on HTL of wet feedstocks, including municipal sludge and upgrading for the production of transportation fuels. The focus of the PNNL is mainly on recovering the nutrients from the aqueous phase and hydrotreatment of the produced biocrude [16].

The biocrude, however, has a high viscosity, high nitrogen content, and low heating value. A significant amount of oxygen and nitrogen heteroatoms was found in the HTL biocrude products from almost all types of feedstock[17]. Thus, upgrading processes for lowering heteroatoms content in the biocrude presents a significant opportunity for wider adaption for converting municipal sewage sludge into biofuels. A catalyst with higher activity and lower cost can play a crucial role here. The catalyst along with optimum reaction temperature and atmosphere can highly

influence the yield and quality of HTL biocrude[18]. Therefore, developing or finding cheap catalysts from waste material for catalytic upgrading of biocrude has attracted scientific attention lately. Red mud (RM) is an industrial waste produced from alumina production. The study reported that approximately 1.5 tons of red mud is discharged per ton of alumina production[19]. The traditional disposal method of this alkaline waste (pH~14) in red mud ponds is risky because of the potential release or leakage of pollutants into groundwater resources [20,21]. Almost 3 billion tons of RM are currently under storage facilities in massive waste ponds or dried mounds [22]. The name red mud came from the color caused by iron (III) oxides, comprising approximately 20–40% of its mass[23,24]. RM can be used as an inexpensive catalyst because of its high iron content. The iron content of this heterogeneous industrial waste is a key factor for its catalytic activity, and different forms of iron can be obtained using various catalyst preparation techniques. The use of iron as the liquefaction catalyst is very attractive since iron is known to react with hot compressed water or steam according to Equation 1, producing in-situ hydrogen for the reduction of the intermediates produced during the liquefaction process [25-27].

$$3Fe + 4H_2O \rightleftharpoons Fe_3O_4 + 4H_2 \quad (1)$$

The use of RM as a catalyst for various applications, including pyrolysis of biomass, hydrogenation, and liquefaction of coal and biomass, hydrodechlorination and desulfurization reactions, methanogenesis reaction, and exhaust gas clean-up, has been demonstrated [28-31]. The hydrodeoxygenation of aqueous-phase produced from the pyrolysis of pinyon-juniper biomass was performed using a synthesized novel multifunctional red mud-supported nickel (Ni/RM) catalyst and compared with commercial $Ni/SiO_2{-}Al_2O_3$ [32]. In another study, reduced red mud (RRM) catalyst removed less reactive organics like alcohols, aldehydes, and acids from hemp-derived bio-oil and increased the stability by alkanes, alkenes, and aromatics for over the course of 90 days,

whereas the untreated bio-oil began to degrade [33]. The study has found out that RM and red clay can enhance biocrude yield with improved quality compared with non-catalytic HTL of food waste [34]. The comparison between activated and raw forms of RM was made in HTL of algae (*Spirulina platensis*). The findings suggested that the increased catalysts to biomass ratio promoted biocrude yield, and activated RM reduced the nitrogen content in the biocrudes [35]. The catalytic activity of an iron-based catalyst for tar elimination was studied, and its efficiency strongly depended on the oxidation state (Fe_2O_3, Fe_3O_4, FeO, or Fe^0). Studies have suggested that metallic iron (Fe^0) is catalytically more active for tar and methane conversion than iron oxides due to the ability of Fe^0 to break C-C and C-H bonds[36,37]. However, the potential of RM as a catalyst in the HTL of municipal sewage sludge has not been studied. The RM can be modified to prepare an HTL catalyst while valorizing it. The reaction atmosphere is an important operating parameter that can affect the distributions of HTL products. Although most HTL studies have been carried out under an inert atmosphere, other gases such as CO_2 ,O_2 have been used during the HTL process[38]. Peng et al. found the following trend: $CO > H_2 > N_2$, for biomass (cornstalk) conversion to biocrude[39]. Wang et al. suggested H_2 gas was more effective than syngas in bio-oil conversion from sawdust, but both of them were better than Ar and CO gaseous environments[40]. In other studies, however, the addition of a heterogeneous catalyst with hydrogen gas during the HTL treatment of algal biomass lowered the O/C ratios of biocrude[41]. To the best of our knowledge, the use of other gases during hydrothermal liquefaction is rare.

In this study, the HTL of municipal sludge has been conducted under an ethylene atmosphere for the first time. We hypothesized that the C=C bond could react with oxygen-, nitrogen- and sulfur-based functional groups, producing a more stable biocrude at higher yield and suppressing in-situ

polymerization reaction. In addition, this study has the potential advantage of gaseous product valorization in thermochemical biomass conversions. For example, fast pyrolysis of polyethylene produces high amounts of ethylene in the gas phase [42-44]. But, the gas product mixture may not be easy to purify. Thus, the proposed pathway can significantly increase the sustainability of other thermochemical processes such as pyrolysis and gasification. However, the cost of ethylene must be taken into account if provided from an external source. Additionally, the in-situ catalytic effects of red mud during the HTL of municipal sewage sludge under both nitrogen and ethylene atmospheres at a temperature of 350℃ were investigated. The contribution of this study is to show an innovative way to convert wet waste feedstocks such as municipal sewage sludge into a liquid (biocrude), upgraded biofuel precursor.

2.2 Materials and methodology

2.2.1 Materials

Municipal sewage sludge was collected, after the belt-filter press, from a local wastewater treatment facility (H.C. Morgan Water Pollution Control Facility, Auburn, Alabama, USA). Red mud was obtained from Almatis Burnside, Inc. (Gonzales, Louisiana, USA). Airgas Inc. (Opelika, Alabama, USA) supplied high purity nitrogen, ethylene, and a gas mixture of 10% hydrogen in 90% nitrogen.

2.2.2 Feedstock characterization

The collected sludge samples were dried at 105℃ for 24 hours, and a planetary ball mill (MSK-SFM-1S, MTI Corporation, Richmond, California, USA) was used to grind the dried samples for uniform size. The EPA 1684 method was followed to measure the total solid content. The ash content was quantified using ASTM E1755 method, and volatile matter content was obtained

according to ASTM E872. The higher heating value (HHV) of dried sludge samples was determined using an oxygen bomb calorimeter (C200, IKA, Wilmington, North Carolina, USA). The elemental analysis (CHNS/O) was performed according to the ASTM D5373-02 method (Vario MICRO cube, Elementar, Ronkonkoma, New York, USA).

2.2.3 Catalyst preparation

The as-received red mud (RM) was calcined at 575°C for four hours without any pretreatment and then sieved to obtain the particle size between 106-595 µm. The three different oxidation states of RM were used in this study as catalysts: calcined red mud at 575°C (CRM), reduced at 500°C (RRM500), and reduced at 700°C(RRM700). The thermogravimetric-temperature programmed reduction (TG-TPR) was used to characterize the reduction behavior. The reduction temperatures for RM were based on the TG-TPR profile of the calcined red mud. For RM reduction, a gas mixture of 10% H_2 and 90% N_2 was used for six hours at the predetermined temperature.

2.2.4 Catalyst characterization

The catalysts were characterized using inductively coupled plasma (ICP) and X-ray diffraction (XRD). The ICP was performed using an outside laboratory (Hazen Research Inc., Golden Colorado, USA). A bench-top powder X-ray diffraction system (AXRD, Proto Manufacturing, Taylor, Michigan, USA) from 20° to 100º (2θ) with 2 seconds of dwell time and 0.014° of Δ2Θ at 30 mA and 40 kV with CuKα radiation (λ = 1.5418 Å) was used to perform XRD analysis.

2.2.5 Experimental setup and procedure

HTL experiments were performed in a high-pressure, high-temperature reactor from Parr Instrument Company (Model 4578, Moline, Illinois, USA). The reactor was equipped with a 1.8 L vessel, PID controlled electrical heating unit, controllable agitator, pressure gauge, and J-type thermocouple to monitor the temperature inside the reactor. For both inert environment (nitrogen)

and ethylene, the HTL experiments were performed at a reaction temperature of 350°C and a residence time of 60 minutes. For each HTL experiment, 600 g as-received municipal sewage sludge (with 17-19% solid content) was loaded into the reactor. For all catalytic HTL experiments, catalyst: feedstock loading was fixed at 1:3 (i.e., ~34 g catalyst per 600 g as-received feedstock). The identical catalyst-to-feedstock ratio was used in HTL conversion of food waste feedstock with red mud and red clay catalyst. Greater carbon yield was found in biocrude by red mud than red clay[34]. The reactor was purged with desired gas (nitrogen or ethylene) three times to remove air from the reactor headspace before pressurizing with it to an initial pressure of 200 psi (1.38 MPa). The reactor was then heated to the desired temperature at the heating rate of ~4°C/min. It was reported that the reaction temperature of 350°C at 3.33°C/min heating rate favored higher biocrude production from sewage sludge feedstock [45]. After holding the reactor at the desired temperature for 1 h, the heater was removed, and the reactor was cooled to room temperature by running cold water in the internal cooling coil. The products (gas, solid, aqueous phase, and biocrude) were separated as described in Section2.2.6. All experiments were performed in duplicates.

2.2.6 Product separation

After cooling down the reactor to room temperature, its pressure was recorded. The gas products were analyzed using a micro-GC (Agilent 3000A). The Agilent 3000 A Micro GC is equipped with three modules: a 10 m Molsieve 5A (MS) column and two 10 m porous polymer (PPU) columns. Each module had a thermal conductivity detector. The instrument has the ability to split the sample into three streams. Each stream would go to one of these modules. MS column was used to analyze hydrogen, methane, and carbon monoxide, while carbon dioxide and ethylene hydrocarbons were analyzed on the PPU columns simultaneously. Argon and helium were used as carrier gases for MS column and PPU column, respectively. The gas composition analysis was

performed in triplicates. After the gas analysis, the remaining gas was vented, and the reactor was opened to recover the liquid and solid products. The content in the reactor was poured into a large flask, and the weight was recorded. Then, the reactor content was filtered through Whatman No.50 filter paper (particle filtration size of 2.7 μm) to separate the solid from dichloromethane mixed liquid products, mainly aqueous phase. Then the remaining solids on the filter paper were washed with dichloromethane (DCM). The aqueous phase was then separated from the DCM mixed bio-oil by decantation. The weight of all liquids (aqueous and organic phases) was recorded for mass balance. The DCM was separated from the biocrude using an IKA rotary evaporator at 60°C and 720 mbar vacuum pressure to obtain DCM extracted bio-oil, which is termed as "biocrude oil" throughout the paper.

2.2.7 Product analysis

The total mass of the gaseous product was calculated back using Equation 2.

$$W_g = \sum x_i . MW_i . n_{tot} \qquad (2)$$

where W_g is the total mass of gaseous product (g), x_i is the mole fraction of gas i, MW_i is the molecular weight of gas i (g/mole), and n_{tot} is the total number of moles of gas product.

In the case of ethylene HTL experiments, Ethylene (C_2H_4) consumption was estimated using Equation 3.

$$Ethylene\ consumption\left(\frac{mole C_2H_4}{kg\ sludge}\right) = \left(n_{iC_2H_4} - x_{fC_2H_4} . n_{ftot}\right) \times \frac{1}{105g\ organic\ Sludge} \times \frac{1000g}{1kg} \qquad (3)$$

where $n_{iC_2H_4}$ is the initial number of mole of ethylene, $x_{fC_2H_4}$ is the final mole fraction of ethylene, n_{ftot} is the total number of moles of gas at the end of the experiment. The yield of liquid, gas and solid product were calculated on dry-ash free basis using Equations 4, 5, and 6, respectively[46,47].

$$Y_{biocrude}(\%) = \frac{w_b}{w_f - w_m - w_a} \times 100 \quad (4)$$

$$Y_{gas}(\%) = \frac{w_g}{w_f - w_m - w_a} \times 100 \quad (5)$$

$$Y_{solid}(\%) = \frac{w_s - w_c}{w_f - w_m - w_a} \times 100 \quad (6)$$

where W_f is the mass of municipal sewage sludge feedstock (g), W_m and W_a are the mass of moisture and ash content of feedstock (g), respectively, W_b is the mass of the biocrude product (g), W_g is the mass of gas product (g), W_s is the weight of total solid residues (g), and W_c is the weight of catalyst (g).

The higher heating value (HHV) of biocrude was determined using an oxygen bomb calorimeter (Model C200, IKA, Wilmington, North Carolina, USA). The elemental analysis was performed on each sample using an elemental analyzer (Vario MICRO, Elementar, Ronkonkoma, New York, USA) according to ASTM D5373-02. The total acid number (TAN) of each sample was determined through titration according to ASTM D664-07 using a Mettler Toledo T50 Titrator. The density and kinematic viscosity of the oils were measured at 20°C using a viscometer (SVM 3001, Anton Paar, Austria). The chemical composition of each sample was subsequently analyzed by Fourier transform infrared (FTIR) and nuclear magnetic resonance (NMR) spectroscopy analyses. The FTIR of biocrudes was performed by using Thermo Nicolet iS10 (Thermo Scientific, Waltham,MA). The samples were analyzed for 34 scans over a range of 400–4000 cm^{-1} wavenumbers. Samples for NMR spectroscopy containing 25mg of oil in 1ml of chloroform (99.9%-D) with 1% v/v tetramethylsilane (TMS) (Acros organic, Switzerland) were prepared in 5 mm 535-PP NMR tubes (Wilmad-LabGlass, Vineland NJ).^{13}C spectra were collected using a Bruker 500 MHZ spectrometer equipped with a broadband nitrogen-cooled prodigy probe. The spectra were referenced to chloroform ($CDCl_3$, $\delta^{13}C$ = 77.2 ppm) and processed in Bruker Topspin

software (3.6.3 version). The Simulated distillation analysis was performed according to ASTM D2887. Approximately 20 mg of each sample was diluted with carbon disulfide (CS_2) until each diluted sample contained an estimated 1 wt. % oil sample[32,48]. The filled vial was then loaded into an Agilent Technologies 7890A GC with Flame-Ionization Detection (FID) System equipped with a 7693 Autosampler. The GC-FID contained a 10 m x 0.53 mm x 3 μm DB-2887 Column. A sample volume of 0.2 μL was injected for the simulated distillation analysis. Each sample was then heated from an initial temperature of 40°C to a final temperature of 350°C at a heating rate of 20°C/min. The GC-FID System was operated in a 1:4 split inlet mode during each simulated distillation analysis.

The aqueous phase was analyzed for total organic carbon (TOC), total nitrogen (TN) with specific species distribution(ammonium (NH_4^+-N), nitrate(NO_3^--N), organic nitrogen (Org-N)), chemical oxygen demand (COD), and pH. The TOC and TN were measured by a TOC/TN analyzer (TOC-L, Shimadzu, Kyoto, Japan). A Prominence Liquid Chromatography (LC) system coupled with a conductivity detector (Shimadzu, Japan) was used to analyze concentrations of ammonium (NH_4^+-N) and nitrate (NO_3^-N) in digestate samples. The detailed procedure can be found in previously published literature [49]. Briefly, A Dionex IonPac CS12 column (4 × 250mm, Thermoscience) and a Dionex IonPac AS22 column (4× 250mm) with suppression (Dionex CERS 500 4mm and Dionex AERS 500 4mm,respectively)were used for ion separation.Acidic eluent (20 mM methanesulfonic acid) was used on the CS12 column, and basic eluent (4.5mM sodium carbonate and 1.4mM sodium bicarbonate solution) was used on the AS22 column. The amount of organic nitrogen (Org-N) was calculated by the difference of total nitrogen and inorganic nitrogen (the sum of NH_4^+-N and NO_3^--N). The COD was determined using a COD assay kit (HACH, Loveland, Colorado, USA) and a spectrometer(DR900, HACH, Loveland, Colorado, USA). The detailed

procedure can be found in previous literature [50]. The pH of the solution was measured using a pH meter (pH510, Oakton, Vernon Hills, Illinois, USA).

2.3 Result and discussion

2.3.1 Feedstock characterization

Table 2.1 shows the proximate and elemental analyses of the municipal sewage sludge feedstock. The elemental composition of feedstock with high ash (29.8±2.7%, on a dry basis), nitrogen, and heavy metal contents are in good agreement with other publications [51,52]. These factors can significantly affect HTL products.

Table 2.1: Characterization of municipal sewage sludge

	Present Study	[51][2]	[52][2]
Proximate Analysis (wt.%)			
Moisture Content	82.4 ± 1.2[1]	2.54	n.r.
Volatile Matter	52.9 ± 0.7[2]	49.77	60.8[4]
Fixed Carbon	3.0±0.5[1,3]	5.42	n.r.
Elemental Composition[2] (wt.%)			
C	33.1±0.3	28.71	31.29
H	5.5±0.1	4.66	3.83
N	5.0±0.1	5.01	4.84
S	0.7±0.1	0.5	3.43
Ash	29.8±2.7	42.27	39.2
O[3]	25.9±0.1	18.82	17.41
HHV[2] (MJ/kg)	14.1±0.9	12.82	n.r.
Heavy Metal[2] (mg/kg)			
Ce	47	150	n.r.
Cd	n.d.	3	2.10
Cr	50	130	87
Cu	270	n.r.	150
Mn	560	n.r.	n.r.
Pb	n.d.	50	61
Zn	560	500	780

[1] as received basis. [2]on dry basis. [3]by difference. [4]including volatile matter and fixed carbon. n.r.=not reported. n.d.=not detected.

2.3.2 Catalysts characterization

Only fresh catalysts were used in this study because the spent catalysts were uniformly mixed with the solid residue after HTL experiments, and we had difficulties separating the spent catalyst from solid residues effectively. The different metal oxides were detected by XRD analysis of the catalysts. Figure 2.1 is showing the most prominent peaks of hematite (Fe_2O_3), magnetite (Fe_3O_4), anatase(TiO_2), goethite($Fe^{3+}O(OH)$), and quartz(SiO_2) at different $2\Theta^o$ positions of all three catalysts with the enlarged view of iron (Fe) peak at $2\Theta = 43^o$ in RRM500 and RRM700.The RRM500 has smaller hematite peaks at $2\Theta^o$ positions of 26, 33, and 54, where intense peaks were found in $2\Theta^o$ positions of 27 and 35 for hematite and magnetite, respectively. A similar trend was found in the RRM700 catalysts. Moreover, one extra peak of magnetite was observed in the XRD peaks of RRM500 and RRM700 at $2\Theta^o$ of 68, which was not seen in CRM. These findings suggested that the reduction process of a catalyst successfully increased the magnetite formation in the catalyst. In other words, the crystallinity of magnetite could have proportional relation with the reduction temperature of the catalysts. Similar results were reported for the XRD pattern of reduced red mud at 450℃, where conversion of hematite to magnetite by reduction process was mentioned[53-56]. The inductively coupled plasma optical emission(ICP-OES) analysis also confirmed the high iron (Fe) content (32.2-37.1 wt.%) in three forms of catalysts. The ICP analysis of catalysts is shown in Table A1 of the supplementary material. The iron (Fe) amount increased in the following order: RRM700>RRM500>CRM. Aluminum(Al), calcium (Ca), sodium (Na), and titanium (Ti) were also present in considerable amounts, along with iron. The characterization tests of RM catalysts proved the reduction process at 500, and 700℃ changed the hematite to magnetite. However, this reduction process could not transform all the hematite into magnetite. In addition, there were a significant amount of other metal oxides (63-67%) in the catalysts.

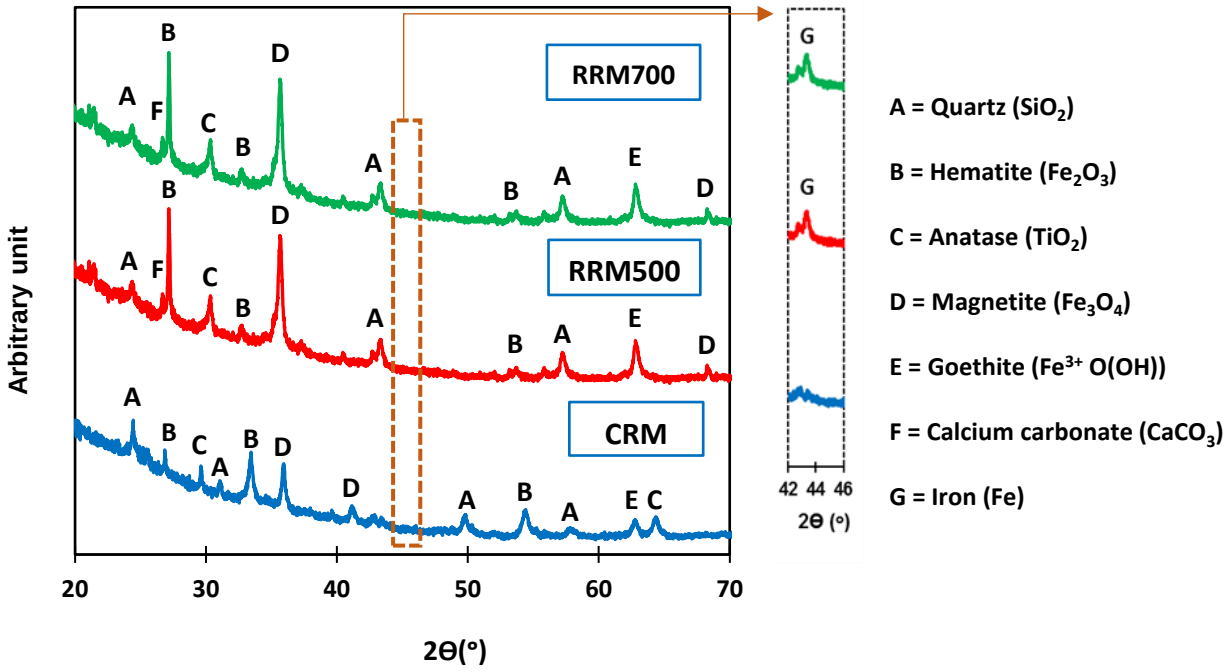

Figure 2.1: XRD analysis of RM catalysts

2.3.3 HTL products characterization

2.3.3.1 Products yield distribution

Figure 2.2 illustrates the effect of catalysts under two reaction conditions over product distribution on dry-ash free basis. In both reaction conditions, the non-catalytic HTL process produced the maximum biocrude yields. Under this scenario, 41.6 wt.% biocrude was produced using ethylene compared to 37.1wt.% with nitrogen. This observation suggested that ethylene could react with municipal sewage sludge-derived components without a catalyst resulting in approximately 5wt.% higher biocrude yield. Among the catalytic experiments, RRM700 in the ethylene environment was the best combination to produce the biocrude yield of 38.2 wt.%. The RRM700 in the nitrogen environment resulted in the lowest liquid yield production (26.7 wt.%), which was about 11wt.% lower than in the ethylene atmosphere.This suggests that the excess 11wt.% biocrude would come

from the direct gas-liquid reaction of C=C with organic molecules, the in-situ stabilization of HTL products that inhibited polymerization, or a combination of both. However, the latter was more likely to happen because the char yield decreased from 21.2 wt.% to 14.5 wt.% in nitrogen and ethylene atmosphere, respectively, using RRM700 catalyst. The gas yields were relatively high primarily because of the reaction temperature of 350°C, where depolymerization can lead to higher gas yield production [7]. From yield analysis, there is a clear indication that a catalyst has reduced the biocrude yield. The biocrude yield reduction is prominent in the nitrogen environment comparing to ethylene. Ethylene gas promoted the gas to biocrude transformation, which increased the biocrude yield both in catalytic and non-catalytic reactions. Subsequently, this reaction condition has also caused a high gas yield in both nitrogen and ethylene conditions. The biocrude yield increased with the reduction temperature of RM under the ethylene atmosphere. This phenomenon can be described as the synergistic effect of reduced RM catalyst and ethylene gaseous environment.

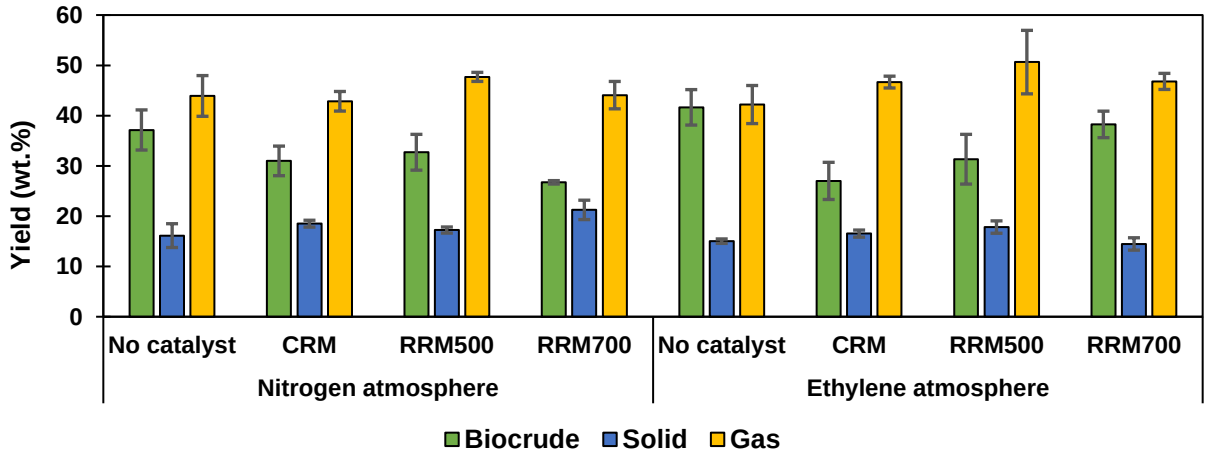

Figure 2.2: Yield distribution (on dry-ash free basis) under different conditions and catalysts.

2.3.3.2 Biocrude characterization

Physicochemical properties

Table 2.2 shows the physicochemical properties of biocrude from each experiment. The biocrude from ethylene experiments had 0.68-5.48 wt.% more carbon compared that with the nitrogen counterpart. This carbon enhancement is another proof that ethylene reacted with organic material in the municipal sewage sludge adding carbon to the biocrude product. Among all the experiments, the lowest nitrogen content was found from the RRM500-ethylene combination. The hydrogen content of biocrude was slightly increased by ethylene. The breakthrough was, however, observed in oxygen removal. The ethylene environment successfully reduced the oxygen content in biocrude by 2-21% compared to the same catalyst combination under an inert (nitrogen) environment. The minimum oxygen content found in the non-catalytic-ethylene combination with a subsequent higher heating value of 29.6 MJ/kg. Furthermore, this may suggest that ethylene reactivity with oxygenated functional groups was more dominant than with sulfur- or nitrogen- heteroatoms. As presented in Table 4, all ethylene experiments produced more CO_2 than nitrogen, suggesting that ethylene might have enhanced decarboxylation reaction. The effects of ethylene over elemental composition also influenced the heating values of the liquids, and all the ethylene experiments (except RRM500) attained higher heating value liquid yields than the nitrogen environment.

Table 2.2: Physicochemical properties of the fresh biocrude.

	Nitrogen				Ethylene			
Elemental Composition (wt.%)	No catalyst	CRM	RRM500	RRM700	No catalyst	CRM	RRM500	RRM700
C	54.13±1.98	63.32±0.67	54.52±2.09	53.53±3.95	59.37±1.68	64±2.49	56.76±1.22	59.43±6.13
H	6.55±0.24	8.34±0.15	6.95±0.05	6.98±0.23	7.62±0.34	8.35±0.20	7.38±0.23	7.33±0.44
N	4.26±0.11	4.8±0.10	4.04±0.08	4.42±0.30	4.80±0.08	4.69±0.33	3.74±0.09	4.11±0.50
S	1.30±0.10	0.90±0.10	0.95±0.10	1.18±0.10	0.95±0.03	1.03±0.12	2.17±0.10	2.67±0.90
O[1]	33.80±2.33	22.64±0.92	33.39±2.33	33.94±3.51	27.97±2.12	22.18±3.14	29.95±1.54	26.47±7.60
HHV (MJ/kg)	28.30±0.53	29.01±0.64	28.53±0.17	26.62±0.15	29.57±0.37	30.43±0.60	28.29±0.77	28.44±0.20
TAN (mgKOH/g)	6.29±0.37	6.45±0.95	5.36±0.46	5.81±0.12	7.75±0.41	8.95±0.44	7.10±0.01	8.76±0.42
Dynamic Viscosity (cP)	3.39±0.58	6.25±1.23	4.18±0.35	1.83±0.03	6.35±1.13	8.83±2.58	4.35±0.81	5.48±0.87
Density (g/cm^3)	1.13±0.01	1.12±0.01	1.12±0.01	1.15±0.01	1.12±0.01	1.11±0.01	1.12±0.01	1.13±0.01

[1]by difference

The use of CRM catalyst resulted in increased carbon content and HHV and the removal of oxygen in both environments. From the XRD pattern of catalysts, it was evident that CRM was full of metal oxides in their highest oxidation state. Such metal oxides (especially hematite) might favor the polymerization reaction over cracking, which would explain higher carbon content (lower oxygen) and HHV compared to other oils. Additionally, CRM increased the nitrogen content of biocrude in nitrogen atmospheres. In ethylene, CRM decreased the nitrogen comparing to non-catalytic reaction. However, the CRM-ethylene biocrude still has higher nitrogen than RRM500 and RRM700 ones. The RRM500 catalyst produced the lowest nitrogen content in the oil in both environments, where the RRM700 catalyst slightly raised the nitrogen content from the non-catalytic ones and had the lowest HHV under the nitrogen environment.Thus, it showed the effect of the reduction process in RM's catalytic effect over biocrude properties. In the case of total acid number (TAN), the ethylene environment raised slightly compared to the nitrogen environment. The highest TAN came from the CRM-ethylene combination, whereas the lowest one came from the RRM500-nitrogen HTL. In both inert and ethylene environments, the RRM500 catalyst was

the best to keep the TAN number lowest. The dynamic viscosity of the fresh biocrude in the nitrogen environment was slightly lower than the ethylene environment. However, the sulfur content and TAN value were also increased by the ethylene reaction environment. Hence, sulfur compounds might have had a more significant impact on TAN than oxygenated functional groups. The biocrude samples used in this study were stored at room temperature (23℃) and atmospheric conditions for nine months (~39 weeks). The aged samples were tested for elemental analysis, higher heating value, viscosity, and total acid number to compare with fresh product. The result is presented in Table A2. It is evident that nine months of storage at room temperature has affected the physicochemical properties of biocrudes. The TAN has significantly increased, which agrees with other aging test results[57]. After nine months of aging, the TAN in the biocrudes from RRM500/nitrogen and RRM500/ethylene conditions have increased up to 64% and 32%, respectively, comparing to the fresh samples. In fact, the biocrudes produced under nitrogen environment have experienced 31-17% higher TAN surges than the ethylene ones. This means an improvement in the storage stability of the ethylene biocrude is the main advantage. The elemental analysis has some minor changes in carbon content in both reaction environments, resulting in lower oxygen content. However, the HHV remained almost the same after nine months of aging.

The dynamic viscosity of the biocrude was measured over four to seven weeks at 40℃ to find the viscosity trend. To verify the effect on viscosity, all oil samples were tested again on the 39th week (~ nine months). Figure 2.3 illustrates the dynamic viscosity of the biocrude measured over four to seven weeks and then 39th week at 40℃. The effect of catalysts was prominent during the viscosity test of aged oil. The biocrude derived under CRM catalysts in both inert, and ethylene conditions solidified within five weeks of production. Thus, we could not measure their viscosity further. Figure 3-A indicates that the RRM700 catalyst worked most efficiently in a nitrogen

environment to generate biocrude with the lowest and most stable viscosity. The viscosity of CRM catalyst biocrude in inert as well as in ethylene environment was the highest. This is another proof that CRM promoted polymerization even at room temperature for weeks. Unlike the nitrogen environment, RRM500 catalyst showed the best performance in the ethylene environment. All biocrudes (except CRM) produced from an ethylene environment gave similar viscosity for the entire test.

One significant effect of the ethylene atmosphere was that the viscosity lines came into a narrower spectrum than the nitrogen atmosphere, where the trend lines under the nitrogen atmosphere were more scattered. However, CRM catalyst did not follow that trend. In the case of CRM-nitrogen condition, the viscosity trend line shown a higher slope in the first three weeks, most probably polymerization reaction continued, and then oil became stable.The biocrude from the CRM-ethylene reaction was more reactive for the first week, and then the reaction slowed down, as evident by the change in the viscosity. These findings indicated that the influence of reaction atmosphere was more pronounced than the effect of catalysts in viscosity trend.

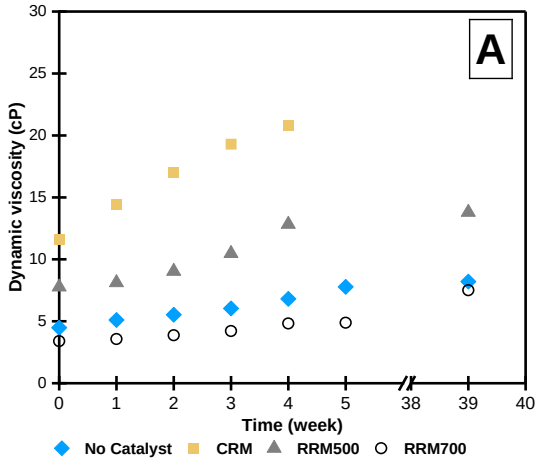

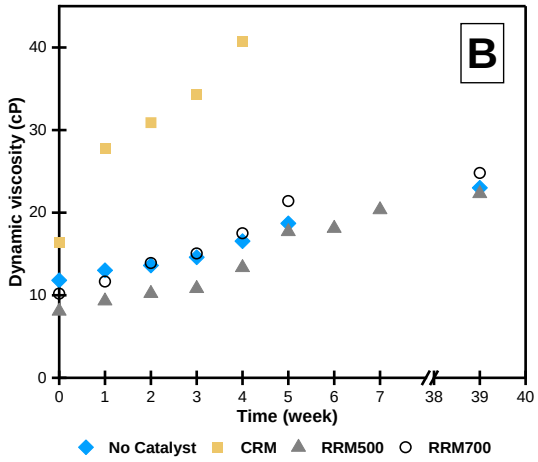

Figure 2.3: Dynamic viscosity of biocrude over time: A-nitrogen environment and B-ethylene environment

Thermogravimetric analysis

Thermogravimetric analysis is presented in Figures 2.4-A, B, C and D. For comparisons, thermograms for the same catalytic condition are plotted in the same figure for nitrogen and ethylene environments.A noticeable mass loss was observed in the derivative thermogravimetric (DTG) curve between 44 and 49℃ in the ethylene environment, which shifted between 50 and 70℃ for the inert environment. It indicated that except for CRM catalyst, the ethylene atmosphere generated some lighter compounds than the inert one in the 44-70℃ temperature range. The CRM-ethylene combination expanded the temperature range up to 400℃ for lightweight compounds production. The DTG curves for "no-catalyst" and CRM conditions are parallel up to 380℃, where biocrude from nitrogen environment has lower mass loss than the ethylene counterpart, but it increased at the end. The DTG curve of the RRM500 catalyst produced sharp loss peaks at 400℃ and 447℃ in nitrogen and ethylene environments, respectively. A similar sharp loss peak was observed at 417℃ only in the non-catalytic experiment of ethylene environment. Thus, the RRM500 catalyst affected the biocrude oil formation with compounds between 400-446℃ boiling points range, irrespective of environment. Otherwise, the lighter compounds were common

between the 203-500℃ range for ethylene. The maximum temperature for TGA experiments was 700℃, and slight biocrude residue (10-14 wt.%) was left at the TGA pan. Similar mass loss was reported in the literature of sewage sludge HTL treatment [58]. Above 80% of the biocrudes obtained in this study had a boiling point under 350℃, suggesting that products were distillable[59]. The simulated distillation of biocrude products is shown in FigureA1 (Appendix A). The biocrude samples from the ethylene environment were mostly inclined towards commercial diesel except for the CRM catalysts.In FigureA2(Appendix), it is evident that the RRM700 catalyst produced the highest gasoline range products (60.3 wt.%) among other conditions, where RRM500 generated the majority of the jet fuel products under the nitrogen environment.The minimum dynamic viscosity in RRM700-nitrogen biocrude oil is in agreement with the highest amount of gasoline range products. Furthermore, CRM catalyst produced the highest heavy diesel fraction under nitrogen environment which is another indication that CRM promoted the polymerization reaction. This finding is in agreement with the dynamic viscosity analysis of previous section. Meanwhile, in ethylene CRM produced slightly (4.28%) more gasoline products than RRM500 but RRM500 had 37.9% more light diesel products than CRM in the biocrude. The RRM500 catalyst also produced additional 21.7% heavy diesel range products in ethylene environment than nitrogen environment. The thermogravimetric analysis has supported this result by showing the shift of the DTG curve towards higher temperature after 400℃ which is equivalent to heavy diesel range (321-425℃). The production of heavy molecular vacuum gas range products by RRM700-ethylene pair can be explained by the higher dynamic viscosity of biocrude than RRM-500 ethylene product. Higher gasoline range products from RRM500-ethylene biocrude, are also in agreement with viscosity result.

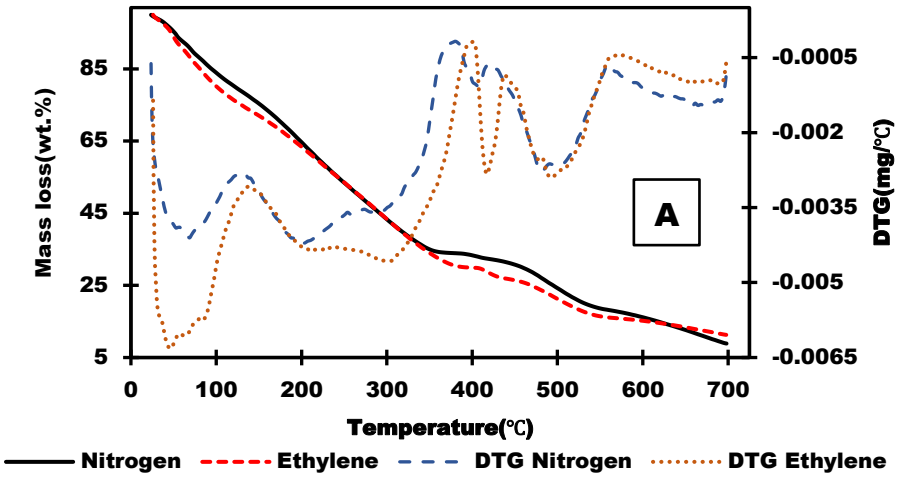
Mass loss(wt.%)
85
65
45
25
5
0
100
200
300
400
500
600
700
-0.0005
-0.002
-0.0035
-0.005
-0.0065
DTG(mg/℃)
A
Temperature(℃)
Nitrogen
Ethylene
DTG Nitrogen
DTG Ethylene

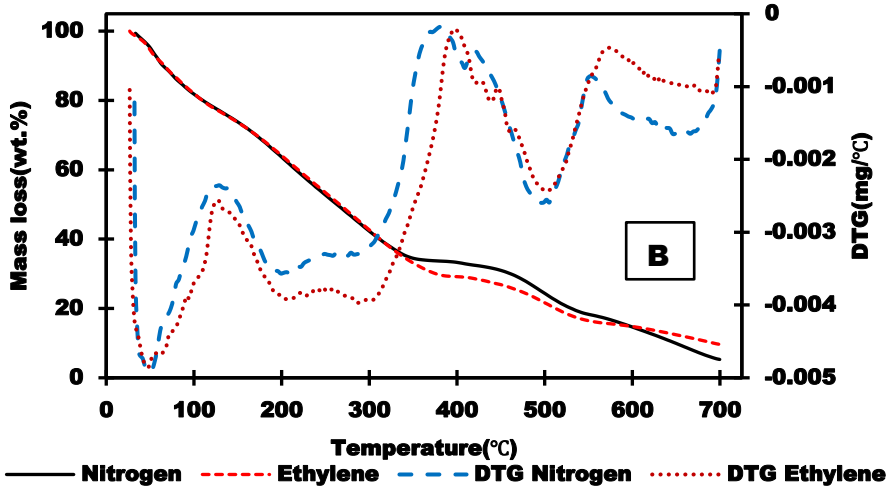
Mass loss(wt.%)
100
80
60
40
20
0
0
100
200
300
400
500
600
700
0
-0.001
-0.002
-0.003
-0.004
-0.005
DTG(mg/℃)
B
Temperature(℃)
Nitrogen
Ethylene
DTG Nitrogen
DTG Ethylene

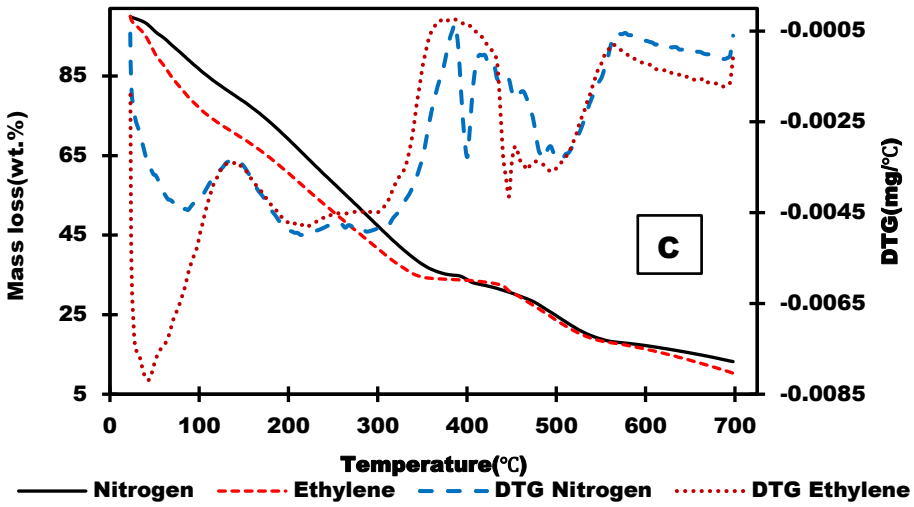
Mass loss(wt.%)
85
65
45
25
5
0
100
200
300
400
500
600
700
-0.0005
-0.0025
-0.0045
-0.0065
-0.0085
DTG(mg/℃)
C
Temperature(℃)
Nitrogen
Ethylene
DTG Nitrogen
DTG Ethylene

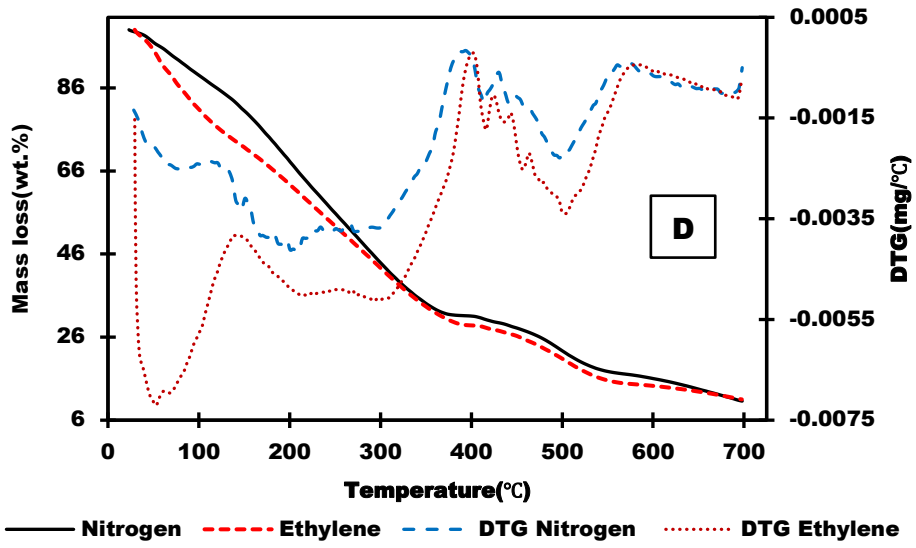

Figure 2.4: Thermogravimetric analysis of biocrude samples from nitrogen and ethylene atmospheres: A- No catalyst, B-CRM, C-RRM500 and D-RRM700.

FTIR and NMR analysis

FTIR and NMR analyses were performed on the biocrude samples for the following conditions: non-catalytic/nitrogen, RRM500/nitrogen, non-catalytic/ethylene, and RRM500/ethylene. The FTIR spectra of non-catalytic/nitrogen and non-catalytic/ethylene biocrudes were presented in Figure 2.5-A. The peak intensity in C=O functional group(1590-1800cm^{-1}) has decreased in the ethylene environment. However, ethylene condition has enhanced the peaks of alcohol, phenolic compounds(1200-1300cm^{-1}), and aromatic compounds (730-800cm^{-1}), comparing to the nitrogen environment. The reduction in -OH peak (3050-3300 cm^{-1}), C=O peak(1590-1800 cm^{-1}) under an ethylene environment has indicated oxygen removal from biocrudes [46]. The elemental analysis of Table 2.2 supported the reduced oxygen content in biocrude produced in an ethylene environment. The gas analysis of Table 2.3 also shown higher CO_2 production under ethylene atmosphere, which indicated more oxygen removal.

The FTIR spectra of non-catalytic/nitrogen and RRM500/nitrogen were compared in Figure 5-B. The RRM500 has reduced the C=O functional groups (1590-1800cm^{-1}) and added more alcohol,

phenolic compounds(1200-1300cm^{-1}) to biocrudes. This catalyst also reduced the -OH peak (3050-3300 cm^{-1}) comparing to a non-catalytic reaction. Figure 2.5-C contained the non-catalytic/ethylene, RRM500/ethylene, and RRM500/nitrogen spectra. The synergistic effects of RRM500 and ethylene atmosphere were the reduction in aromatic compounds(730-800cm^{-1}), alcohol, phenolic compounds(1200-1300cm^{-1}), and in the -OH peak (3050-3300 cm^{-1}).

^{13}C NMR spectra of the biocrudes are shown in Figure A3 (in Appendix A). Only aliphatic groups were found in the biocrudes from four conditions in Figure A3. The FTIR spectra in 2.5-A, B and C, also have the highest peaks in the aliphatic region (2700-3100 cm^{-1}). The aliphatic groups were divided into saturated aliphatic groups (0-28ppm) and unsaturated aliphatic groups (28-55ppm)[58],[59]. The semiquantitative ^{13}C NMR spectra integral (Table A4) has shown that the RRM500 catalyst has reduced saturated aliphatic groups but increased the unsaturated group in biocrude samples, irrespective of the reaction environment. The ethylene environment has slightly decreased (0.1%) the saturated aliphatic group and promoted the unsaturated group in a very small scale for both catalytic (RRM500) and non-catalytic reactions. The unsaturated bond of ethylene gas had probably reacted with the feedstock component and added more unsaturated aliphatic groups in the biocrude. However, the FTIR spectra of the biocrudes (Figure 2.5-A, B, and C) have not indicated much difference in the aliphatic regions (2700-3100cm^{-1}). From individual peak area (Table A3),6.3% decrease was found at 0 ppm chemical shift, in non-catalytic/nitrogen biocrude, compared to non-catalytic/ethylene one. On the other hand, the addition of RRM500 catalyst has increased the same peak area in a nitrogen environment. The most significant difference was found in the peak area at 1ppm. The addition of RRM500 has decreased the area by 64.3% in the biocrudes from the nitrogen environment. The peak area at 1 ppm has also decreased for both non-catalytic and catalytic reactions in ethylene ambiance with a lower rate. Although changes were

observed within individual peak, saturated and/or unsaturated regions, given the complexity of the biocrude molecules, it is unclear what these changes in NMR signals are associated with. Thus, further isotopic studies are needed to clarify the exact reaction mechanisms between ethylene and feedstock.

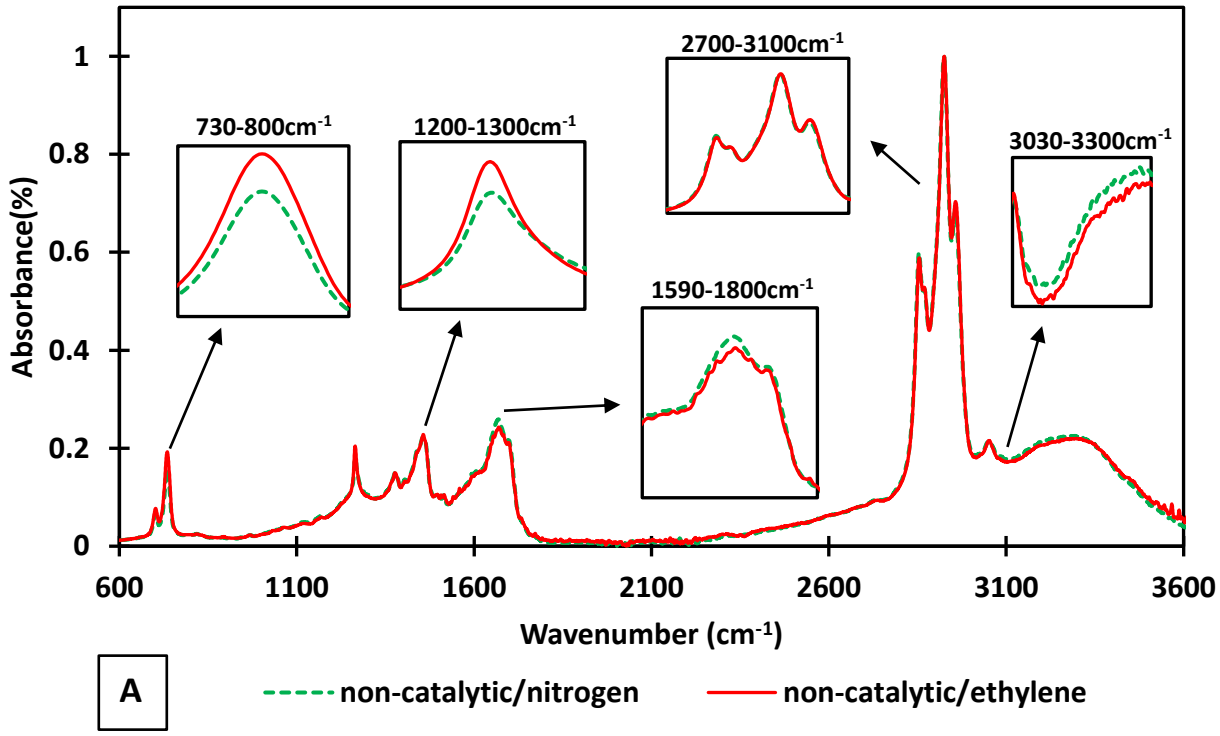

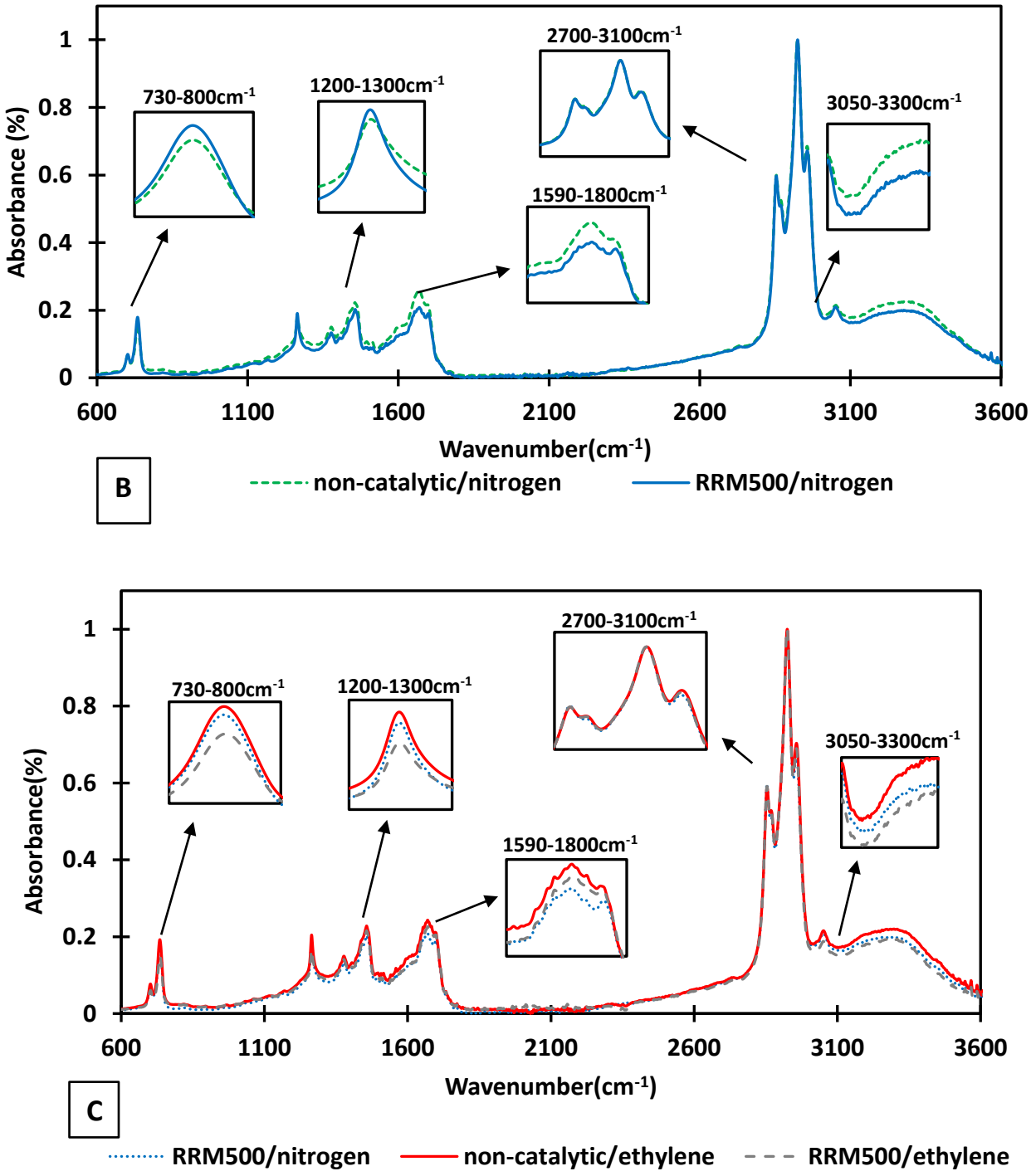

Figure 2.5: FTIR spectra of biocrudes, A-non-catalytic/nitrogen and non-catalytic/ethylene, B-non-catalytic/ nitrogen and RRM500/nitrogen and C- non-catalytic/ethylene, RRM500/ethylene, and RRM500/nitrogen

Analysis of byproducts

Table 2.3 illustrates the characterization of all byproducts: aqueous phase, solid residue, and gas phase. The non-catalyst-inert condition gave the highest TOC of the aqueous phase, whereas RRM500 gave the highest TOC under an ethylene environment. However, TOC remained less than 8 g/L under all conditions. The inorganic nitrogen mainly consisted of NH_4^+-N with very low NO_3^--N. The ethylene environment slightly raised NH_4^+-N concentration in the aqueous phase comparing to nitrogen ones. The nitrate (NO_3^--N) concentration was, however, much higher in ethylene environment products. The highest (NO_3^--N) was found from RRM500/ethylene condition with 34.7 mg/L. The nitrogen atmosphere-derived aqueous products have more organic nitrogen (Org-N) in non-catalytic and CRM conditions where RRM500 and RRM700 have increased Org-N transfer in the aqueous phase derived from the ethylene atmosphere. Thus, the results appear to suggest that ethylene transformed some of the organic nitrogen into nitrates, while red mud catalyst (regardless of its oxidation state) caused a decrease in total nitrogen. For TN, nitrogen transfer decreased by the catalyst in both atmospheres. The same trend was found for the COD of the aqueous phase produced under inert conditions. However, in ethylene, the COD has increased by RRM500 and RRM700. In pH analysis, there is increasing alkalinity in the aqueous phase from non-catalytic to catalytic reactions, irrespective of the reaction environment.

The elemental analysis was performed to characterize the solid residue, and the results are reported on catalyst-free basis. The carbon content is higher in an inert environment comparing to an ethylene one. The opposite trend was observed in elemental analysis of biocrude samples where the ethylene environment raised the carbon content. It suggested that the ethylene environment successfully transferred more carbon towards biocrude than the solid char. From a catalytic point of view, the non-catalytic reactions generated the maximum carbon and oxygen in the char

irrespective of the atmosphere. Among catalysts, only RRM700 increased the carbon, hydrogen, nitrogen, and sulfur content in char. There was enough evidence in this study to show CRM enhanced polymerization reaction. Moreover, the ash content has increased with the use of catalysts. This effect was common in both ambiances. Most probably, the catalysts have played a role in transferring the ash content of the feedstock to the solid char. However, there is no other evidence except the increased ash content in solid residue to verify this phenomenon as catalytic activity.

For gas product analysis, it is important to note that only N_2, CH_4, H_2, CO, and CO_2 gases were quantified using the method discussed in the previous work[60]. The introduction of reduced red mud catalysts has promoted in-situ hydrogen production. In inert conditions, this effect is more prominent, and RRM500 raised the hydrogen production by 2.3-4.5 mol% comparing to no catalyst reaction. RRM500 also increased methane (CH_4) production in the inert atmosphere from 0.2 – 2.4 mol%. The CO_2 production in inert conditions was almost similar except CRM. CRM generated the lowest hydrogen and CH_4, their composition was 0.8mol % and 4.7 mol%, respectively, while increasing CO_2 production significantly (93.3 mol%). These results show the effect of reduced red mud catalyst under inert conditions over HTL gas products. The ethylene atmosphere has increased the H_2 and CO_2 production by 0.5 and 7.5 mol% in the non-catalytic experiment, comparing to the inert one. The reaction between ethylene and feedstock might be responsible for this change in gaseous products. When catalysts were introduced in an ethylene environment, the synergetic effects of atmosphere and catalysts were observed on gaseous products. For example, the hydrogen production efficiency of RRM500 catalysts was suppressed by 2.4 mol% comparing to the inert atmosphere. Another example was the catalytic activity of CRM catalyst, which raised the CH_4 (by 2.1 mol%) and minimized the CO_2 (6.4 mol.%) production

in ethylene compared to the nitrogen atmosphere. The performance of RRM700 was similar in both ambiances except for almost 3mol% more CO_2 generation in the ethylene atmosphere.The ethylene consumption was calculated for the HTL experiments in ethylene. The RRM500 has consumed the least amount of ethylene, where the CRM catalyst consumed the most. The ethylene consumption trend in this study, CRM>No Catalyst>RRM700>RRM500. This means that the catalytic reactions by RRM catalysts absorbed less ethylene to influence the HTL products from municipal sewage sludge feedstock. The minimum ethylene consumption was another proof of the superiority of RRM500 over the other two catalysts.

Table 2.3: Properties of Sludge HTL byproducts

Ambiance	Nitrogen				Ethylene			
Catalyst	No Catalyst	CRM	RRM500	RRM700	No Catalyst	CRM	RRM500	RRM700
Aqueous phase								
TOC (g/L)	7.6±0.2	3.2±0.2	3.7±0.1	3.8±0.1	3.±0.1	2.8±0.1	3.9±0.1	3.4±0.1
NH_4^+-N(g/L)	5.5±0.3	4.6±0.1	4.5±0.5	5.3±0.2	5.7±0.4	5.2±0.8	4.6±1.2	5±0.5
NO_3^--N(mg/L)	17.5±1.2	21.3±0.2	0.3±1.2	12.8±0.4	34.7±0.8	35.3±1.1	28.6±0.8	29.8±0.3
Org-N[1] (g/L)	3.3±0.5	2.2±0.6	0.9±0.7	1.1±0.5	2±0.4	1.7±0.2	1.6±0.5	1.8±0.7
TN (g/L)	8.9±0.1	5.6±0.8	5.4±0.3	6.5±0.3	7.7±0.1	7±0.2	6.4±0.2	7±0.1
COD (g/L)	36.8±1.8	29.7±0.2	21.6±0.3	33.4±1.2	21.5±1.4	19.2±0.3	32.8±0.9	32.7±1.2
pH	8.5±0.1	9.2±0.1	9.2±0.1	9±0.1	8.9±0.1	8.7±0.1	9.2±0.1	9.1±0.1
Solid Residue (wt.%)								
C	27.3±0.1	17.7±0.1	17.6±1.3	22.8±0.4	21.1±0.1	15.9±0.1	17.1±0.4	20.2±0.5
H	2.6±0.1	2.1±0.1	1.9±0.1	2.3±0.1	1.9±0.1	1.8±0.1	1.9±0.4	2.2±0.1
N	2.2±0.1	1.8±0.1	1.7±0.2	2±0.2	1.7±0.1	1.7±0.2	1.7±0.3	1.9±0.1
S	0.6±0.2	0.5±0.1	0.5±0.1	0.7±0.1	0.6±0.1	0.5±0.1	1±0.1	0.7±0.1
Ash	57.1±0.9	75.2±0.9	72.3±0.4	63.7±0.5	62±1	71.5±1.2	73.5±0.5	73.6±0.1
O[1]	10.3±1	2.8±0.9	6±1.9	8.5±0.1	12.5±1	8.8±1.2	4.9±0.4	1.3±0.6
Gas Phase (mol%)								
H_2	0.9±0.1	0.8±0.1	5.3±0.6	2.9±0.3	1.4±0.5	1.1±0.2	2.9±1.1	2.9±1.7
CH_4	6.4±0.3	4.7±0.7	7.1±0.2	6.8±1.3	3.6±0.7	6.8±0.8	5.7±1.1	5.9±2
CO_2	85.3±0.4	93.3±1.9	85.8±2.1	88.2±0.2	92.9±2.2	86.9±2	88.6±2.1	91.1±0.1
Balance	7.4±0.6	1.3±1.2	1.9±1.7	2.1±1.8	2.2±1.3	5.3±3	2.9±2.1	0.1±0.1
Ethylene Consumption (mol/kg feedstock)	NA	NA	NA	NA	1.2±0.4	1.3±0.5	1±0.3	1.2±0.6

[1] by difference. NA = Not applicable.

2.3.4 Nitrogen and heavy metal distribution

The feedstock characterization confirmed the high nitrogen content in the municipal sewage sludge, and it is necessary to know the distribution of nitrogen compounds in HTL products. Especially the presence of nitrogen heavily affects the upgrading of biocrude products and the safe disposal of the aqueous phase[61]. Several research works have confirmed that the nitrogen content in biocrude from municipal sewage sludge is significantly higher comparing to that derived from other biomasses such as barley straw or barks of white pine, white spruce, and white birch[62]. The nitrogen transfer from feedstock to HTL products of the present work is shown in Figure 2.6-A by calculating the percentage of feedstock nitrogen that was distributed in each HTL product. The unquantified nitrogen was accounted as balance since the nitrogen content in HTL gases was not determined. As shown in Figure 2.6-A, the highest amount of nitrogen (31-64%) was transferred to the aqueous phase, which is in agreement with other HTL works on sludge and livestock manure [61,11,63]. The non-catalytic reactions in both environments obtained the maximum nitrogen in biocrude. The catalysts reduced the nitrogen transfer to the biocrudes irrespective of environments. Probably the catalytic reaction produced more ammonium in the aqueous phase and removed the nitrogen from the biocrudes. The least nitrogen transfer to biocrude was observed using RRM500 catalyst (14.6% and 16.8% under nitrogen and ethylene, respectively).

The trace of cerium (Ce), chromium (Cr), copper (Cu), manganese (Mn), and zinc (Zn) in HTL products suggests the heavy metal immobilization from the feedstock to all HTL products. The distribution of these metals in the HTL process is shown in Figure 2.6-B. Only samples produced using RRM500 catalyst in the ethylene environment were analyzed. It is evident that the transfer of heavy metals mostly from feedstock (municipal sewage sludge) to solid residues composed of

char and catalyst rather than biocrude. Only Cu (30 mg/kg) and Zn (100 mg/kg) were found in the biocrude where previous study has reported Pb(0.7mg/kg), Zn(121.0mg/kg), Cu(30.6mg/kg) and Ni(7.9mg/kg) in municipal sewage sludge derived HTL biocrudes. However, the heavy metal content in regular petro-diesel is much lower (Pb=0, Zn=0.11–0.14, , Cu=0.081–0.097 and Ni=0–0.045 mg/kg) [64]. Therefore, the biocrude sample requires further processing to lower its Cu and Zn contents. The accumulation of heavy metals in solid residue after the catalytic HTL process was reported by previous work by other researchers as well[45,65].We could not compare heavy metal contents in the aqueous phase with other HTL work on sewage sludge as they were below detection limits [9]. ICP detection limits for Cu, Zn, Cr, Mn, and Ce were 0.0025, 0.001, 0.005, 0.0005, and 0.0005 wt.%, respectively.

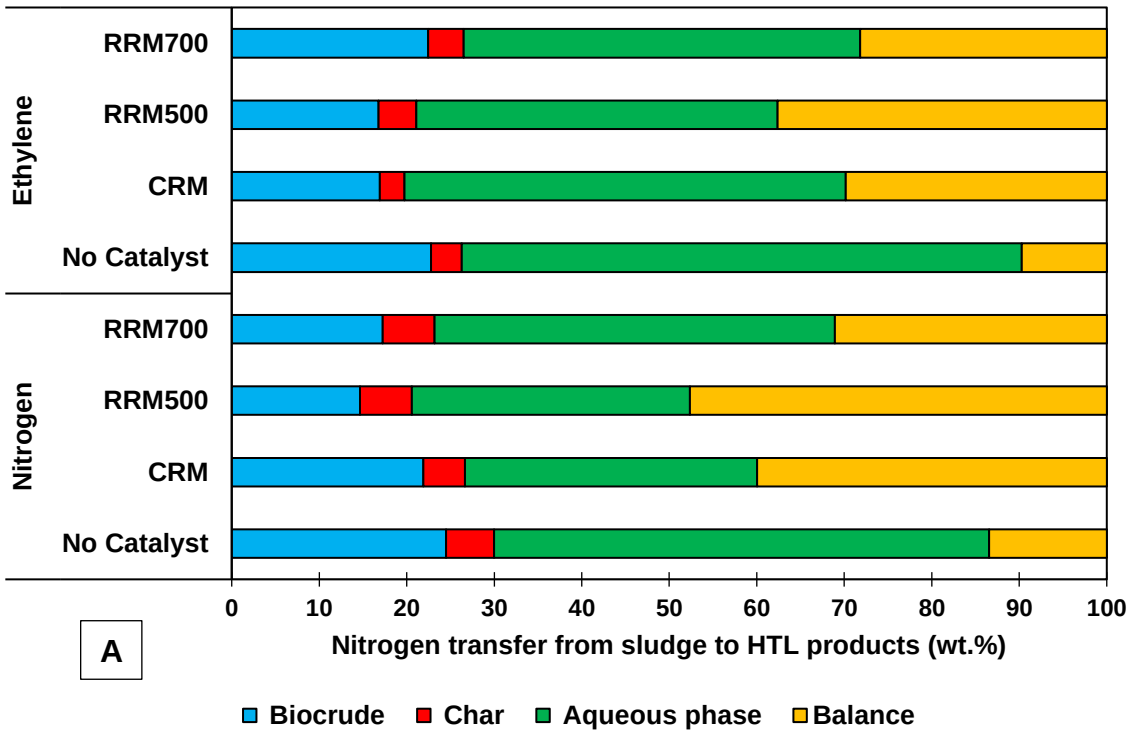

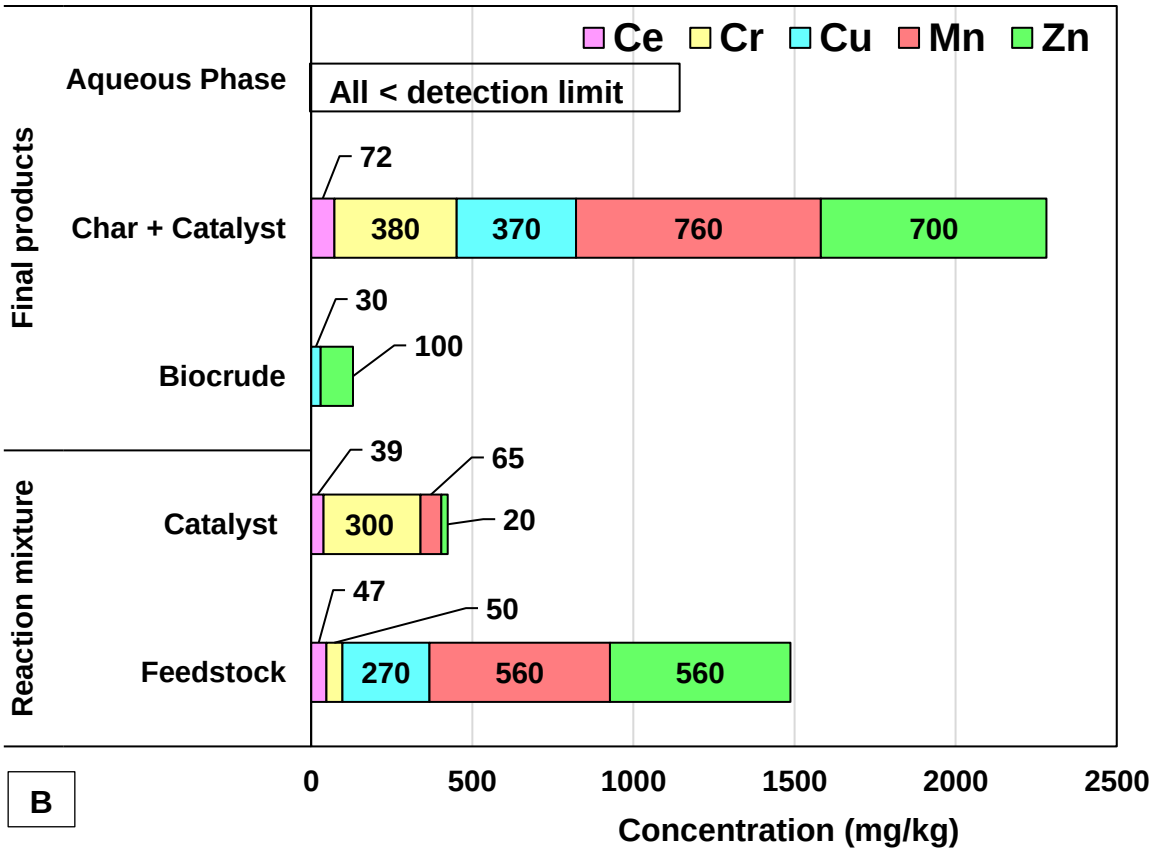

Figure 2.6: A-Nitrogen distribution and B-heavy metal distribution in HTL system using RRM500 catalyst under ethylene ambiance.

2.4 Conclusion

The hydrothermal liquefaction (HTL) of municipal sewage sludge was investigated using three forms of red mud (RM) catalysts, namely calcined red mud (CRM), reduced red mud at 500°C (RRM500), and red mud reduced at 700°C (RRM700), under inert (nitrogen) and ethylene atmosphere. The RRM500 and RRM700 lowered acidity and viscosity, whereas CRM promoted polymerization in biocrude products. However, the ethylene atmosphere gave a higher biocrude yield with consistent viscosity. The RRM500-ethylene combination reduced nitrogen content and viscosity of biocrude. Therefore, ethylene atmosphere and reduced RM catalyst were better conditions to produce biocrude from municipal sewage sludge.

2.5 References

[1] US EPA O. Basic Information about Biosolids. US EPA 2021. https://www.epa.gov/biosolids/basic-information-about-biosolids (accessed May 18, 2021).

[2] Jahromi R, Rezaei M, Hashem Samadi S, Jahromi H. Biomass gasification in a downdraft fixed-bed gasifier: Optimization of operating conditions. Chemical Engineering Science 2021;231:116249. https://doi.org/10.1016/j.ces.2020.116249.

[3] Marulanda VA, Gutierrez CDB, Alzate CAC. Chapter 4 - Thermochemical, Biological, Biochemical, and Hybrid Conversion Methods of Bio-derived Molecules into Renewable Fuels. In: Hosseini M, editor. Advanced Bioprocessing for Alternative Fuels, Biobased Chemicals, and Bioproducts, Woodhead Publishing; 2019, p. 59–81. https://doi.org/10.1016/B978-0-12-817941-3.00004-8.

[4] Zhang Y, Chen W-T. 5 - Hydrothermal liquefaction of protein-containing feedstocks. In: Rosendahl L, editor. Direct Thermochemical Liquefaction for Energy Applications, Woodhead Publishing; 2018, p. 127–68. https://doi.org/10.1016/B978-0-08-101029-7.00004-7.

[5] Patil V, Adhikari S, Cross P, Jahromi H. Progress in the solvent depolymerization of lignin. Renewable and Sustainable Energy Reviews 2020;133:110359. https://doi.org/10.1016/j.rser.2020.110359.

[6] Qian L, Wang S, Savage PE. Hydrothermal liquefaction of sewage sludge under isothermal and fast conditions. Bioresource Technology 2017;232:27–34. https://doi.org/10.1016/j.biortech.2017.02.017.

[7] Wang W, Yu Q, Meng H, Han W, Li J, Zhang J. Catalytic liquefaction of municipal sewage sludge over transition metal catalysts in ethanol-water co-solvent. Bioresource Technology 2018;249:361–7. https://doi.org/10.1016/j.biortech.2017.09.205.

[8] Xu D, Lin G, Liu L, Wang Y, Jing Z, Wang S. Comprehensive evaluation on product characteristics of fast hydrothermal liquefaction of sewage sludge at different temperatures. Energy 2018;159:686–95. https://doi.org/10.1016/j.energy.2018.06.191.

[9] Fan Y, Fonseca FG, Gong M, Hoffmann A, Hornung U, Dahmen N. Energy valorization of integrating lipid extraction and hydrothermal liquefaction of lipid-extracted sewage sludge. Journal of Cleaner Production 2021;285:124895. https://doi.org/10.1016/j.jclepro.2020.124895.

[10] Shah AA, Toor SS, Conti F, Nielsen AH, Rosendahl LA. Hydrothermal liquefaction of high ash containing sewage sludge at sub and supercritical conditions. Biomass and Bioenergy 2020;135:105504. https://doi.org/10.1016/j.biombioe.2020.105504.

[11] Mishra S, Mohanty K. Co-HTL of domestic sewage sludge and wastewater treatment derived microalgal biomass – An integrated biorefinery approach for sustainable biocrude production. Energy Conversion and Management 2020;204:112312. https://doi.org/10.1016/j.enconman.2019.112312.

[12] Yang T, Liu X, Li R, Li B, Kai X. Hydrothermal liquefaction of sewage sludge to produce bio-oil: Effect of co-pretreatment with subcritical water and mixed surfactants. The Journal of Supercritical Fluids 2019;144:28–38. https://doi.org/10.1016/j.supflu.2018.10.005.

[13] Chen G, Hu M, Du G, Tian S, He Z, Liu B, et al. Hydrothermal Liquefaction of Sewage Sludge by Microwave Pretreatment. Energy Fuels 2020;34:1145–52. https://doi.org/10.1021/acs.energyfuels.9b02155.

[14] Liu R, Tian W, Kong S, Meng Y, Wang H, Zhang J. Effects of inorganic and organic acid pretreatments on the hydrothermal liquefaction of municipal secondary sludge. Energy Conversion and Management 2018;174:661–7. https://doi.org/10.1016/j.enconman.2018.08.058.

[15] Wet Waste Hydrothermal Liquefaction and Biocrude Upgrading to Hydrocarbon Fuels: 2019 State of Technology | PNNL n.d. https://www.pnnl.gov/publications/wet-waste-hydrothermal-liquefaction-and-biocrude-upgrading-hydrocarbon-fuels-2019 (accessed July 19, 2021).

[16] Jarvis JM, Albrecht KO, Billing JM, Schmidt AJ, Hallen RT, Schaub TM. Assessment of Hydrotreatment for Hydrothermal Liquefaction Biocrudes from Sewage Sludge, Microalgae, and Pine Feedstocks. Energy Fuels 2018;32:8483–93. https://doi.org/10.1021/acs.energyfuels.8b01445.

[17] Xu D, Lin G, Guo S, Wang S, Guo Y, Jing Z. Catalytic hydrothermal liquefaction of algae and upgrading of biocrude: A critical review. Renewable and Sustainable Energy Reviews 2018;97:103–18. https://doi.org/10.1016/j.rser.2018.08.042.

[18] Kumar S, Kumar R, Bandopadhyay A. Innovative methodologies for the utilisation of wastes from metallurgical and allied industries. Resources, Conservation and Recycling 2006;48:301–14. https://doi.org/10.1016/j.resconrec.2006.03.003.

[19] Agrawal A, Sahu KK, Pandey BD. Solid waste management in non-ferrous industries in India. Resources, Conservation and Recycling 2004;42:99–120. https://doi.org/10.1016/j.resconrec.2003.10.004.

[20] Sushil S, Batra VS. Catalytic applications of red mud, an aluminium industry waste: A review. Applied Catalysis B: Environmental 2008;81:64–77. https://doi.org/10.1016/j.apcatb.2007.12.002.

[21] Service RF. Red mud is piling up. Can scientists figure out what to do with it? Science | AAAS 2020. https://www.sciencemag.org/news/2020/08/red-mud-piling-can-scientists-figure-out-what-do-it (accessed May 18, 2021).

[22] Evans K, Nordheim E, Tsesmelis K. Bauxite Residue Management. In: Suarez CE, editor. Light Metals 2012, Cham: Springer International Publishing; 2016, p. 63–6. https://doi.org/10.1007/978-3-319-48179-1_11.

[23] Tsakiridis PE, Agatzini-Leonardou S, Oustadakis P. Red mud addition in the raw meal for the production of Portland cement clinker. Journal of Hazardous Materials 2004;116:103–10. https://doi.org/10.1016/j.jhazmat.2004.08.002.

[24] Xu C, Etcheverry T. Hydro-liquefaction of woody biomass in sub- and super-critical ethanol with iron-based catalysts. Fuel 2008;87:335–45. https://doi.org/10.1016/j.fuel.2007.05.013.

[25] Miyata Y, Yamazaki Y, Hirano Y, Kita Y. Quantitative analysis of the aqueous fraction from the Fe-assisted hydrothermal liquefaction of oil palm empty fruit bunches. Journal of Analytical and Applied Pyrolysis 2018;132:72–81. https://doi.org/10.1016/j.jaap.2018.03.013.

[26] Miyata Y, Sagata K, Yamazaki Y, Teramura H, Hirano Y, Ogino C, et al. Mechanism of the Fe-Assisted Hydrothermal Liquefaction of Lignocellulosic Biomass. Ind Eng Chem Res 2018;57:14870–7. https://doi.org/10.1021/acs.iecr.8b03725.

[27] Yathavan BK, Agblevor FA. Catalytic Pyrolysis of Pinyon–Juniper Using Red Mud and HZSM-5. Energy Fuels 2013;27:6858–65. https://doi.org/10.1021/ef401853a.

[28] Lim X, Sanna A, Andrésen JM. Influence of red mud impregnation on the pyrolysis of oil palm biomass-EFB. Fuel 2014;119:259–65. https://doi.org/10.1016/j.fuel.2013.11.057.

[29] Klopries B, Hodek W, Bandermann F. Catalytic hydroliquefaction of biomass with red mud and CoO□MoO3 catalysts. Fuel 1990;69:448–55. https://doi.org/10.1016/0016-2361(90)90312-E.

[30] Pratt KC, Christoverson V. Hydrogenation of a model hydrogen-donor system using activated red mud catalyst. Fuel 1982;61:460–2. https://doi.org/10.1016/0016-2361(82)90072-2.

[31] Jahromi H, Agblevor FA. Hydrodeoxygenation of Aqueous-Phase Catalytic Pyrolysis Oil to Liquid Hydrocarbons Using Multifunctional Nickel Catalyst. Ind Eng Chem Res 2018;57:13257–68. https://doi.org/10.1021/acs.iecr.8b02807.

[32] Karimi E, Briens C, Berruti F, Moloodi S, Tzanetakis T, Thomson MJ, et al. Red Mud as a Catalyst for the Upgrading of Hemp-Seed Pyrolysis Bio-oil. Energy Fuels 2010;24:6586–600. https://doi.org/10.1021/ef101154d.

[33] Cheng F, Tompsett GA, Murphy CM, Maag AR, Carabillo N, Bailey M, et al. Synergistic Effects of Inexpensive Mixed Metal Oxides for Catalytic Hydrothermal Liquefaction of Food Wastes. ACS Sustainable Chem Eng 2020;8:6877–86. https://doi.org/10.1021/acssuschemeng.0c02059.

[34] Saral JS, Ranganathan P. Catalytic hydrothermal liquefaction of Spirulina platensis for biocrude production using Red mud. Biomass Conv Bioref 2021. https://doi.org/10.1007/s13399-021-01447-4.

[35] Kuhn JN, Zhao Z, Felix LG, Slimane RB, Choi CW, Ozkan US. Olivine catalysts for methane- and tar-steam reforming. Applied Catalysis B: Environmental 2008;81:14–26. https://doi.org/10.1016/j.apcatb.2007.11.040.

[36] Guan G, Chen G, Kasai Y, Lim EWC, Hao X, Kaewpanha M, et al. Catalytic steam reforming of biomass tar over iron- or nickel-based catalyst supported on calcined scallop shell. Applied Catalysis B: Environmental 2012;115–116:159–68. https://doi.org/10.1016/j.apcatb.2011.12.009.

[37] Singh R, Chaudhary K, Biswas B, Balagurumurthy B, Bhaskar T. Hydrothermal liquefaction of rice straw: Effect of reaction environment. The Journal of Supercritical Fluids 2015;104:70–5. https://doi.org/10.1016/j.supflu.2015.05.027.

[38] Peng W, Wu C, Wu S, Wu Y, Gao J. The Effects of Reaction Atmosphere on Composition, Oxygen Distribution, and Heating Value of Products from the Hydrothermal Liquefaction of Corn Stalk. Energy Sources, Part A: Recovery, Utilization, and Environmental Effects 2014;36:347–56. https://doi.org/10.1080/15567036.2010.540636.

[39] Wang G, Li W, Li B, Chen H. Direct liquefaction of sawdust under syngas. Fuel 2007;86:1587–93. https://doi.org/10.1016/j.fuel.2006.11.010.

[40] Duan P, Savage PE. Hydrothermal Liquefaction of a Microalga with Heterogeneous Catalysts. Ind Eng Chem Res 2011;50:52–61. https://doi.org/10.1021/ie100758s.

[41] Kalargaris I, Tian G, Gu S. Experimental evaluation of a diesel engine fuelled by pyrolysis oils produced from low-density polyethylene and ethylene–vinyl acetate plastics. Fuel Processing Technology 2017;161:125–31. https://doi.org/10.1016/j.fuproc.2017.03.014.

[42] Diaz-Silvarrey LS, Zhang K, Phan AN. Monomer recovery through advanced pyrolysis of waste high density polyethylene (HDPE). Green Chem 2018;20:1813–23. https://doi.org/10.1039/C7GC03662K.

[43] Dikgang J, Leiman A, Visser M. Elasticity of demand, price and time: lessons from South Africa's plastic-bag levy. Applied Economics 2012;44:3339–42. https://doi.org/10.1080/00036846.2011.572859.

[44] Zhai Y, Chen H, Xu B, Xiang B, Chen Z, Li C, et al. Influence of sewage sludge-based activated carbon and temperature on the liquefaction of sewage sludge: Yield and composition of bio-oil, immobilization and risk assessment of heavy metals. Bioresource Technology 2014;159:72–9. https://doi.org/10.1016/j.biortech.2014.02.049.

[45] Jahromi H, Agblevor FA. Hydrodeoxygenation of pinyon-juniper catalytic pyrolysis oil using red mud-supported nickel catalysts. Applied Catalysis B: Environmental 2018;236:1–12. https://doi.org/10.1016/j.apcatb.2018.05.008.

[46] Jahromi H, Agblevor FA. Upgrading of pinyon-juniper catalytic pyrolysis oil via hydrodeoxygenation. Energy 2017;141:2186–95. https://doi.org/10.1016/j.energy.2017.11.149.

[47] Tanneru SK, Steele PH. Pretreating bio-oil to increase yield and reduce char during hydrodeoxygenation to produce hydrocarbons. Fuel 2014;133:326–31. https://doi.org/10.1016/j.fuel.2014.05.026.

[48] Wang Q, Prasad R, Higgins BT. Aerobic bacterial pretreatment to overcome algal growth inhibition on high-strength anaerobic digestates. Water Research 2019;162:420–6. https://doi.org/10.1016/j.watres.2019.07.011.

[49] Wang P, Peng H, Adhikari S, Higgins B, Roy P, Dai W, et al. Enhancement of biogas production from wastewater sludge via anaerobic digestion assisted with biochar amendment. Bioresource Technology 2020;309:123368. https://doi.org/10.1016/j.biortech.2020.123368.

[50] Li M, Wang H, Huang Z, Yuan X, Tan M, Jiang L, et al. Comparison of atmospheric pressure and gas-pressurized torrefaction of municipal sewage sludge: Properties of solid products. Energy Conversion and Management 2020;213:112793. https://doi.org/10.1016/j.enconman.2020.112793.

[51] Yuan X, Leng L, Huang H, Chen X, Wang H, Xiao Z, et al. Speciation and environmental risk assessment of heavy metal in bio-oil from liquefaction/pyrolysis of sewage sludge. Chemosphere 2015;120:645–52. https://doi.org/10.1016/j.chemosphere.2014.10.010.

[52] Wimmers OJ, Arnoldy P, Moulijn JA. Determination of the reduction mechanism by temperature-programmed reduction: application to small iron oxide (Fe2O3) particles. J Phys Chem 1986;90:1331–7. https://doi.org/10.1021/j100398a025.

[53] Pineau A, Kanari N, Gaballah I. Kinetics of reduction of iron oxides by H2: Part I: Low temperature reduction of hematite. Thermochimica Acta 2006;447:89–100. https://doi.org/10.1016/j.tca.2005.10.004.

[54] Pineau A, Kanari N, Gaballah I. Kinetics of reduction of iron oxides by H2: Part II. Low temperature reduction of magnetite. Thermochimica Acta 2007;456:75–88. https://doi.org/10.1016/j.tca.2007.01.014.

[55] Samouhos M, Taxiarchou M, Pilatos G, Tsakiridis PE, Devlin E, Pissas M. Controlled reduction of red mud by H2 followed by magnetic separation. Minerals Engineering 2017;105:36–43. https://doi.org/10.1016/j.mineng.2017.01.004.

[56] Wang Y, Zhang Y, Liu Z. Effect of Aging in Nitrogen and Air on the Properties of Biocrude Produced by Hydrothermal Liquefaction of Spirulina. Energy Fuels 2019;33:9870–8. https://doi.org/10.1021/acs.energyfuels.9b01846.

[57] Ali Shah A, Sohail Toor S, Hussain Seehar T, Sadetmahaleh KK, Helmer Pedersen T, Haaning Nielsen A, et al. Bio-crude production through co-hydrothermal processing of swine manure with sewage sludge to enhance pumpability. Fuel 2021;288:119407. https://doi.org/10.1016/j.fuel.2020.119407.

[58] Huang H, Yuan X, Li B, Xiao Y, Zeng G. Thermochemical liquefaction characteristics of sewage sludge in different organic solvents. Journal of Analytical and Applied Pyrolysis 2014;109:176–84. https://doi.org/10.1016/j.jaap.2014.06.015.

[59] Jahromi H, Adhikari S, Roy P, Hassani E, Pope C, Oh T-S, et al. Production of green transportation fuels from Brassica carinata oil: A comparative study of noble and transition metal catalysts. Fuel Processing Technology 2021;215:106737. https://doi.org/10.1016/j.fuproc.2021.106737.

[60] Lu J, Li H, Zhang Y, Liu Z. Nitrogen Migration and Transformation during Hydrothermal Liquefaction of Livestock Manures. ACS Sustainable Chem Eng 2018;6:13570–8. https://doi.org/10.1021/acssuschemeng.8b03810.

[61] Hao B, Xu D, Jiang G, Sabri TA, Jing Z, Guo Y. Chemical reactions in the hydrothermal liquefaction of biomass and in the catalytic hydrogenation upgrading of biocrude. Green Chem 2021;23:1562–83. https://doi.org/10.1039/D0GC02893B.

[62] Lu J, Zhang J, Zhu Z, Zhang Y, Zhao Y, Li R, et al. Simultaneous production of biocrude oil and recovery of nutrients and metals from human feces via hydrothermal liquefaction. Energy Conversion and Management 2017;134:340–6. https://doi.org/10.1016/j.enconman.2016.12.052.

[63] Huang H, Yuan X. Recent progress in the direct liquefaction of typical biomass. Progress in Energy and Combustion Science 2015;49:59–80. https://doi.org/10.1016/j.pecs.2015.01.003.

[64] Huang H, Yuan X. The migration and transformation behaviors of heavy metals during the hydrothermal treatment of sewage sludge. Bioresource Technology 2016;200:991–8. https://doi.org/10.1016/j.biortech.2015.10.099.

Chapter 3

Influence of red mud catalyst and reaction atmosphere on hydrothermal liquefaction of algae

Abstract

This study investigated the effects of reaction environments on biocrude production from "*Tetraselmis sp*" algae strain by hydrothermal liquefaction (HTL) process using red mud (RM) based catalyst. The inert (N_2), ethylene (C_2H_4), reducing ($10\%H_2/90\%N_2$), and oxidizing ($10\%O_2/90\%N_2$) atmospheres were applied to the non-catalytic as well as catalytic HTL treatments with two forms of RM catalysts: RM reduced at 500°C (RRM) and nickel-supported RM (Ni/RM). The Ni/RM catalyst produced the highest biocrude yield (37 wt.%) in an ethylene environment, generated the lowest total acid number (14 mgKOH/g) under inert atmosphere, and lowered sulfur (33-66%) and oxygen (18-30%) from biocrude products irrespective of environments. The RRM catalyst maximized the biocrude carbon content (61 wt.%) under reducing environment and minimized the heavy metal and phosphorus transfer from the feedstock to biocrude in studied ambiances. Among the non-catalytic experiments, the reducing atmosphere optimized carbon content (54.3 wt.%) and calorific value (28 MJ/kg) with minimum oxygen amount (27 wt.%) in biocrudes.

Keywords: Hydrothermal liquefaction, algae, red mud, reaction environment, catalyst

3.1 Introduction

Hydrothermal liquefaction (HTL) is a widely studied conversion technology for biomass liquefaction where the conversion of biomass takes place under sub- or super- critical condition of water, acting it as both reactant and catalyst and produces liquid (a.k.a biocrude), aqueous, solid and gaseous products [1]. Algae are a diverse group of aquatic organism, gained worldwide

attention for renewable biofuel production by HTL process as drying stage can be avoided [2]. Therefore, several researchers have explored the HTL technology for various algae conversion. Recently, Jazie et al. have maximized algae (*F. vesiculosus) derived* biocrude oil yield by 27.6%, utilizing 15% of Hβ zeolite catalyst loading with residence time of 20 min and at reaction temperature of 300 °C [3]. Xia et al. produced 10% higher biocrude yield from a co-liquefaction of rice straw and algae (*Nannochloropsis)* using alkali catalyst (K_2CO_3) in glycerol-water solvent compared to pure rice straw feedstock [4]. Norouzi et al. have utilized functionalized graphene oxide/polyurethane composite as catalyst for HTL of *Cladophora glomerata* and effectively repealed the undesired chemicals formation in biocrudes [5]. According to Yu et al., HTL product of polyculture algae could be utilized as fuel (biocrude) as well as hydrocar which can be used as renewable anode material in lithium ion batteries [6]. Guo et al. have showed that the addition of dichloromethane solvent induced about 9 wt.% higher biocrude yields of microalgae *Chlorella vulgaris,* compared to non-solvent separation technique [7]. Biswas et al. have explored the co-hydrothermal liquefaction of Prot lignin and *Sargassum tenerrimum* macroalgae in water, ethanol, and water–ethanol solvent mixture and found 7:3 ratio of lignin:macroalgae feedstock under water–ethanol solvent mixture could maximize the biocrude yield [8]. To reduce the algae production cost, researchers around the world adopted various strategies. Islam et al. increased the fecal sludge portion in co-liquefaction of algae and sludge mixture and noticed that the blend of 25% microalgae: 75% fecal sludge could produce the highest biocrude yield with a lighter hydrocarbon contents[9]. Kim and Lee incorporated a transparent low-density polyethylene film-based floating photobioreactor to culture *Tetraselmis* sp. microalga strain in the ocean [10]. Fon Sing et al. also determined that *Tetraselmis* sp species can maintain high growth rate under various

salinity levels ranging from saline to hypersaline conditions [11]. For low production cost and high growth rate *Tetraselmis* sp. can be a promising algal feedstock for HTL biocrude production.

The HTL derived biocrude using algae has high viscosity, high oxygen and nitrogen, and low heating value. Catalytic HTL treatment is a suitable option to upgrade this product. The bauxite plant residue called red mud (RM), can be used as an inexpensive catalyst by modifying its properties. The heterogeneity of this industrial waste with high iron content can work as a liquefaction catalyst as iron is known to react with hot compressed water or steam and produce in-situ hydrogen to react with the organic fractions of feedstock [12]. Red mud has been employed as catalyst support due to its low cost, strong stability, high surface area, sintering resistance, and resistance to poisoning [13]. In separate studies, Ni-based catalysts supported by Al_2O_3 has been used for hydrotreatment of the algal biocrude oil which removed sulfur, nitrogen and oxygen heteroatoms from oil with increased higher heating value (HHV)[14,15]. Red mud supported nickel (Ni/RM) catalyst successfully utilized for hydrodeoxygenation of pyrolysis oil and hydrogen production by ammonia decomposition [13,16]. Due to the perceived potential of Ni/RM, it is being tested for HTL process as well. The reaction atmosphere is an important operating parameter that can affect the distributions of HTL products. Peng et al. found that under CO,H_2 and N_2 gaseous reaction environments biocrude yield from cornstalk followed this trend: CO > H_2 > N_2 [17]. Wang et al. also used H_2, syngas (H_2: 68.1%, CO: 30.1%, C_1–C_4: 0.9% and CO_2: 0.9%.), Ar and CO gases in HTL conversion of sawdust feedstock and mentioned that H_2 gas generated more biocrude yield than syngas, Ar, and CO [18]. Yang et al. found out that Ni/REHY(REHY, Y zeolite exchanged with rare earth) catalyst achieved further deoxygenation and desulfurization of algae (*Dunaleilla salina)* derived HTL biocrude product under hydrogen

gas [19]. However, understanding the effect of reaction environment over catalytic and non-catalytic HTL conversion of any algal feedstock is still rare.

This work aims to investigate the effect of inert, ethylene, reducing and oxidizing reaction environments over non-catalytic as well as catalytic HTL treatment of "*Tetraselmis sp"* algae strain. Our previous work showed the superiority of ethylene reaction atmosphere with reduced red mud (RRM) catalysts over inert (nitrogen) condition by increased yield and stability of municipal sewage sludge derived HTL biocrude[20]. Current study assesses the influence of four different reaction atmospheres over HTL process of highly productive *Tetraselmis sp*. algae strain with the reduced red mud (RRM) and Ni metal on RM support (Ni/RM) catalysts. The hypothesis of this study is that the RRM and Ni/RM will enhance biocrude yield, carbon recovery from *Tetraselmis* feedstock. It is also expected that the RM catalysts under reducing environment could promote mild hydrogenation of *Tetraselmis* derived biocrude during the HTL reactions and the oxidizing environment may lead to oxidation of reactive functional groups in biocrude. Thus, the goal is to enhance biocrude production from algal feedstock with improved quality, which can be further upgraded via hydrotreatment.

3.2 Materials and methods

3.2.1 Material

Tetraselmis sp. microalga was purchased from Reed Mariculture Inc. (Campbell, California, USA). Red mud (RM) was obtained from Almatis Burnside, Inc. (Gonzales, Louisiana, USA). Airgas Inc. (Opelika, Alabama, USA) supplied high purity nitrogen, ethylene, and a gas mixture of 10% H_2/90%N_2 and 10%O_2/90%N_2 which denoted as reducing and oxidizing reaction ambiance, respectively, in this study. Nickel (II) nitrate hexahydrate (99 wt.% crystalline), was purchased from Sigma–Aldrich (St. Louis, MO, USA) and was used as received.

3.2.2 Feedstock characterization

For feedstock characterization, the algae samples were dried at 105℃ for 24 hours, and a planetary ball mill (MSK-SFM-1S, MTI Corporation, Richmond, California, USA) was used to grind the dried samples for uniform size. The EPA 1684 method was followed to measure the total solid content. The ash content was quantified using ASTM E1755 method. Biochemical composition of *Tetraselmis sp.* strain was provided by the supplier. The elemental analysis (CHNS/O) was performed according to the ASTM D5373-02 method in Vario MICRO cube, Elementar (New York, USA). The higher heating value (HHV) of dried algae samples was determined using a unified correlation (Equation 1) based on elemental analysis, proposed by Channiwala et al.

$$HHV = 0.3491*C+1.1783*H+0.1005*S-0.1034*O-0.015*N-0.0211*A \quad (1)$$

where, C, H, O, N, S and A represents carbon, hydrogen, oxygen, nitrogen, sulfur, and ash contents of material, respectively, expressed in mass percentages on dry basis [21].

3.2.3 Catalyst preparation

The RRM500 catalyst was prepared according to our previous work [20]. The as-received RM was calcined at 575℃ for four hours without any pretreatment and then sieved to obtain the particle size between 106-595 µm. The sieved calcined RM was reduced at 500°C temperature. The reduction temperatures for RM were based on TG-TPR profile. For RM reduction, a gas mixture of 10% H_2 and 90% N_2 was used for six hours at the predetermined temperature. Incipient wetness impregnation method was used to prepare Ni/RM catalysts with nickel nitrate hexahydrate ($Ni(NO_3)_2 \cdot 6H_2O$) salt. The details of Ni/RM catalyst preparation and characterization such as TG-TPR analysis can be found in published document elsewhere [16]. In brief, 20g of calcined RM with 106-595 µm particle size was mixed with 350 mL deionized water. To this slurry, calculated amount of $Ni(NO_3)_2 \cdot 6H_2O$ salt was added to give 10% Ni loading in the final catalyst. The metallic

salts mixed with calcined red mud slurry was stirred at 80℃ for 4 h to obtain a thick mixture. The mixture was then dried at 105℃ overnight to obtain catalyst precursors. The catalyst precursor was calcined for 5 h in air at 620 °C in a muffle furnace (Thermo Scientific, Inc., Waltham, MA, USA). Then, the calcined material was reduced for 6 h at 500 °C using a reducing gas mixture of 10% H_2 and 90% N_2 to obtain the final catalyst.

3.2.4 Catalyst characterization

Inductively coupled plasma-optical emission spectrometry (ICP-OES), X-ray diffraction (XRD) techniques and surface analyzer methods were used to characterize the catalysts. The Soil, Plant, And Water Laboratory (University of Georgia, Athens, USA) performed ICP-OES analysis. XRD analysis was performed by the method discussed in our previous work[22]. Briefly, a bench-top powder X-ray diffraction system (AXRD, Proto Manufacturing, Taylor, Michigan, USA) was utilized from 20° to 100º (2θ) with 2 seconds of dwell time and 0.014° of Δ2Θ at 30 mA and 40 kV with CuKα radiation (λ = 1.5418 Å). An Autosorb-iQ (Quantachrome Instruments, USA) measured specific surface area of the catalysts by BET (Brunauer–Emmett–Teller) equation using N_2-adsorption–desorption isotherm in an adsorption analyzer. The chemisorption macro steps can be found in our previous work [23].

3.2.5 Experimental setup and procedure

A high-pressure, high-temperature reactor from Parr Instrument Company (Model 4578, Moline, Illinois, USA) was used for HTL experiments. The reactor setup was the same as our previous work [20]. The reactor has 1.8 L vessel, PID controlled electrical heating unit, controllable agitator, pressure gauge, and J-type thermocouple to monitor the temperature inside the reactor. For all reaction environments (nitrogen, ethylene, reducing and oxidizing), the HTL experiments were performed at a reaction temperature of 275°C, agitator speed of 550 rpm and a residence time of

60 minutes. For each HTL experiment, 450 g as-received *Tetraselmis sp.* (with 18-19% solid content) was loaded into the reactor. For all catalytic HTL experiments, catalyst:feedstock loading was fixed at 1:10 on basis of solid content of feedstock (i.e., ~8 g catalyst per 450 g as-received feedstock).The reactor was purged with desired gas (nitrogen, ethylene,10%H_2/90%N_2 and 10%O_2/90%N_2) three times to remove air from the reactor headspace before pressurizing with it to an initial pressure of 200 psi (1.38 MPa). The reactor was then heated to the desired temperature at the heating rate of ~3°C/min. After holding the reactor at 275°C temperature for 1 h, the heater was removed, and the reactor was cooled to room temperature by running cold water in the internal cooling coil. The products (gas, solid, aqueous phase, and biocrude) were separated as described in Section 3.2.6. All experiments were performed in duplicates.

3.2.6 Product separation

After cooling down the reactor to room temperature, the gas was vented followed by the gas analysis and the reactor was opened to recover the liquid and solid products. The content in the reactor was poured into a large flask, and the weight was recorded. Then, the reactor content was filtered through Whatman No.50 filter paper (particle filtration size of 2.7 μm) to separate the solid from aqueous phase. Then the remaining solids on the filter paper were washed with methanol (MEOH). The weight of all liquids (aqueous and organic phases) was recorded for mass balance. The MEOH was separated from the biocrude using an IKA rotary evaporator at 85°C and 230 mbar vacuum pressure to obtain MEOH extracted bio-oil, which is termed as “biocrude oil” throughout the paper.

3.2.7 Product analysis

The gas products were analyzed using a micro-GC (Agilent 3000A) as discussed elsewhere [20]. The Agilent 3000 A Micro GC is equipped with three modules: a 10 m Molsieve 5A (MS) column

and two 10 m porous polymer (PPU) columns. Each module had a thermal conductivity detector. The instrument can split the sample into three streams. Each stream would go to one of these modules. MS column was used to analyze hydrogen, methane, and carbon monoxide, while carbon dioxide and ethylene hydrocarbons were analyzed on the PPU columns simultaneously. Argon and helium were used as carrier gases for MS column and PPU column, respectively. The gas composition analysis was performed in triplicates.

The mass of the gaseous product was calculated by using Equation 2

$$W_g = \sum x_i . MW_i . n_{tot} \qquad (2)$$

where W_g is the total mass of gaseous product (g), x_i is the mole fraction of gas i, MW_i is the molecular weight of gas i (g/mole), and n_{tot} is the total number of moles of gas product.

In the case of ethylene, reducing, oxidizing HTL experiments, ethylene (C_2H_4), hydrogen(H_2), oxygen(O_2) consumption was estimated using Equation 3.

$$Gas\ consumption\left(\frac{mole\ of\ gas}{kg\ Algae}\right) = \left(n_{igas} - x_{fgas} . n_{ftot}\right) \times \frac{1}{mass\ of\ algae} \times \frac{1000g}{1kg} \quad (3)$$

where n_{igas} is the initial number of moles of ethylene, hydrogen, or oxygen, x_{fgas} is the final mole fraction of ethylene, hydrogen and oxygen. n_{ftot} is the total number of moles of gas at the end of the experiment [20]. The yield of biocrude and solid product were calculated on dry-ash free basis using Equations 4 and 5, respectively [24]. The remaining product fraction was regarded as "balance" and calculated using Equation 6.

$$Y_{biocrude}(\%) = \frac{w_b}{w_f - w_m - w_a} \times 100 \qquad (4)$$

$$Y_{solid}(\%) = \frac{w_s - w_c}{w_f - w_m - w_a} \times 100 \qquad (5)$$

$$Y_{balance}(\%) = 100 - Y_{biocrude} - Y_{solid} \qquad (6)$$

where w_f is the mass of *Tetraselmis sp.* algae feedstock (g), w_m and w_a are the mass of moisture and ash content of feedstock (g), respectively, w_b is the mass of the biocrude product (g), w_s is the weight of total solid residues (g), and w_c is the weight of catalyst (g).

The elemental analysis was performed on each sample using an elemental analyzer (Vario MICRO, Elementar, New York, USA) according to ASTM D5373-02. Effects and interactions of catalysts and reaction environments on biocrude yield, carbon, sulfur, ash and oxygen content were analyzed by the two-way analysis of variance (ANOVA) at 0.05 significance level followed by Tukey HSD test ,using statistical programming software R [25]. The higher heating value (HHV) of biocrude was determined using Equation 1. The total acid number (TAN) of each sample was determined through titration according to ASTM D664-07 using a Mettler Toledo T50 Titrator. Thermogravimetric analysis (TGA) of biocrude was performed by using a Shimadzu TGA-50 (Shimadzu, Japan) under nitrogen atmosphere (flow rate:20 ml/min) with heating rate of 10 °C/min from room temperature up to 800 °C[26]. The chemical composition of each biocrude sample was subsequently analyzed by Fourier transform infrared (FTIR) and nuclear magnetic resonance (NMR) spectroscopy analyses. The FTIR of biocrudes was performed by using Thermo Nicolet iS10 (Thermo Scientific, Waltham, MA). The samples were analyzed for 34 scans over a range of 400–4000 cm^{-1} wavenumbers. Samples for NMR spectroscopy containing 15mg of oil in 1ml of ethanol-d6 (99.9 atom% D) (Acros organic, Switzerland) were prepared in 5 mm 535-PP NMR tubes (Wilmad-LabGlass, Vineland NJ).^{13}C spectra were collected using a Bruker 500 MHZ spectrometer equipped with a broadband nitrogen-cooled prodigy probe. The spectra were referenced to ethanol-d6 (C_2D_6O, $\delta^{13}C$ = 56.96 and 17.31 ppm) and processed in Bruker Topspin software (4.1.3 version).

The aqueous phase analysis followed the procedure as discussed in the published document elsewhere [20]. Total organic carbon (TOC), total nitrogen (TN) with specific species distribution (ammonium (NH_4^+-N), nitrate (NO_3^--N), organic nitrogen (Org-N)), chemical oxygen demand (COD), and pH, were measured to characterize the aqueous products. The TOC and TN were measured by a TOC/TN analyzer (TOC-L, Shimadzu, Kyoto, Japan). A Prominence Liquid Chromatography (LC) system coupled with a conductivity detector (Shimadzu, Japan) was used to analyze concentrations of ammonium (NH_4^+-N) and nitrate (NO_3^--N) in digestate samples. The detailed procedure can be found elsewhere [27]. Briefly, A Dionex IonPac CS12 column (4 × 250mm, Thermoscience) and a Dionex IonPac AS22 column (4× 250mm) with suppression (Dionex CERS 500 4mm and Dionex AERS 500 4mm, respectively) were used for ion separation. Acidic eluent (20 mM methane sulfonic acid) was used on the CS12 column, and basic eluent (4.5mM sodium carbonate and 1.4mM sodium bicarbonate solution) was used on the AS22 column. The amount of organic nitrogen (Org-N) was calculated by the difference of total nitrogen and inorganic nitrogen (the sum of NH_4^+-N and NO_3^--N). The COD was determined using a COD assay kit (HACH, Loveland, Colorado, USA) and a spectrometer (DR900, HACH, Loveland, Colorado, USA). The detailed procedure can be found in a published document [28]. The pH of the solution was measured using a pH meter (pH510, Oakton, Vernon Hills, Illinois, USA).

3.3 Results and discussion

3.3.1 Feedstock characterization

The physicochemical properties of the chosen algae feedstock (*Tetraselmis Sp.*) were studied by elemental composition analysis (CHNS/O), higher heating value (HHV), ash content and the biochemical composition. The characterization result of *Tetraselmis sp* along with other algae strains on dry basis, is presented in Table 3.1. The carbon content and HHV of *Tetraselmis sp.*

was lower than other strains, which is supported by previous *Tetraselmis* reports [29,30]. The biochemical composition of the algae varied widely with the strain. *Teteraselmis* strain has high protein content similar to *Nannochloropsis* strain[31]. The ash content of *Tetraselmis* sp. was also in agreement with the previous work. The saline growth culture for this algae might be responsible for ash content [29].

Table 3.1: Characterization of *Tetraselmis sp.* feedstock and comparison with other algae strains[31].

	Tetraselmis	*Nannochloropsis*	*Pavlova*	*Isochrysis*
Proximate Analysis [a] (wt.%)				
Moisture	82±1.2	68.88 ± 1.24	75.80 ± 0.42	73.93 ± 1.44
Ash	2.6±0.1	3.42 ± 0.38	3.47 ± 0.33	3.39 ± 0.29
Volatile content	13.2±0.3	22.51 ± 1.28	17.74 ± 0.77	18.20 ± 1.01
Elemental Composition [b] (wt.%)				
C	32.2±0.3	56.83 ± 0.33	54.34 ± 1.36	55.76 ± 1.14
H	5.1±0.2	9.32 ± 0.06	8.69 ± 0.41	8.70 ± 0.34
N	4.4±0.1	10.13 ± 0.06	8.67 ± 0.21	7.96 ± 0.06
S	0.8±0.1	0.37 ± 0.19	0.82 ± 0.09	0.62 ± 0.10
Ash	15±0.2	3.42 ± 0.38	3.47 ± 0.33	3.39 ± 0.29
O [c]	42.4±0.2	19.93 ± 0.26	24.01 ± 2.07	23.57 ± 1.65
H/C ratio	1.9	1.96	1.91	1.87
HHV [b] (MJ/kg)	12.6±0.2	24.02 ± 0.07	22.69 ± 0.07	22.97 ± 0.02
Biochemical Composition [b] (wt.%)				
Protein	63	62.79	46.94	44.36
Lipid	11	18.12	13.88	18.98
Carbohydrate	11	8.92	28	25.46

[a] as received basis, [b] dry basis, [c] by difference

3.3.2 Catalyst characterization

Due to difficulties in separation of catalysts from char, only fresh catalysts were analyzed. Figure 3.1 illustrates the XRD analysis of RRM500 and Ni/RM catalysts. Metal oxides such as gibbsite ($Al(OH)_3$), quartz(SiO_2), hematite(Fe_2O_3), calcite($CaCO_3$), anatase(TiO_2) and magnetite(Fe_3O_4) were detected in these RM based catalysts. Major peaks of iron (hematite, magnetite) were detected by XRD analysis in both catalysts. ICP-OES analysis (Table B1, Appendix B) also determined

significant amount of Fe metal in RRM500 and Ni/RM catalysts where RRM500 contained 11.8% more iron than Ni/RM catalyst. The prominent XRD peak of nickel (Ni) in Ni/RM catalyst indicated the successful incorporation of this transition metal on RM support. 10.5wt.%(104802ppm) of Ni metal was detected by ICP OES analysis in Ni/RM catalyst, which was very close to the desired Ni loading. However, no significant difference was observed in BET surface area (Table B2) of Ni/RM (22.4m^2/g) and RRM (21.9m^2/g) catalysts.

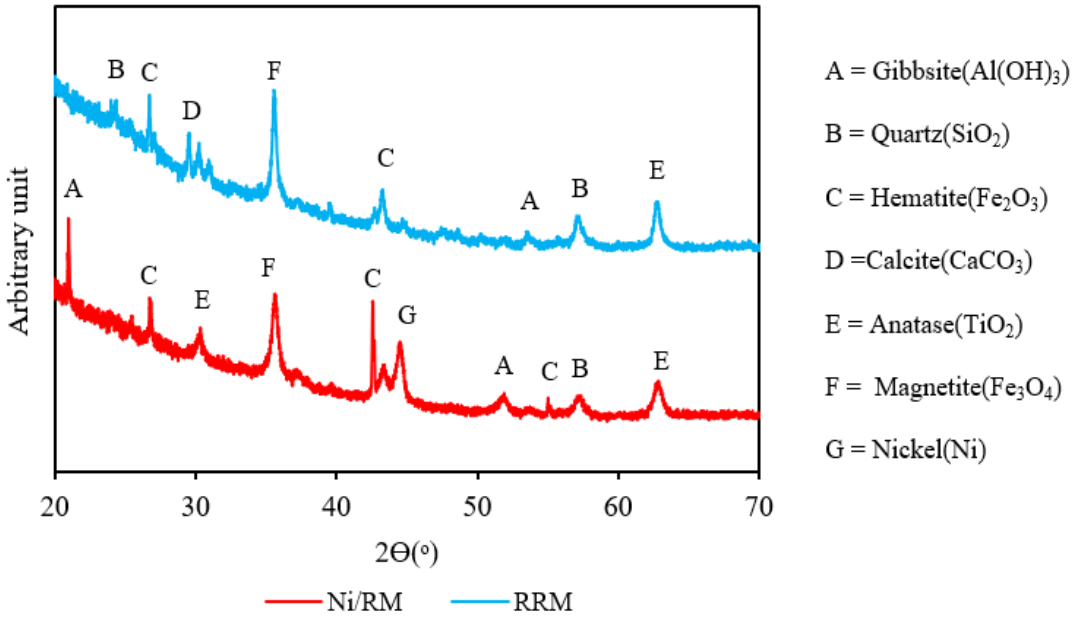

Figure 3.1: XRD pattern of RRM500 and Ni/RM catalysts

3.3.3 HTL products characterization

3.3.3.1 Products yield distribution

Figure 3.2 demonstrated the product distribution (on dry-ash free basis) for catalytic and non-catalytic HTL experiments of *Tetraselmis* under four reaction environments. Without the use of catalyst, the inert(nitrogen) environment generated the highest biocrude yield by 22.8 wt.% where the reducing environment produced the lowest biocrude yield by 17wt.%. The trend of biocrude

yield in non-catalytic reactions under studied reaction environments was as followed: nitrogen> oxidizing> ethylene>reducing. The biocrude yield of this study was lower compared to other *Tetraselmis* HTL biocrude studies where biocrude products were extracted by dichloromethane(DCM) solvent[29,32]. The increased biocrude yield by DCM solvent from *Chlorella vulgaris* microalgae and municipal sewage sludge feedstock was observed in previous HTL works [7,33]. The use of MEOH instead of DCM, for biocrude separation might be a reason to obtain lower yield from *Tetraselmis* feedstock in the current work. Incorporation of catalyst has increased the biocrude yield in inert, ethylene and reducing ambiances. Except oxidizing environment, biocrude yield enhanced by the following trend: no catalyst<RRM500<Ni/RM. The influence of catalysts over biocrude yield was found statistically significant (d.f.=2, F=32.9, p=0.000) but there was no interaction between the environment and catalysts (TableB3). The Ni/RM catalyst successfully maximized the biocrude yield up to 37.4 wt.% in ethylene environment which closely matched with *Tetraselmis* biocrude yield from HTL study by Pacific Northwest National Laboratory , at higher temperature (350℃) in inert environment [34]. According to Wang et al., Ni catalyst ($Ni/SiO_2{-}Al_2O_3$) is able to reduce the activation energy for algae building blocks (protein and carbohydrate) conversion which could generate more biocrude with higher nitrogen and oxygen content [35]. In this study, the elemental analysis (Table 3.2) of biocrude showed that Ni/RM catalyst has increased the nitrogen content of biocrude irrespective of reaction environment. This finding suggested that Ni/RM catalyst might facilitate the higher conversion of protein from *Tetrsaselmis* during HTL process comparing to noncatalytic or RRM500 reactions in all four reaction ambiances. In addition, the Ni/RM catalyst appeared to catalyze deoxygenation reaction under reactive ambiances (ethylene, reducing, and oxidizing environments). The reducing reaction environment and Ni/RM catalyst combination produced

almost 91% more biocrude products comparing to non-catalytic reaction in reducing environment. The hydrogenation ability of hydrogen gas could be a reason for higher feedstock conversion during HTL process [18]. In oxidizing reaction ambiance, the biocrude yield was also increased by the catalysts compared to non-catalytic condition. Unlike other three reaction conditions, RRM500 catalyst promoted more biocrude production than Ni/RM one under oxidizing environment.

The solid residue increased with catalyst regardless of the reaction environment. Except oxidizing environment, the solid residue increasing trend as followed: no catalyst<RRM500<Ni/RM. The oxidizing environment increased the solid residue in both catalytic and non-catalytic reactions compared to other three reaction environments. The oxidizing atmosphere might promote oxidation of feedstock in HTL condition and raised the char yield. The RRM500 catalyst under oxidizing environment produced the highest solid residue by 24 wt.% whereas the lowest solid residue (14wt.%) was found from no catalyst-reducing environment combination. The addition of Ni/RM catalyst led to 46% more solid residue production than non-catalytic reaction under reducing ambiance.

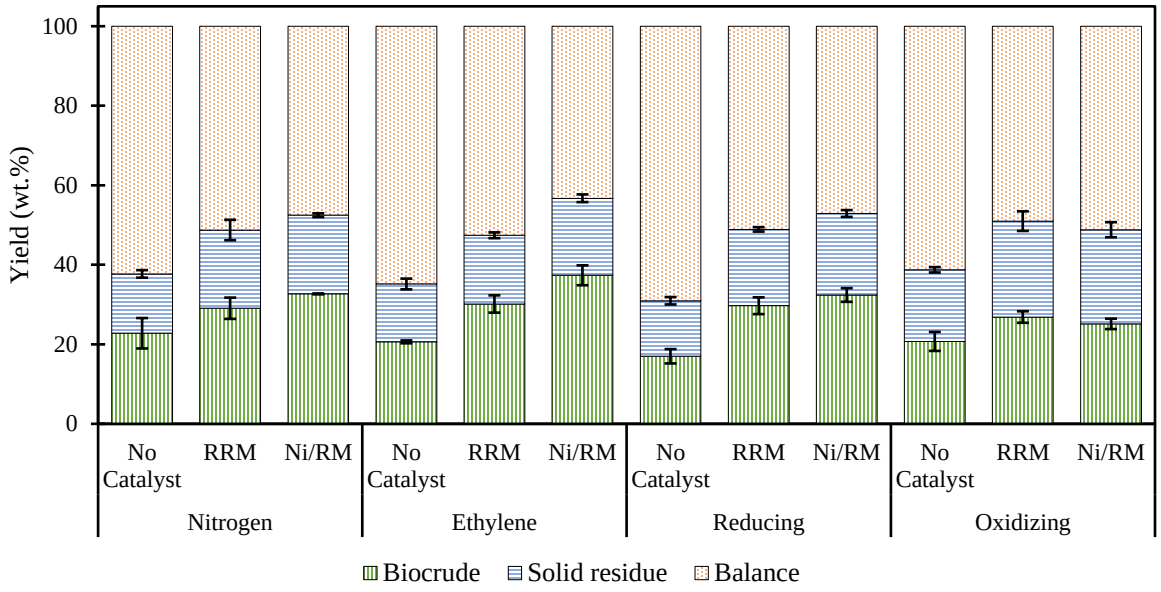

Figure 3.2: Yield distribution of *Tetraselmis sp.* (on dry-ash free basis) under different reaction environments and catalysts.

3.3.3.2 Biocrude characterization

Physicochemical properties

Table 3.2 has showed the physicochemical properties of HTL biocrude from *Tetraselmis* algal feedstock. Among non-catalytic reactions, the reducing environment has maximized the carbon content with 54±1.0 wt.% and subsequently minimized the oxygen content (27.4±0.9wt.%). This result suggested that the reducing environment performed deoxygenation reaction without catalyst during HTL process. The ash and sulfur contents were also lowered by reducing ambiance in non-catalytic reaction. Therefore, the HHV of the same biocrude subsequently increased by 10.67% compared to inert-no catalyst reaction derived biocrude. The hydrogen and nitrogen percentages in biocrudes remained almost the same in non-catalytic reactions under four reaction environments. Among catalytic and non-catalytic reactions, the inert environment-no catalyst combination generated highest ash (6 wt.%), oxygen percentage (32.3 wt.%) with the lowest

carbon content of 47.9 wt.% in biocrude, which ultimately led to the minimum HHV of 25.4 MJ/kg. Ethylene reaction atmosphere reduced acidity (TAN) by 15-39% in non-catalytic biocrude compared to other non-catalytic experiments.

Prominent catalytic effects were observed in carbon, ash, sulfur, oxygen content and HHV of the biocrudes in all studied environments. Irrespective of reaction environments, both RRM500 and Ni/RM catalyst increased carbon and nitrogen percentage with reduced ash content in biocrudes compared to non-catalytic reactions. As a result, the oxygen percentage was lowered in catalyst derived biocrudes with higher HHV. The interaction of reaction environment and catalyst over the carbon (d.f.=6,F=41.9,p=0.000), ash (d.f.=6,F=28.2,p=0.000) and oxygen(d.f.=6,F=12.7,p=0.000) content of biocrude were statistically significant. The RRM500 catalyst in inert and reducing environments and Ni/RM catalyst in oxidizing environments were successful to maximize carbon percentage in *Tetraselmis* biocrude by 61 wt.% and 60.2 wt.%, respectively. Increased carbon percentage was also found in HTL conversion of *Nannochloropsis salina* (*N. salina*) with Ni–Mo/Al_2O_3 catalyst under H_2 reaction ambiance [36]. However, the catalytic HTL reactions raised the nitrogen content of the biocrudes. As discussed earlier (section 3.3.3.1), the catalyst probably converted more protein compounds compared to non-catalytic reactions and increased the nitrogen content of the biocrudes. Incorporation of Ni metal on RM support has clearly favored deoxygenation reaction. The oxygen removal by Ni/RM followed this trend: inert<ethylene<reducing<oxidizing reaction environment. The low (1.35wt.%) oxygen content in hydrotreated pyrolysis oil from pinyon-juniper was observed by Ni/RM catalyst at high pressure hydrogen (6.2 MPa initial pressure)[37]. In this study, the Ni/RM catalyst under reducing environment lowered oxygen percentage of biocrude by 24% compared to the Ni/RM-inert reactions under lower hydrogen pressure (1.37 MPa initial pressure). This finding suggested that

Ni/RM catalyst might perform mild hydrodeoxygenation at lower hydrogen pressure of HTL process. Addition of Ni/RM catalyst also reduced the sulfur content of the biocrudes by 33-66% compared to non-catalytic and RRM500 catalytic reactions in four ambiances. This desulfurization of the biocrudes might occur due to the adsorption ability of Ni/RM catalyst [38]. The sulfur removal from biocrudes by catalyst found to be statistically significant (d.f.=2, F=8.3,p=0.005) without any interaction between environment and catalyst(Table B3).

The catalytic reactions increased TAN of *Tetraselmis* biocrude in all reaction environments, except inert atmosphere. Higher TAN was reported in HTL conversion of *Nannochloropsis* by Ni/TiO_2 catalyst in inert atmosphere. Most probably, Ni/TiO_2 catalyst promoted the hydrolysis of protein and lipids from algae in HTL process which generated more TAN increasing compounds such as carboxyl group enriched fatty acid, carboxylates, amino acid or phenolic compounds from amino acid conversion [35]. However, Ni/RM-inert reaction generated minimum acidity in the biocrude of this study. The presence of TiO_2 with other metal oxides of $Al(OH)_3$, SiO_2,Fe_2O_3,$CaCO_3$, and Fe_3O_4 in Ni/RM catalyst, was confirmed by XRD analysis (Figure 3.1). Most probably the mixed metal oxides of RM support affected the Ni/RM catalytic activity and suppressed the generation of TAN increasing compounds in *Tetraselmis* biocrude. From ICP analysis, RRM500 catalysts found to be more effective than Ni/RM catalyst, to suppress the migration of heavy metals such as copper (Cu) and zinc (Zn) and phosphorus (P) compounds to biocrudes irrespective of reaction environments. It is well established that treated or untreated RM can absorb heavy metals and phosphate from soil and water [39]. However, the effect of RM-based catalyst on metal content of HTL biocrude was rarely investigated. The lowest Cu (0.49 ppm) and Zn (<2.50 ppm) contents were observed in biocrude from RRM500-reducing reaction environment. However, the minimum values of Cu, Zn or P from *Tetraselmis* biocrude were

higher than conventional petroleum crude oil [40,41]. Significant leaching of iron (Fe) took place in catalytic reactions derived biocrude. The introduction of Ni metal on RM support also increased the Ni content in the biocrudes regardless of the reaction atmospheres. Under oxidizing environment, RRM500 catalyst reduced the iron migration to biocrude by 8-62% compared to other reaction conditions. The ethylene environment was successful to repeal the Ni leaching from Ni/RM catalyst to biocrude products by 30-74% compared to other three reaction environments.

Table 3.2: Physicochemical properties of *Tetraselmis* HTL biocrude

	Nitrogen			Ethylene			Reducing			Oxidizing		
	No Catalyst	RRM500	Ni/RM	No Catalyst	RRM500	Ni/RM	No Catalyst	RRM500	Ni/RM	No Catalyst	RRM500	Ni/RM
Elemental Composition [a](wt.%)												
C	47.9±0.6	61.0±0.1	53.9±0.5	48.9±0.2	57.0±0.3	58.2±0.3	54.3±1.0	61.0±0.1	59.3±0.3	52.5±0.3	54.6±0.6	60.2±0.3
H	10.3±0.4	10.6±0.2	10.2±0.1	10.4±0.2	10.6±0.1	10.5±0.3	10.2±0.5	10.9±0.1	11.2±0.1	10.1±0.6	10.4±0.1	9.5±0.8
N	3.1±0.1	4.4±0.1	4.0±0.1	3.1±0.1	4.1±0.1	4.2±0.1	3.5±0.1	4.5±0.1	4.5±0.1	3.5±0.1	3.9±0.1	4.4±0.1
S	0.4±0.1	0.5±0.1	0.2±0.1	0.5±0.1	0.6±0.1	0.2±0.1	0.3±0.2	0.4±0.1	0.2±0.1	0.5±0.3	0.6±0.1	0.3±0.1
Ash	6.0±0.1	4.9±0.1	4.5±0.0	5.3±0.1	3.8±0.0	4.4±0.2	4.4±0.1	3.9±0.1	2.9±0.1	5.6±0.0	3.4±0.1	4.5±0.0
O[b]	32.3±1.3	18.8±0.4	27.2±0.7	31.8±0.6	23.9±0.3	22.5±0.8	27.2±1.9	19.4±0.3	21.9±0.7	27.7±1.2	27.1±0.9	21.2±1.1
HHV (MJ/kg)	25.4±0.8	31.7±0.3	27.9±0.3	26.0±0.3	29.8±0.2	30.3±0.6	28.0±1.1	32.1±0.2	31.5±0.4	27.3±0.9	28.4±0.4	29.9±1.1
TAN (mgKOH/g)	21.9±0.1	27.3±1.0	14.0±01	18.9±0.4	24.6±0.3	27.5±0.3	26.3±0.1	28.5±0.1	28.3±0.4	24.4±1.8	27.1±0.2	30.0±0.8
Heavy Metal and Phosphorus (ppm)												
Co	37.91	44.29	16.71	40.31	64.96	57.1	22.40	22.12	71.19	20.64	50.11	52.59
Cr	1.34	1.54	0.97	<1.47	0.44	0.55	<0.90	<3.66	2.71	0.20	1.85	1.409
Cu	13.06	4.02	8.73	<0.50	<0.50	13.38	4.03	0.49	4.69	<0.50	<0.50	14.63
Fe	1075.02	2788.08	3173.14	1145.24	3408.60	3253.54	854.05	2405.33	1518.86	588.35	1050.53	2233.65
Mn	<2.50	<2.50	<2.50	<5.00	<5.00	<2.50	<5.00	<5.00	5.60	9.60	<5.00	<2.50
Ni	280.50	15.48	1448.69	12.67	87.39	1113.24	8.06	6.83	1938.18	16.53	16.11	1540.07
P	37.52	9.62	32.00	42.97	6.14	9.30	160.44	34.93	535.39	25.47	2.48	8.71
Zn	13.49	5.873	12.24	<2.50	<2.50	8.87	13.99	<2.50	8.96	9.91	<2.50	9.76

[a] dry basis, [b] by difference

Thermogravimetric analysis

Figure 3.3 presents the thermogravimetric analysis of biocrude products from catalytic and non-catalytic HTL conversion of *Tetraselmis* feedstock under nitrogen, ethylene, reducing and oxidizing reaction environments. Based on decomposition patterns, the TGA thermograms of the biocrudes were divided into three regions: 100-300°C (referred to as light fraction), 300-550°C

(medium fraction), and 550-800°C (heavy fraction). The biocrude products of this work contained 32-38wt.% light fraction, 28-36 wt.% medium fraction and 13-22 wt.% of heavy fraction. Among all non-catalytic reactions, the reducing environment generated 1.2-9.2% higher light fraction in biocrude. Regardless of the reaction environment, incorporation of catalysts increased the decline of biocrude weight percentage or mass loss in both medium and heavy fraction regions of the TGA graphs compared to non-catalytic reactions. The lowest heavy fraction was found in biocrude sample from non-catalytic reaction under oxidizing ambiance. The Ni/RM catalyst increased the mass loss in heavy fraction region by 90% compared to non-catalytic reaction in oxidizing environment. The heavy fraction decomposition in oxidizing environment showed following trend: No Catalyst < RRM500 <Ni/RM. At 130°C, the biocrude mass loss in oxidizing environment exhibited following trend: No Catalyst>RRM500>Ni/RM. This finding suggested that non-catalytic reaction under oxidizing environment might favor gasoline range products in *Tetraselmis* biocrude. The Ni/RM-reducing environment combination decreased heavy fraction of biocrude by 30.8-12.4% compared to other three reaction ambiances with same catalyst.

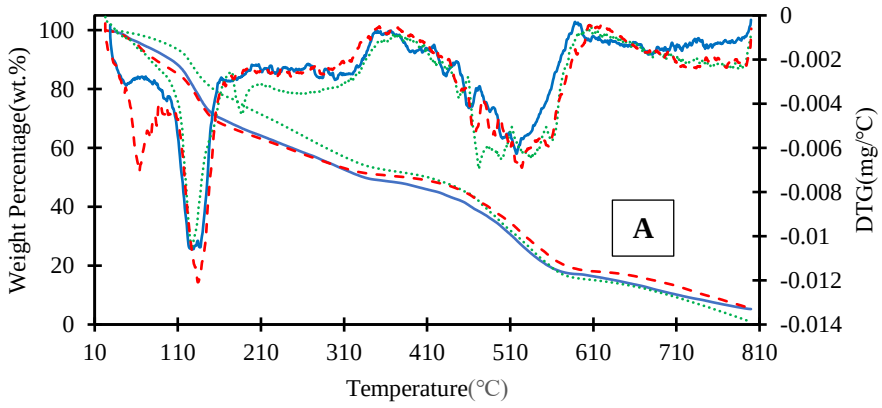

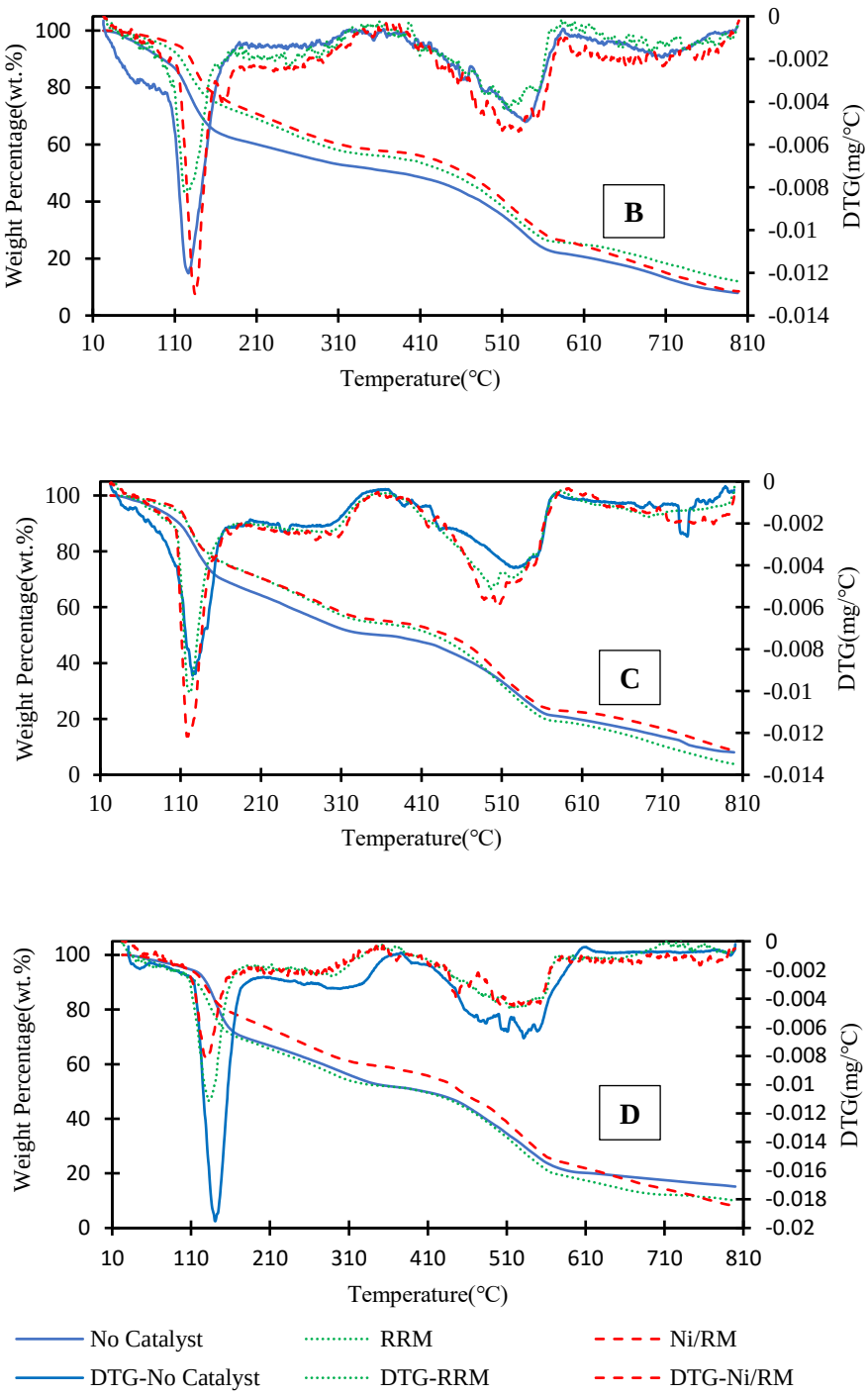

Figure 3.3: Thermogravimetric analysis of biocrude samples from non-catalytic and catalytic reactions: A-Nitrogen, B-Ethylene, C-Reducing and D-Oxidizing reaction environments.

FTIR analysis

FTIR spectra of *Tetraselmis* biocrude are presented in Figure 3.4. The non-catalytic reactions derived biocrude spectra are compared in Figure 3.4A; the effect of RRM500 and Ni/RM catalysts under inert ambiance are shown in Figure 3.4B whereas Figure 3.4C has compared the biocrude spectra of non-catalytic, RRM500 and Ni/RM catalyst under reducing environment.

In Figure 3.4A, reducing environment without catalyst showed higher intensity in four regions of hydroxyl and phenolic groups (3050-3700cm^{-1}), methylene groups (2800-3000cm^{-1}) and in bands of 1300-1750cm^{-1} compared to other three reaction ambiances. The sharp peaks of 2800–3000 cm^{-1} band under reducing environment suggested strong presence of C-H stretching in biocrude [42]. The increased peak in 3050-3700cm^{-1} region under reducing environment might appear due to high biocrude TAN value as oxygen content was lower in biocrude[35]. Variation in location of 980-1080cm^{-1} might cause by lowest aliphatic esters by the oxidizing environment where reducing environment has generated the maximum amount.

From Figure 3.4B, the reduction in peak of 3050-3700cm^{-1}, might took place due to the decline of -OH group as minimum oxygen content was reported (Table 3.2) from RRM500 catalyst under inert environment. Both RRM500 and Ni/RM increased methylene groups (2800-3000cm^{-1}) and the bands of 980-1080cm^{-1} and 1300-1750cm^{-1} which suggested that catalysts might promote nitrogen heteroatom under inert condition which was consistent with the increasing nitrogen content (Table 3.2) of the catalytic biocrudes [42].

In Figure 3.4C, lower intensity in 3050-3700cm^{-1} area suggested that RRM500 and Ni/RM catalysts effectively reduced -OH group in reducing environment. This finding was also supported by the elemental analysis of the biocrude products where oxygen content of RRM500 catalytic

reactions derived biocrude under reducing environment was lower compared to no catalyst and Ni/RM conditions.

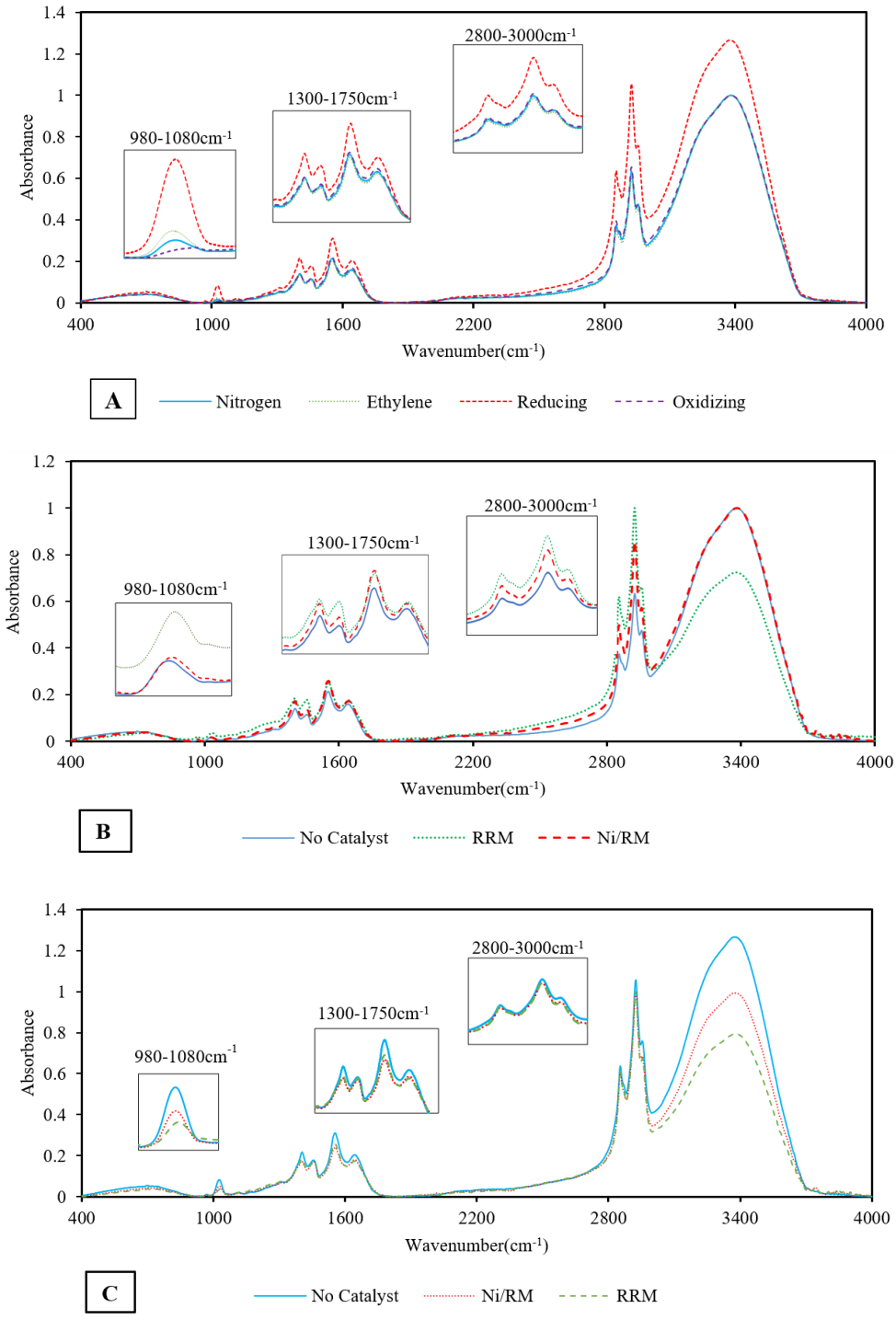

Figure 3.4: FTIR spectra of *Tetraselmis* biocrudes, A- non-catalytic reactions, B- reactions under nitrogen environment, C- reactions under reducing environment

NMR analysis

Figure 3.5 illustrated the functional groups of *Tetraselmis* biocrudes generated under four reaction atmospheres from three different catalytic conditions, by semi-quantitative integration of ^{13}C NMR spectra. The aliphatic groups found (such as methyl and methylene carbon atoms) within 0–28 ppm was assigned to saturated aliphatic groups where 28-55 ppm region was attributed to unsaturated aliphatic groups (separated from oxygen atoms by at least two bonds). The region of 55-95 ppm was designated to alcohols, esters, and anhydrous carbohydrates [43]. The reaction atmosphere significantly affected saturated aliphatic groups of biocrudes. The ethylene environment with Ni/RM catalyst has produced the highest saturated aliphatic groups percentage. The incorporation of catalyst has generated more saturated aliphatic compounds compared to non-catalytic reaction under reducing environment. This result suggested that both the RRM500 and Ni/RM catalyst have performed hydrogenation of unsaturated carbon in biocrude during HTL process under reducing environment [43]. According to absolute integral value (Table B5), Ni/RM catalyst produced 33% more saturated aliphatic groups in biocrudes than RRM500 catalyst under reducing ambiance. This finding agreed with the previous hydrodeoxygenation study by Ni/RM catalyst where incorporation of Ni metal increased the saturated aliphatic compounds in upgraded pinyon-juniper catalytic pyrolysis oil [37].The maximum alcohols, esters, and anhydrous carbohydrates were observed in the biocrudes from reducing-RRM500 condition. This result agreed with aliphatic ester region of FTIR biocrude spectra from the same reaction condition. The Ni/RM catalyst repealed the aliphatic groups with oxygen, compared to RRM500 catalyst under reducing environment which can be considered as the catalytic activity of Ni/RM catalyst [37]. The alcohols, esters, and anhydrous carbohydrates groups content were lower in all catalytic conditions under oxidizing environment compared to other three reaction environments. This

finding agreed with the aliphatic ester region (980-1080cm^{-1}) of oxidizing environment (Figure 3.4A) where the oxidizing environment showed the minimum aliphatic esters peak in non-catalytic biocrude spectra.

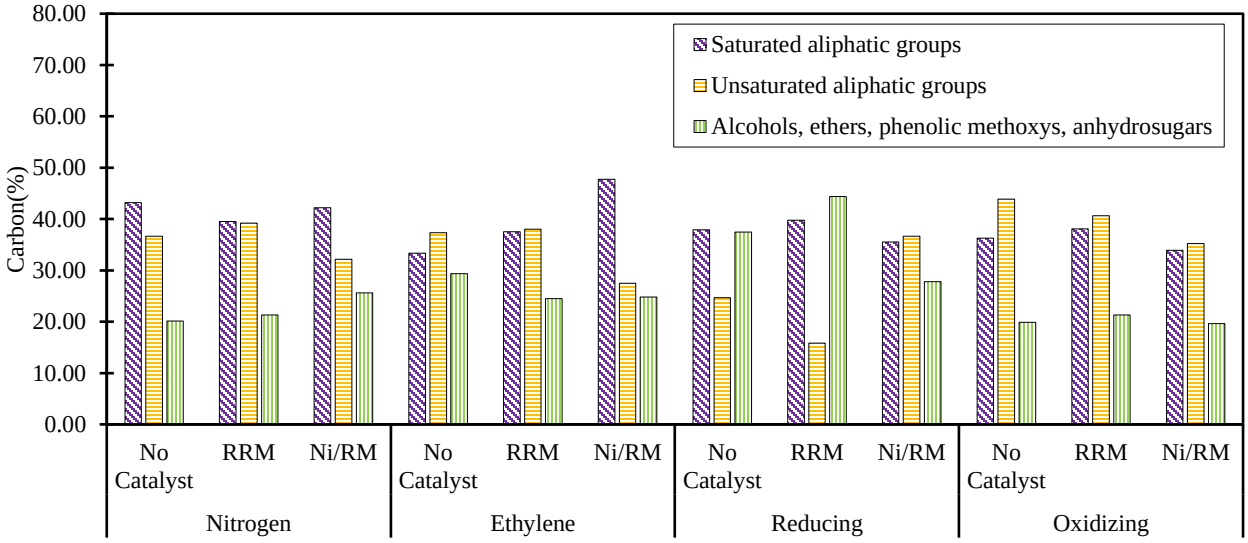

Figure 3.5: Functional group distribution in ^{13}C NMR analysis of *Tetraselmis* biocrudes

3.3.3.3 Analysis of byproducts

Table 3.3 presents the analysis of three HTL byproducts: aqueous phase, solid residue, and gaseous phase. The aqueous phase was characterized by TOC, TN with NH_4^+-N, NO_3^--N, COD, and pH. Among the non-catalytic reactions, the reducing environment has maximized TOC of aqueous phase where the minimum was found in inert environment. This result suggested that the reducing ambiance in the absence of catalyst, has solubilized some organic compounds into the aqueous phase. The addition of catalysts increased TOC value in the aqueous products. The highest TOC (16.41g/L) was observed in the aqueous phase produced from oxidizing-Ni/RM reaction. Since pH of aqueous phase was not in acidic side for oxidizing-Ni/RM condition, the TOC increase was

probably due to the formation of more hydroxyl groups from alcohols and low molecular weight phenolics. Almost 70% of TN was occupied by Org-N. The majority of Org-N in TN could be the confirmation of protein decomposition as the nitrogen source in aqueous phase [44]. Incorporation of catalysts increased the NH_4^+-N content of the aqueous products and highest amount was detected in oxidizing-RRM500 reaction. Both RRM500 and Ni/RM catalysts increased COD of the aqueous phases irrespective of reaction environments which indicated the negative effects of catalysts over aqueous phase treatment for reuse. The highest COD was observed in the aqueous product of reducing-Ni/RM reactions. The Ni/RM catalyst under reducing environment also reduced the pH value of the aqueous byproduct by 2-7% compared to other reactions of this study.

The solid residues of this study were analyzed by elemental composition and the analysis results were presented as catalyst free basis.The addition of catalyst clearly decreased the carbon content of solid chars compared to non-catalytic reaction. The carbon percentage of the char showed the opposite trend of biocrudes: Ni/RM<RRM500<No Catalyst. It suggested that catalysts transferred the carbon from feedstock to biocrude rather than solid char. The lowered nitrogen content in catalyst derived solid char was the result of enhanced nitrogen content of biocrude and aqueous phase. Regardless of reaction environment, increased oxygen and sulfur was found in the solid residues of catalytic reactions which indicated that the RM based catalysts assisted the migration of oxygen and sulfur-based compounds from *Tetraselmis* feedstock to char by HTL treatment in inert, ethylene, reducing and oxidizing reaction environments. The catalysts also increased ash in the char under four reaction atmospheres. The similar phenomenon was observed in sewage sludge HTL study with reduced red mud catalysts under nitrogen and ethylene atmospheres[20].

The gas phase analysis only quantified H_2, CH_4, CO and CO_2 gases. The RRM500 catalyst has promoted in-situ hydrogen production in nitrogen, ethylene and oxidizing ambiances. The hydrogen production maximized under ethylene environment by 1.3-7 mol%. The reaction ambiance consumption was significantly high with Ni/RM catalyst in ethylene and hydrogen reaction atmospheres. Addition of catalysts suppressed the CO_2 production for all four reaction atmospheres. The maximum CO_2 production was observed from non-catalytic oxidizing environment which suggested that the decarboxylation is a dominant pathway in this condition.

Table 3.3: Properties of *Tetraselmis* HTL byproducts

	Nitrogen			Ethylene			Reducing			Oxidizing		
	No Catalyst	RRM500	Ni/RM	No Catalyst	RRM500	Ni/RM	No Catalyst	RRM500	Ni/RM	No Catalyst	RRM500	Ni/RM
Aqueous phase(g/L)												
TOC	11.42	13.19	13.65	12.53	13.98	13.79	12.65	13.26	15.80	12.06	13.95	16.41
$NH4^+$-N	2.87	4.00	3.92	2.71	3.74	2.83	3.13	3.15	4.02	3.00	4.20	3.64
NO_3^--N	0.02	0.06	0.02	0.01	0.02	0.05	0.03	0.02	0.06	0.02	0.05	0.06
Org-N[a]	7.41	7.24	7.12	7.54	7.62	7.83	7.52	7.37	6.68	6.98	7.19	7.86
TN	10.30	11.30	11.06	10.26	11.38	10.71	10.68	10.54	10.76	10.00	11.44	11.56
COD	86±0.3	99.6±0.0	89.2±0.1	87.6±0.1	110.0±0.1	96.4±3.6	89.9±0.2	101.1±0.8	119.1±0.2	91.2±0.3	103±0.2	107.6±0.1
pH	8.3±0.6	8.6±0.1	8.4±0.3	8.7±0.1	8.3±0.5	8.7±0.2	8.3±0.2	8.5±0.1	7.9±0.1	8.2±0.2	8.1±0.1	8.2±0.3
Solid Residue (wt.%)												
C	34.2±2.3	25.1±0.1	21.1±1.4	36.9±0.1	18.3±1.0	22.5±0.1	28.9±0.9	20.7±0.3	18.0±0.2	37.4±1.6	24.9±1.4	24.7±0.1
H	4.8±0.1	2.7±0.1	2.5±0.2	4.4±0.1	2.1±0.2	2.4±0.1	3.4±0.2	1.9±1.4	2.7±0.1	3.5±0.6	3.4±0.3	3.2±0.1
N	2.3±0.2	1.6±0.1	1.4±0.1	2.2±0.1	1.3±0.1	1.5±0.4	1.9±0.1	1.4±0.1	1.2±0.1	2.8±0.1	1.8±0.2	1.8±0.1
S	0.3±0.1	0.5±0.1	1.2±0.1	0.4±0.2	0.4±0.1	1.2±0.1	0.3±0.1	0.4±0.1	1.4±0.1	0.3±0.1	0.4±0.1	0.8±0.2
Ash	55.4±0.1	58.1±0.2	64.3±0.1	55.3±0.3	68.5±0.2	62.9±0.4	59.6±0.2	57.2±0.1	70.5±0.1	46.7±0.1	47.8±0.2	56.9±0.3
O[a]	3.1±2.8	12.0±0.4	9.5±1.8	0.9±0.7	9.4±1.5	9.6±0.9	5.9±1.3	18.4±1.8	6.1±0.4	9.4±2.4	21.8±2.1	12.6±0.8
Gas Phase (mol%)												
H_2	1.5±0.0	6.1±0.2	4.8±0.1	1.1±0.0	8.0±0.1	6.7±0.1		Consumed		1.0±0.1	3.9±0.2	2.5±0.1
CH_4	0.1±0.0	1.5±0.1	0.1±0.0	0.1±0.0	1.4±0.1	3.0±0.1	0.1±0.0	1.1±0.1	0.1±0.0	0.1±0.0	0.7±0.1	0.1±0.0
CO	3.2±0.1	0.8±0.1	4.8±0.1	2.2±0.0	2.5±0.1	0.1±0.0	3.1±0.1	2.4±0.1	8.4±0.1	1.7±0.0	3.8±0.2	2.9±0.0
CO_2	80.8±0.9	62.1±0.1	65.8±0.3	72.7±1.2	41.0±1.6	58.7±0.1	82.8±0.8	67.5±0.6	69.8±0.2	85.1±1.5	52.9±0.5	72.7±0.1
Balance[a]	14.4±0.9	29.4±0.3	24.6±0.3	23.9±1.3	47.1±1.5	31.5±0.1	14.0±0.7	29.1±0.8	21.8±0.1	12.2±1.5	38.1±1.0	21.7±0.1
Consumption (mol/kg feedstock)	0	0	0	0.11±0.02	0.72±0.2	1.48±0.4	0.01±0.0	0.04±0.01	1.52±0.3	1.22±0.1	1.07±0.2	1.23±0.4

[a] by difference

3.3.4 Carbon and nitrogen distribution

Carbon distribution in the *Tetraselmis* HTL products is illustrated in Figure 3.6-A. The carbon recovery was calculated based on the elemental analysis of *Tetraselmis* feedstock, biocrude, solid residue and total organic carbon (TOC) content of the aqueous phase. The carbon addition to the HTL system by ethylene atmosphere was calculated using the ethylene consumption rate from Table 3. The carbon mostly transferred from feedstock to biocrude products and carbon transfer was increased by catalytic reactions. The elemental analysis (Table 3.2) of the biocrudes and carbon distribution showed the identical carbon transfer trend: No Catalyst<RRM500<Ni/RM. The carbon recovery in biocrudes were comparatively lower in oxidizing atmosphere. Therefore, the carbon transfer to solid residue and aqueous phase was increased by oxidizing environment. Significant carbon transfer to balance (gas phase) portion in non-catalytic reactions of inert, ethylene and reducing reaction environments was supported by increased CO_2 production from non-catalytic reactions (Table 3.3).

Nitrogen distribution of *Tetraselmis* HTL products was presented in Figure 3.6-B. The N distribution was calculated based on nitrogen content of feedstock, biocrude, solid residue from elemental analysis and TN value of aqueous phase. Almost 64-73% of the N ended up in the aqueous phase whereas 9-25% transferred to the biocrude. There was an unwanted rise of N transfer in biocrude and aqueous phase. It was evident that the addition of catalysts promoted higher decomposition of the protein rich *Tetraselmis* feedstock during HTL process and the produced nitrogenated compounds distributed among the HTL products. The higher nitrogen content of biocrudes indicated that further upgrading process was required to use it as transportation fuel [45].

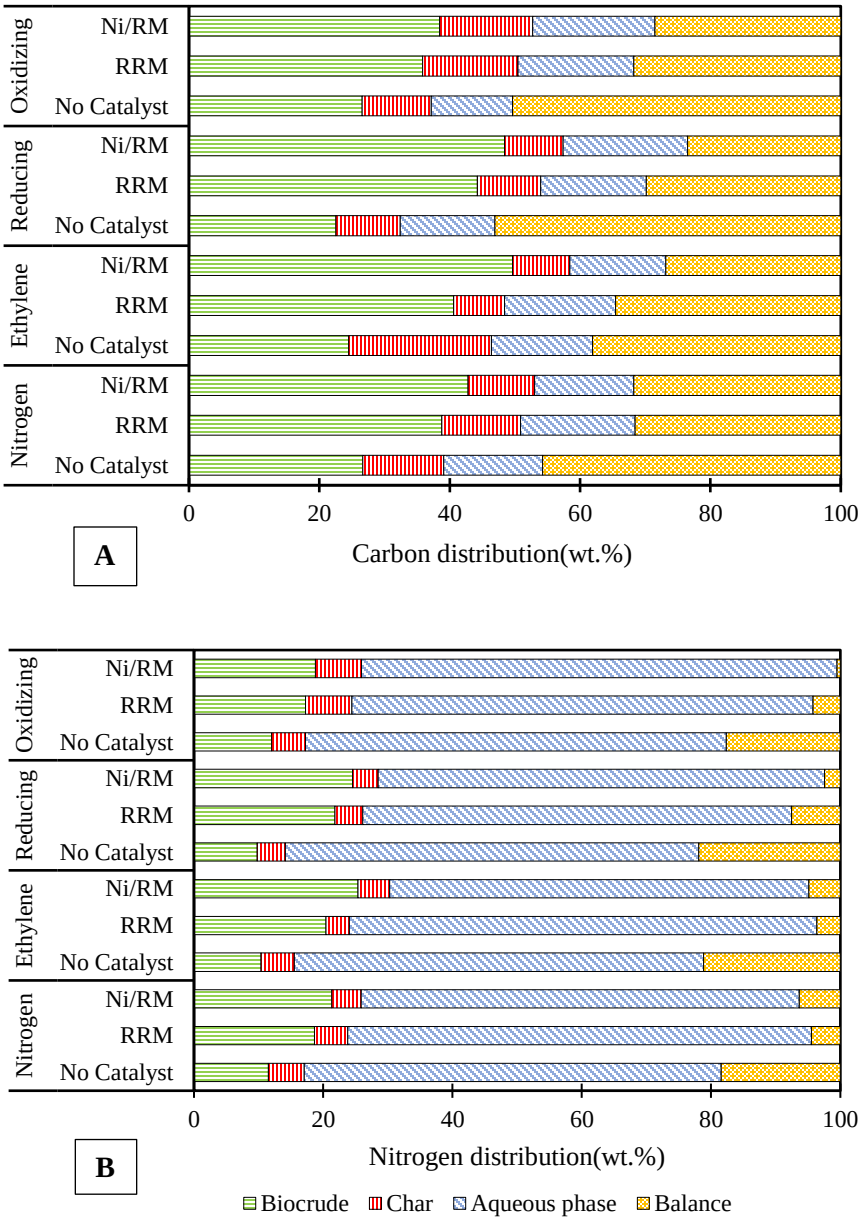

Figure 3.6: Carbon and nitrogen distribution in HTL products, A-Carbon distribution, and B- Nitrogen distribution

3.4 Conclusions

The red mud (RM) based catalysts, reduced red mud (RRM500) and red mud supported nickel (Ni/RM), were applied to hydrothermal liquefaction (HTL) of *Tetraselmis sp.* algae strain under nitrogen, ethylene, reducing and oxidizing reaction environments. Regardless of reaction environments, the use of catalysts has increased the yield of *Tetraselmis* derived biocrude. Under nitrogen, ethylene and reducing environment, the biocrude yield increased by following trend: No Catalyst<RRM500<Ni/RM. The highest biocrude yield of 37 wt.% was produced under ethylene environment with Ni/RM catalyst. Both RRM500 and Ni/RM catalysts promoted deoxygenation, reaction with increased the carbon content and calorific value for the biocrude products in four reaction atmospheres. The Ni/RM catalyst under inert environment reduced biocrude acidity by 20-50% compared to other reaction conditions. The desulfurization activity of Ni/RM catalysts and demetallization effect of RRM500 catalyst were observed in all biocrude products, irrespective of reaction environments. Major portion of nitrogen migrated to aqueous phase from protein enriched *Tetraselmis* feedstock after HTL treatment where most of the carbon ended up in the biocrudes. The reducing environment facilitated mild hydrotreatment during HTL reaction in presence of both RRM500 and Ni/RM catalysts. Among the non-catalytic HTL reactions, inert environment maximized biocrude production from *Tetraslmis* feedstock, ethylene environment lowered total acid number (TAN) of the biocrudes and reducing environment added maximum carbon and minimum oxygen and sulfur content to *Tetraselmis* biocrude.

3.5 References

[1] A.A. Peterson, F. Vogel, R.P. Lachance, M. Fröling, J. Michael J. Antal, J.W. Tester, Thermochemical biofuel production in hydrothermal media: A review of sub- and supercritical water technologies, Energy Environ. Sci. 1 (2008) 32–65. https://doi.org/10.1039/B810100K.

[2] J. Watson, T. Wang, B. Si, W.-T. Chen, A. Aierzhati, Y. Zhang, Valorization of hydrothermal liquefaction aqueous phase: pathways towards commercial viability, Progress in Energy and Combustion Science. 77 (2020) 100819. https://doi.org/10.1016/j.pecs.2019.100819.

[3] A.A. Jazie, J. Haydary, S.A. Abed, M.F. Al-Dawody, Hydrothermal liquefaction of *Fucus vesiculosus* algae catalyzed by Hβ zeolite catalyst for biocrude oil production, Algal Research. 61 (2022) 102596. https://doi.org/10.1016/j.algal.2021.102596.

[4] J. Xia, L. Han, C. Zhang, H. Guo, N. Rong, H.A. Baloch, P. Wu, G. Xu, K. Ma, Hydrothermal co-liquefaction of rice straw and *Nannochloropsis*: The interaction effect on mechanism, product distribution and composition, Journal of Analytical and Applied Pyrolysis. 161 (2022) 105368. https://doi.org/10.1016/j.jaap.2021.105368.

[5] O. Norouzi, S. Mazhkoo, S.A. Haddadi, M. Arjmand, A. Dutta, Hydrothermal liquefaction of green macroalgae *Cladophora glomerata*: Effect of functional groups on the catalytic performance of graphene oxide/polyurethane composite, Catalysis Today. (2022). https://doi.org/10.1016/j.cattod.2022.01.021.

[6] J. Yu, M. Audu, M.T. Myint, F. Cheng, J.M. Jarvis, U. Jena, N. Nirmalakhandan, C.E. Brewer, H. Luo, Bio-crude oil production and valorization of hydrochar as anode material from hydrothermal liquefaction of algae grown on brackish dairy wastewater, Fuel Processing Technology. 227 (2022) 107119. https://doi.org/10.1016/j.fuproc.2021.107119.

[7] B. Guo, B. Yang, P. Weil, S. Zhang, U. Hornung, N. Dahmen, The effect of dichloromethane on product separation during continuous hydrothermal liquefaction of *Chlorella vulgaris* and aqueous product recycling for algae cultivation, Energy Fuels. 36 (2022) 922–931. https://doi.org/10.1021/acs.energyfuels.1c02523.

[8] B. Biswas, A. Kumar, R. Kaur, B.B. Krishna, T. Bhaskar, Co-hydrothermal liquefaction of lignin and macroalgae: effect of process parameters on product distribution, Bioenerg. Res. (2022). https://doi.org/10.1007/s12155-022-10437-x.

[9] Md.B. Islam, M. Khalekuzzaman, S.B. Kabir, Md.R. Hossain, Md.A. Alam, Substituting microalgal biomass with faecal sludge for high-quality biocrude production through co-liquefaction: A sustainable biorefinery approach, Fuel Processing Technology. 225 (2022) 107063. https://doi.org/10.1016/j.fuproc.2021.107063.

[10] Z.-H. Kim, H.P. and C.-G. Lee, Seasonal assessment of biomass and fatty acid productivity by *Tetraselmi*s sp. in the ocean using semi-permeable membrane photobioreactors, 26 (2016) 1098–1102. https://doi.org/10.4014/jmb.1601.01031.

[11] S. Fon Sing, A. Isdepsky, M.A. Borowitzka, D.M. Lewis, Pilot-scale continuous recycling of growth medium for the mass culture of a halotolerant *Tetraselmis* sp. in raceway ponds under increasing salinity: A novel protocol for commercial microalgal biomass production, Bioresource Technology. 161 (2014) 47–54. https://doi.org/10.1016/j.biortech.2014.03.010.

[12] Y. Miyata, K. Sagata, M. Hirose, Y. Yamazaki, A. Nishimura, N. Okuda, Y. Arita, Y. Hirano, Y. Kita, Fe-Assisted hydrothermal liquefaction of lignocellulosic biomass for producing high-grade bio-Oil, ACS Sustainable Chem. Eng. 5 (2017) 3562–3569. https://doi.org/10.1021/acssuschemeng.7b00381.

[13] J.-L. Cao, Z.-L. Yan, Q.-F. Deng, Y. Wang, Z.-Y. Yuan, G. Sun, T.-K. Jia, X.-D. Wang, H. Bala, Z.-Y. Zhang, Mesoporous modified-red-mud supported Ni catalysts for ammonia decomposition to hydrogen, International Journal of Hydrogen Energy. 39 (2014) 5747–5755. https://doi.org/10.1016/j.ijhydene.2014.01.169.

[14] K. Pongsiriyakul, W. Kiatkittipong, S. Adhikari, J.W. Lim, S.S. Lam, K. Kiatkittipong, A. Dankeaw, P. Reubroycharoen, N. Laosiripojana, K. Faungnawakij, S. Assabumrungrat, Effective Cu/Re promoted Ni-supported γ-Al_2O_3 catalyst for upgrading algae bio-crude oil produced by hydrothermal liquefaction, Fuel Processing Technology. 216 (2021) 106670. https://doi.org/10.1016/j.fuproc.2020.106670.

[15] B. Guo, V. Walter, U. Hornung, N. Dahmen, Hydrothermal liquefaction of *Chlorella vulgaris* and *Nannochloropsis gaditana* in a continuous stirred tank reactor and hydrotreating of biocrude by nickel catalysts, Fuel Processing Technology. 191 (2019) 168–180. https://doi.org/10.1016/j.fuproc.2019.04.003.

[16] H. Jahromi, F.A. Agblevor, Hydrotreating of guaiacol: A comparative study of red mud-supported nickel and commercial Ni/SiO_2-Al_2O_3 catalysts, Applied Catalysis A: General. 558 (2018) 109–121. https://doi.org/10.1016/j.apcata.2018.03.016.

[17] W. Peng, C. Wu, S. Wu, Y. Wu, J. Gao, The effects of reaction atmosphere on composition, oxygen distribution, and heating value of products from the hydrothermal liquefaction of corn stalk, Energy Sources, Part A: Recovery, Utilization, and Environmental Effects. 36 (2014) 347–356. https://doi.org/10.1080/15567036.2010.540636.

[18] G. Wang, W. Li, B. Li, H. Chen, Direct liquefaction of sawdust under syngas, Fuel. 86 (2007) 1587–1593. https://doi.org/10.1016/j.fuel.2006.11.010.

[19] C. Yang, L. Jia, C. Chen, G. Liu, W. Fang, Bio-oil from hydro-liquefaction of *Dunaliella salina* over Ni/REHY catalyst, Bioresource Technology. 102 (2011) 4580–4584. https://doi.org/10.1016/j.biortech.2010.12.111.

[20] T. Rahman, H. Jahromi, P. Roy, S. Adhikari, E. Hassani, T.-S. Oh, Hydrothermal liquefaction of municipal sewage sludge: Effect of red mud catalyst in ethylene and inert ambiances, Energy Conversion and Management. 245 (2021) 114615. https://doi.org/10.1016/j.enconman.2021.114615.

[21] S.A. Channiwala, P.P. Parikh, A unified correlation for estimating HHV of solid, liquid and gaseous fuels, Fuel. 81 (2002) 1051–1063. https://doi.org/10.1016/S0016-2361(01)00131-4.

[22] P. Roy, H. Jahromi, S. Adhikari, Y. Zou Finfrock, T. Rahman, Z. Ahmadi, M. Mahjouri-Samani, F. Feyzbar-Khalkhali-Nejad, T.-S. Oh, Performance of biochar assisted catalysts during hydroprocessing of non-edible vegetable oil: Effect of transition metal source on catalytic activity, Energy Conversion and Management. 252 (2022) 115131. https://doi.org/10.1016/j.enconman.2021.115131.

[23] K. Harun, S. Adhikari, H. Jahromi, Hydrogen production via thermocatalytic decomposition of methane using carbon-based catalysts, RSC Adv. 10 (2020) 40882–40893. https://doi.org/10.1039/D0RA07440C.

[24] H. Jahromi, S. Adhikari, P. Roy, E. Hassani, C. Pope, T.-S. Oh, Y. Karki, Production of green transportation fuels from Brassica carinata oil: A comparative study of noble and transition metal catalysts, Fuel Processing Technology. 215 (2021) 106737. https://doi.org/10.1016/j.fuproc.2021.106737.

[25] RStudio Team, RStudio: Integrated Development Environment for R, (2019). https://www.rstudio.com/ (accessed May 6, 2022).

[26] H. Jahromi, S. Adhikari, P. Roy, M. Shelley, E. Hassani, T.-S. Oh, Synthesis of novel biolubricants from waste cooking oil and cyclic oxygenates through an integrated catalytic Process, ACS Sustainable Chem. Eng. 9 (2021) 13424–13437. https://doi.org/10.1021/acssuschemeng.1c03523.

[27] Q. Wang, R. Prasad, B.T. Higgins, Aerobic bacterial pretreatment to overcome algal growth inhibition on high-strength anaerobic digestates, Water Research. 162 (2019) 420–426. https://doi.org/10.1016/j.watres.2019.07.011.

[28] P. Wang, H. Peng, S. Adhikari, B. Higgins, P. Roy, W. Dai, X. Shi, Enhancement of biogas production from wastewater sludge via anaerobic digestion assisted with biochar amendment, Bioresource Technology. 309 (2020) 123368. https://doi.org/10.1016/j.biortech.2020.123368.

[29] T.K. Vo, S.-S. Kim, H.V. Ly, E.Y. Lee, C.-G. Lee, J. Kim, A general reaction network and kinetic model of the hydrothermal liquefaction of microalgae Tetraselmis sp., Bioresource Technology. 241 (2017) 610–619. https://doi.org/10.1016/j.biortech.2017.05.186.

[30] B.E. Eboibi, D.M. Lewis, P.J. Ashman, S. Chinnasamy, Effect of operating conditions on yield and quality of biocrude during hydrothermal liquefaction of halophytic microalga *Tetraselmis* sp., Bioresource Technology. 170 (2014) 20–29. https://doi.org/10.1016/j.biortech.2014.07.083.

[31] R. Shakya, J. Whelen, S. Adhikari, R. Mahadevan, S. Neupane, Effect of temperature and Na2CO3 catalyst on hydrothermal liquefaction of algae, Algal Research. 12 (2015) 80–90. https://doi.org/10.1016/j.algal.2015.08.006.

[32] B.E.-O. Eboibi, D.M. Lewis, P.J. Ashman, S. Chinnasamy, Hydrothermal liquefaction of microalgae for biocrude production: Improving the biocrude properties with vacuum distillation, Bioresource Technology. 174 (2014) 212–221. https://doi.org/10.1016/j.biortech.2014.10.029.

[33] H. Jahromi, T. Rahman, P. Roy, S. Adhikari, Hydrotreatment of solvent-extracted biocrude from hydrothermal liquefaction of municipal sewage sludge, Energy Conversion and Management. 263 (2022) 115719. https://doi.org/10.1016/j.enconman.2022.115719.

[34] S.B. Jones, Y. Zhu, D.B. Anderson, R.T. Hallen, D.C. Elliott, A.J. Schmidt, K.O. Albrecht, T.R. Hart, M.G. Butcher, C. Drennan, L.J. Snowden-Swan, R. Davis, C. Kinchin, Process design and economics for the conversion of algal biomass to hydrocarbons: Whole algae hydrothermal liquefaction and upgrading, 2014. https://doi.org/10.2172/1126336.

[35] W. Wang, Y. Xu, X. Wang, B. Zhang, W. Tian, J. Zhang, Hydrothermal liquefaction of microalgae over transition metal supported TiO_2 catalyst, Bioresource Technology. 250 (2018) 474–480. https://doi.org/10.1016/j.biortech.2017.11.051.

[36] H. Li, J. Hu, Z. Zhang, H. Wang, F. Ping, C. Zheng, H. Zhang, Q. He, Insight into the effect of hydrogenation on efficiency of hydrothermal liquefaction and physico-chemical properties of biocrude oil, Bioresource Technology. 163 (2014) 143–151. https://doi.org/10.1016/j.biortech.2014.04.015.

[37] H. Jahromi, F.A. Agblevor, Hydrodeoxygenation of pinyon-juniper catalytic pyrolysis oil using red mud-supported nickel catalysts, Applied Catalysis B: Environmental. 236 (2018) 1–12. https://doi.org/10.1016/j.apcatb.2018.05.008.

[38] P. Duan, P.E. Savage, Hydrothermal liquefaction of a microalga with heterogeneous catalysts, Ind. Eng. Chem. Res. 50 (2011) 52–61. https://doi.org/10.1021/ie100758s.

[39] S. Sushil, V.S. Batra, Catalytic applications of red mud, an aluminium industry waste: A review, Applied Catalysis B: Environmental. 81 (2008) 64–77. https://doi.org/10.1016/j.apcatb.2007.12.002.

[40] J.B. Stigter, H.P.M. de Haan, R. Guicherit, C.P.A. Dekkers, M.L. Daane, Determination of cadmium, zinc, copper, chromium and arsenic in crude oil cargoes, Environmental Pollution. 107 (2000) 451–464. https://doi.org/10.1016/S0269-7491(99)00123-2.

[41] M.F. Gazulla, M. Rodrigo, M. Orduña, M.J. Ventura, C. Andreu, Determination of phosphorus in crude oil and middle distillate petroleum products by inductively coupled plasma–optical emission spectrometry, Analytical Letters. 50 (2017) 2465–2474. https://doi.org/10.1080/00032719.2017.1296853.

[42] Y. Han, K. Hoekman, U. Jena, P. Das, Use of Co-Solvents in Hydrothermal liquefaction (HTL) of microalgae, Energies. 13 (2020) 124. https://doi.org/10.3390/en13010124.

[43] X. Zhang, L. Chen, W. Kong, T. Wang, Q. Zhang, J. Long, Y. Xu, L. Ma, Upgrading of bio-oil to boiler fuel by catalytic hydrotreatment and esterification in an efficient process, Energy. 84 (2015) 83–90. https://doi.org/10.1016/j.energy.2015.02.035.

[44] Yang Han, S. Kent Hoekman, Zheng Cui, Umakanta Jena, Probir Das, Hydrothermal liquefaction of marine microalgae biomass using co-solvents, 38 (2019) 101421. https://doi.org/10.1016/j.algal.2019.101421.

[45] C. Jazrawi, P. Biller, A.B. Ross, A. Montoya, T. Maschmeyer, B.S. Haynes, Pilot plant testing of continuous hydrothermal liquefaction of microalgae, Algal Research. 2 (2013) 268–277. https://doi.org/10.1016/j.algal.2013.04.006.

Chapter 4

Depolymerization of household plastic waste via catalytic hydrothermal liquefaction

Abstract

In this work, a mixture of five prominent plastic polymers as simulated household waste was depolymerized using the hydrothermal liquefaction (HTL) process using pretreated red mud catalyst for crude products. The selected plastics were polyethylene terephthalate (PET), high-density polyethylene (HDPE), low-density polyethylene (LDPE), polypropylene (PP), and polystyrene (PS). For proper comparison, each plastic material was treated individually in control experiments. Among the single plastics, HDPE generated the maximum biocrude yield of 76 wt.%, whereas PET produced only solid (80wt.%) and gaseous products. The biocrude yield production from non-catalytic reactions followed this trend: HDPE>PS>PP>LDPE. When PET (42wt.%), HDPE (20wt.%), LDPE (20wt.%), PP (4wt.%) and PS (14wt.%) were blended together, the crude yield was 22 wt.%. The catalyst facilitated cracking and gasification with suppressed liquid and solid formation from individual plastic feedstock and played a vital role in reducing the viscosity and acidity of HTL liquid products. The plastic crude oil possessed 36-92 wt.% gasoline-range compounds, while the chemical composition varied with the feedstock. Without a catalyst, HDPE decomposed into straight-chain alkanes, whereas PP and PS-derived products consisted of aromatic and cyclic compounds. The catalyst promoted aromatization in plastic mix-derived crudes and increased the gasoline boiling range of compounds.

Keywords: Plastic, Red Mud, Hydrothermal Liquefaction, Crude Oil

4.1 Introduction

Due to their durability, lightweight with low production cost, plastic materials are widely used in home appliances to delicate instruments [1]. The excessive use of plastic has created enormous

amounts of plastic waste with serious impacts on waste management facilities and on the environment [2]. The heterogeneity of plastic waste makes it difficult to separate different plastic materials from the waste stream and treat them individually [3]. Hydrothermal liquefaction (HTL) technology is a promising thermochemical depolymerization process for mixed plastic waste and individual plastic [4]. The HTL process can depolymerize almost any organic feedstock into liquid biocrude oil, solid char, and gaseous products at moderate temperature (typically 200–400°C) and high pressure (typically 10–25 MPa) [5]. Recently plastic materials have gained global attention as feedstock for the HTL process. Zhao et al. investigated HTL conversion of e-waste plastics, and the produced organic yield varied from 81.4 to 97.6 wt.% at 350 °C temperature, which mostly composed of styrene monomers, styrene derivatives, bisphenol A, and caprolactam [6]. Hongkong et al. explored the non-catalytic co-liquefaction of nylon and *Fucus Serratus* macroalgae under 350°C with different blend ratios. They reported a maximum of 17 wt.% biocrude yields, enriched with nylon monomer (caprolactam), from a 1:1 blend of nylon six and microalgae [7]. Poravou et al. investigated the HTL of plastic waste mix and polypropylene by conventional heating and solar energy-aided within 350 to 450 °C temperature where single polypropylene produced maximum HTL fuel, and solar simulator facilitated more biocrude production [8].

The catalysts can play a critical role in improving the thermochemical conversion energy efficiency and can promote targeted reactions with product selectivity [9]. Wu et al. commented that there are significant knowledge gaps and challenges that remain in the development of low-cost, efficient catalysts for the thermochemical conversion of biomass [10]. Widely abundant waste slag materials, such as red mud (RM), can be utilized as a catalyst in the HTL process. RM is a byproduct of the alumina production process, composed of mainly iron oxide with other metal oxides, and poses a serious threat to the environment due to its high alkalinity [11]. This iron-

enriched industrial waste has been successfully used as a catalyst for HTL conversion of municipal sewage sludge, food waste, algae, and lignocellulosic biomass. It was found that the RM catalyst is capable of increasingcarbon conversion efficiency and energy recovery of the HTL Process [12–14].Caprariis et al. liquefied woody biomass with red mud catalyst by HTL process and found that red mud actively produced hydrogen in the HTL system, thus increasing the bio-crude yield with lower oxygen content and higher HHV. This zero-value waste could be recovered from the oak char and reused again in the HTL system after reduction treatment [15]. Saral et al. successfully minimized the nitrogen content of algae-derived HTL biocrude by red mud catalyst [16]. The use of RM catalysts is not rare in the pyrolysis treatment of plastic and polymers. Lopez et al. studied the influence of ZSM-5 zeolite and RM in the pyrolysis of mixed plastic wastes at 440 and 500 °C. They reported that the RM catalyst required a higher reaction temperature to have a similar catalytic effect of ZSM-5 catalysts over plastic mixture pyrolysis [17]. Ahmed et al. modified the catalytic properties of RM by rearranging the agglomerated phases for the co-pyrolysis of biomass and polyethylene, which showed better performance than ZSM-5 by promoting decarbonylation over dehydration [18]. To the best of our knowledge, the effect of RM catalyst in HTL of plastic materials has not been explored yet.

This study aims to investigate the influence of modified RM catalysts over the HTL decomposition of five different plastic materials such as polyethylene terephthalate (PET), high-density polyethylene (HDPE), low-density polyethylene (LDPE), polypropylene (PP) and polystyrene (PS) and the plastic mixture that resemble municipal solid waste. The objective of this study is to evaluate the efficacy of HTL treatment for mixed plastic streams. We hypothesize that the different plastics from the mixture during HTL depolymerization will promote the crude formation, and RM will influence the HTL decomposition by cracking reaction. This study explored the perspectives

of a mixed plastic product as feedstock for fuel production in association with a zero-value, mixed metal oxide catalyst.

4.2 Materials and methods

4.2.1 Material

Unused plastic products such as water bottles, food containers, shopping bags, and utensils made of polyethylene terephthalate (PET), high-density polyethylene (HDPE), low-density polyethylene (LDPE), polypropylene (PP), and polystyrene (PS) were purchased from a local market. A plastic granulator (Shini USA, Model: SG-2042NCH) was used to shred each plastic component separately, and the shredded plastics were sieved to obtain a 2mm particle size. The sieved, shredded plastics were blended at weight percentage (Table C1, Appendix C) based on the US Army Research Laboratory (ARL) study and denoted as "PM" throughout this study [19]. The red mud (RM) was collected from Almatis Burnside, Inc. (Gonzales, Louisiana, USA). Airgas Inc. (Opelika, Alabama, USA) supplied high-purity nitrogen gas that was used in this study

4.2.2 Feedstock characterization

The shredded plastic feedstocks were characterized for ultimate and proximate analyses and heavy metal content. The elemental analysis (CHNS/O) was performed according to the ASTM D5373-02 method in Vario MICRO cube, Elementar (New York, USA) [20]. The EPA 1684 method was followed to measure the moisture content. The ash content and volatile matter content were determined using ASTM E1755 and ASTM E872methods, repectively. The heavy metals of the feedstocks were measured by inductively coupled plasma-optical emission spectrometry (ICP-OES). The Soil, Plant, and Water Laboratory (University of Georgia, Athens, USA) performed the ICP-OES analysis of the plastics.

4.2.3 Catalyst preparation

The RM based catalyst was prepared according to our previous work [12]. Briefly, the as-received RM was calcined at 575℃ for four hours and then sieved to obtain the particle size between 106-595 μm. The calcined, sieved RM was reduced at 500℃(RRM500) using a gas mixture of 10% H_2 and 90% N_2 for six hours and stored for the future use in HTL.

4.2.4 Catalyst characterization

The catalyst was characterized by inductively coupled plasma-optical emission spectrometry (ICP-OES), X-ray diffraction (XRD) techniques and surface analyzer methods. The methodology of XRD analysis was discussed in our previous work [21]. Briefly, a bench-top powder X-ray diffraction system (AXRD, Proto Manufacturing, Taylor, Michigan, USA) was utilized from 20° to 100º (2θ) with 2 seconds of dwell time and 0.014° of Δ2Θ at 30 mA and 40 kV with CuKα radiation (λ = 1.5418 Å). The surface area of the catalyst was measured by an Autosorb-iQ (Quantachrome Instruments, USA) with BET (Brunauer–Emmett–Teller) equation using N_2-adsorption–desorption isotherm in an adsorption analyzer. The chemisorption macro steps can be found in our previous work [22].

4.2.5 Experimental setup and procedure

The reaction temperature of all HTL experiment of this study was set at 450℃. However, all single plastic materials or plastic mixture feedstocks could not reach that high temperature inside the reactor even after a prolong heating period. Therefore, heating period was fixed with heating rate of 3℃/min for seven hours (starting from room temperature) for each HTL experiment and then the reactor was cooled to room temperature. The highest attained temperature along with pressure inside reactor during HTL depolymerization of each feedstock is provided at supporting material (Appendix C, Table C3). A high-pressure, high-temperature reactor from Parr Instrument

Company (Model 4578, Moline, Illinois, USA) was used for HTL experiments of the plastics. Details of the reactor setup was discussed in our previous work [12]. Briefly, the reactor has 1.8 L vessel, PID controlled electrical heating unit, controllable agitator, pressure gauge, and J-type thermocouple to monitor the temperature inside the reactor. For each HTL experiment, 50 g of shredded and sieved single plastic or plastic mixture was loaded into the reactor with 87.5 g (feedstock and water ratio of 1:1.75) deionized water as per the published work [23]. For all catalytic HTL experiments, catalyst: feedstock loading was fixed at 1:10 i.e., 5 g catalyst per 50 g plastic feedstock. Once the plastic, water and catalyst (if applicable) were loaded in the reactor, the reactor was sealed. The reactor was then purged with inert gas (nitrogen) three times to remove air from the reactor headspace before pressurizing with it to an initial pressure of 90 psi (0.62 MPa) with nitrogen gas. The agitator was turned on with fixed speed 300 rpm above 400°C temperature to avoid any interruption by thermally degraded semi-solid plastic. After 7 h heating, the heater was removed, and the reactor was cooled to room temperature by electrical fan and ice bath. The products (gas, solid, aqueous phase, and plastic oil) were separated as described in Section 4.2.6. All experiments were performed in duplicates.

4.2.6 Product separation

After cooling the reactor to room temperature, the gas composition was analyzed . Then the reactor was opened to recover the liquid and solid products. The reactor content was poured into a large flask, and the weight was recorded. Then, the reactor content was filtered through Whatman No.50 filter paper (particle filtration size of 2.7 μm) to separate solid from the liquid phase. The liquid products were transferred to separatory funnel to decant the organic product after draining the aqueous phase. The remaining solids on the filter paper were then washed with dichloromethane (DCM). The DCM was separated from the organics using an IKA rotary evaporator at 65°C and

700 mbar vacuum pressure to obtain DCM extracted organic phase. The weight of all liquids (aqueous and organic phases) was recorded for mass balance. The decanted and DCM extracted organic phases were termed as "crude oil" throughout the paper.

4.2.7 Product analysis

A micro-GC (Agilent 3000A) was used to analyze gaseous products. Details of micro-GC analysis was discussed elsewhere [12]. Briefly, the Agilent 3000 A micro-GC is equipped with three modules alongside thermal conductivity detector: a 10 m Molsieve 5A (MS) column and two 10 m porous polymer (PPU) columns. The sample could be split into three streams to go into one of these modules. MS column analyzed hydrogen, methane, and carbon monoxide, while carbon dioxide and ethylene hydrocarbons were analyzed on the PPU columns simultaneously. Argon and helium were used as carrier gases for MS column and PPU column, respectively.

The yield of biocrude and solid product were calculated on dry-ash free basis using Equations 1and 2, respectively [24]. The remaining product fraction was regarded as "balance" and calculated using Equation 3.

$$Y_{crude}(\%) = \frac{w_b}{w_f - w_m - w_a} \times 100 \qquad (1)$$

$$Y_{solid}(\%) = \frac{w_s - w_c}{w_f - w_m - w_a} \times 100 \qquad (2)$$

$$Y_{balance}(\%) = 100 - Y_{crude} - Y_{solid} \qquad (3)$$

where w_f is the mass of *plastic* feedstock (g), w_m and w_a are the mass of moisture and ash content of feedstock (g), respectively. w_b is the mass of the crude product (g), w_s is the weight of total solid residues (g), and w_c is the weight of catalyst (g).

The elemental analysis was performed on each sample using an elemental analyzer (Vario MICRO, Elementar, New York, USA). The higher heating value (HHV) of biocrude was

determined using IKA Model C2000 basic bomb calorimeter (IKA Works, Inc., Wilmington, NC, USA)[25].The total acid number (TAN) of each sample was determined through titration according to ASTM D664-07 using a Mettler Toledo T50 Titrator. Thermogravimetric analysis (TGA) of biocrude was performed by using a Shimadzu TGA-50 (Shimadzu, Japan) under nitrogen atmosphere (flow rate: 20 ml/min) with heating rate of 10 °C/min from room temperature up to 800 °C [26].

The simulated distillation analysis was performed according to ASTM D2887 [27]. The diluted samples (20 mg oil in 2ml of CS_2) were analyzed by Agilent Technologies 7890A GC-FID (flame-ionization detector) system with a 7693 autosampler and a 10 m x 0.53 mm x 3 μm DB-2887 Column. A sample volume of 0.2 μL was injected for the simulated distillation analysis and then heated from 40°C to 350°C at a heating rate of 20°C/min. The GC-FID system was operated in a 1:4 split inlet mode during each analysis. The chemical composition of biocrude samples was analyzed by an Agilent Technologies 7890A Gas Chromatograph (GC) System with a 7683B Series Injector, 5975C Inert Mass Selective Detector (MSD) with Triple-Axis Detector. The details of GC-MS instrument were reported elsewhere [26]. In a brief, 30 m × 250 μm × 0.25 μm DB-35MS column was used while the GC oven was heated up to 50 °C and held for 2 min and then ramped at a heating rate of 5 °C/min to 280 °C and kept for 15 min. The chemical structures identified by the National Institute of Standards and Technology (NIST) MS Library of the GC–MS, were then grouped into paraffins, olefins, cyclic-aromatics and oxygenated compounds based on their peak area percent from semi-quantification.

The aqueous phase was analyzed for total organic carbon (TOC), total nitrogen (TN) and pH. The TOC and TN were measured by a TOC/TN analyzer (TOC-L, Shimadzu, Kyoto, Japan). The pH of the solution was measured by a pH meter (pH510, Oakton, Vernon Hills, Illinois, USA).

4.3 Results and discussion

4.3.1 Feedstock characterization

Table 4.1 presents the ultimate and proximate analyses of the studied plastic materials. The physicochemical properties of plastic mixtures (PM) were calculated based on the individual plastic properties with mixing proportion. Among five plastics polymers, polystyrene possessed the highest amount of carbon by 92.7 wt.%. The minimum carbon of 65 wt.% was found in LDPE. The oxygen content was significantly low in plastic materials compared to traditional HTL feedstock, such as sludge, algae, woody biomass, etc. [12,28]. The volatile content was a prominent part of the ultimate analysis of the plastics. The HDPE contained the highest amount of volatile (97.1wt.%), and the LDPE had the lowest volatile quantity (78.3 wt.%). The ash content of LDPE was unusually high. A high concentration of metals was also detected in LDPE samples (Appendix C, Table C5). The LDPE samples of this study were collected from shredded commercial shopping bags. The metals are generally incorporated with plastic as additives, colorants, antioxidants, or stabilizers to improve the quality of the polymer. These additives might be responsible for higher metal content as well as the ash of LDPE plastic feedstock [29,30]. Both the elemental composition and ultimate analysis results of the plastic mixtures varied with the blending ratio and plastic components.

Table 4.1: Properties of the plastic feedstocks

	PET	HDPE	LDPE	PP	PS	PM [b]
Elemental Analysis(wt.%)						
C	65.3±0.0	86.4±0.2	65.0±2.0	86.4±0.0	92.7±0.0	74.2±0.7
H	3.5±0.3	13.2±0.1	8.5±0.3	13.0±0.1	7.1±0.0	7.4±0.4
Ash	0.4±0.1	0	20.3±0.2	0.2±0.0	0	4.2±0.1
O[a]	30.8±0.4	0.4±0.1	6.2±2.5	0.4±0.1	0.2±0.0	14.2±1.2
Proximate Analysis(wt.%)						
Moisture	0.3±0.0	0.1±0.0	0.4±0.0	0.1±0.0	0.4±0.0	0.3±0.1
Ash	0.4±0.1	0	20.3±0.2	0.2±0.0	0	4.2±0.1
Volatile Content	94.0±0.0	97.1±0.0	78.3±0.2	96.2±0.0	96.3±0.0	90.9±0.2
Fixed Carbon[a]	5.3±0.1	2.8±0.0	1.0±0.4	3.5±0.0	3.3±0.0	4.6±0.4

[a] by difference, [b] calculated with the plastic ratio and individual plastic properties

4.3.2 Catalyst characterization

The properties of RRM500 catalyst were discussed in our prior work [12]. The XRD analysis (Figure 4.1) of RRM500 has distinguished the iron oxide peaks of hematite (Fe_2O_3), magnetite (Fe_3O_4) along with other metal oxides of calcite($CaCO_3$), gibbsite($Al(OH)_3$), anatase(TiO_2)and quartz(SiO_2). A high concentration of iron was verified by the ICP analysis data (Appendix C: Table C3) of the catalyst with 43 wt.% (435473.0 ppm) of iron content. The metal composition of RRM500 also included a notable amount of aluminum (7wt.%), calcium (2.4wt.%), and sodium (3.2wt.%). The surface area (Table C4) of this catalyst was only 21.92 m^2/g with 6.15 nm of pore size. The metal content and physisorption data of RRM500 were within the range of other red mud reports [31].

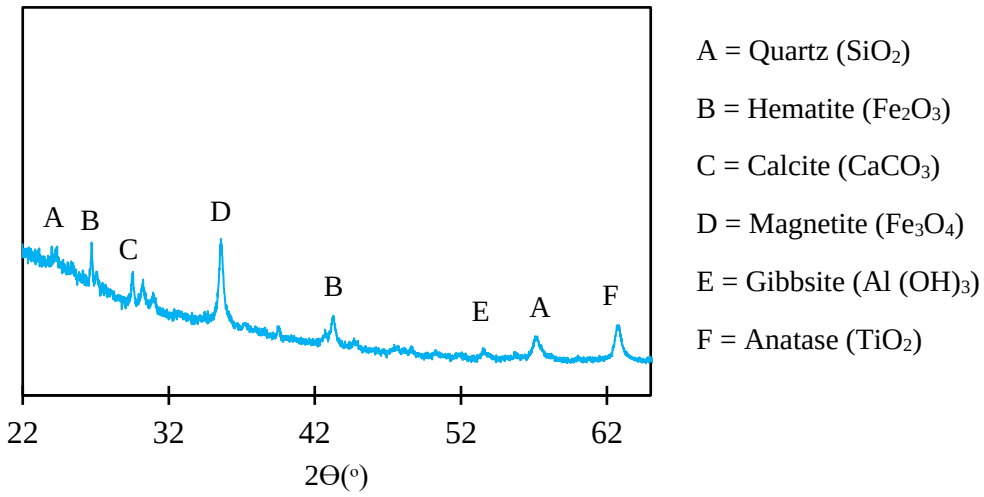

Figure 4.1: XRD analysis of RRM500

4.3.3 HTL products characterization

4.3.3.1 Yield Analysis

Figure 4.2-A shows the yield distribution of plastic HTL reactions on dry-ash free basis. Depending on the plastic types, HTL product distribution varied widely in both catalytic and non-catalytic reactions. Without a catalyst, HPDE polymers produced the maximum crude yield of 76 wt.%, and the lowest crude yield of 28 wt.% was generated by LDPE feedstock. Maximum 87 wt.% HTL crude yield from high density and low density polyethylene (PE) was reported at 425 °C with 2.5 h residence time in 500 ml size reactor [23]. Larger HTL reactor (1800 ml) might be a reason for slightly lower HDPE crude yield of this study. The second highest non catalytic crude yield (73wt.%) was produced from PS feedstock. This specific plastic material is well known for high crude oil production (maximum 86 wt.%) even in sub-critical temperature (350℃)[32]. Regardless of catalyst, PET was converted to solid and gas under HTL condition. The solid production was reduced by 11% by RRM500 catalyst. Higher depolymerization of PET has

previously been reported in the presence of an alkali catalyst [33]. The RM is also highly alkaline in nature (10-15 pH) which might affect the decomposition of PET [34,35]. High solid yield (84wt.%) from HTL treatment of PET plastic was also observed in other report where DCM could not dissolve the PET HTL products [32]. Therefore, DCM was not added to PET derived wax products in this study. Using PET in a plastic mixture of PM also resulted in 22 wt.% solid productions, separated from biocrude by gravity. The RRM500 catalyst did not favor biocrude formation from individual plastic materials. The high balance fraction indicated that the plastic might be decomposed into more gaseous products in this high temperature rather than crudes or solid products. However, the RRM500 catalyst increased the biocrude yield from the PM and plastic mixture compared to the non-catalytic condition. Approximately 63 % less solid was obtained from HTL conversion of PM mixture with RRM500 catalyst, compared to non-catalytic experiments. Figure 4.2-B compares the experimental value of solid from PET and crude yield with the calculated yield. The experimental crude yield from each plastic and the experimental solid yield value of PET were multiplied with their blending ratio to determine the theoretical "calculated yield" of the PM mixture. The details of calculated yield determination from plastic mixture was reported elsewhere [36]. It was evident from the comparison that irrespective of catalyst, less solid was generated from PET in plastic mixture. The lower solid production from mixed plastic suggested the synergistic effects of plastic mixture in solid generation from PET. A similar trend was observed in an equi-mass mixture of PP, PET, PS, and PC, where the experimental biocrude yield exceeded the calculated yield [36]. The opposite effects were observed in non-catalytic HTL reactions where the experimental yield from PM was less than the calculated yield from the same condition. Therefore, it can be concluded that the RRM500 catalyst

promoted crude production from mixed plastic feedstocks rather than an individual plastic component.

In absence of catalyst, the LDPE has generated the maximum solid residue products with 25 wt.% yield where polypropylene produced the lowest solid yield of 2 wt.%. The solid production from the non-catalytic conversion of the individual plastic component has the following order: LDPE>PS>HDPE>PP. The catalyst promoted the solid formation from individual plastic material, except PET. The most significant rise was observed in PS-RRM500 reaction where solid yield was increased by three times with the catalyst. In case of mixture, the catalytic char yield remained almost same as the non-catalytic reaction.

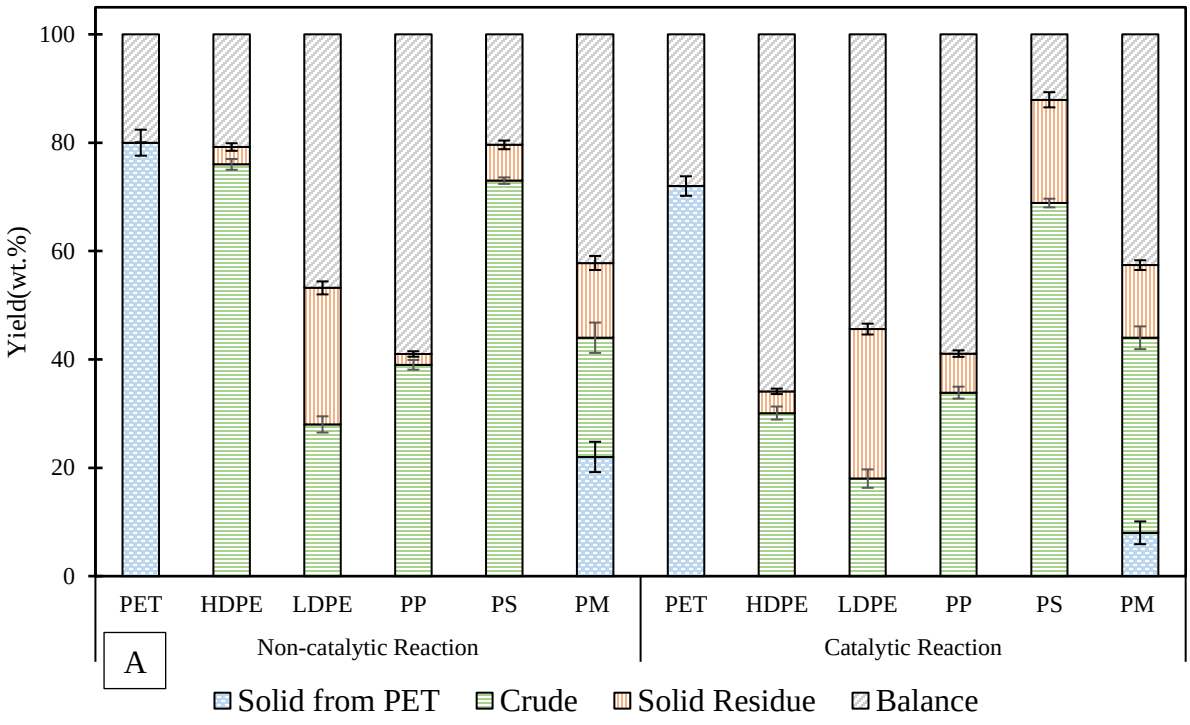

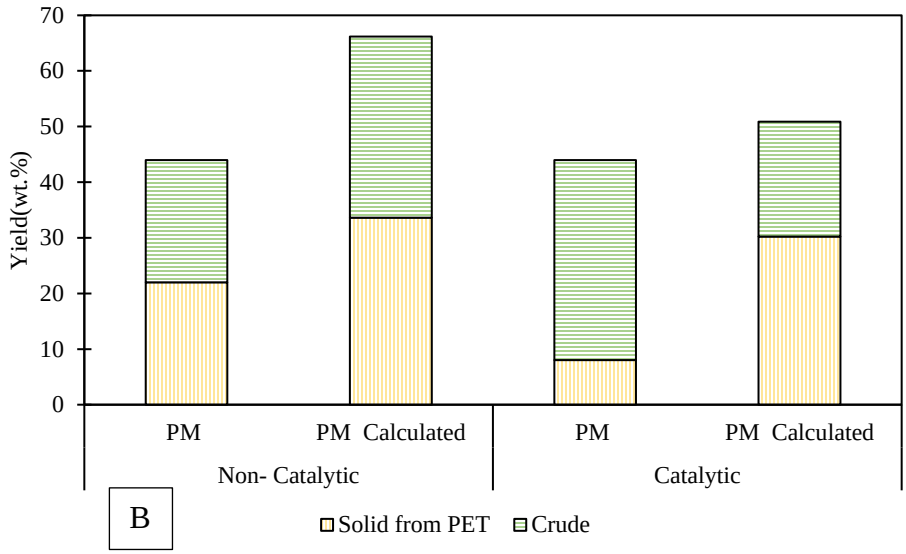

Figure 4.2: Product distribution of Plastic HTL – A: Yield distribution of individual and plastic mixtures, B: Comparison between calculated and experimental biocrude yields of plastic mixtures

4.3.3.2 Biocrude characterization

Physicochemical properties

Table 4.2 shows the physicochemical properties of plastic biocrudes in this study. Due to little nitrogen and sulfur content, only carbon, hydrogen, and ash were reported as elemental compositions of plastic biocrudes. In non-catalytic conditions, the maximum carbon, hydrogen, and minimum oxygen were found in HDPE-derived HTL crude, leading to this study's highest HHV (45.8 MJ/kg). Without a catalyst, no notable change was found in the carbon content of four individual plastic biocrudes. Depending on the plastic type, the non-catalytic hydrogen content ranged from 13.4 to 7.8 wt.%. The HHV of the single plastic biocrudes showed the following order: HDPE>PP>LDPE>PS. Amidst the single plastic non-catalytic treatments, crude from PP plastic possessed the maximum oxygen of 8.2 wt.%. The carbon and hydrogen contents drastically

declined in crude oils from the plastic mixture. As a result, high oxygen was detected in mixed plastic biocrude. The biocrude from PM had the maximum oxygen (27 wt.%) with the lowest HHV (28.6 MJ/kg) in non-catalytic HTL reactions. When RRM500 catalyst was introduced to HTL systems, the carbon content of LDPE, PP, and PS was reduced by 7.4 to 11 % in comparison with the non-catalytic biocrudes from the sample plastic. Most probably, the high reaction temperature of plastic HTL depolymerization released carbon as gas(CO, CO_2) from the HTL system. The oxygen content of catalytic PScrude was almost three times higher than the no catalyst PS crude product. The catalyst added little carbon (1%) to HDPE crude but lowered the hydrogen content compared to no catalyst reaction-derived HDPE crude. For these adverse effects of RRM500 catalyst, the HHV of catalytical biocrudes from single plastic were 1.6 to 20% less than the biocrudes from no catalyst HTL condition. The elemental composition and HHV of the catalytic PM-derived biocrude were almost identical to the non-catalytic one, with few differences.

The acidity of HTL plastic crudes was significantly less than our prior HTL study of municipal sewage sludge [12]. However, the TAN values of plastic crudes were almost two times higher than commercial diesel fuel [37]. In single plastic non-catalytic HTL conversion, the maximum TAN value was observed in the biocrude from HDPE, and the minimum was found in the LDPE biocrude. The PM mixture-derived crude has the highest acidity in this study, with a TAN value of 20.30 mgKOH/g. The hydrolysis of PET in supercritical water could release acidic compounds such as terephthalic acid and raise the TAN value of the oil [38]. The RRM500 catalyst significantly reduced acidity in HDPE, LDPE, PS, and PM-derived biocrude products. The acidity reduction by RM catalyst was also reported in corn stalk and pine wood chips pyrolysis bio-oil [39,40]. The RM-based catalyst might play a role in neutralizing the acidic compounds from liquid products of thermochemical conversion processes.

The utilization of catalysts has reduced the dynamic viscosity of HDPE, LDPE, and PM mixtures-derived biocrudes compared with non-catalytic biocrudes. It was reported that the mixed metal (Fe, Al, and Mg) content of red mud (RM) could crack the heavy compounds of feedstock during the pyrolysis process [40]. The RRM500 catalyst might crack some plastic components under HTL conditions and produce less viscous biocrude products. Further evidence of cracking reaction can be found in the enhanced gaseous yield (balance) within the catalytic product distribution (Figure 4.2-A) of HDPE, LDPE, and PM mixture conversion. The biocrude density was slightly higher from catalytic HTL conversions. Among non-catalytic HTL reactions, the HDPE biocrude has the minimum density of 0.79g/cm^3, where PM-derived biocrudes had the highest one with 0.95g/cm^3.

Heavy metal content (Table C6) of non-catalytic plastic oil was lower than other HTL oil but higher than petroleum products [12,41]. Some heavy metals (Co and Fe) from RRM500 were likely leached into the catalytic plastic biocrudes. The catalytic PP and PS biocrude contained significantly higher Co and Fe metals than non-catalytic products. When all the heavy metals found in each HTL product from every feedstock were added, the heavy metals from RRM500 mostly deposited to solid HTL products (Figure C3).

Table 4.2: Physicochemical properties of plastic HTL biocrudes.

		Elemental Analysis (wt.%)							
		C	H	Ash	O[a]	HHV (MJ/kg)	TAN (mgKOH/g)	Dynamic Viscosity (cP)	Density (g/cm3)
Non-Catalytic	HDPE	86.2±0.0	13.4±0.1	0.2±0.0	0.3±0.2	45.8±0.2	1.80±0.21	2.82±0.54	0.79±0.01
	LDPE	83.8±0.8	8.6±0.1	0.1±0.0	7.5±1.0	38.7±0.5	0.35±0.10	1.08±0.43	0.95±0.02
	PP	82.6±1.6	9.2±0.3	0.0	8.2±1.9	38.8±1.2	0.4±0.12	0.72±0.20	0.81±0.01
	PS	84.9±3.0	7.8±0.2	0.1±0.0	7.2±3.2	38.0±1.6	0.58±0.0	0.60±0.17	0.87±0.03
	PM	65.5±1.4	7.3±0.1	0.1±0.0	27.1±1.5	28.6±0.6	20.30±0.52	0.95±0.33	0.95±0.03
Catalytic	HDPE	87.3±1.6	10.1±0.2	0.1±0.0	2.5±1.8	42.0±0.5	0.35±0.10	1.19±0.25	0.85±0.02
	LDPE	77.6±0.7	8.5±0.3	0.3±0.0	13.6±1.0	35.7±0.4	0.28±0.10	0.92±0.14	0.90±0.02
	PP	73.6±2.0	7.7±0.4	0.0	18.7±2.4	32.8±1.5	0.44±0.1	0.91±0.10	0.86±0.03
	PS	73.7±0.4	5.4±0.3	0.1±0.0	20.8±0.7	29.9±0.2	0.24±0.11	0.86±0.12	0.90±0.02
	PM	65.4±0.5	6.6±0.1	0.1±0.0	27.9±0.6	27.8±0.3	8.39±1.3	0.77±0.30	0.96±0.03

[a] by difference

Thermogravimetric analysis

Figure 4.3 presents the thermogravimetric analysis (TGA) of the plastic HTL crude products. The TGA profile of each plastic and plastic mixtures derived non-catalytic crudes were compared with the catalytic counterpart to evaluate the effect of the RRM500 catalyst. From Figure 4.3-A, it was evident that the RRM500 catalyst has promoted volatile components in HDPE biocrude. This finding was in agreement with the simulated distillation result (Figure C4), where catalytic HDPE biocrude has approximately 80% and 52% more gasoline and jet fuel boiling point range molecules, respectively than the non-catalytic one. There were slightly high (5% higher) low boiling point compounds in catalytic LDPE biocrude relative to the no catalyst product. It is another proof that the RRM500 catalyst assisted the cracking reaction of plastic molecules during HTL conversion, and light compounds were released [40]. TGA thermographs of PP and PS were also matched with the boiling point distribution of sim distillation. The catalytic PP biocrude contained 0.5%, and the non-catalytic PS biocrude possessed 8% more gasoline and jet fuel range compounds than their non-catalytic and catalytic counterparts. The catalytic PM-derived biocrude contained a 15% higher gasoline range product than the non-catalytic one. On the other hand, the non-catalytic PM biocrude has 13% more jet fuel range products than the catalytic product.

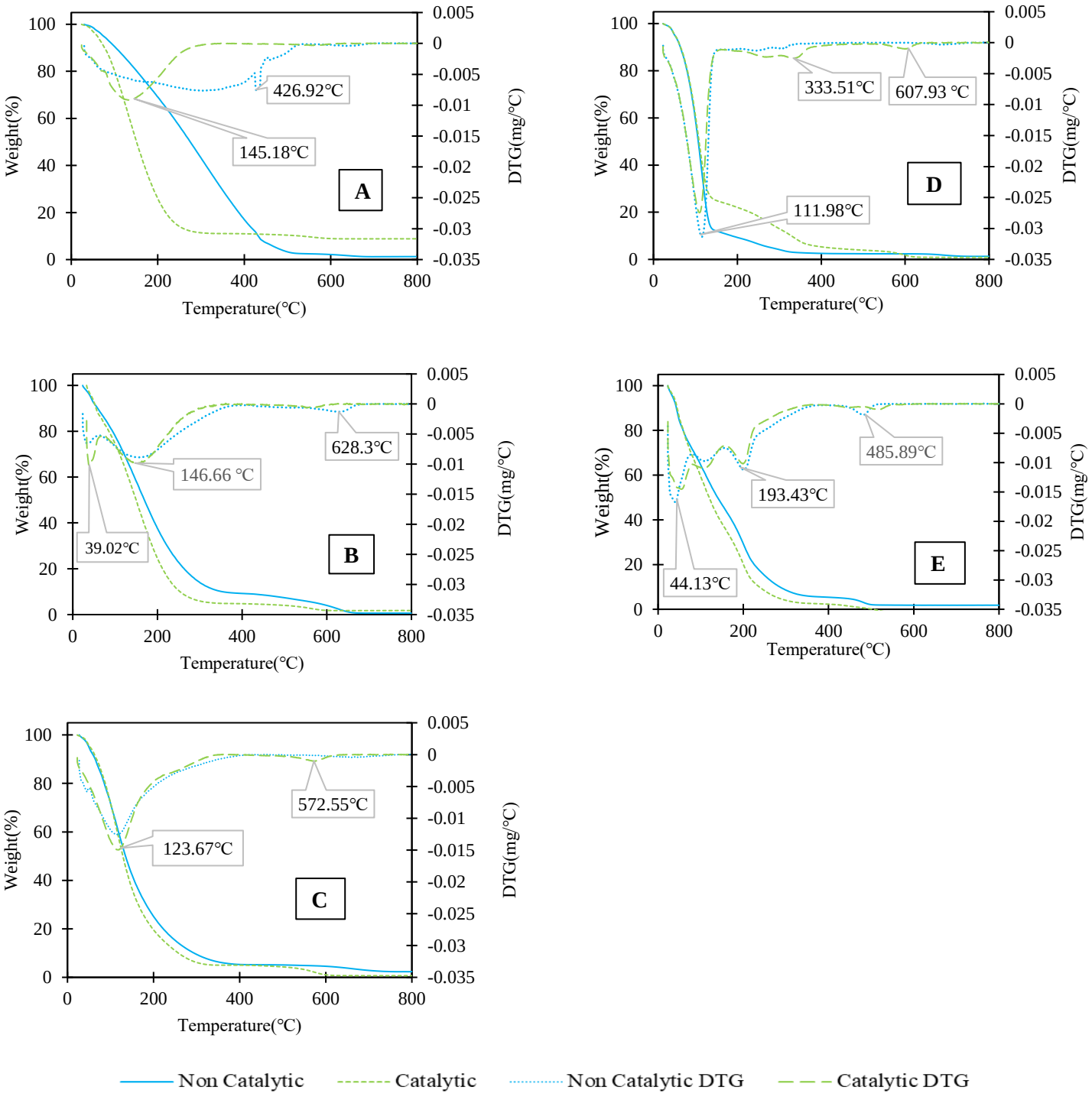

Figure 4.3: Thermogravimetric analysis of biocrude samples from no catalytic and catalytic HTL reactions: A- HDPE, B-LDPE, C-PP, D-PS and E- PM

Chemical Composition

Figure 4.4 shows the semi-quantification and classification of plastic and plastic mixture crude products. The compounds were presented according to the area percentages, and they were divided into paraffin, olefins, cyclic and aromatics, and oxygenated compounds (Table C7-C16). Maximum paraffin was detected in non-catalytic HDPE crude. It is established that the thermal cracking of HDPE by supercritical water mainly produces alkanes and alkenes products[42]. Olefin, along with a small amount of oxygenates and aromatics-cyclic, were also detected in HDPE non-catalytic crudes. The catalyst suppressed the olefin production in HDPE crude and increased the cyclic, aromatic groups, especially in C9-C12 (Appendix C, Figure C5) groups, significantly relative to non-catalytic HDPE biocrude. Generally, Gasoline products' carbon atom number ranges between C4 and C12 [43]. This result was in agreement with the sim distillation of catalytic HDPE crude oil(Figure C4), where gasoline boiling point range products were significantly high in catalytic oil compared to non-catalytic one. There is a possibility that the iron oxide (Fe_2O_3, Fe_3O_4) from RRM500 accelerated the dehydrogenation reaction and facilitated the aromatization of HDPE products [23,44]. In the case of LDPE crude, the RRM500 catalyst promoted the paraffin compound in biocrude by two times and reduced the cyclic compound by 37%, compared to no catalyst condition. Lin et al. hypothesized that the iron might increase the active sites of the catalyst and promote deoxygenation, dehydrogenation, rearrangement, cyclization, and aromatization reactions [45]. According to other researchres, the untreated and cation-exchanged RM catalysts were found to be effective for the aromatization of olefins in co-pyrolysis of LDPE, which was not observed in HTL conversion of LDPE with RRM500 catalyst [17,46]. The excess metal content of LDPE feedstock (Table C5) might be responsible for this opposite catalytic effect over LDPE crude product. Regardless of the catalyst, the cyclic and aromatic compounds were the only

compound group in PP and PS crudes. The formation of cyclic and aromatics from HTL treatment of PP at or above 425℃ was reported before. Xylene was the prominent product in PP crude which agrees with the current study [47]. The RRM500 catalyst slightly raised the xylene production from PP (Table C12), which can be considered a catalytic effect. Xylene is a useful chemical commodity, and RRM500 catalyst can enhance this product recovery from HTL conversion of PP polymer [48]. The catalyst slightly increased the compounds with C11 and C12 carbon numbers in PP crude oil, but that difference was not detected in the simulated distillation of the same oil. The HTL reaction of PS polymer mainly produced toluene, benzene, and ethyl benzene which is supported by the previous studies [49]. The styrene monomers were not detected in the PS crude of this study. Long reaction hours might promote the hydrogenation of styrene and raise the amount of ethylbenzene in PS-derived biocrudes [50].

The plastic mixture biocrude components largely depend on the plastic materials and the mixture ratio. The paraffin and cyclic-aromatics were the dominant compound groups alongside small olefins and oxygenated in non-catalytic PM crudes. The catalyst has increased the cyclic-aromatic group by 11%, where olefin and paraffin formation was suppressed by two times and 14%, respectively, compared to non-catalytic reaction- PM oil product. Ethylbenzene was the major aromatic compound in both catalytic and non-catalytic biocrude from the PM mixture. Moreover, the use of a catalyst has increased ethylbenzene production in PM mixture biocrude rather than PS biocrude alone. Seshasayee et al. have speculated that the presence of PP in an equi-mass plastic mixture of PP, PET, PS, and PC(polycarbonate) might be responsible for higher cyclic aliphatics, and polycyclic aromatics in the HTL biocrude at 400 and 425°C reaction temperature [36]. In this study, both PP and PS were major constituents of PM mixtures. The high amount of ethylbenzene indicated that the decomposition of polystyrene might be the dominant reaction in the HTL

conversion of the PM mixture. Additionally, the RRM500 could be more active in PS decomposition in PM mixture than individual HTL reactions.

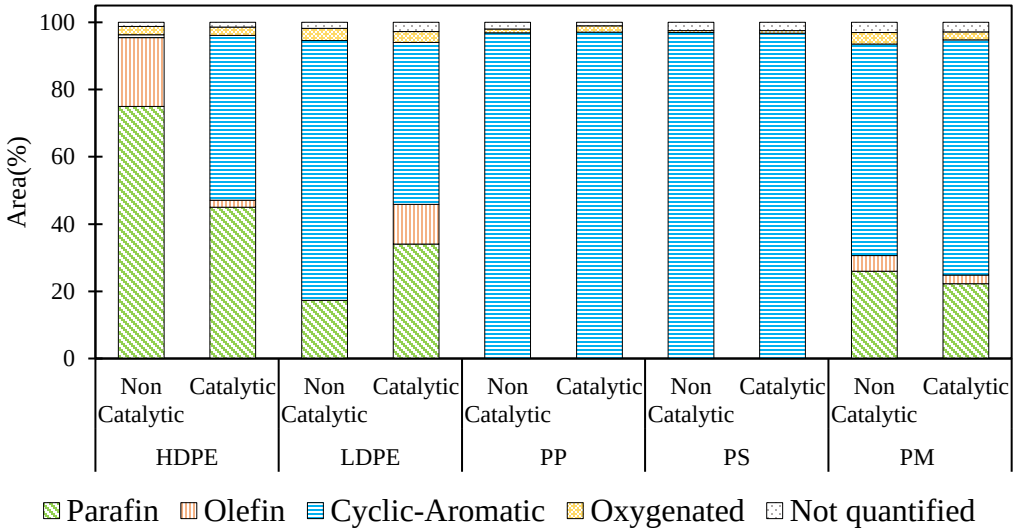

Figure 4.4: Chemical composition of plastic HTL biocrudes

4.3.3.3 Analysis of byproducts

Table 4.3 presents the three byproducts of this plastic HTL work. The aqueous products were characterized by probing total organic carbon (TOC), total nitrogen (TN), and pH. In single plastic non-catalytic criteria, the PET aqueous phase contained the maximum TOC concentration. The presence of PET in a plastic mixture significantly raised the TOC level in the aqueous products of the plastic mixture of PM. A similar trend was observed in the co-liquefaction study of pistachio hulls with PE, PP, and PET plastics, where an increased PET ratio in the mixture raised the TOC content of the HTL aqueous phase [51]. Except for HDPE, PET, and PP, the RRM500 catalyst has increased the carbon content of the aqueous phase from single plastic and two plastic mixtures. There was a sharp decline (almost four times reduction) in the TOC of PP aqueous products by RRM500. However, still, the PM aqueous phase possessed the maximum TOC of 10.70 g/L. The

TN level in the aqueous product was negligible as the plastic feedstocks do not have nitrogenated products. The non-catalytic aqueous products of PET, PP, and PS plastics have lower pH than other feedstocks of this study. Most probably, these plastics released some acidic compounds during the HTL reaction. There is a high chance PET was decomposed into terephthalic acid, and it reduced the pH of the water [38,52]. In general, the catalyst shifted the aqueous pH towards the basic side. Most probably, there was some leaching from the RRM500 catalyst, which raised the pH level of the aqueous product [53].

The solid residues or char by-products of plastic HTL were analyzed by elemental analysis. The elemental composition of PET-derived solids was also shown here. A sharp decline in carbon content was observed in non-catalytic char from PET, LDPE, and PM mixture compared to the carbon percentage of each feedstock. The carbon in solid products of no catalyst – PS reaction remained almost the same as PS plastic, but PP char obtained 8% more carbon than PP feedstock. The hydrogen content was relatively lower in every non-catalytic char product from single and mixture of plastic feedstocks. The RRM500 catalyst has suppressed the carbon content of the char by-products. It is noteworthy that the use of a catalyst almost doubled the ash and oxygen content of the solid residue in both individual and plastic mixtures. The increment of ash in char was also observed in our previous HTL work with an RRM500 catalyst [12].

In the gas product analysis, the mol fraction (mol%) of H_2, CO, CO_2, and CH_4 was presented. There was an expected rise in hydrogen production by the RRM500 catalyst. The gaseous product of PS plastic has the maximum hydrogen fraction of 12 mol%. The CO and CO_2 production were dramatically increased by the catalyst in PS gas products, but the gas yield was low (Figure 2). Therefore, the deoxygenation reaction did not occur for the PS biocrude.

Table 4.3: Byproducts of Plastic HTL

	Non-Catalytic						Catalytic					
	PET	HDPE	LDPE	PP	PS	PM	PET	HDPE	LDPE	PP	PS	PM
Aqueous Phase(g/L)												
TOC	4.97	1.02	1.96	3.14	0.90	8.12	6.98	0.95	2.45	0.81	1.06	10.70
TN	0.01	0.13	0.09	0.01	0.02	0.01	0.09	0.01	0.05	0	0.01	0.06
pH	4.43	8.01	8.07	3.72	3.97	4.71	4.98	8.28	7.76	8.49	6.91	4.86
Solid Residue(wt.%)												
C	46.7±1.5	82.2±1.0	21.5±0.2	93.6±0.3	93.2±0.2	59.6±0.0	42.2±0.9	76.5±1.1	14.7±0.5	11.8±0.8	65.3±1.5	36.7±0.4
H	5.5±0.2	10.5±0.3	0.1±0.1	4.2±0.2	5.0±0.2	2.3±0.2	3.8±0.1	11.8±0.3	2.1±0.0	3.5±1.0	2.4±0.1	1.6±0.1
S	0	0.1±0.0	0.1±0.0	0.1±0.0	0.1±0.0	0.1±0.0	0	0.1±0.0	0.2±0.0	0.2±0.1	0.2±0.1	0.4±0.1
Ash	10.5±0.3	5.1±0.5	77.5±0.2	1.3±0.1	0.3±0.0	30.8±2.1	12±0.1	7.3±0.4	79.5±1.5	81.2±1.0	26.7±1.2	48.4±2.6
O[a]	37.3±2.0	2.1±1.8	0.8±0.5	0.8±0.6	1.4±0.4	7.2±2.3	42±1.1	4.3±1.8	3.5±2.0	3.3±2.9	5.4±2.4	13.0±3.2
Gaseous Product(mol%)												
H_2	2.0±0.1	5.5±0.3	4.5±0.2	4.7±0.2	0.4±0.3	0.4±0.0	3.2±0.0	8.7±0.0	6.8±0.0	5.4±0.0	12.1±0.1	5.9±0.0
CO	40.2±0.2	80.6±0.3	65.7±0.4	92.6±1.2	1.4±1.1	7.6±0.2	44.0±0.6	88.6±0.1	67.0±0.1	91.1±0.2	49.4±0.3	54.6±0.0
CO_2	42.3±0.1	1.4±0.2	2.8±0.1	0.6±0.0	1.4±0.7	17.6±0.1	45.5±0.2	2.5±0.0	3.4±1.2	1.0±0.3	4.6±0.0	14.4±0.0
CH_4	0	0	0	0	0	0	0	0	0	0	0	1.2±0.0
Balance[a]	15.5±0.4	12.5±0.8	27.0±0.7	2.1±1.4	96.8±2.1	74.4±0.3	7.3±0.8	0.2±0.1	22.8±1.3	2.5±0.5	33.9±0.4	24.0±0.0

[a] by difference

4.3.4 Carbon distribution

Figure 4.5 shows the carbon distribution in plastic HTL products. The carbon recovery was calculated based on the elemental composition of the feedstock, biocrude, char, and total organic carbon (TOC) of the aqueous phase. Irrespective of catalyst and feedstock, the majority of carbon shifted towards biocrude products. HDPE crude oil has the maximum carbon transfer among other HTL products, whereas LDPE has the minimum one. In the case of PM mixture, 13wt.%, and 19wt.% carbon transferred to solid from PET and crude products, respectively. From yield analysis, both solid PET and biocrude products have the same yield, but their individual carbon content (Tables 4.2 and 4.3) made the real difference here. Among the non-catalytic aqueous phases, the PM has the maximum carbon recovery as TOC was higher. Most probably, the PET content of the mixture was responsible for this carbon transfer to aqueous products. The catalyst promoted the carbon transfer towards gaseous products(balance) rather than biocrudes in each

feedstock. This is another proof of a cracking reaction by the RRM500 catalyst. The high reaction temperature for catalytic HTL depolymerization of this study might be responsible for the further decomposition of plastic feedstocks and high gas (balance) production, which ultimately led to more carbon transfer towards gas products. The maximum carbon transfer towards gas (balance) took place in a catalytic PS-RRM500 experiment where carbon transfer increased by 20% in comparison with a non-catalytic PS reaction. This excess carbon toward gas was supported by the gas yield data (Table 4.3). In the case of PET, most of the carbon was deposited to solid fraction than gas as the solid yield was higher.

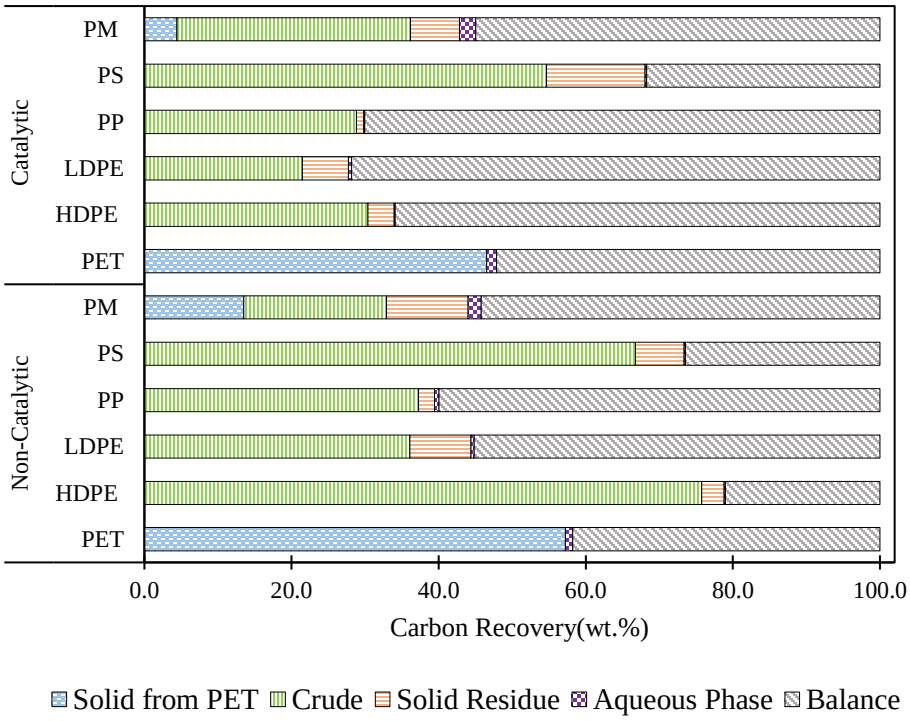

Figure 4.5**:** Carbon distribution in Plastic HTL products.

4.4 Conclusions

This work investigated the liquefaction of mixed plastic of polyethylene terephthalate (PET), high-density polyethylene (HDPE), low-density polyethylene (LDPE), polypropylene (PP), polystyrene (PS) plastics by supercritical water with reduced red mud (RRM500) catalyst. In individual plastic HTL treatment, the PET converted into a solid, whereas the HDPE produced a high crude yield (76wt.%). The liquefaction of simulated mixed plastic feedstock composed of PET (42wt.%), HDPE (20wt.%), LDPE (20wt.%), PP (4wt.%) and PS (14wt.%), generated 22wt.% liquid crude product along with 22wt.% solid from PET. The addition of catalyst repealed the crude and solid from PET production and induced low viscosity and acidity to crudes regardless of the reaction condition. The GC-MS analysis revealed that HDPE oil mainly consisted of paraffin compounds where PP and PS decomposed into aromatic or cyclic compounds. The RRM500 catalyst facilitated the paraffin formation in LDPE oils. Moreover, increased gasoline range low boiling products were recovered from catalytic plastic crudes by simulated distillation. The synergistic effect of the plastic mix was found in decreased char from PET production, where the utilization of catalysts in mixed feedstock accelerated liquid crude formation. The result of this plastic depolymerization study can be used to mitigate the plastic waste problem with energy-enriched liquid fuel production.

4.5 References

[1] A. Brems, J. Baeyens, R. Dewil, Recycling and recovery of post-consumer plastic solid waste in a European context, Thermal Science. 16 (2012) 669–685.

[2] D. Munir, Abdullah, F. Piepenbreier, M.R. Usman, Hydrocracking of a plastic mixture over various micro-mesoporous composite zeolites, Powder Technology. 316 (2017) 542–550. https://doi.org/10.1016/j.powtec.2017.01.037.

[3] P. Zhao, Z. Yuan, J. Zhang, X. Song, C. Wang, Q. Guo, A.J. Ragauskas, Supercritical water co-liquefaction of LLDPE and PP into oil: properties and synergy, Sustainable Energy Fuels. 5 (2021) 575–583. https://doi.org/10.1039/D0SE01486A.

[4] P. Biller, I. Johannsen, J.S. dos Passos, L.D.M. Ottosen, Primary sewage sludge filtration using biomass filter aids and subsequent hydrothermal co-liquefaction, Water Research. 130 (2018) 58–68. https://doi.org/10.1016/j.watres.2017.11.048.

[5] Y. Zhang, W.-T. Chen, 5 - Hydrothermal liquefaction of protein-containing feedstocks, in: L. Rosendahl (Ed.), Direct Thermochemical Liquefaction for Energy Applications, Woodhead Publishing, 2018: pp. 127–168. https://doi.org/10.1016/B978-0-08-101029-7.00004-7.

[6] X. Zhao, Y. Xia, L. Zhan, B. Xie, B. Gao, J. Wang, Hydrothermal treatment of e-waste plastics for tertiary recycling: Product slate and decomposition mechanisms, ACS Sustainable Chem. Eng. 7 (2019) 1464–1473. https://doi.org/10.1021/acssuschemeng.8b05147.

[7] S. Hongthong, H.S. Leese, M.J. Allen, C.J. Chuck, Assessing the conversion of various nylon polymers in the hydrothermal liquefaction of macroalgae, Environments. 8 (2021) 34. https://doi.org/10.3390/environments8040034.

[8] C.A. Poravou, N.I. Tsongidis, C. Lekkos, V.A. Zacharopoulou, A.G. Konstandopoulos, Valorization of Plastic Waste: A lab-scale approach with the aid of solar hydrothermal liquefaction technology, Waste Biomass Valor. 13 (2022) 3835–3844. https://doi.org/10.1007/s12649-022-01837-3.

[9] R.-X. Yang, K. Jan, C.-T. Chen, W.-T. Chen, K.C.-W. Wu, Thermochemical conversion of plastic waste into fuels, chemicals, and value-added materials: A critical review and outlooks, ChemSusChem. 15 (2022) e202200171. https://doi.org/10.1002/cssc.202200171.

[10] Y. Wu, H. Wang, H. Li, X. Han, M. Zhang, Y. Sun, X. Fan, R. Tu, Y. Zeng, C.C. Xu, X. Xu, Applications of catalysts in thermochemical conversion of biomass (pyrolysis, hydrothermal

liquefaction and gasification): A critical review, Renewable Energy. 196 (2022) 462–481. https://doi.org/10.1016/j.renene.2022.07.031.

[11] H. Jahromi, F.A. Agblevor, Hydrodeoxygenation of pinyon-juniper catalytic pyrolysis oil using red mud-supported nickel catalysts, Applied Catalysis B: Environmental. 236 (2018) 1–12. https://doi.org/10.1016/j.apcatb.2018.05.008.

[12] T. Rahman, H. Jahromi, P. Roy, S. Adhikari, E. Hassani, T.-S. Oh, Hydrothermal liquefaction of municipal sewage sludge: Effect of red mud catalyst in ethylene and inert ambiances, Energy Conversion and Management. 245 (2021) 114615. https://doi.org/10.1016/j.enconman.2021.114615.

[13] F. Cheng, G.A. Tompsett, C.M. Murphy, A.R. Maag, N. Carabillo, M. Bailey, J.J. Hemingway, C.I. Romo, A.D. Paulsen, P.E. Yelvington, M.T. Timko, Synergistic effects of inexpensive mixed metal oxides for catalytic hydrothermal liquefaction of food wastes, ACS Sustainable Chem. Eng. 8 (2020) 6877–6886. https://doi.org/10.1021/acssuschemeng.0c02059.

[14] W. Zhang, Y. Liang, Hydrothermal liquefaction of sewage sludge – effect of four reagents on relevant parameters related to biocrude and PFAS, Journal of Environmental Chemical Engineering. 10 (2022) 107092. https://doi.org/10.1016/j.jece.2021.107092.

[15] De Caprariis Benedetta, Damizia Martina, Tai Lingyu, De Filippis Paolo, Hydrothermal liquefaction of biomass using waste material as catalyst: Effect on the bio-crude yield and quality, Chemical Engineering Transactions. 92 (2022) 607–612. https://doi.org/10.3303/CET2292102.

[16] J.S. Saral, P. Ranganathan, Catalytic hydrothermal liquefaction of *Spirulina platensis* for biocrude production using red mud, Biomass Conv. Bioref. (2021). https://doi.org/10.1007/s13399-021-01447-4.

[17] A. López, I. de Marco, B.M. Caballero, M.F. Laresgoiti, A. Adrados, A. Aranzabal, Catalytic pyrolysis of plastic wastes with two different types of catalysts: ZSM-5 zeolite and Red Mud, Applied Catalysis B: Environmental. 104 (2011) 211–219. https://doi.org/10.1016/j.apcatb.2011.03.030.

[18] M. HM Ahmed, N. Batalha, Z.A. ALOthman, Y. Yamauchi, Y. Valentino Kaneti, M. Konarova, Transforming red mud into an efficient Acid-Base catalyst by hybridization with mesoporous ZSM-5 for Co-pyrolysis of biomass and plastics, Chemical Engineering Journal. 430 (2022) 132965. https://doi.org/10.1016/j.cej.2021.132965.

[19] J.A. Margolin, P.A. Marrone, M.A. Randel, W.R. Allmon, R.B. McLean, P.M. Bozoian, Test standards for contingency base waste-to-energy technologies:, Defense Technical Information Center, Fort Belvoir, VA, 2015. https://doi.org/10.21236/ADA623363.

[20] P. Roy, H. Jahromi, T. Rahman, S. Adhikari, F. Feyzbar-Khalkhali-Nejad, E. Barbary Hassan, T.-S. Oh, Understanding the effects of feedstock blending and catalyst support on hydrotreatment of algae HTL biocrude with non-edible vegetable oil, Energy Conversion and Management. 268 (2022) 115998. https://doi.org/10.1016/j.enconman.2022.115998.

[21] P. Roy, H. Jahromi, S. Adhikari, Y. Zou Finfrock, T. Rahman, Z. Ahmadi, M. Mahjouri-Samani, F. Feyzbar-Khalkhali-Nejad, T.-S. Oh, Performance of biochar assisted catalysts during hydroprocessing of non-edible vegetable oil: Effect of transition metal source on catalytic activity, Energy Conversion and Management. 252 (2022) 115131. https://doi.org/10.1016/j.enconman.2021.115131.

[22] K. Harun, S. Adhikari, H. Jahromi, Hydrogen production via thermocatalytic decomposition of methane using carbon-based catalysts, RSC Adv. 10 (2020) 40882–40893. https://doi.org/10.1039/D0RA07440C.

[23] K. Jin, P. Vozka, G. Kilaz, W.-T. Chen, N.-H.L. Wang, Conversion of polyethylene waste into clean fuels and waxes via hydrothermal processing (HTP), Fuel. 273 (2020) 117726. https://doi.org/10.1016/j.fuel.2020.117726.

[24] H. Jahromi, S. Adhikari, P. Roy, E. Hassani, C. Pope, T.-S. Oh, Y. Karki, Production of green transportation fuels from Brassica carinata oil: A comparative study of noble and transition metal catalysts, Fuel Processing Technology. 215 (2021) 106737. https://doi.org/10.1016/j.fuproc.2021.106737.

[25] H. Jahromi, T. Rahman, P. Roy, S. Adhikari, Hydrotreatment of solvent-extracted biocrude from hydrothermal liquefaction of municipal sewage sludge, Energy Conversion and Management. 263 (2022) 115719. https://doi.org/10.1016/j.enconman.2022.115719.

[26] H. Jahromi, S. Adhikari, P. Roy, M. Shelley, E. Hassani, T.-S. Oh, Synthesis of novel biolubricants from waste cooking oil and cyclic oxygenates through an integrated catalytic process, ACS Sustainable Chem. Eng. 9 (2021) 13424–13437. https://doi.org/10.1021/acssuschemeng.1c03523.

[27] H. Jahromi, F.A. Agblevor, Hydrodeoxygenation of aqueous-phase catalytic pyrolysis oil to liquid hydrocarbons using multifunctional nickel catalyst, Ind. Eng. Chem. Res. 57 (2018) 13257–13268. https://doi.org/10.1021/acs.iecr.8b02807.

[28] R. Shakya, J. Whelen, S. Adhikari, R. Mahadevan, S. Neupane, Effect of temperature and Na_2CO_3 catalyst on hydrothermal liquefaction of algae, Algal Research. 12 (2015) 80–90. https://doi.org/10.1016/j.algal.2015.08.006.

[29] S.S. Núñez, J. Moltó, J.A. Conesa, A. Fullana, Heavy metals, PAHs and POPs in recycled polyethylene samples of agricultural, post-commercial, post-industrial and post-consumer origin, Waste Management. 144 (2022) 113–121. https://doi.org/10.1016/j.wasman.2022.03.016.

[30] J.N. Hahladakis, C.A. Velis, R. Weber, E. Iacovidou, P. Purnell, An overview of chemical additives present in plastics: Migration, release, fate and environmental impact during their use, disposal and recycling, Journal of Hazardous Materials. 344 (2018) 179–199. https://doi.org/10.1016/j.jhazmat.2017.10.014.

[31] K. Kang, G. Loebsack, T. Sarchami, N.B. Klinghoffer, S. Papari, K.K.-C. Yeung, F. Berruti, Production of a bio-magnetic adsorbent via co-pyrolysis of pine wood waste and red mud, Waste Management. 149 (2022) 124–133. https://doi.org/10.1016/j.wasman.2022.06.009.

[32] M.S. Seshasayee, P.E. Savage, Oil from plastic via hydrothermal liquefaction: Production and characterization, Applied Energy. 278 (2020) 115673. https://doi.org/10.1016/j.apenergy.2020.115673.

[33] B.-Z. Wan, C.-Y. Kao, W.-H. Cheng, Kinetics of depolymerization of poly(ethylene terephthalate) in a potassium hydroxide solution, Ind. Eng. Chem. Res. 40 (2001) 509–514. https://doi.org/10.1021/ie0005304.

[34] Y. Liu, R. Naidu, Hidden values in bauxite residue (red mud): Recovery of metals, Waste Management. 34 (2014) 2662–2673. https://doi.org/10.1016/j.wasman.2014.09.003.

[35] Y. Liu, C. Lin, Y. Wu, Characterization of red mud derived from a combined Bayer Process and bauxite calcination method, Journal of Hazardous Materials. 146 (2007) 255–261. https://doi.org/10.1016/j.jhazmat.2006.12.015.

[36] M.S. Seshasayee, P.E. Savage, Synergistic interactions during hydrothermal liquefaction of plastics and biomolecules, Chemical Engineering Journal. 417 (2021) 129268. https://doi.org/10.1016/j.cej.2021.129268.

[37] M.H. mat Yasin, R. Mamat, A.F. Yusop, R. Rahim, A. Aziz, L.A. Shah, Fuel physical characteristics of biodiesel blend fuels with alcohol as additives, Procedia Engineering. 53 (2013) 701–706. https://doi.org/10.1016/j.proeng.2013.02.091.

[38] M. Goto, Chemical recycling of plastics using sub- and supercritical fluids, The Journal of Supercritical Fluids. 47 (2009) 500–507. https://doi.org/10.1016/j.supflu.2008.10.011.

[39] W. Shaoqing, X. Meili, W. Fang, L. Zhihe, Preparation of bio-oil by catalytic pyrolysis of corn stalks using red mud, International Journal of Agricultural and Biological Engineering. 9 (2016) 177–183. https://doi.org/10.25165/ijabe.v9i5.2214.

[40] A. Veses, M. Aznar, J.M. López, M.S. Callén, R. Murillo, T. García, Production of upgraded bio-oils by biomass catalytic pyrolysis in an auger reactor using low cost materials, Fuel. 141 (2015) 17–22. https://doi.org/10.1016/j.fuel.2014.10.044.

[41] Akpoveta, O. V, S.A. Osakwe, Determination of heavy metal content in refined petroleum products sold in Agbor metropolis, in: 33 Rd International Conference of The Chemical Society Of Nigeria. Kuto, 2010: p. 10.

[42] T. Moriya, H. Enomoto, Characteristics of polyethylene cracking in supercritical water compared to thermal cracking, Polymer Degradation and Stability. 65 (1999) 373–386. https://doi.org/10.1016/S0141-3910(99)00026-9.

[43] C.D. Collins, Implementing phytoremediation of petroleum hydrocarbons, in: N. Willey (Ed.), Phytoremediation: Methods and Reviews, Humana Press, Totowa, NJ, 2007: pp. 99–108. https://doi.org/10.1007/978-1-59745-098-0_8.

[44] A. Boddien, D. Mellmann, F. Gärtner, R. Jackstell, H. Junge, P.J. Dyson, G. Laurenczy, R. Ludwig, M. Beller, Efficient dehydrogenation of formic acid using an iron catalyst, Science. 333 (2011) 1733–1736. https://doi.org/10.1126/science.1206613.

[45] X. Lin, H. Lei, E. Huo, M. Qian, W. Mateo, Q. Zhang, Y. Zhao, C. Wang, E. Villota, Enhancing jet fuel range hydrocarbons production from catalytic co-pyrolysis of Douglas fir and low-density polyethylene over bifunctional activated carbon catalysts, Energy Conversion and Management. 211 (2020) 112757. https://doi.org/10.1016/j.enconman.2020.112757.

[46] M.H.M. Ahmed, N. Batalha, T. Qiu, M.M. Hasan, L. Atanda, N. Amiralian, L. Wang, H. Peng, M. Konarova, Red-mud based porous nanocatalysts for valorisation of municipal solid waste, Journal of Hazardous Materials. 396 (2020) 122711. https://doi.org/10.1016/j.jhazmat.2020.122711.

[47] W.-T. Chen, K. Jin, N.-H. Linda Wang, Use of supercritical water for the liquefaction of polypropylene into oil, ACS Sustainable Chem. Eng. 7 (2019) 3749–3758. https://doi.org/10.1021/acssuschemeng.8b03841.

[48] P.T. Williams, E. Slaney, Analysis of products from the pyrolysis and liquefaction of single plastics and waste plastic mixtures, Resources, Conservation and Recycling. 51 (2007) 754–769. https://doi.org/10.1016/j.resconrec.2006.12.002.

[49] H.-Y. Shin, S.-Y. Bae, Thermal decomposition of polystyrene in supercritical methanol, Journal of Applied Polymer Science. 108 (2008) 3467–3472. https://doi.org/10.1002/app.27960.

[50] J.A. Onwudili, N. Insura, P.T. Williams, Composition of products from the pyrolysis of polyethylene and polystyrene in a closed batch reactor: Effects of temperature and residence time, Journal of Analytical and Applied Pyrolysis. 86 (2009) 293–303. https://doi.org/10.1016/j.jaap.2009.07.008.

[51] S. Hongthong, S. Raikova, H.S. Leese, C.J. Chuck, Co-processing of common plastics with pistachio hulls via hydrothermal liquefaction, Waste Management. 102 (2020) 351–361. https://doi.org/10.1016/j.wasman.2019.11.003.

[52] J.S. dos Passos, M. Glasius, P. Biller, Screening of common synthetic polymers for depolymerization by subcritical hydrothermal liquefaction, Process Safety and Environmental Protection. 139 (2020) 371–379. https://doi.org/10.1016/j.psep.2020.04.040.

[53] M. Czop, J. Motyka, O. Sracek, M. Szuwarzyński, Geochemistry of the hyperalkaline Gorka Pit Lake (pH > 13) in the Chrzanow Region, Southern Poland, Water Air Soil Pollut. 214 (2011) 423–434. https://doi.org/10.1007/s11270-010-0433-x.

Chapter 5

Hydrothermal liquefaction of southern yellow pine

Abstract

In this study, pine sawdust was liquefied using a water and water-ethanol mixture at 250, 300, and 350℃ reaction temperatures via hydrothermal liquefaction (HTL) process. Metallic iron (Fe) powder was added to the HTL system to evaluate its catalytic effects. Increasing the ethanol concentration increased biocrude yield regardless of reaction temperature. The equal ethanol and water (1:1, wt./wt.) mixture produced a maximum of 34 wt.% biocrude yields (on a dry basis) at 300℃. The effect of reaction temperature was prominent in pure water medium where biocrude yield followed this trend: 250℃<300℃<350℃. The maximum biocrude yield from the water medium was 18wt.%, obtained at 350℃. The iron catalyst promoted biocrude production within the water at studied reaction temperatures. The highest catalytic biocrude yield of 27wt.% was found at 300℃ in the water reaction medium. The oxygen content and acidity of the pine biocrudes significantly declined with the iron catalyst in the water-ethanol reaction medium. The pine HTL biocrudes were mainly composed of phenolic and acidic compounds. The ethanol converted acids to esters while the catalyst promoted esterification during liquefaction. This study showed the potential of ethanol and cheap iron catalyst for enhanced biocrude yield with improved properties from pine feedstock.

Keywords: Pine sawdust, Hydrothermal liquefaction, Iron catalyst, Ethanol co-solvent

5.1 Introduction

Lignocellulosic biomass is a green and abundant resource to produce energy and chemicals. Mother nature takes millions of years to convert this abundant resource into fossil fuel [1]. The thermochemical processes can produce the equivalent energy within a few seconds to a few hours by converting lignocellulosic biomass into value-added products. Among different thermochemical technologies, hydrothermal liquefaction (HTL) is a prominent method for producing biofuels and bio-based chemicals from lignocellulosic feedstock. HTL process converts biomass feedstock into liquid biocrude, gas, and solid products using subcritical or supercritical water or other solvents at elevated temperature (250–370℃) and pressure (2–24 MPa) [2]. The most important fact of the HTL process is that the feedstock does not require any pre-drying step, and the debris-free lignocellulosic biomass can be used just after washing [3]. Techno-economic analysis has proved that carbon-neutral HTL biocrude has a significant potential for commercialization [1]. Recently, HTL conversion of wood feedstock has been extensively studied, where product yields varied with process parameters such as temperature, pressure, residence time, type of biomass, and biomass-to-solvent ratio. In general, the molecular structure of biomass is more complex than other feedstock of first-generation biofuels [4]. Therefore, using suitable catalysts to improve biocrude yields and quality has gained worldwide attention. Three broad categories of heterogeneous catalysts for biomass HTL conversion process are redox metals or acidic metal oxides (e.g., CeO2, ZrO_2, Fe and Cu based), noble metals (e.g., Pd, Pt, Ru based), and non-noble metals (e.g., all other transition metals) [5]. Wu et al. performed catalytic hydrothermal liquefaction of eucalyptus in the presence of NaOH, KOH, and Pd/C catalysts at 260 and 300℃. They have mentioned that alkali catalysts (NaOH, KOH) enhanced the gaseous products at higher temperatures (300℃), where the same catalysts increased the biocrude yields from 32.5-61.2% at

260℃ [6]. Maldonado et al. have utilized a mixture of Ni–Mo nitrides and carbides catalyst (Mo_2C–Ni_2Mo_3N) doped with nickel in HTL conversion of pretreated pine chip and generated reduced solid char and an increased gaseous product with higher nickel amount. They recovered a maximum of 80.41% liquid and 6.43% solid char from pine feedstock at optimal 10% nickel loading [4]. Tekin et al. have performed HTL treatment of Scotch pine using sodium perborate monohydrate ($NaBO_3 \cdot H_2O$) and observed enhanced biocrude yield (~35-40%) from Scotch pine wood with significantly lower solid residue yields(12-15%) at 300 and 350 °C [7]. Alper et al. have studied the influence of a Lewis acid ($Mg(ClO_4)_2$), Brønsted acid($HClO_4$), and their combined use ($HClO_4$/$Mg(ClO_4)_2$) over the HTL of teak wood. Although higher $Mg(ClO_4)_2$ loading improved the teak HTL biocrude property by deoxygenation reaction,the increasing ratio of $Mg(ClO_4)_2$, $HClO_4$, and $HClO_4$/$Mg(ClO_4)_2$ catalysts in general suppressed biocrude formation[8].

The catalysts decompose large biomass molecular chains at high temperatures in HTL reactors, but the production costs of biocrude can be higher depending on the catalyst materials [4]. Iron (Fe) based redox catalysts are low cost and well known for in situ hydrogen production in water medium by oxidation of Fe into Fe_3O_4 while the released hydrogen can take part in the hydrogenation of reactive chemical species during HTL reaction. Moreover, the iron (Fe) based catalysts can be easily regenerated because of their fast oxidation–reduction kinetics properties [5,9]. Several researchers have explored the role of iron-based catalysts in the wood HTL process. Capariis et al. have studied the HTL process of oak wood biomass with 10wt.% iron powder catalyst (Fe, Fe_3O_4, Fe_2O_3) loading at 260–320 °C reaction temperature. It was found that the zerovalent Fe maximized oak biocrude production with a 40% yield, whereas the oxidized Fe (Fe_3O_4, Fe_2O_3) led to a minor improvement in the biocrude generation [9]. The zerovalent Fe was

utilized in catalytic HTL of lignocellulosic palm oil fruit bunch, which promoted biocrude oil yield by 2-25% with increasing solvent(water) to biomass ratio [10]. The choice of solvents has a great impact on the biocrude yield and chemical composition [11]. Yuan et al. have concluded from a rice straw HTL study that the ethanol co-solvent can act as a hydrogen donor solvent and might stabilize the highly reactive free radicals of HTL products [12]. Cheng et al. have found that the co-solvent of 50 wt. % ethanol with water, significantly raised the eastern white pine-derived biocrude yield(up to 65wt.%) at 300 °C for 15 min than those in a mono-solvent of alcohol or water [13]. Several researchers investigated the role of Fe-based catalysts in the ethanol-water mixture. Wu et al. have introduced Fe_x-$Co_{(1-x)/}Al_2O_3$ catalyst to HTL conversion of poplar biomass within water along with low-content (10%) ethanol co-solvent. They found that the catalyst significantly increased the biocrude yield and energy recovery rate with lower oxygen and diverse lignin-derived phenolic compounds. The highest biocrude yield from poplar was 67.35% with 60Fe-40Co/Al2O3 catalyst at 260 °C reaction temperature [14]. Hassan et al. have employed ethanol and water mixture in HTL conversion of giant miscanthus (Miscanthus giganteus) perennial feedstock where 1:1 water-ethanol mixture at 280℃ temperature with 15 min residence time was the optimum condition to produce a maximum 51% of biocrude yield [15].

This study has focused on the HTL conversion of southern yellow pine biomass in different water-ethanol mixtures with fixed pure iron powder catalyst loading at the varying reaction temperature. The chosen lignocellulosic feedstock was the southern yellow pine, one of the most common tree species in the southeastern United States of America. According to the U.S. Forest Service surveys, loblolly pine is the second-most common tree species in the United States, after red maple [16]. Our previous studies evaluated non-catalytic HTL decomposition of bark and leaf-free loblolly

pine wood chips and southern yellow pine planer shavings in water-ethanol solvent (1/1, wt./wt.) at different reaction temperatures [17,18]. This work investigates the influence of zerovalent Fe catalyst over the HTL reaction of southern yellow pine at 250, 300, and 350℃ temperatures in only water and a 1:1 (wt./wt.) water-ethanol mixture. This work provides important information on the synergistic effects of hydrogen donor solvent and hydrogen-producing catalyst over HTL conversion of lignocellulosic biomass.

5.2 Materials and methods

5.2.1 Material

The hammermilled pine sawdust were collected from local timber plants of Alabama. The as received pine dust was sieved to maintain 106-595 μm particle size. The 200-proof ethanol and the zero valent iron (Fe) were bought from Sigma Aldrich. The pure nitrogen gas was supplied by Airgas Inc. (Opelika, Alabama, USA).

5.2.2 Feedstock characterization

The pine sawdust was analyzed for ultimate, proximate, and biochemical composition (hemicellulose, cellulose, and lignin) analyses. The feedstock characterization is presented in Table D1 (Appendix D). The elemental analysis (CHNS/O) was performed according to the ASTM D5373-02 method in the Vario MICRO cube, Elementar (New York, USA) [19]. The ash content was quantified using ASTM E1755 method, and volatile matter content was obtained according to ASTM E872. For biochemical composition analysis, pine samples were sent to the Agricultural and Environmental Science Laboratory (University of Georgia, Athens, USA). The detergent fiber analyses developed by Van Soest and Wine were followed to determine the hemicellulose, cellulose, and lignin content of biomass [20–22]. In this procedure, neutral detergent fiber (NDF) and acid detergent fiber (ADF) of the biomass were determined at the initial step. The neutral

detergent fiber (NDF) is the residue remaining after digesting the sample in a neutral detergent solution, predominantly hemicelluloses, cellulose, and lignin. The acid detergent fiber (ADF) is the residue remaining after digesting the sample with an acid detergent solution composed of cellulose and lignin. The analyses of NDF and ADF were carried out on an Ankom Fiber Analyzer (ANKOM Technology, NY) using F57 filter bags (ANKOM Technology, NY). The contents of hemicellulose and cellulose were estimated from NDF, ADF, lignin, and ash, as shown in Equations 1 and 2.

$$\%\text{Hemicellulose} = \%\text{NDF} - \%\text{ADF} \quad (1)$$

$$\%\text{Cellulose} = \%\text{ADF} - (\%\text{Lignin} + \%\text{Ash}) \quad (2)$$

5.2.3 Catalyst characterization

The pure iron was characterized by X-ray diffraction (XRD) techniques. The methodology of XRD analysis was discussed in our previous work [23]. Briefly, a bench-top powder X-ray diffraction system (AXRD, Proto Manufacturing, Taylor, Michigan, USA) was utilized from 20° to 100º (2θ) with 2 seconds of dwell time and 0.014° of Δ2Θ at 30 mA and 40 kV with CuKα radiation (λ = 1.5418 Å). The XRD peaks at a 2Θ value of 44.9° and additional peaks at 65.22°, and 82.50° (Figure D1) confirmed zero valent state of iron [24,25].No iron oxide peak was detected.

5.2.4 Experimental setup and procedure

A high-pressure, high-temperature reactor from Parr Instrument Company (Model 4578, Moline, Illinois, USA) was used for HTL experiments of the plastics. Details of the reactor setup was discussed in our previous work [26]. The reactor has 1.8 L vessel, PID controlled electrical heating unit, controllable agitator, pressure gauge, and J-type thermocouple to monitor the temperature inside the reactor. The HTL experiments were performed at 250℃,300℃ and 350℃ reaction temperature. The HTL reaction kept at desired temperature for 30 min. For HTL experiment 50

g of pine sawdust was loaded into the reactor with feedstock and solvent ratio of 1:15. The mixed solvents of water and ethanol were prepared on weight basis such as 50g water was mixed with 50 g of ethanol for 1:1(wt./wt.) water-ethanol mixture. For all catalytic HTL experiments, catalyst: feedstock loading was fixed at 1:10 i.e., ~5 g catalyst per 50 g as-received pine feedstock. The reactor was purged with inert gas (nitrogen) three times to remove air from the reactor headspace before pressurizing with it to an initial pressure of 200 psi (0.62 MPa) in pure water medium. In case of high temperature (350°C), no initial pressure was applied and feedstock-solvent ratio was identical (1:15) with reduced loading such as 15g of pine feedstock with 225g of solvent. The agitator speed was kept at 550 rpm for all experiments. After 30 min heating at desired temperature, the heater was removed, and the reactor was cooled to room temperature by electrical fan and ice bath. The products (gas, solid, aqueous phase, and biocrude) were separated as described in Section 5.2.5 All experiments were performed in duplicates.

5.2.5 Product separation

After cooling the reactor to room temperature, the gas was vented followed by the gas analysis and the reactor was opened to recover the liquid and solid products. The content in the reactor was poured into a large flask, and the weight was recorded. Then, the reactor content was filtered through Whatman No.50 filter paper (particle filtration size of 2.7 μm) to separate the solid from liquid phase. Then the remaining solids on the filter paper were washed with dichloromethane (DCM). The DCM was separated from the organics using an IKA rotary evaporator at 65°C and 700 mbar vacuum pressure to obtain DCM extracted organic phase. The weight of all liquids (aqueous and organic phases) was recorded for mass balance. The DCM extracted organic phases were termed as “biocrude oil” throughout the paper.

5.2.6 Product analysis

A micro-GC (Agilent 3000A) was used to analyzed gaseous products. The details of micro-GC was discussed elsewhere [26]. Briefly, the Agilent 3000 A Micro GC is equipped with three modules alongside thermal conductivity detector: a 10 m Molsieve 5A (MS) column and two 10 m porous polymer (PPU) columns. The sample could be split into three streams to go one of these modules. MS column analyzed hydrogen, methane, and carbon monoxide, while carbon dioxide and ethylene hydrocarbons were analyzed on the PPU columns simultaneously. Argon and helium were used as carrier gases for MS column and PPU column, respectively. The gas composition analysis was performed in triplicates.

The mass of the gaseous product was calculated by using Equation 3

$$W_g = \sum x_i . MW_i . n_{tot} \qquad (3)$$

where W_g is the total mass of gaseous product (g), x_i is the mole fraction of gas i, MW_i is the molecular weight of gas i (g/mole), and n_{tot} is the total number of moles of gas product.

The yield of biocrude and solid product were calculated on dry-ash free basis using Equations 4 and 5, respectively [27]. The remaining product fraction was regarded as "balance" and calculated using Equation 6.

$$Y_{biocrude}(\%) = \frac{w_b}{w_f - w_m - w_a} \times 100 \qquad (4)$$

$$Y_{solid}(\%) = \frac{w_s - w_c}{w_f - w_m - w_a} \times 100 \qquad (5)$$

$$Y_{balance}(\%) = 100 - Y_{biocrude} - Y_{solid} \qquad (6)$$

where w_f is the mass of pine feedstock (g), w_m and w_a are the mass of moisture and ash content of feedstock (g), respectively, w_b is the mass of the biocrude product (g), w_s is the weight of total solid residues (g), and w_c is the weight of catalyst (g).

The elemental analysis was performed on each sample using an elemental analyzer (Vario MICRO, Elementar, New York, USA) according to ASTM D5373-02. Effects and interactions of reaction mediums,temperatures on biocrude yield was analyzed by the two-way analysis of variance (ANOVA) at 0.05 significance level,using statistical programming software R [28]. The higher heating value (HHV) of pine biocrudes was determined using a unified correlation (Equation 7) based on elemental analysis, proposed by Channiwala et al.

$$HHV = 0.3491*C+1.1783*H+0.1005*S-0.1034*O-0.015*N-0.0211*A \quad (7)$$

where, C, H, O, N, S and A represents carbon, hydrogen, oxygen, nitrogen, sulfur, and ash contents of material, respectively, expressed in mass percentages on dry basis [29].

The total acid number (TAN) of each sample was determined through titration according to ASTM D664-07 using a Mettler Toledo T50 Titrator. Thermogravimetric analysis (TGA) of biocrude was performed by using a Shimadzu TGA-50 (Shimadzu, Japan) under nitrogen atmosphere (flow rate:20 ml/min) with heating rate of 10 °C/min from room temperature up to 800 °C [30]. The chemical composition of biocrude samples was analyzed by an Agilent Technologies 7890A Gas Chromatograph (GC) System outfitted with a 7683B Series Injector and 5975C Inert Mass Selective Detector (MSD) with Triple-Axis Detector. The details of GC-MS instrument were reported elsewhere [30]. In a brief, 30 m × 250 μm × 0.25 μm DB-35MS column was used in GC-MS to analyze the product. During analysis, the GC oven was heated to an initial temperature of 50 °C and held for 2 min and then ramped at a heating rate of 5 °C/min to a final temperature of 280 °C and holding time of 15 min. The chemical structures identified by the National Institute of Standards and Technology (NIST) MS Library of the GC–MS were then grouped into acids, phenols, alcohol, ester, aliphatic and others. The compounds were then semi-quantified based on their peak area percent. The pine biocrudes were analyzed by electrospray ionization- mass

spectroscopy (ESI-MS,m/z 90-2000) on a Bio-oil samples (1 mg)were dissolved in methanol containing 1% acetic acid (1 mL) and directly analyzed in both positive and negative ion electrospray ionization–mass spectrometry (ESI–MS, m/z 90–2000) on a Finnigan LCQ-Deca instrument (Thermoquest, San Jose, CA). The detailed procedure reported elsewhere [31]. Briefly ,1mg of biocrude samples were diluted by methanol with 1% acetic acid (1ml) and analyzed by positive and negative ESI-MS at a flowrate of 10μL/min. The number average molar mass (Mn) and weight average molar mass(Mw) was calculated by Equation 8 and 9, respectively.

$$M_n = \sum M_i N_i / \sum N_i \qquad (8)$$

$$M_w = \sum M_i^2 N_i / \sum M_i N_i \qquad (9)$$

The aqueous phase was analyzed for total organic carbon (TOC), total nitrogen (TN)and pH. The TOC and TN were measured by a TOC/TN analyzer (TOC-L, Shimadzu, Kyoto, Japan). The pH of the solution was measured using a pH meter (pH510, Oakton, Vernon Hills, Illinois, USA).

5.3 Results and discussion

5.3.1 HTL products characterization

5.3.1.1 Products yield distribution

Effect of Reaction Temperature

Figure 5.1 shows the HTL product distribution of pine feedstocks on a dry basis. The effects of reaction temperature on pine HTL products in varying ethanol concentrations of water-ethanol mixtures are depicted in Figure 5.1-A. It was evident that the increased reaction temperature promoted biocrude with the lower solid formation and increased gas in the water reaction medium from pine feedstock. The HTL conversion in water resulted in a maximum of 18 wt.% biocrude yield at 350℃ reaction temperature. The pine biocrude production in water followed this trend: 250℃<300℃<350℃. The biocrude yields were within range of other reports on pine HTL work.

In separate studies, Hu et al. and Wang et al. have recovered 11.35 and 12 wt.% biocrude yield, respectively, from pine feedstock in pure water medium at 300℃ and [32,33]. Hardi et al. have mentioned improved pine biomass conversion with the increase in the reaction temperature [34]. The solid yield in a water medium confirmed that the reaction temperature of 250℃ was not enough to depolymerize pine biomass, where the majority of pine decomposed at 350°C [35].

Regardless of reaction temperature, the trace of ethanol in the reaction medium has brought a dramatic change in HTL product distribution. The increasing ethanol concentration facilitated more biocrude formation, suppressed the solid products, and also produced more gas. At a reaction temperature of 250℃, the water-ethanol equal mass mixture enhanced biocrude yield by almost 60% and suppressed the solid formation by 26% compared to the biocrude products from the water medium. The biocrude yield using a 1:1 water-ethanol mixture at 300℃ was 34 wt.% with only 5.4 wt.% char yield. The biocrude enhancement by 1:1 (wt./wt.) water-ethanol mixture was statistically significant. The maximization of pine biocrude yield under (1:1, wt./wt.) water-ethanol mixture at a reaction temperature of 300℃ was also observed in other pine HTL reports [17,32,36]. It was found that ethanol donated hydrogen in the HTL system, which stabilized the pine-derived free radicals by repealing the recombination of free radicals into solid char [37]. The HTL product distribution of pine in a water-ethanol reaction medium ranging from 0 to 100% ethanol was shown in the supplementary material (Figure D2). The ethanol addition suppressed the solid production remarkably up to 50 wt.% ethanol concentration. The solid yield from a single reaction medium (only water or only ethanol) was almost identical. Liu et al. explained this low solid product in a mixed reaction medium as a synergistic effect of a water-ethanol mixture. Besides hydrogen donation, the water-ethanol mixture could dissolve more oily or high molecular products at subcritical conditions and thus promote biocrude production and suppress char formation [38].

However, the maximum biocrude yield (38wt.%) was derived from 100 wt.% ethanol reaction medium at 300℃ (Figure D2). Cheng et al. produced a similar biocrude yield (~42wt.%) from pine sawdust at 300℃ using ethanol [39]. The lower dielectric constant, critical temperature, and pressure of ethanol could accelerate biomass degradation and result in more biocrude than water medium [40]. The increasing ethanol concentration in the water-ethanol mixture led to more gas and solid production at 350℃ reaction temperature. The elevated reaction temperature might promote pine decomposition via condensations or cracking reactions which could transform the biocrude products or intermediates into gas and char [13].

Effect of catalyst

The effect of the iron catalyst was shown in Figure 5.1-B and 5.1-C in water and water-ethanol (1:1, wt./wt.) mixture, respectively. The addition of iron powder to pine HTL conversion has enhanced biocrude formation significantly in pure water (Figure 5.1-B). The maximum catalytic pine biocrude yield was 27 wt.%, obtained at 300℃. Zhao et al. reported a pine biocrude yield of 36 wt.% at the same reaction temperature and catalyst loading. The authors described the metallic Fe as a reducing agent and hydrogen donor in the HTL system. In the presence of water, Fe produced hydrogen, which might react with pine HTL intermediates during the HTL process and increase biocrude production [41]. The catalytic biocrude yield from the water was raised by increasing reaction temperature, where the highest biocrude yield was 29 wt.% at 350℃. However, the catalyst slightly (4-13%) reduced the biocrude formation and promoted more gas products in mixed solvents compared to pure water medium (Figure 5.1-C). In a separate study, Zhao et al. liquefied cornstalk in a water-ethanol (1:1,v/v) mixture with metallic Fe at 300℃ and found that the biocrude yield was significantly enhanced by the Fe addition with much lower char yield [42]. In this study, iron catalyst did not show such an effect over pine biocrude yield in a water-ethanol

mixture regardless of reaction temperature. The use of a higher biocrude extraction temperature (35℃ higher) in the current study to ensure the removal of ethanol and DCM could be a probable reason for lower biocrudes yield. The iron catalyst also suppressed biocrude formation in pure ethanol medium and increased the char yield (Figure D3). The absence of water might affect the catalytic activity of the iron catalyst in a pure ethanol medium. However, the reduced catalytic char yield was found by increasing reaction temperature in both water and water-ethanol medium. Generally, the reactivity of iron (Fe) in HTL conditions increased with higher reaction temperature, which promoted hydrogen production and limited the char formation [9]. It is notable that the solid amount gradually decreased by elevated temperature in the water-ethanol mixture. The combined effect of iron reactivity in higher temperatures and hydrogen donation by ethanol might be responsible for lower solid char formation in a water-ethanol mixed medium.

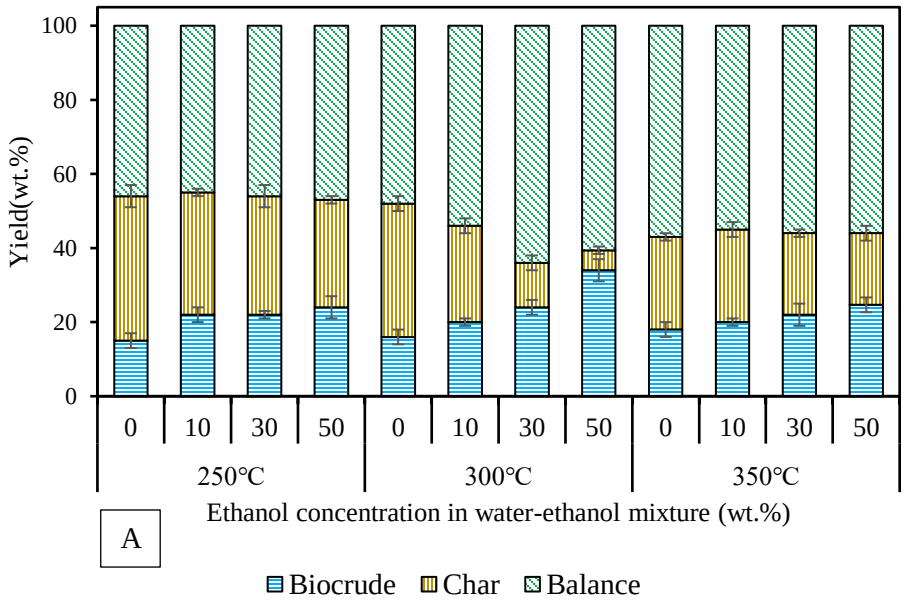

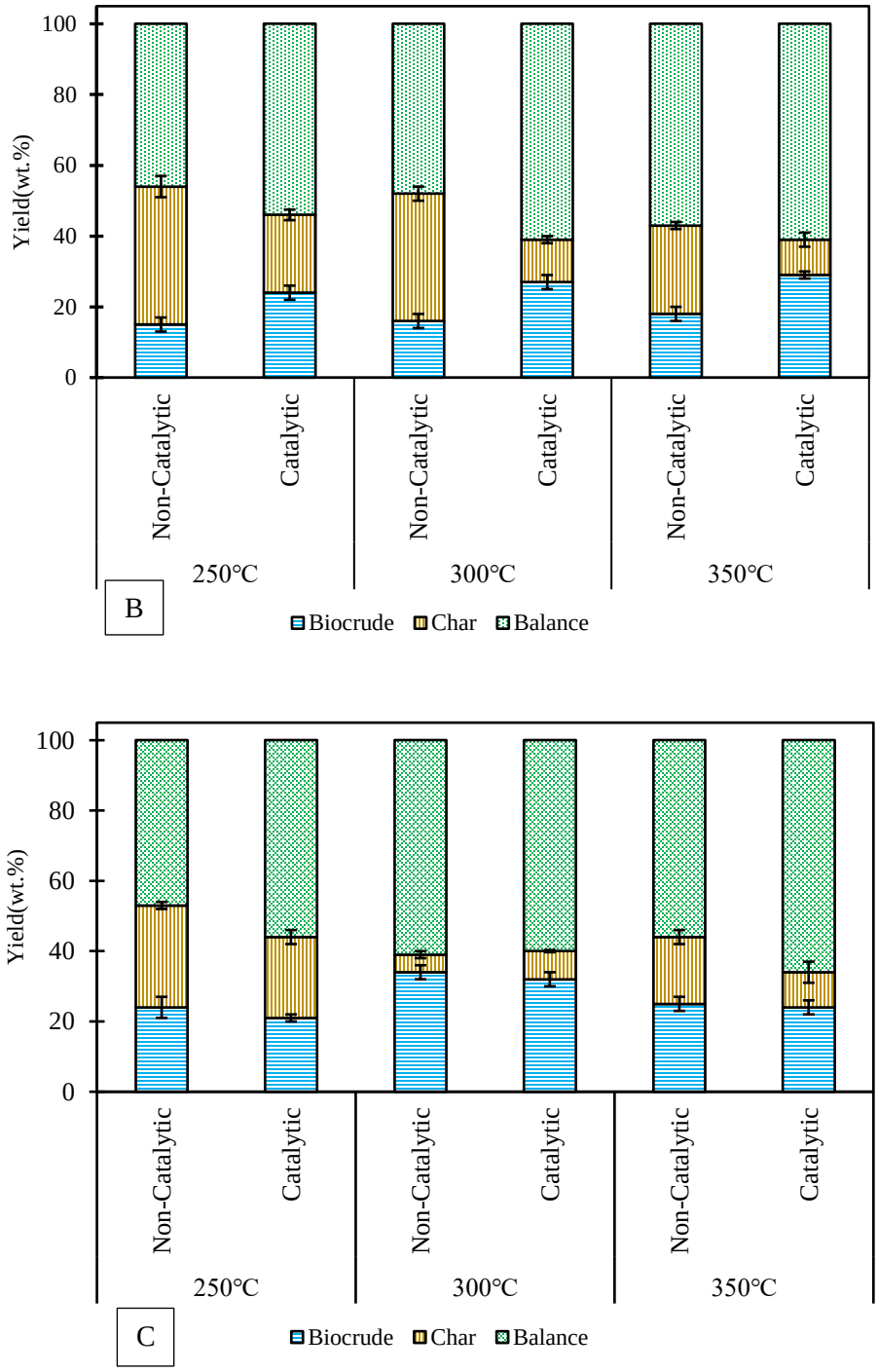

Figure 5.1: Products yield distribution in Pine HTL: A- Influence of reaction temperatures and ethanol concentration without catalyst , in B- Effect of iron catalyst at various temperatures using pure water medium and C- Effects of iron catalyst and temperatures using 1:1 (wt./wt.) water-ethanol medium

5.3.1.2 Biocrude characterization

Physicochemical properties

Table 5.1 shows the physicochemical properties of pine-derived HTL biocrude products with increasing ethanol concentration in water-ethanol mixtures under varying reaction temperatures and catalytic conditions. It is evident that the carbon content of the biocrudes is enhanced by the higher reaction temperature in pure water regardless of catalytic conditions. As a result, the lower oxygen content with increased HHV was found in the biocrudes with increasing reaction temperatures. In water, the carbon content of 73.7 wt.% was obtained at 350℃ by non-catalytic reaction where iron slightly raised the carbon concentration to 75.1 wt.%. The enhanced carbon with lower oxygen and subsequent high HHV in the biocrude from the increasing liquefaction temperature was also found in the HTL conversion of pine, hay, oak wood, walnut shell, and cellulose [35,43]. The greatly reduced oxygen content in the pine HTL biocrudes with the increasing temperature in the range of 250–350 ℃ could be attributed to the dehydration reactions along with CO or CO_2 formation during the liquefaction process, which will be discussed in the gaseous product section [44]. The catalyst did not bring much change in carbon, oxygen, and HHV of biocrudes produced from 250℃ and 300℃ within a pure water reaction medium.

The acidity was also affected by reaction temperatures. The reaction temperature of 350℃ reduced total acid number (TAN) by 51% in comparison with a lower reaction temperature (250℃). The reduction of biocrude TAN by enhanced reaction temperature was also found in algae HTL conversion. The organic acid influences the TAN value of biocrudes [45]. The evidence could be found in the chemical composition (GC-MS) analysis of the pine biocrudes.

The increasing ethanol concentration in the water-ethanol mixture suppressed the carbon content of biocrudes in three reaction temperatures. Therefore, a higher oxygen content with reduced HHV was found in the biocrude products from water-ethanol mediums. The higher oxygen content of pine HTL biocrude by water-ethanol co-solvent was also observed in the previous literature [32]. It suggested the formation of oxygenated compounds within water-ethanol mixtures. It also could be the result of competition between hydrogen donor reduction of oxygen and CO–CO_2 reduction of oxygen [44]. The increasing ethanol concentration in water-ethanol co-solvent has raised the oxygen content in pine HTL biocrudes. In the presence of ethanol, the oxygen of feedstock could be transformed into CO or CO_2 rather than water and suppress the carbon content [46]. The increasing gas yield ("balance" in Figure 5.1) was another proof of higher CO or CO_2 formation from water/ethanol mixtures. The high gas formation might be responsible for the minimum carbon content of the pine biocrude from 1:1(wt./wt.) water-ethanol mixed medium at 300℃. The effect of the reaction temperature in the water-ethanol mixture was similar to the water medium, and high temperature shifted more carbon towards biocrudes. The maximum carbon of 74.8 wt.% was observed within 10/90 (wt./wt.) ethanol/water mixture at 350℃. The biocrude products from only ethanol (Table D1) have increased carbon concentration with subsequent oxygen reduction. The decrement of oxygen contents in sludge HTL biocrudes obtained from the higher ethanol ratios run (7/3 and pure ethanol) was observed elsewhere. The abundance of ethanol could promote the hydrogen-donor reduction of oxygen and suppress the CO–CO_2 reduction of oxygen [44]. The lower gas fraction (others in FigureD1) from pure ethanol also supported this theory.

The incorporation of an iron catalyst increased the carbon content of biocrudes leading to a corresponding reduction in oxygen in both pure water and water-ethanol mixtures. The HHV was raised by 2-18% throughout the temperature range of 250-350℃ with the addition of Fe. Higher

HHV with metallic Fe when compared with non-catalytic products, suggesting that the in-situ hydrogen generated from metallic Fe could improve the bio-oil quality via hydro treatment. The catalyst remarkably reduced the TAN value within the water-ethanol reaction medium by increasing reaction temperatures. The iron might provide excess hydrogen by reacting with water and accelerate the esterification process by ethanol of the reaction medium. The TAN value of catalytic biocrudes from 300℃ reaction temperature (Table D1) followed this trend: water<ethanol<water-ethanol mixture. It suggested that acid neutralization by iron catalyst required both water and ethanol.

Table 5.1: Physicochemical properties of pine HTL Biocrudes

			Elemental Composition(wt.%)					
	Reaction Temperature (℃)	Ethanol (wt.%)	C	H	Ash	O[a]	HHV (MJ/Kg)	TAN (mgKOH/g)
Non -Catalytic Reaction	250℃	0	65.1±0.0	6.2±0.0	0.4±0.3	28.3±0.3	27.1±0.1	59.3±1.5
		10	65.3±0.4	6.0±0.0	0.3±0.2	28.4±0.6	26.9±0.2	51.4±1.9
		30	60.5±0.3	6.5±0.1	0.4±0.1	32.6±0.5	25.4±0.3	48.4±4.9
		50	60.3±1.3	6.8±0.6	0.4±0.1	32.5±2.0	25.7±1.4	24.5±2.0
	300℃	0	66.0±0.0	6.0±0.1	0.5±0.2	27.5±0.3	27.2±0.1	45.3±2.2
		10	65.7±0.1	6.0±0.0	0.4±0.2	27.2±0.3	28.0±0.1	40.2±2.2
		30	63.8±0.3	6.7±0.0	0.5±0.2	29.0±0.5	27.2±0.2	32.9±1.0
		50	55.8±1.2	6.9±0.1	0.2±0.1	37.1±1.4	23.8±0.7	30.4±1.4
	350℃	0	73.7±0.0	6.7±0.1	0.4±0.2	19.2±0.3	31.6±0.1	39.1±1.8
		10	74.6±0.2	6.9±0.1	0.6±1.0	18.0±1.4	32.2±0.3	29.8±1.2
		30	74.8±0.4	6.8±0.2	0.6±0.1	17.8±0.7	32.3±0.4	28.5±1.0
		50	71.8±0.2	7.2±0.3	0.6±0.2	20.4±0.7	31.4±0.5	9.8±0.3
Catalytic Reaction	250℃	0	65.7±0.5	6.5±0.2	0.6±0.2	27.2±0.9	27.8±0.5	33.9±3.0
		50	67.6±0.1	7.0±0.3	0.8±0.2	24.6±0.2	29.3±0.4	8.8±0.2
	300℃	0	67.0±3.0	6.4±0.7	0.7±0.2	25.9±3.9	28.2±2.3	32.2±1.7
		50	67.7±0.3	6.1±0.2	0.8±0.3	25.4±0.2	28.2±0.4	6.6±0.5
	350℃	0	75.1±3.0	6.5±0.1	0.5±0.1	17.9±3.2	32.0±1.5	26.5±3.3
		50	77.4±0.0	6.8±0.6	0.7±0.1	15.1±0.7	33.5±0.8	3.2±0.2

[a] by difference

Thermogravimetric analysis

Figure 5.2 shows the thermogravimetric analysis of biocrude products from catalytic and non-catalytic HTL conversion of pine feedstock in pure water, ethanol, and water-ethanol co-solvent at 300℃ reaction temperature. The effect of ethanol addition was shown in Figure 5.2-A, and the catalytic effect of iron in pure water, water/ethanol mixture, and pure ethanol were shown in Figures 5.2- B, C, and D, respectively. Based on the degradation profile, the TGA thermograms of the biocrudes could be divided into three basic regions: 100-350°C (referred to as light fraction), 350-600°C (medium fraction), and 600-800°C (heavy fraction). The increasing ethanol in the reaction medium has remarkably enhanced the light fraction for non-catalytic biocrudes. The 1:1(wt./wt.) water-ethanol mixture raised the light fraction by 5%, whereas pure ethanol increased that fraction by 62% in comparison with the pure water biocrude thermogram. The temperature range of 100-350℃ could decompose phenolic compounds, vanillin, and other oligomer compounds, which possibly formed due to the polymerization of the biocrudes. The degradation below 100℃ temperatures could be attributed to the loss of moisture or low molecular weight compounds such as alcohols, carboxylic acids, and aldehydes. The loss of medium and heavy fractions could occur due to the chemical bond cleavage of the lignin-derived heavy compounds from the biocrudes [18]. There was a sharp decomposition peak in pure ethanol at 546℃ temperature, which was absent in pure water or water-ethanol mixture. As a result, the medium fraction of pure ethanol biocrude was 16% higher than pure water biocrude product. The heavy fraction of pure ethanol was almost five times lower than pure water medium. The higher heavy fraction loss for pure water biocrudes indicated the presence of high boiling point aromatic compounds [18]. These findings suggested the formation of lower boiling point compounds in pure ethanol-derived HTL biocrudes. The increasing biocrude reaction temperature also influenced

the weight loss pattern (Figure D4). The pine biocrude produced at 350℃ has a maximum decomposition peak at 334℃ where derivative weight loss curves (DTG) for this biocrude were much sharper than the biocrude products from 250℃ and 300℃. This could be an indication that higher reaction temperature promoted low boiling point compounds in the biocrudes. The addition of an iron catalyst has increased the weight loss in all three fractions of pure water and water-ethanol mixture. In pure water, the maximum decomposition peaks were at 87 and 130℃ TG temperature, where the highest weight loss peak was at 130℃. The addition of alcohol with iron catalyst has increased the weight loss at a TG temperature of 130℃. This might be the synergistic effect of water-ethanol co-solvent and iron catalysts. The thermograms of catalytic and non-catalytic pure ethanol-derived biocrudes were similar except for the sharp decomposition peak at the medium fraction region (546℃) of catalytic biocrude, which suggested more medium fraction compounds generation by the iron catalyst. From ESI-MS characterization (Figure D5), the catalytic pine oil from pure ethanol has more monomers and dimers ($m/z<400$) than non-catalytic biocrude. As a result, catalytic pine biocrude from pure ethanol has almost 20% lower number average molar mass (Mn) than non-catalytic biocrude from the same medium. This result indicated that an iron catalyst might promote a cracking reaction and reduce the molar mass of the ethanol-derived pine biocrude [31].

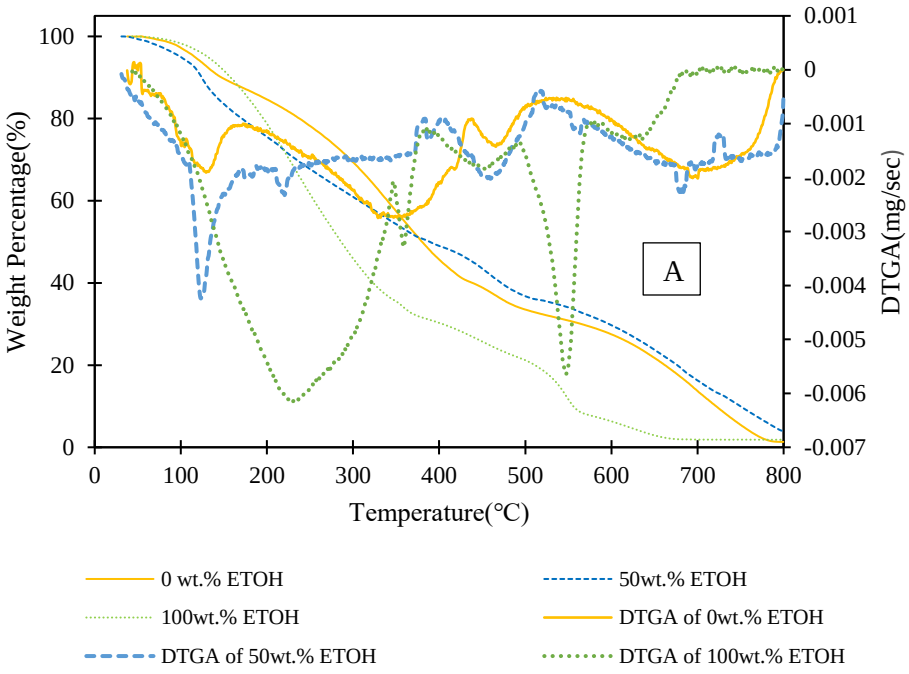
Weight Percentage(%)
DTGA(mg/sec)
Temperature(℃)
A
0 wt.% ETOH
50wt.% ETOH
100wt.% ETOH
DTGA of 0wt.% ETOH
DTGA of 50wt.% ETOH
DTGA of 100wt.% ETOH

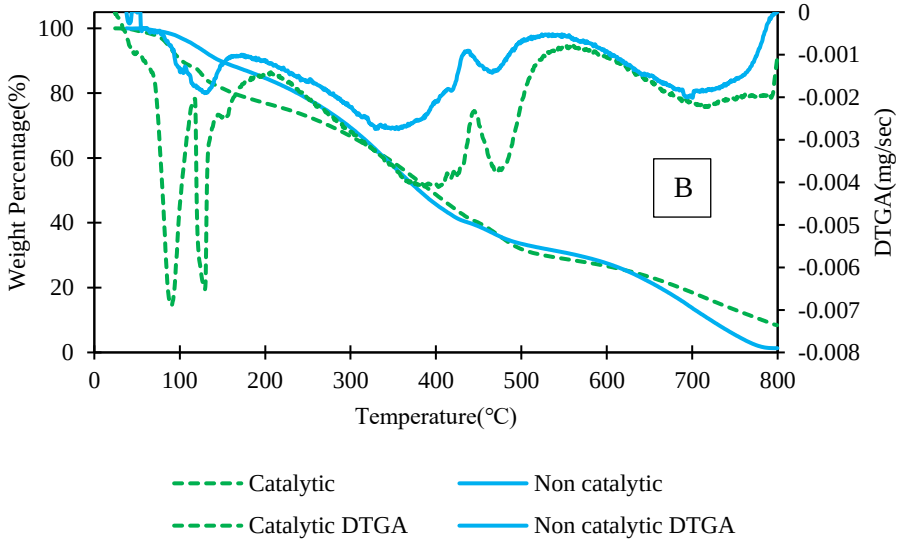
Weight Percentage(%)
DTGA(mg/sec)
Temperature(℃)
B
Catalytic
Non catalytic
Catalytic DTGA
Non catalytic DTGA

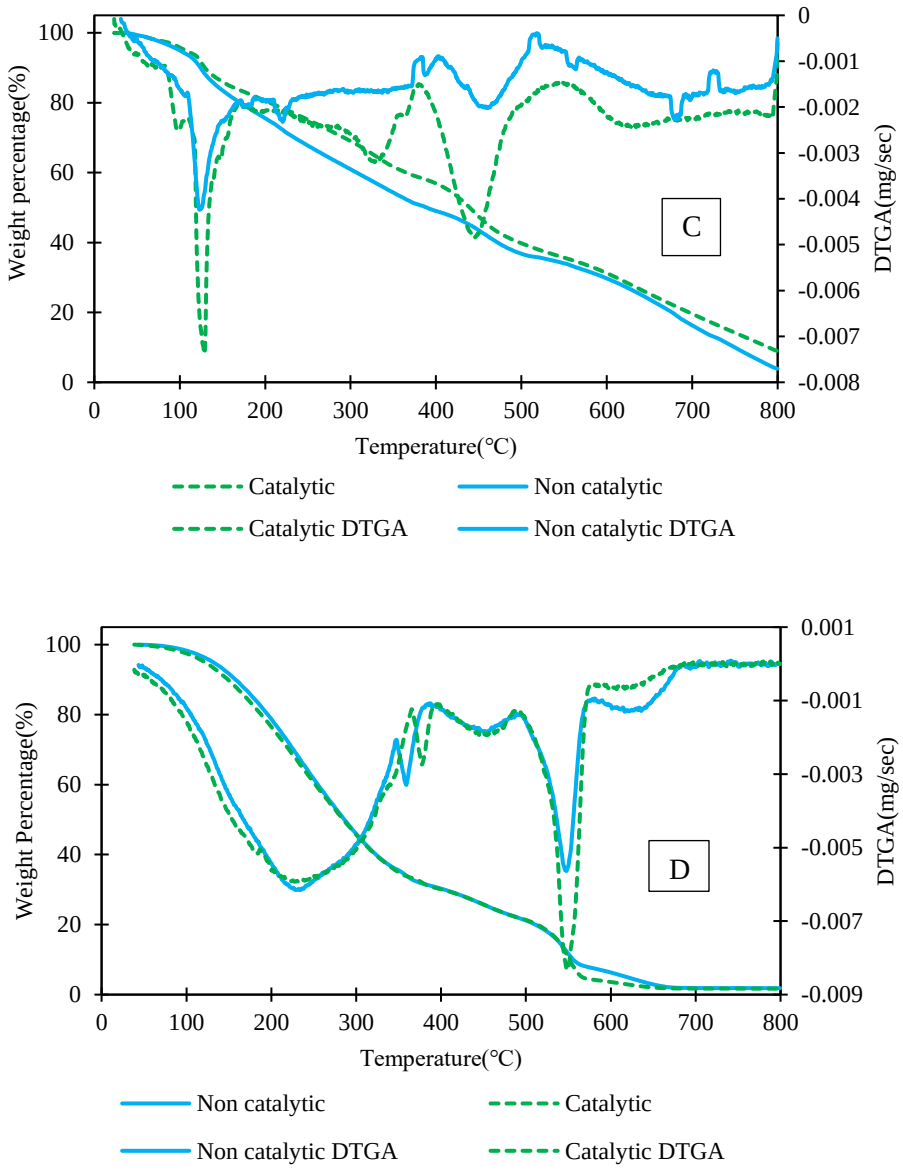

Figure 5.2: Thermogravimetric analysis of pine HTL biocrude samples produced at 300℃: A-Effect of ethanol addition in non-catalytic reaction and, B- Effect of catalyst in pure water, C-Influence of catalyst in water-ethanol mixture(1:1,wt./wt.), D-Influence of catalyst in pure ethanol reaction medium

GC-MS analysis

Figure 5.3 shows the GC-MS analysis of the pine-derived biocrudes under pure water, ethanol, and mixed (1:1, wt./wt.) reaction mediums with and without catalyst at a reaction temperature of 300℃. The biocrudes from the HTL experiment of 300℃ were selected to compare single and

mixed reaction mediums with and without catalysts at a fixed temperature. Moreover, this specific temperature (300°C) promoted the biocrude yield significantly in the water-ethanol mixture in comparison with the other two reaction temperatures.

The HTL biocrudes from pine sawdust are mainly composed of phenol, acids, and esters, along with aliphatic and other aromatics. A similar biocrude composition was reported in previous wood liquefaction works [47]. The major compound group distribution based on carbon number and area percentage is reported in the Appendix (Figure D6). The acid and phenol groups were dominant compounds in the biocrudes of this study. The presence of carboxylic acids and phenol was also observed in other pine HTL biocrude studies [48–50]. The hydrolysis reaction of cellulose generally produces esters, organic acids, furfural, and derivatives during HTL conversion [36,51]. The carboxylic acids could also be produced from pine extractives [52–54]. The phenols might originate from the lignin fraction of the pine feedstocks, as lignin contains phenol, hydroxyl, carboxyl, carbonyl, ether, and ester groups [55]. Lignin is generally depolymerized in water to form phenolic compounds by hydrolysis of ether and ester bonds [56]. The production of organic acid was significantly suppressed in the ethanol reaction medium with subsequent higher ester production. Most probably, ethanol has underwent esterification reaction with the acidic intermediates from HTL liquefaction and formed acid ethyl esters [57]. More evidence could be found in the chemical composition of pine biocrude from pure ethanol, where 28% lower acidic groups with 53% more esters compared to the water-ethanol medium were detected by GC-MS analysis. There was a 10% reduction in the phenol group in water-ethanol mixtures compared to pure water, which was also in good agreement with pine liquefaction in water-ethanol co-solvent [58]. The condensation reaction between ethanol and lignin-derived phenol could be the possible reason for less phenol detection [17]. Higher amounts of GC-MS compounds were found in the

biocrudes from pure ethanol medium compared to pure water or water-ethanol mixtures. Pure ethanol might promote lignin depolymerization and, at the same time, could suppress the re-polymerization of lignin products which raised the GC-MS detectable compounds [36,57].

The incorporation of iron catalyst has brought a change in acid, phenol, ester, and aliphatic contents of pine HTL biocrudes. The reduction of acid groups and subsequent rise in esters were observed in studied catalytic biocrudes, which was supported by lower TAN values of the biocrude (Table 5.1). This was another proof that iron catalyst has played a role in the acid neutralization of biocrude. The phenol content of catalytic pine biocrude was increased by 5-31% in all three reaction mediums. The increment of phenol by iron catalyst was also observed in other HTL work [59,60]. Iron has significantly increased aliphatic compounds in water and water-ethanol medium. From Figure D5, the carbon number of aliphatic compounds in catalytic biocrudes from mixed solvents (1:1(wt./wt.) water-ethanol) has shifted towards a lower carbon number. The surge of aliphatic with lower carbon number could be attributed to the in-situ hydrogen production by the Fe catalyst in the HTL system [9]. The increased phenol, ester, and aliphatic were also observed in biocrudes from reaction temperatures of 250 and 350°C (Figure D7 and Figure D8) underwater and water-ethanol mixture. These results suggested that the catalytic activities of iron catalysts could be more influenced by reaction mediums than temperature.

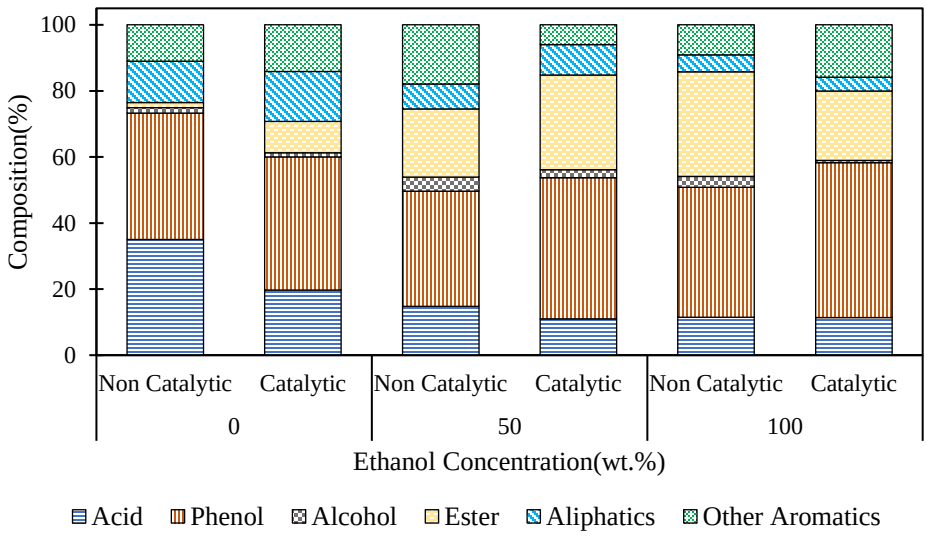

Figure 5.3: GC-MS analysis of pine HTL biocrudes at 300°C

5.3.1.3 Analysis of byproducts

Aqueous Phase

Table 5.2 shows the TOC and pH of the aqueous products of this study. It was evident that the addition of ethanol to the reaction medium gradually elevated the TOC level of the aqueous phase in studied reaction temperatures. The increasing reaction temperature has suppressed the TOC values. This finding indicated lower carbon transfer towards the aqueous product at the elevated reaction temperature, which will be discussed more in the carbon recovery section. The iron catalyst added more carbon to the aqueous phase, and the maximum TOC of 63g/L was found at 250°C within the water-ethanol (1:1, wt./wt.) mixture. The pH was mostly acidic, which confirmed the organic acid production from pine HTL conversion. At higher temperatures, the pH slightly moved towards the basic sides, and the ethanol accelerated neutralization. However, the acidity of aqueous products was still considerably high and required further treatment before releasing to the environment.

Solid Residue

The elemental composition of the solid residues of this study is shown in Table 5.2. Due to the negligible or zero sulfur and nitrogen content of the char products, only carbon, hydrogen, and oxygen (by difference) were reported here. The increasing reaction temperature has added more carbon to solid chars, which was also observed in the elemental composition of the biocrude products (Table 5.1). The ethanol suppressed the carbon content of the chars. The metallic Fe significantly repealed the carbon percentage of the char products. The catalytic effect over gaseous products will be discussed in the next section. From the elemental composition of biocrudes and solid char, it was clear that the iron catalyst had actively taken part in the deoxygenation reaction. From Figure D9 (Appendix D), it was found that the zero-valent iron catalyst has transformed into iron oxide, mostly magnetite (Fe_3O_4), after participating in an HTL reaction with pine. This study has not explored the recovery or reuse of iron catalysts. But this transformation of the catalyst could be beneficial for easy separation from char. Moreover, Alam et al. have investigated composites synthesized from magnetite nanoparticles and willow biochar for the removal of heavy metal (Cr(VI)) from an aqueous solution [61]. The literature on magnetite mixed pine biochar for heavy metal removal or other use is still rare. Further investigation is required to value add this by-product of the HTL process.

Table 5.2: Properties of aqueous phase and solid residue from pine HTL conversion

			Aqueous Phase		Solid Residue Elemental Composition (wt.%)		
	Temperature (°C)	Ethanol (wt.%)	TOC (g/L)	pH	Carbon	Hydrogen	Oxygen[a]
Non-Catalytic	250	0	6.7	2.74	68.7±0.2	4.7±0.0	26.6±0.3
		10	12.2	2.92	65.3±0.0	4.8±0.1	29.9±0.1
		30	32.6	3.82	58.3±0.7	5.7±0.1	36.0±0.8
		50	62.3	3.72	47.9±0.6	5.6±0.0	46.5±0.7
	300	0	5.2	2.8	67.9±0.3	4.5±0.2	22.6±0.4
		10	18.6	3.18	68.0±0.0	4.5±0.0	22.5±0.0
		30	34.9	3.3	66.1±0.1	4.3±0.1	24.5±0.2
		50	60.3	3.4	69.3±0.5	4.4±0.1	26.3±0.6
	350	0	4.6	3.32	76.9±0.1	4.2±0.0	18.9±0.1
		10	7.8	3.51	77.2±0.1	4.1±0.0	18.6±0.1
		30	14.3	4.18	78.8±0.6	4.2±0.0	17.1±0.6
		50	18.2	4.21	79.7±0.3	3.7±0.0	16.6±0.3
Catalytic	250	0	9.2	3.92	51.6±0.2	3.4±0.1	45.0±0.3
		50	63.0	4.54	45.0±0.3	4.1±0.3	50.9±0.6
	300	0	7.5	3.4	46.4±0.8	2.7±0.3	50.9±1.0
		50	60.7	4.6	66.7±0.3	6.1±0.2	27.3±0.5
	350	0	6.5	3.28	38.7±0.4	2.6±0.1	58.7±0.5
		50	20.1	4.2	77.1±0.3	3.7±0.1	19.2±0.5

[a] by difference

Gaseous Products

Figure 5.4 represents gaseous product composition from non-catalytic (Figure 5.4-A) and catalytic (Figure 5.4-B) HTL conversion of pine feedstock. The gaseous products were determined by hydrogen(H_2), carbon monoxide (CO), carbon dioxide (CO_2), and methane (CH_4) composition, and the rest of the gases were denoted as balance. The production of H_2, CO, and CO_2 was increased by elevated reaction temperature in pure water. At a reaction temperature of 350°C, a notable amount (5-6 mol%) of CH_4 was also detected in water-derived gas products. The enhanced CO and CO_2 fractions supported the oxygen removal from biocrudes at higher reaction temperatures (Table 5.1). The addition of ethanol has raised the H_2 and CO_2 concentrations in the gaseous product. The maximum hydrogen concentration was observed in the 1:1 (wt./wt.) water-

ethanol reaction medium. The CO_2 concentration gradually increased by ethanol percentage in the reaction medium. From the elemental composition of biocrudes (Table 5.1), the carbon percentages of biocrudes were decreased by increasing ethanol concentration at three studied reaction temperatures. It was evident that the extra carbon from ethanol was released in gaseous form (CO and CO_2) rather than biocrude or solid products. However, the production of H_2 and CO_2 started reducing from 70 wt.% ethanol reaction medium. This explained the excess carbon percentages of pure ethanol-derived biocrude(Table D1).

Except for the pure ethanol reaction medium, the iron catalyst has multiplied the hydrogen production in the gas product. This might occur due to the hydrogen production by metallic Fe in a water and water-ethanol mixture, which did not occur in the presence of ethanol. This excess hydrogen might be the reason low oxygen content of the catalytic biocrudes. The methane (CH_4) was not detected in high temperatures of catalytic HTL conversion.

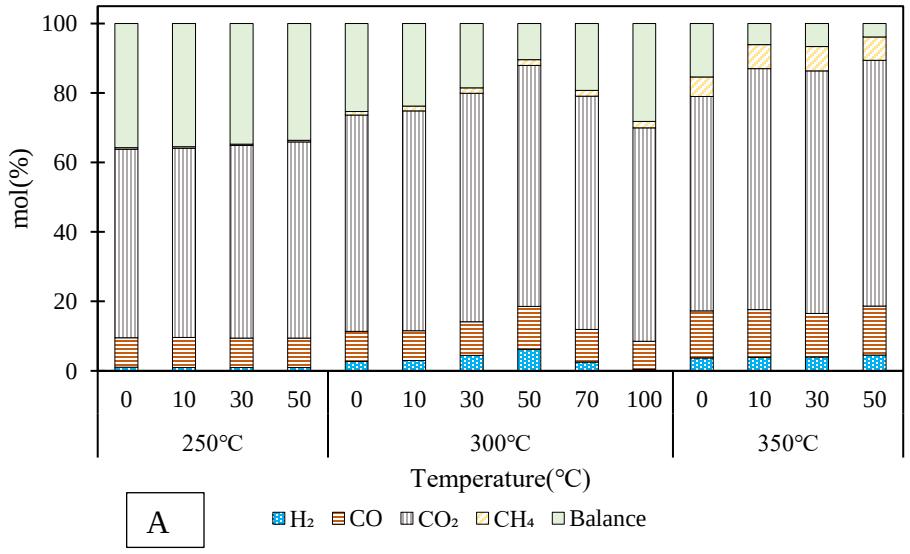

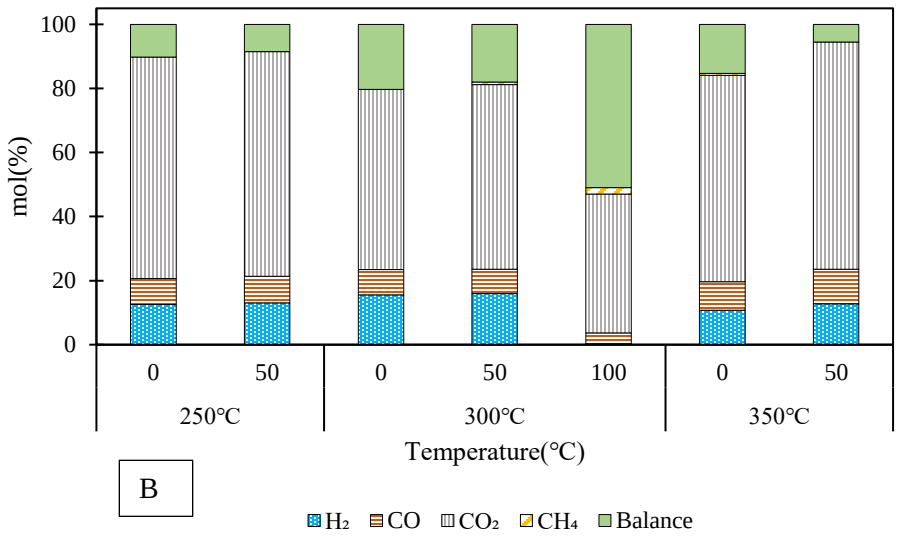

Figure 5.4: Gaseous product distribution: A- Non-Catalytic Reaction, B-Catalytic Reaction

5.3.2 Carbon distribution

Figure 5.5 shows the carbon distribution in this pine HTL study. Carbon distribution was calculated based on the elemental composition of biocrudes, solid residue, and TOC of the aqueous phase. Figure 5.5-A presents the carbon recovery of non-catalytic reactions, and Figure 5.5-B depicts the catalytic one. In Figure 5.5-A, the carbon movement toward biocrude products was suppressed by increasing ethanol with the subsequent rise of carbon in gaseous products. These findings were supported by the gas product analysis where CO and CO_2 were increased by ethanol concentration in the reaction medium. Thus, the excess carbon from ethanol was released by gas rather than biocrudes or solid products. The maximum carbon transfer to the biocrude product took place at the reaction temperature of 350℃ within the water reaction medium, while the highest amount of carbon shifted towards gaseous products of water-ethanol mixtures. Throughout the study, the lower carbon transfer to the solid residue was in agreement with the declining solid yield by rising ethanol concentration.

The catalytic HTL conversion of pine added 2-78% more carbon to the biocrudes in the pure water reaction medium. However, the incorporation of ethanol repealed carbons to biocrude products and shifted more carbon to gaseous (balance) products compared to only water medium. The reduction of biocrude yield in the water-ethanol medium by catalyst was the reason for lower carbon transfer to biocrudes.

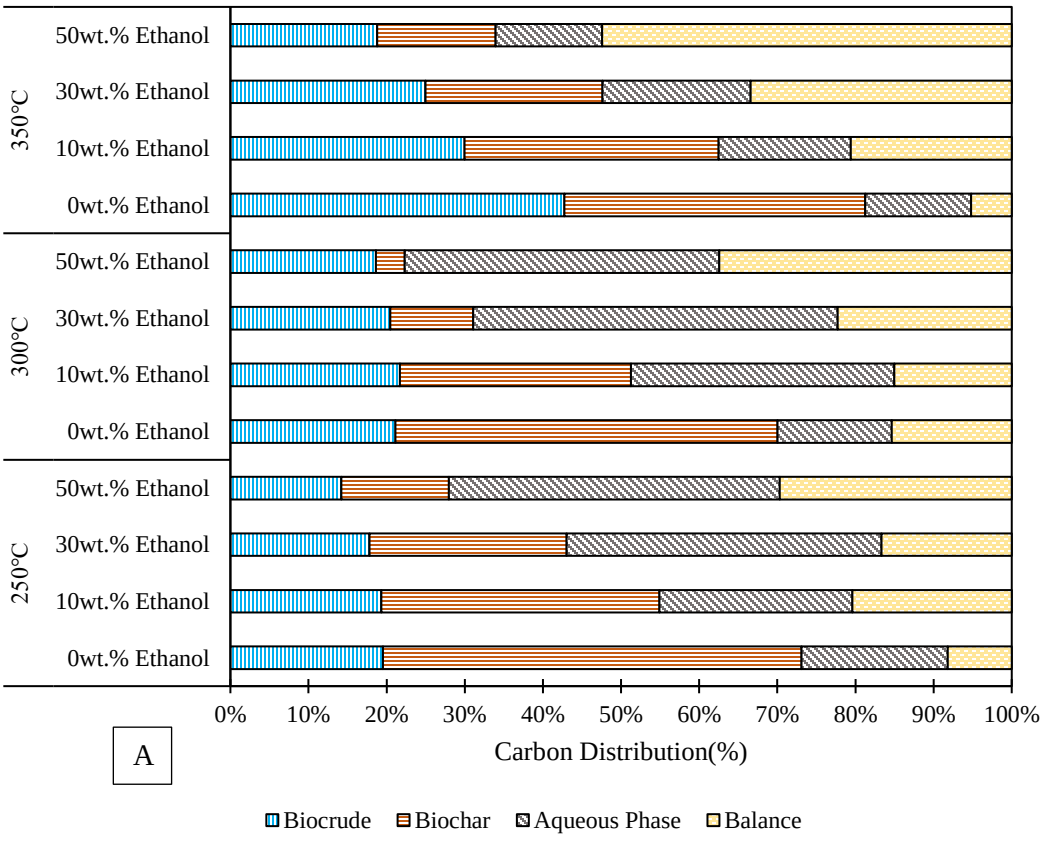

A

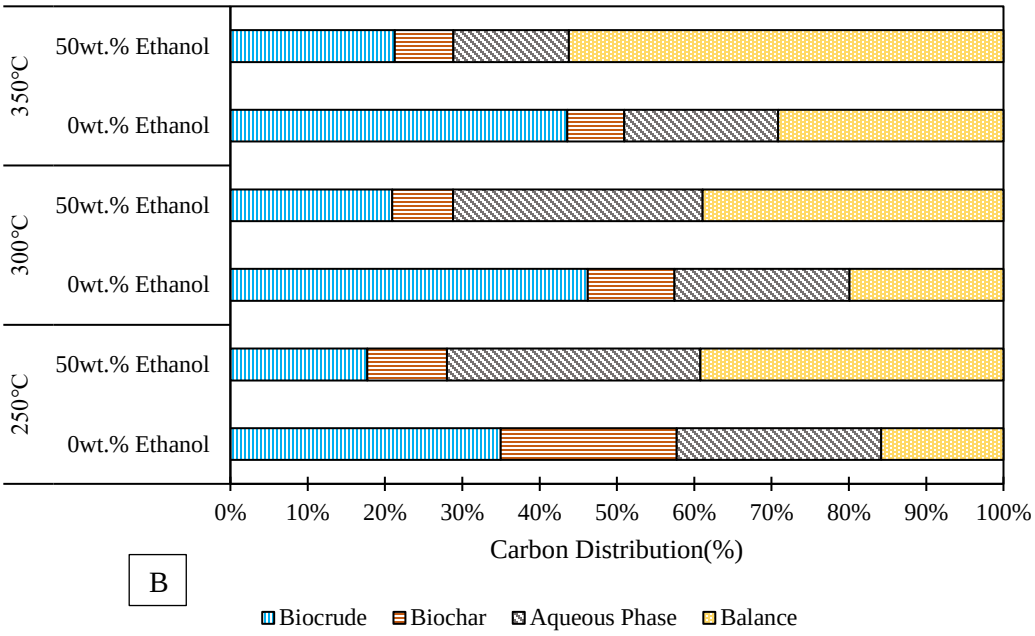

Figure 5.5: Carbon distribution of Pine HTL products: A- Non-Catalytic and B-Catalytic reaction

5.4 Conclusions

The hydrothermal liquefaction of pine sawdust under water and water-ethanol was explored with metallic iron (Fe) catalyst within a 250-350℃ reaction temperature range. The reaction temperature, presence of ethanol in the reaction medium, and catalyst significantly affected the biocrude production from pine feedstock. The biocrude production from pure water was influenced by the reaction temperature, and the highest biocrude yield was 27 wt.% at 350℃. The gradually increasing ethanol ratio in the water-ethanol reaction medium facilitated biocrude production and raised the biocrude yield by two-fold in the equal water-ethanol ratio (wt./wt.) at 300℃, compared to pure water medium. The catalytic effect of iron powder was prominent in a single water medium by enhanced biocrude production. In a mixed medium, zero-valent iron reduced the oxygen and acidity of the pine biocrudes. The chemical composition of pine-derived biocrudes was influenced by the reaction medium and catalyst. The elevated ethanol concentration transformed the acidic compounds into esters, while the catalyst increased the phenolic compounds in biocrude products.

The carbon transfer to the biocrudes was improved by the higher reaction temperature with the catalyst. However, the addition of ethanol led carbon to gaseous products rather than biocrudes or solids. This study has demonstrated the prospects of single and mixed solvents along with the metallic iron (Fe) catalyst in pine biomass conversion for enhanced biocrude products with improved properties.

5.5 Reference

[1] D.C. Elliott, P. Biller, A.B. Ross, A.J. Schmidt, S.B. Jones, Hydrothermal liquefaction of biomass: Developments from batch to continuous process, Bioresource Technology. 178 (2015) 147–156. https://doi.org/10.1016/j.biortech.2014.09.132.

[2] M.P. Gundupalli, S.P. Gundupalli, A.S. Somavarapu Thomas, M. Jayakumar, D. Bhattacharyya, B. Gurunathan, Chapter 4 - Hydrothermal liquefaction of lignocellulosic biomass for production of biooil and by-products: current state of the art and challenges, in: B. Gurunathan, R. Sahadevan, Z.A. Zakaria (Eds.), Biofuels and Bioenergy, Elsevier, 2022: pp. 61–84. https://doi.org/10.1016/B978-0-323-85269-2.00001-0.

[3] C.D. Venkatachalam, S.R. Ravichandran, M. Sengottian, Lignocellulosic and algal biomass for bio-crude production using hydrothermal liquefaction: Conversion techniques, mechanism and process conditions: A review, Environmental Engineering Research. 27 (2022). https://doi.org/10.4491/eer.2020.555.

[4] J.J. Malpica-Maldonado, A.L. Martínez-Salazar, B. Portales-Martínez, M.A. Coronel-García, Y. Salazar-Cerda, Biocrude production by catalytic hydrothermal liquefaction of wood chips using NiMo series catalysts, International Journal of Hydrogen Energy. 47 (2022) 30160–30171. https://doi.org/10.1016/j.ijhydene.2022.06.109.

[5] Y. Hirano, Y. Miyata, M. Taniguchi, N. Funakoshi, Y. Yamazaki, C. Ogino, Y. Kita, Fe-assisted hydrothermal liquefaction of cellulose: Effects of hydrogenation catalyst addition on

properties of water-soluble fraction, Journal of Analytical and Applied Pyrolysis. 145 (2020) 104719. https://doi.org/10.1016/j.jaap.2019.104719.

[6] X.-F. Wu, J.-J. Zhang, M.-F. Li, J. Bian, F. Peng, Catalytic hydrothermal liquefaction of eucalyptus to prepare bio-oils and product properties, Energy Conversion and Management. 199 (2019) 111955. https://doi.org/10.1016/j.enconman.2019.111955.

[7] K. Tekin, S. Karagöz, S. Bektaş, Effect of sodium perborate monohydrate concentrations on product distributions from the hydrothermal liquefaction of Scotch pine wood, Fuel Processing Technology. 110 (2013) 17–23. https://doi.org/10.1016/j.fuproc.2013.01.010.

[8] K. Alper, Y.-Y. Wang, X. Meng, K. Tekin, S. Karagoz, A.J. Ragauskas, Use of a Lewis acid, a Brønsted acid, and their binary mixtures for the hydrothermal liquefaction of lignocellulose, Fuel. 304 (2021) 121398. https://doi.org/10.1016/j.fuel.2021.121398.

[9] B. de Caprariis, I. Bavasso, M.P. Bracciale, M. Damizia, P. De Filippis, M. Scarsella, Enhanced bio-crude yield and quality by reductive hydrothermal liquefaction of oak wood biomass: Effect of iron addition, Journal of Analytical and Applied Pyrolysis. 139 (2019) 123–130. https://doi.org/10.1016/j.jaap.2019.01.017.

[10] Y. Miyata, K. Sagata, M. Hirose, Y. Yamazaki, A. Nishimura, N. Okuda, Y. Arita, Y. Hirano, Y. Kita, Fe-Assisted hydrothermal liquefaction of lignocellulosic biomass for producing high-grade bio-oil, ACS Sustainable Chem. Eng. 5 (2017) 3562–3569. https://doi.org/10.1021/acssuschemeng.7b00381.

[11] Z. Liu, F.-S. Zhang, Effects of various solvents on the liquefaction of biomass to produce fuels and chemical feedstocks, Energy Conversion and Management. 49 (2008) 3498–3504. https://doi.org/10.1016/j.enconman.2008.08.009.

[12] X.Z. Yuan, H. Li, G.M. Zeng, J.Y. Tong, W. Xie, Sub- and supercritical liquefaction of rice straw in the presence of ethanol–water and 2-propanol–water mixture, Energy. 32 (2007) 2081–2088. https://doi.org/10.1016/j.energy.2007.04.011.

[13] S. Cheng, I. D'cruz, M. Wang, M. Leitch, C. (Charles) Xu, Highly efficient liquefaction of woody biomass in hot-compressed alcohol−water co-solvents, Energy Fuels. 24 (2010) 4659–4667. https://doi.org/10.1021/ef901218w.

[14] H. Wu, U. Shakeel, Q. Zhang, K. Zhang, X. Xu, J. Xu, Ethanol-assisted hydrothermal liquefaction of poplar using Fe-Co/Al2O3 as Catalyst, Energies. 15 (2022) 3057. https://doi.org/10.3390/en15093057.

[15] I. Hafez, E.B. Hassan, Rapid liquefaction of giant miscanthus feedstock in ethanol–water system for production of biofuels, Energy Conversion and Management. 91 (2015) 219–224. https://doi.org/10.1016/j.enconman.2014.12.016.

[16] U. of Georgia, Ten most common trees in the United States, Treehugger. (n.d.). https://www.treehugger.com/ten-most-common-trees-united-states-3971258 (accessed October 6, 2022).

[17] Y. Celikbag, B.K. Via, S. Adhikari, G. Buschle-Diller, M.L. Auad, The effect of ethanol on hydroxyl and carbonyl groups in biopolyol produced by hydrothermal liquefaction of loblolly pine: 31P-NMR and 19F-NMR analysis, Bioresource Technology. 214 (2016) 37–44. https://doi.org/10.1016/j.biortech.2016.04.066.

[18] O.A. Asafu-Adjaye, Y. Celikbag, J. Street, M.S. Peresin, M.L. Auad, S. Adhikari, B. Via, Elucidation of the effect of fast pyrolysis and hydrothermal liquefaction on the physico-chemical properties of bio-oil from southern yellow pine biomass as a chemical feedstock, BioRes. 17 (2022) 2176–2192. https://doi.org/10.15376/biores.17.2.2176-2192.

[19] P. Roy, H. Jahromi, T. Rahman, S. Adhikari, F. Feyzbar-Khalkhali-Nejad, E. Barbary Hassan, T.-S. Oh, Understanding the effects of feedstock blending and catalyst support on hydrotreatment of algae HTL biocrude with non-edible vegetable oil, Energy Conversion and Management. 268 (2022) 115998. https://doi.org/10.1016/j.enconman.2022.115998.

[20] P.J.V. Soest, Use of detergents in the analysis of fibrous feeds. I. Preparation of fiber residues of low nitrogen content, Journal of Association of Official Agricultural Chemists. 46 (1963) 825–829. https://doi.org/10.1093/jaoac/46.5.825.

[21] P.J.V. Soest, Use of detergents in the analysis of fibrous feeds. II. A rapid method for the determination of fiber and lignin, Journal of Association of Official Agricultural Chemists. 46 (1963) 829–835. https://doi.org/10.1093/jaoac/46.5.829.

[22] P.J.V. Soest, R.H. Wine, Use of Detergents in the analysis of fibrous feeds. IV. Determination of plant cell-wall constituents, Journal of Association of Official Analytical Chemists. 50 (1967) 50–55. https://doi.org/10.1093/jaoac/50.1.50.

[23] P. Roy, H. Jahromi, S. Adhikari, Y. Zou Finfrock, T. Rahman, Z. Ahmadi, M. Mahjouri-Samani, F. Feyzbar-Khalkhali-Nejad, T.-S. Oh, Performance of biochar assisted catalysts during hydroprocessing of non-edible vegetable oil: Effect of transition metal source on

catalytic activity, Energy Conversion and Management. 252 (2022) 115131. https://doi.org/10.1016/j.enconman.2021.115131.

[24] R.K. Singhal, B. Gangadhar, H. Basu, V. Manisha, G.R.K. Naidu, A.V.R. Reddy, Remediation of malathion contaminated soil using zero valent iron nano-particles, American Journal of Analytical Chemistry. 3 (2012) 76–82. https://doi.org/10.4236/ajac.2012.31011.

[25] Y.-P. Sun, X. Li, J. Cao, W. Zhang, H.P. Wang, Characterization of zero-valent iron nanoparticles, Advances in Colloid and Interface Science. 120 (2006) 47–56. https://doi.org/10.1016/j.cis.2006.03.001.

[26] T. Rahman, H. Jahromi, P. Roy, S. Adhikari, E. Hassani, T.-S. Oh, Hydrothermal liquefaction of municipal sewage sludge: Effect of red mud catalyst in ethylene and inert ambiances, Energy Conversion and Management. 245 (2021) 114615. https://doi.org/10.1016/j.enconman.2021.114615.

[27] H. Jahromi, S. Adhikari, P. Roy, E. Hassani, C. Pope, T.-S. Oh, Y. Karki, Production of green transportation fuels from Brassica carinata oil: A comparative study of noble and transition metal catalysts, Fuel Processing Technology. 215 (2021) 106737. https://doi.org/10.1016/j.fuproc.2021.106737.

[28] RStudio Team, RStudio: Integrated Development Environment for R, (2019). https://www.rstudio.com/ (accessed May 6, 2022).

[29] S.A. Channiwala, P.P. Parikh, A unified correlation for estimating HHV of solid, liquid and gaseous fuels, Fuel. 81 (2002) 1051–1063. https://doi.org/10.1016/S0016-2361(01)00131-4.

[30] H. Jahromi, S. Adhikari, P. Roy, M. Shelley, E. Hassani, T.-S. Oh, Synthesis of novel biolubricants from waste cooking oil and cyclic oxygenates through an integrated catalytic process, ACS Sustainable Chem. Eng. 9 (2021) 13424–13437. https://doi.org/10.1021/acssuschemeng.1c03523.

[31] Y. Han, D.N. McIlroy, A.G. McDonald, Hydrodeoxygenation of pyrolysis oil for hydrocarbon production using nanospring based catalysts, Journal of Analytical and Applied Pyrolysis. 117 (2016) 94–105. https://doi.org/10.1016/j.jaap.2015.12.011.

[32] Y. Hu, Z. Gu, W. Li, C. (Charles) Xu, Alkali-catalyzed liquefaction of pinewood sawdust in ethanol/water co-solvents, Biomass and Bioenergy. 134 (2020) 105485. https://doi.org/10.1016/j.biombioe.2020.105485.

[33] Y. Wang, H. Wang, H. Lin, Y. Zheng, J. Zhao, A. Pelletier, K. Li, Effects of solvents and catalysts in liquefaction of pinewood sawdust for the production of bio-oils, Biomass and Bioenergy. 59 (2013) 158–167. https://doi.org/10.1016/j.biombioe.2013.10.022.

[34] F. Hardi, M. Mäkelä, K. Yoshikawa, Non-catalytic hydrothermal liquefaction of pine sawdust using experimental design: Material balances and products analysis, Applied Energy. 204 (2017) 1026–1034. https://doi.org/10.1016/j.apenergy.2017.04.033.

[35] M. Wądrzyk, M. Berdel, R. Janus, D.W.F. Brilman, Hydrothermal processing of pine wood: effect of process variables on bio-oil quality and yield, E3S Web Conf. 108 (2019) 02004. https://doi.org/10.1051/e3sconf/201910802004.

[36] S. Feng, R. Wei, M. Leitch, C.C. Xu, Comparative study on lignocellulose liquefaction in water, ethanol, and water/ethanol mixture: Roles of ethanol and water, Energy. 155 (2018) 234–241. https://doi.org/10.1016/j.energy.2018.05.023.

[37] N.P. Vasilakos, D.M. Austgen, Hydrogen-donor solvents in biomass liquefaction, Ind. Eng. Chem. Proc. Des. Dev. 24 (1985) 304–311. https://doi.org/10.1021/i200029a015.

[38] Y. Liu, X. Yuan, H. Huang, X. Wang, H. Wang, G. Zeng, Thermochemical liquefaction of rice husk for bio-oil production in mixed solvent (ethanol–water), Fuel Processing Technology. 112 (2013) 93–99. https://doi.org/10.1016/j.fuproc.2013.03.005.

[39] S. Cheng, L. Wei, J. Julson, P.R. Kharel, Y. Cao, Z. Gu, Catalytic liquefaction of pine sawdust for biofuel development on bifunctional Zn/HZSM-5 catalyst in supercritical ethanol, Journal of Analytical and Applied Pyrolysis. 126 (2017) 257–266. https://doi.org/10.1016/j.jaap.2017.06.001.

[40] B. Biswas, A. Kumar, R. Kaur, B.B. Krishna, T. Bhaskar, Catalytic hydrothermal liquefaction of alkali lignin over activated bio-char supported bimetallic catalyst, Bioresource Technology. 337 (2021) 125439. https://doi.org/10.1016/j.biortech.2021.125439.

[41] B. Zhao, H. Li, H. Wang, Y. Hu, J. Gao, G. Zhao, M.B. Ray, C.C. Xu, Synergistic effects of metallic Fe and other homogeneous/heterogeneous catalysts in hydrothermal liquefaction of woody biomass, Renewable Energy. 176 (2021) 543–554. https://doi.org/10.1016/j.renene.2021.05.115.

[42] B. Zhao, Y. Hu, L. Qi, J. Gao, G. Zhao, M.B. Ray, C.C. Xu, Promotion effects of metallic iron on hydrothermal liquefaction of cornstalk in ethanol-water mixed solvents for the production of biocrude oil, Fuel. 285 (2021) 119150. https://doi.org/10.1016/j.fuel.2020.119150.

[43] B. de Caprariis, P. De Filippis, A. Petrullo, M. Scarsella, Hydrothermal liquefaction of biomass: Influence of temperature and biomass composition on the bio-oil production, Fuel. 208 (2017) 618–625. https://doi.org/10.1016/j.fuel.2017.07.054.

[44] H. Li, X. Yuan, G. Zeng, D. Huang, H. Huang, J. Tong, Q. You, J. Zhang, M. Zhou, The formation of bio-oil from sludge by deoxy-liquefaction in supercritical ethanol, Bioresource Technology. 101 (2010) 2860–2866. https://doi.org/10.1016/j.biortech.2009.10.084.

[45] R. Shakya, J. Whelen, S. Adhikari, R. Mahadevan, S. Neupane, Effect of temperature and Na_2CO_3 catalyst on hydrothermal liquefaction of algae, Algal Research. 12 (2015) 80–90. https://doi.org/10.1016/j.algal.2015.08.006.

[46] A. Yerrayya, A.K. Shree Vishnu, S. Shreyas, S.R. Chakravarthy, R. Vinu, Hydrothermal liquefaction of rice straw using methanol as co-Solvent, Energies. 13 (2020) 2618. https://doi.org/10.3390/en13102618.

[47] Z. Pan, H. Huang, C. Zhou, X. Xiao, X. He, F. Lai, J. Xiong, Highly efficient conversion of camphor tree sawdust into bio-oil and biochar products by liquefaction in ethanol-water cosolvent, Journal of Analytical and Applied Pyrolysis. 136 (2018) 186–198. https://doi.org/10.1016/j.jaap.2018.10.006.

[48] L. Nazari, Z. Yuan, S. Souzanchi, M.B. Ray, C. (Charles) Xu, Hydrothermal liquefaction of woody biomass in hot-compressed water: Catalyst screening and comprehensive characterization of bio-crude oils, Fuel. 162 (2015) 74–83. https://doi.org/10.1016/j.fuel.2015.08.055.

[49] E. Akalin, Y.-M. Kim, K. Alper, V. Oja, K. Tekin, I. Durukan, M.Z. Siddiqui, S. Karagöz, Co-hydrothermal liquefaction of lignocellulosic biomass with Kukersite oil shale, Energy Fuels. 33 (2019) 7424–7435. https://doi.org/10.1021/acs.energyfuels.9b01473.

[50] N. Sudasinghe, J.R. Cort, R. Hallen, M. Olarte, A. Schmidt, T. Schaub, Hydrothermal liquefaction oil and hydrotreated product from pine feedstock characterized by heteronuclear two-dimensional NMR spectroscopy and FT-ICR mass spectrometry, Fuel. 137 (2014) 60–69. https://doi.org/10.1016/j.fuel.2014.07.069.

[51] N. Shimizu, B. Zeng, K. Kushima, Hydrothermal liquefaction of wood chips under supercritical and subcritical water reaction conditions, SN Appl. Sci. 3 (2021) 577. https://doi.org/10.1007/s42452-021-04561-0.

[52] S. Karagöz, T. Bhaskar, A. Muto, Y. Sakata, Comparative studies of oil compositions produced from sawdust, rice husk, lignin and cellulose by hydrothermal treatment, Fuel. 84 (2005) 875–884. https://doi.org/10.1016/j.fuel.2005.01.004.

[53] C. Xu, N. Lad, Production of heavy oils with high caloric values by direct liquefaction of woody biomass in sub/near-critical water, Energy Fuels. 22 (2008) 635–642. https://doi.org/10.1021/ef700424k.

[54] G.W. Huber, S. Iborra, A. Corma, Synthesis of transportation fuels from biomass: Chemistry, catalysts, and engineering, Chem. Rev. 106 (2006) 4044–4098. https://doi.org/10.1021/cr068360d.

[55] Wahyudiono, T. Kanetake, M. Sasaki, M. Goto, Decomposition of a lignin model compound under hydrothermal conditions, Chemical Engineering & Technology. 30 (2007) 1113–1122. https://doi.org/10.1002/ceat.200700066.

[56] G. Brunner, Chapter 8 - Processing of biomass with hydrothermal and supercritical water, in: G. Brunner (Ed.), Supercritical Fluid Science and Technology, Elsevier, 2014: pp. 395–509. https://doi.org/10.1016/B978-0-444-59413-6.00008-X.

[57] Y. Chen, Y. Wu, P. Zhang, D. Hua, M. Yang, C. Li, Z. Chen, J. Liu, Direct liquefaction of *Dunaliella tertiolecta* for bio-oil in sub/supercritical ethanol–water, Bioresource Technology. 124 (2012) 190–198. https://doi.org/10.1016/j.biortech.2012.08.013.

[58] Y. Celikbag, S. Meadows, M. Barde, S. Adhikari, G. Buschle-Diller, M.L. Auad, B.K. Via, Synthesis and characterization of bio-oil-based self-curing epoxy resin, Ind. Eng. Chem. Res. 56 (2017) 9389–9400. https://doi.org/10.1021/acs.iecr.7b02123.

[59] P. Sun, M. Heng, S.-H. Sun, J. Chen, Analysis of liquid and solid products from liquefaction of paulownia in hot-compressed water, Energy Conversion and Management. 52 (2011) 924–933. https://doi.org/10.1016/j.enconman.2010.08.020.

[60] P. Sun, M. Heng, S. Sun, J. Chen, Direct liquefaction of paulownia in hot compressed water: Influence of catalysts, Energy. 35 (2010) 5421–5429. https://doi.org/10.1016/j.energy.2010.07.005.

[61] M.S. Alam, B. Bishop, N. Chen, S. Safari, V. Warter, J.M. Byrne, T. Warchola, A. Kappler, K.O. Konhauser, D.S. Alessi, Reusable magnetite nanoparticles–biochar composites for the efficient removal of chromate from water, Sci Rep. 10 (2020) 19007. https://doi.org/10.1038/s41598-020-75924-7.

Chapter 6

Conclusion and future recommendation

6.1 Conclusions

This research work studied the hydrothermal liquefaction of selected waste material-based feedstocks for improved biocrude production. Among four feedstocks, two were wet feedstocks: municipal sewage sludge and algae, and the other two were dry ones: waste plastic mix and woody residue. This work included four objectives to understand: 1) the effect of ethylene ambiance and red mud catalyst over municipal sewage sludge liquefaction, 2) the influence of red mud-supported nickel catalyst and four reaction ambiances in algae conversion, 3) the catalytic activity of red mud in mixed plastic feedstock and 4) the role of hydrogen donor solvent in different reaction temperature and iron catalyst over lignocellulosic biomass conversion. The major findings of these objectives are provided below.

Objective 1: The inert (nitrogen) and ethylene atmosphere were applied to the hydrothermal liquefaction (HTL) of municipal sewage sludge at 350℃ using three forms of red mud (RM) catalysts given their oxidation state: calcined red mud (CRM), reduced red mud at 500°C (RRM500), and red mud reduced at 700°C (RRM700). The ethylene atmosphere promoted higher biocrude yield with consistent viscosity. The RRM500 and RRM700 catalyst reduced acidity and viscosity, whereas the use of CRM catalyst led to the polymerization of biocrude products. The mutual effect of RRM500-ethylene was observed by the reduced nitrogen content and viscosity of the biocrude. Therefore, the ethylene atmosphere and reduced RM catalyst were capable of improving biocrude formation from municipal sewage sludge.

Objective 2: The reactive environments by inert (nitrogen), ethylene, reducing, and oxidizing gases were imposed over the HTL conversion of *Tetraselmis sp.* algae at 275℃ temperature in the presence of reduced red mud (RRM) and red mud-supported nickel (Ni/RM) catalysts. Irrespective of the reaction atmosphere, the use of catalysts has increased the yield of Tetraselmis-derived biocrude, where the Ni/RM showed better performance in yield and carbon content enhancement with lower oxygen, sulfur percentage, and acidity of biocrudes, compared to RRM catalysts. The reducing environment facilitated mild hydrotreatment during the HTL reaction in the presence of both RRM and Ni/RM catalysts. Among the non-catalytic HTL reactions, an inert environment maximized biocrude production, the ethylene environment lowered the total acid number (TAN) of the biocrudes, and the reducing environment added maximum carbon and minimum oxygen and sulfur content to *Tetraselmis* biocrude.

Objective 3: This work investigated the liquefaction of polyethylene terephthalate(PET), high-density polyethylene (HDPE), low-density polyethylene (LDPE), polypropylene (PP), polystyrene (PS) plastics by supercritical water with reduced red mud (RM) catalyst. The addition of catalyst repealed the liquid crude from HDPE, LDPE, PP, PS, and solid from PET production. The RM catalyst also induced low viscosity and acidity to biocrudes regardless of the reaction condition. The plastic-derived crude oil contained 36-92% gasoline range low boiling products where HDPE produced paraffin compounds and PP and PS decomposed into aromatic or cyclic compounds. The combined effect of the RM catalyst and the extra metal content of the LDPE sample has promoted paraffin formation in LDPE oils. The synergistic effect of the plastic mix was found in higher crude oil production, which can be utilized to mitigate the plastic waste problem with energy-enriched liquid fuel production.

Objective 4: The hydrothermal liquefaction of pine sawdust under water and water-ethanol and pure ethanol was explored with metallic iron (Fe) catalyst within a 250-350℃ reaction temperature range. The maximum biocrude production in pure water was 18 wt.% at 350℃, whereas the highest biocrude yield of 34wt.% was produced from an equal water-ethanol mixture at 300℃. The iron powder catalyst enhanced biocrude production in a water medium and reduced the oxygen and acidity of the pine biocrudes in a mixed medium. The elevated ethanol concentration transformed the acidic compounds into esters, while the catalyst increased the phenolic compounds in biocrude products. The carbon transfer to the biocrudes is improved by the catalytic HTL at the higher reaction temperature. However, adding ethanol led to carbon to gaseous products rather than biocrudes or solids.

6.2 Future recommendation

The hydrothermal liquefaction (HTL) of organic materials has been extensively studied with a wide range of feedstocks, catalysts, and process parameters. This study has explored the HTL conversion of multiple feedstocks under different HTL conditions. A few research gaps were detected during the experimental work and data analysis, which were not investigated further. Based on the findings of this study, recommendations for future research are given below.

a. **Model compound analysis:** The current study has investigated the HTL conversion of selected feedstocks as a received basis primarily to determine the biocrude yield and biocrude quality. However, the model compound analysis can be performed to understand the depolymerization process. Several researchers have studied the HTL conversion chemistry with monomers of lipid, carbohydrate, protein, and lignin [1–3]. Best to our knowledge, the reaction mechanism between monomer or model compound and reaction atmosphere during the HTL process has not been explored yet. To fully understand the reaction mechanism of

biomass components in hydrothermal media under a reactive gaseous environment, the conversion of model compounds into desired gas needs to be performed.

b. **Co-liquefaction**: The concept of co-liquefaction is well-established and extensively studied. The feedstocks of recent co-liquefaction studies included various wastes such as household mixed waste(food, plastic), biogenic wastes(sludge, food residue) with algae, and post-consumer mixed textile wastes (PET, cotton) [4–6]. The co-HTL of studied waste feedstocks can be performed to add important information about waste valorization with industrial residue-based catalysts.

c. **Catalyst reuse**: The red mud was applied as the catalyst to the HTL systems of the four feedstocks. Due to the difficulties in separation and utilization of zero-value industrial waste (red mud) as a catalyst, this research work did not include catalyst recovery or regeneration. Moreover, the iron catalyst was also not recovered and reused in the pine sawdust liquefaction study. These iron-based catalyst mixed char can be used for other application such as waste water treatment or graphene production [7].

d. **Parametric study:** This study did not include investigating the HTL process by varying reaction time, feedstock, or catalyst loading. The parametric study can provide important information about the optimum condition for biocrude production from a specific feedstock. In the case of catalytic plastic depolymerization, a parametric study is required to determine the optimum temperature for maximum crude products with improved properties.

e. **Effect of solvent:** The type of solvent greatly influences the biocrude production and properties [8]. The chlorine content of dicholormethane extracted biocrude can be determined. The hydrogen donor solvent ethanol was used in this study to improve the woody biomass liquefaction. Other hydrogen donor solvents, such as tetralin and formic acid, can be used to

compare HTL depolymerization's effect. The attachment of solvent to biocrude can be determined by ^{13}C labeled solvent.Moreover, the current study could not break down polyethylene terephthalate (PET) plastic polymer by hydrolysis at high temperatures. Using hexane or octane as a solvent can depolymerize PET and other plastic polymers in the HTL process.

f. **Bi-products recycling:** The HTL depolymerization of plastic has produced a significant amount of gas fraction. The gaseous products, especially ethylene gas from polyethylene decomposition, can be utilized in the HTL reaction environment. Moreover, the recovered aqueous phase from wet feedstock can be applied as a reaction medium for dry feedstock to study the effect over crude and other by-products from the HTL process.

6.3 Reference

[1] R. Obeid, D.M. Lewis, N. Smith, T. Hall, P. van Eyk, Reaction kinetics and characterisation of species in renewable crude from hydrothermal liquefaction of monomers to represent organic fractions of biomass feedstocks, Chemical Engineering Journal. 389 (2020) 124397. https://doi.org/10.1016/j.cej.2020.124397.

[2] Y. Fan, U. Hornung, N. Dahmen, A. Kruse, Hydrothermal liquefaction of protein-containing biomass: study of model compounds for Maillard reactions, Biomass Conv. Bioref. 8 (2018) 909–923. https://doi.org/10.1007/s13399-018-0340-8.

[3] C. Yang, S. Wang, J. Yang, D. Xu, Y. Li, J. Li, Y. Zhang, Hydrothermal liquefaction and gasification of biomass and model compounds: a review, Green Chem. 22 (2020) 8210–8232. https://doi.org/10.1039/D0GC02802A.

[4] J. Rajagopal, K.P. Gopinath, R. Neha, K. Aakriti, R.S. Jayaraman, J. Arun, A. Pugazhendhi, Processing of household waste via hydrothermal gasification and hydrothermal liquefaction for bio-oil and bio-hydrogen production: Comparison with RSM studies, Journal of Environmental Chemical Engineering. 10 (2022) 107218. https://doi.org/10.1016/j.jece.2022.107218.

[5] M. Ellersdorfer, Hydrothermal co-liquefaction of chlorella vulgaris with food processing residues, green waste and sewage sludge, Biomass and Bioenergy. 142 (2020) 105796. https://doi.org/10.1016/j.biombioe.2020.105796.

[6] A. Matayeva, P. Biller, Hydrothermal liquefaction of post-consumer mixed textile waste for recovery of bio-oil and terephthalic acid, Resources, Conservation and Recycling. 185 (2022) 106502. https://doi.org/10.1016/j.resconrec.2022.106502.

[7] S. Mura, Y. Jiang, I. Vassalini, A. Gianoncelli, I. Alessandri, G. Granozzi, L. Calvillo, N. Senes, S. Enzo, P. Innocenzi, L. Malfatti, Graphene Oxide/Iron Oxide Nanocomposites for Water Remediation, ACS Appl. Nano Mater. 1 (2018) 6724–6732. https://doi.org/10.1021/acsanm.8b01540.

[8] H. Jahromi, T. Rahman, P. Roy, S. Adhikari, Hydrotreatment of solvent-extracted biocrude from hydrothermal liquefaction of municipal sewage sludge, Energy Conversion and Management. 263 (2022) 115719. https://doi.org/10.1016/j.enconman.2022.115719.

[9] H.V. Halleraker, S. Ghoreishi, T. Barth, Investigating reaction pathways for formic acid and lignin at HTL conditions using 13C-labeled formic acid and 13C NMR, Results in Chemistry. 2 (2020) 100019. https://doi.org/10.1016/j.rechem.2019.100019.

Appendix
A

Supporting information for Chapter 2

Hydrothermal liquefaction of municipal sewage sludge

Table A1: ICP analysis of catalysts in wt.%

CRM		RRM500		RRM700	
Fe	32.2	Fe	36.1	Fe	37.1
Al	8.58	Al	8.55	Al	10.7
Na	3.37	Na	3.81	Na	5.17
Ca	1.69	Ca	1.86	Ca	2.57
Ti	1.43	Ti	1.7	Ti	2.34
Mg	0.147	Mg	0.159	Mg	0.24
V	0.091	V	0.0902	V	0.0799
Zr	0.0469	Zr	0.0598	Zr	0.0684
K	0.041	K	0.038	K	0.051
Cr	0.031	Cr	0.03	Cu	0.041
P	0.009	P	0.021	Cr	0.035
Mn	0.0065	Mn	0.0065	Ni	0.017
Sr	0.006	Sr	0.006	Mn	0.0091
Th	0.0046	Th	0.0059	Zn	0.008
Ce	0.0033	Ce	0.0039	Th	0.0079
Re	0.0017	Re	0.0028	Sr	0.007
Y	0.001	Zn	0.002	Ce	0.005
Zn	0.001	Y	0.0013	Re	0.0028
La	0.0008	La	0.001	Y	0.0016
Cu	<0.0025	Cu	<0.0025	La	0.0014
Ni	<0.0025	Ni	<0.0025	P	<0.005

Table A2: Physicochemical properties of the biocrude after nine months.

Elemental Composition (wt.%)	Nitrogen				Ethylene			
	No catalyst	CRM	RRM500	RRM700	No catalyst	CRM	RRM500	RRM700
C	58.20±1.48	64.73±1.94	61.23±1.2	57.72±1.64	60.81±1.19	64.87±1.10	62.96±1.48	62.93±1.02
H	6.88±0.50	8.55±0.59	7.90±0.41	7.27±0.67	8.18±0.71	8.58±0.04	7.96±0.55	7.72±0.5
N	4.78±0.04	4.98±0.17	4.17±0.27	4.74±0.29	4.76±0.26	4.83±0.11	4.17±0.14	4.45±0.1
S	1.08±0.07	0.92±0.05	0.95±0.1	1.13±0.07	0.95±0.01	1.03±0.12	2.17±0.03	2.67±0.01
O[1]	29.06±2.10	20.82±1.11	25.74±1.5	29.14±1.33	25.30±1.73	20.70±1.07	22.74±1.83	22.23±1.64
HHV	28.54±0.23	30.53±0.30	28.05±0.12	25.74±0.22	28.27±0.32	30.64±0.56	29.15±0.24	28.96±0.15
TAN (mgKOH/g)	11.63±0.16	15.38±0.41	15.16±1.23	10.73±0.43	10.42±0.6	15.2±0.66	10.56±0.34	10.27±0.33
Dynamic Viscosity (cP)	8.20±0.50	n.d.[2]	13.81±1.20	7.51±0.23	23±0.12	n.d.	22.30±0.57	24.81±1.12
Density (g/cm3)	1.13±0.01	1.12±0.01	1.12±0.01	1.15±0.01	1.12±0.01	1.11±0.01	1.12±0.01	1.13±0.01

[1]by difference, [2] n.d.= not determined.

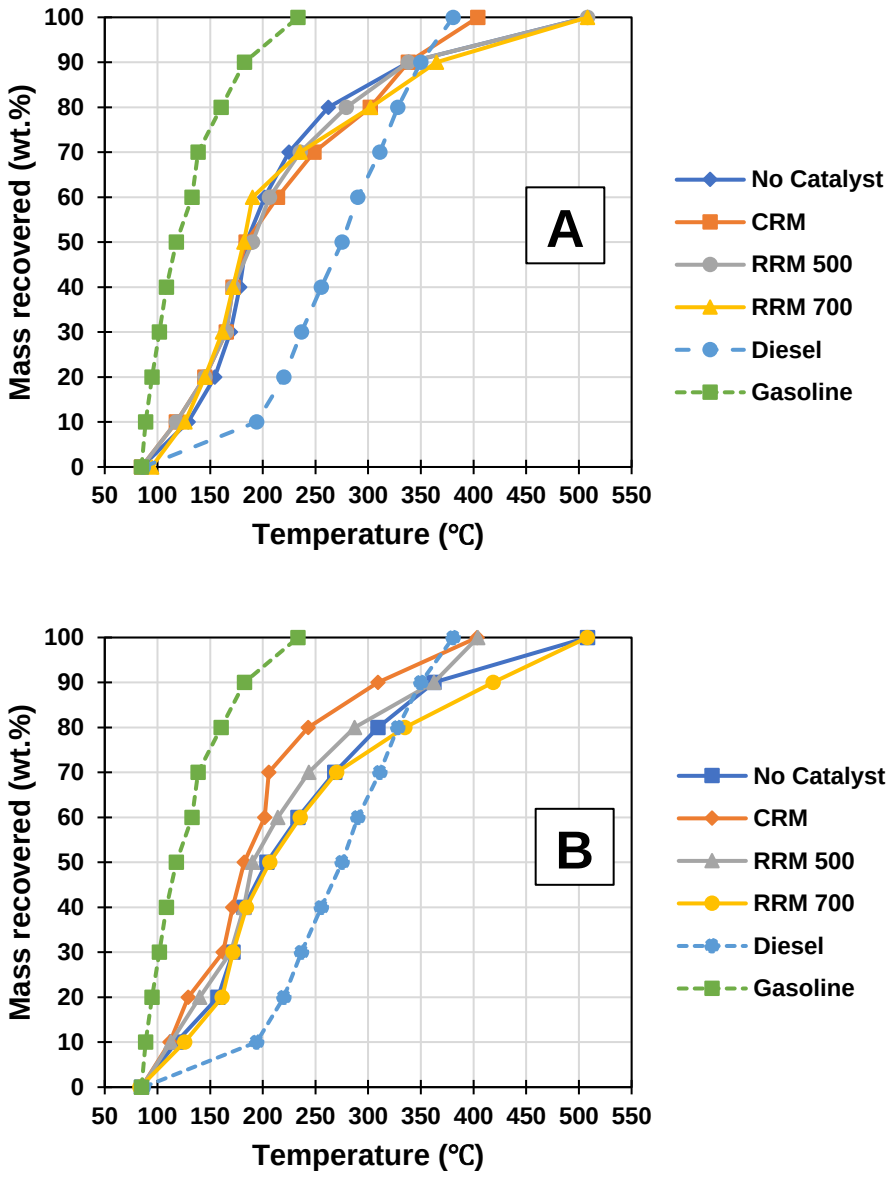

Figure A1: Simulated distillation of biocrude products: A-nitrogen atmosphere, B-ethylene atmosphere

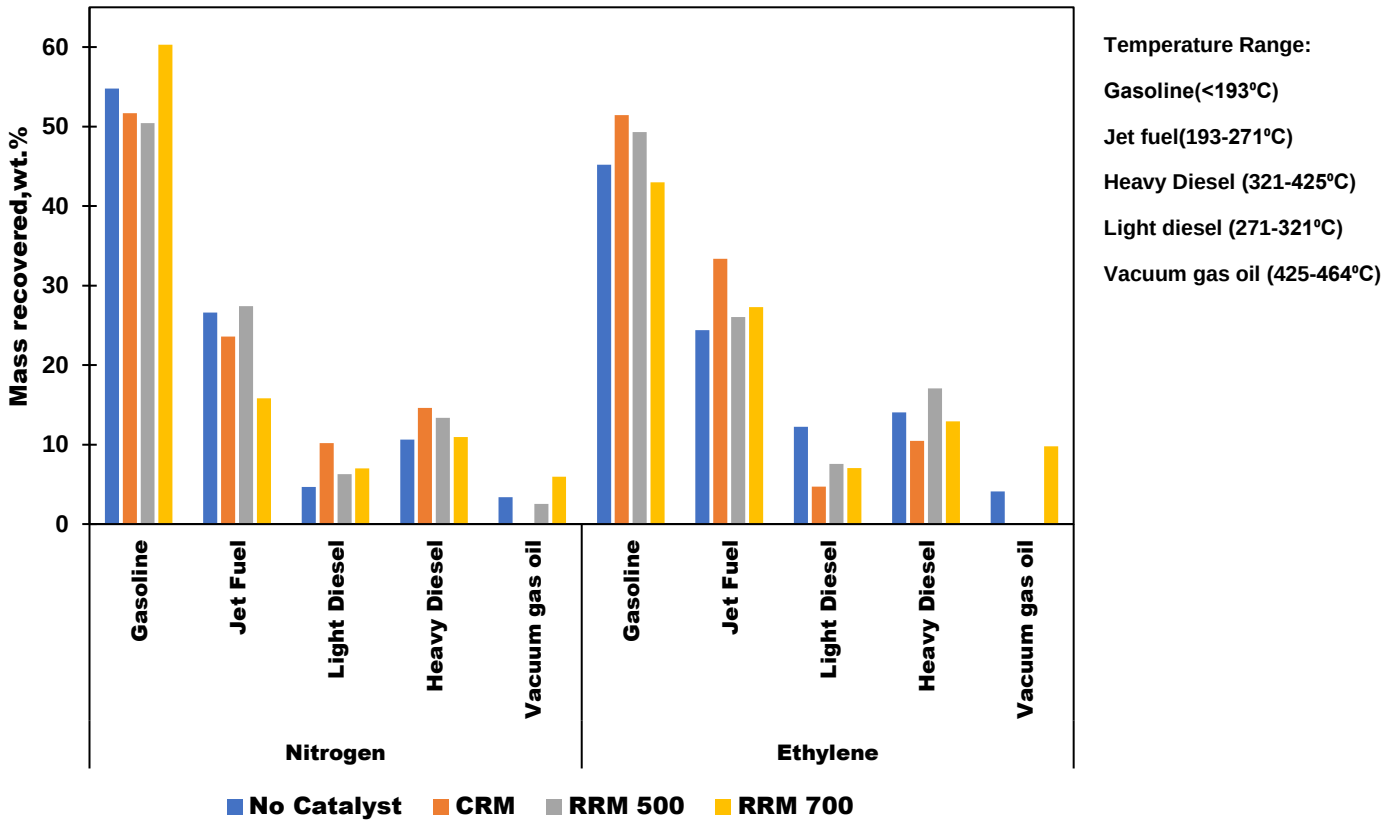

Figure A2: Comparison between HTL biocrudes and petroleum crude oil

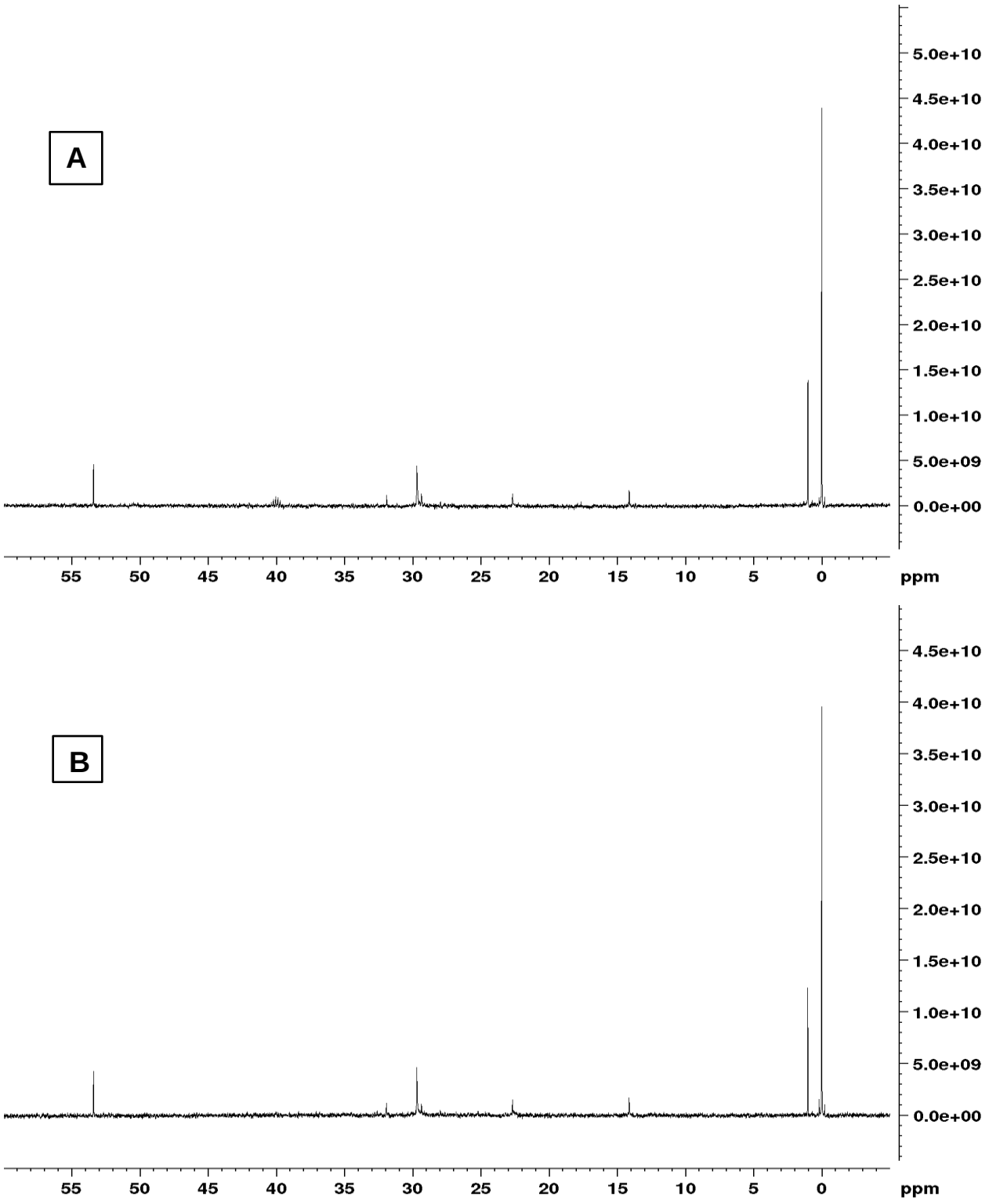
A
5.0e+10
4.5e+10
4.0e+10
3.5e+10
3.0e+10
2.5e+10
2.0e+10
1.5e+10
1.0e+10
5.0e+09
0.0e+00
55 50 45 40 35 30 25 20 15 10 5 0
ppm
B
4.5e+10
4.0e+10
3.5e+10
3.0e+10
2.5e+10
2.0e+10
1.5e+10
1.0e+10
5.0e+09
0.0e+00
55 50 45 40 35 30 25 20 15 10 5 0
ppm

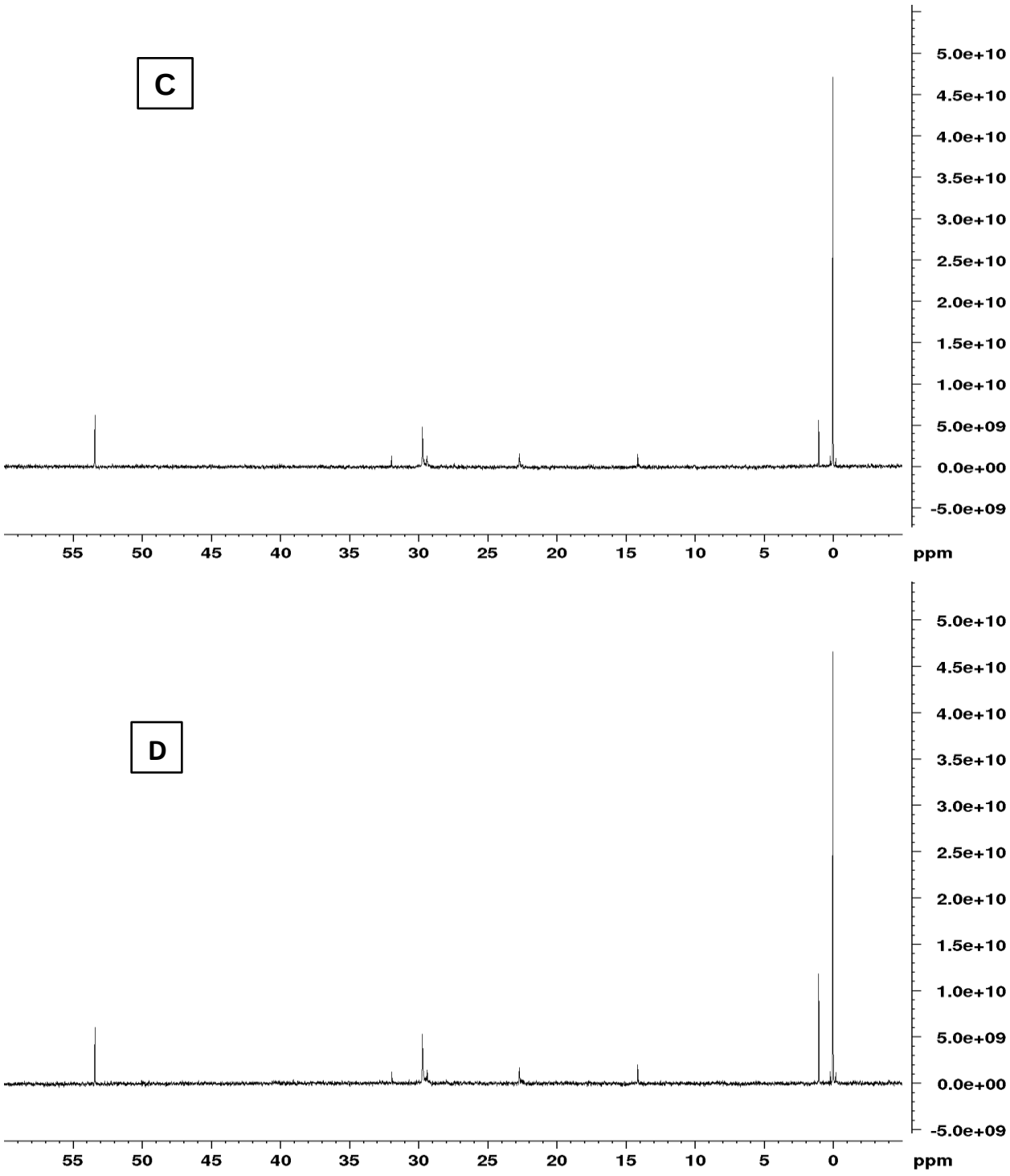

Figure A3: ^{13}C NMR spectra of biocrudes: A- Non-catalytic/nitrogen, B- Non-catalytic/ethylene , C- RRM500/nitrogen and D- RRM500/ethylene

Table A3: Individual peak area from ^{13}C NMR spectral integration

Peak chemical shift (ppm)		Peak area based on ^{13}C analysis[1]			
		Under nitrogen		Under ethylene	
		No catalyst	RRM500	No catalyst	RRM500
Saturated aliphatic (0-28 ppm)	0	8.08	8.84	8.63	8.01
	1	3.73	1.33	2.21	2.15
	14	0.62	0.44	0.84	0.65
	22	0.74	0.87	1.16	0.89
Unsaturated aliphatic (28-55 ppm)	29	4.16	4.13	4.38	4.52
	31	0.25	0.3	0.32	0.44
	53	1.39	1.59	1	1.22

[1]Relative integral

Table A4: Functional group distribution in biocrudes from ^{13}C NMR spectral integration

		Percentage of carbon based on ^{13}C NMR analysis[1]			
		Nitrogen		Ethylene	
Dominant type of carbon	Chemical Shift Region (ppm)	No Catalyst	RRM500	No Catalyst	RRM500
Saturated Aliphatic Groups	0-28ppm	69.4	65.6	69.3	65.4
Unsaturated Aliphatic Groups	28-55ppm	30.6	34.4	30.7	34.6

[1] Absolute integral

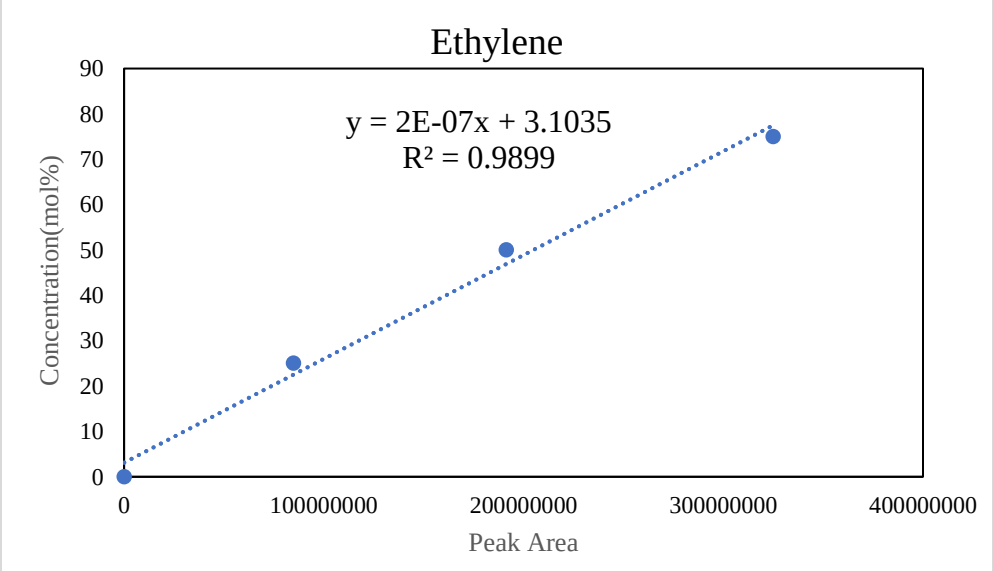

Figure A4: Calibration curve for the quantification of Ethylene using micro-GC peak area.

Appendix

B

Supporting Materials for Chapter 3

Influence of red mud catalyst and reaction atmosphere on hydrothermal liquefaction of algae

Table B1: ICP analysis of feedstock (*Tetraselmis* sp.*)* and catalysts (RRM, Ni/RM)

	ppm (parts per million)		
Metals	*Tetraselmis* sp.	RRM	Ni/RM
Al	5.0	70102.7	100829.0
B	95.9	193.7	214.5
Ca	16101.6	24391.6	18215.7
Cd	0.5	10.0	10.9
Co	41.2	7.5	37.6
Cr	1.5	253.4	273.8
Cu	13.5	15.4	6.7
Fe	1150.1	435473.0	317557.0
K	13150.1	247.2	195.3
Mg	2328.3	2201.6	1846.2
Mn	186.3	2.5	2.5
Mo	142.6	13.7	18.7
Na	107736.0	32176.4	33415.7
Ni	2.0	19.2	114802.0
P	17556.1	165.1	385.6
Pb	0.1	62.1	44.9
S	528.7	620.6	765.8
Si	17.4	24.7	333.5
Zn	5.0	25.9	386.7

Table B2: Physisorption data of the catalysts

Catalyst	Specific Surface area (m^2/g)	Average Pore Size nm	Total Pore Volume (cc/g)
RRM	21.92	6.15	0.07
Ni/RM	22.39	6.95	0.08

Table B3: F and p values from two-way ANOVA of *Tetraselmis* biocrude yields, carbon,sulfur,ash and oxygen content with reaction environment and catalysts as independent variables

	Source of variation	Degree of freedom(d.f.)	F	p
Biocrude yield	Environment	3	3.38	0.054
	Catalyst	2	32.96	0.000*
	Environment: Catalyst	6	2.07	0.132
Biocrude carbon content	Environment	3	45.58	0.000*
	Catalyst	2	340.61	0.000*
	Environment: Catalyst	6	41.9	0.000*
Biocrude sulfur content	Environment	3	1.26	0.330
	Catalyst	2	8.32	0.005*
	Environment: Catalyst	6	0.39	0.872
Biocrude ash content	Environment	3	107.79	0.000*
	Catalyst	2	255.52	0.000*
	Environment: Catalyst	6	28.15	0.000*
Biocrude oxygen content	Environment	3	7.74	0.003*
	Catalyst	2	72.36	0.000*
	Environment: Catalyst	6	12.65	0.000*

*Statistical difference ($p<0.05$)

Table B4: p values from Tukey HSD test for interaction between reaction environment and catalyst in carbon, ash, and oxygen content of *Tetraselmis* biocrude

	p value		
Environment: Catalyst	Carbon	Ash	Oxygen
Nitrogen:Ni/RM-Ethylene:Ni/RM	0.0008487*	1	0.1035373
Oxydizing:Ni/RM-Ethylene:Ni/RM	0.1822591	0.9999984	0.9954156
Reducing:Ni/RM-Ethylene:Ni/RM	0.7972486	0.0000024*	0.999998
Ethylene:No Catalyst-Ethylene:Ni/RM	0.0000002*	0.0009896*	0.0006409*
Nitrogen:No Catalyst-Ethylene:Ni/RM	0.0000001*	0.0000029*	0.000377*
Oxydizing:No Catalyst-Ethylene:Ni/RM	0.0000502*	0.0000541*	0.0612154
Reducing:No Catalyst-Ethylene:Ni/RM	0.0020856*	1	0.1041109
Ethylene:RRM-Ethylene:Ni/RM	0.8096817	0.0118237*	0.9924072
Nitrogen:RRM-Ethylene:Ni/RM	0.0323904*	0.1239269	0.3038562
Oxydizing:RRM-Ethylene:Ni/RM	0.0037532*	0.0002843*	0.1156699
Reducing:RRM-Ethylene:Ni/RM	0.0286355*	0.0456621*	0.5176787
Oxydizing:Ni/RM-Nitrogen:Ni/RM	0.0000182*	1	0.0223732*
Reducing:Ni/RM-Nitrogen:Ni/RM	0.0000834*	0.0000018*	0.0532349
Ethylene:No Catalyst-Nitrogen:Ni/RM	0.0001884*	0.0015001*	0.1284009
Nitrogen:No Catalyst-Nitrogen:Ni/RM	0.0000276*	0.0000038*	0.0701269
Oxydizing:No Catalyst-Nitrogen:Ni/RM	0.5657464	0.0000766*	0.9999998
Reducing:No Catalyst-Nitrogen:Ni/RM	0.9999035	1	1
Ethylene:RRM-Nitrogen:Ni/RM	0.0116095*	0.0075044*	0.4361003
Nitrogen:RRM-Nitrogen:Ni/RM	0.0000057*	0.19098	0.0015006*
Oxydizing:RRM-Nitrogen:Ni/RM	0.9931314	0.0001949	1
Reducing:RRM-Nitrogen:Ni/RM	0.0000053*	0.0287249*	0.0028877*
Reducing:Ni/RM-Oxydizing:Ni/RM	0.9572158	0.0000016*	0.9999752
Ethylene:No Catalyst-Oxydizing:Ni/RM	0*	0.0017943*	0.0001773*
Nitrogen:No Catalyst-Oxydizing:Ni/RM	0*	0.0000043*	0.0001086*
Oxydizing:No Catalyst-Oxydizing:Ni/RM	0.000002*	0.0000889*	0.0131297*
Reducing:No Catalyst-Oxydizing:Ni/RM	0.0000366*	0.9999999	0.0225013*
Ethylene:RRM-Oxydizing:Ni/RM	0.0117515*	0.0062019*	0.6782947
Nitrogen:RRM-Oxydizing:Ni/RM	0.9868103	0.2277283	0.8028771
Oxydizing:RRM-Oxydizing:Ni/RM	0.0000579*	0.0001665*	0.0250984*
Reducing:RRM-Oxydizing:Ni/RM	0.9787808	0.0236022*	0.957929
Ethylene:No Catalyst-Reducing:Ni/RM	0.0000001*	0*	0.0003604*
Nitrogen:No Catalyst-Reducing:Ni/RM	0*	0*	0.0002159*
Oxydizing:No Catalyst-Reducing:Ni/RM	0.0000072*	0*	0.0311727*
Reducing:No Catalyst-Reducing:Ni/RM	0.0001817*	0.0000022*	0.0535384
Ethylene:RRM-Reducing:Ni/RM	0.09562	0.0005971*	0.9241546
Nitrogen:RRM-Reducing:Ni/RM	0.439781	0.0000001*	0.5063414
Oxydizing:RRM-Reducing:Ni/RM	0.000303*	0.0283938*	0.0596805
Reducing:RRM-Reducing:Ni/RM	0.401482	0.0001931*	0.7528926
Nitrogen:No Catalyst-Ethylene:No Catalyst	0.8757436	0.0089185*	0.9999991
Oxydizing:No Catalyst-Ethylene:No Catalyst	0.0041054*	0.5406252	0.2107926
Reducing:No Catalyst-Ethylene:No Catalyst	0.0000863*	0.0011303*	0.1277049
Ethylene:RRM-Ethylene:No Catalyst	0.0000011*	0.0000034*	0.002828*

Nitrogen:RRM-Ethylene:No Catalyst	0*	0.1714494	0.0000218*
Oxydizing:RRM-Ethylene:No Catalyst	0.0000538*	0.0000003*	0.1150365
Reducing:RRM-Ethylene:No Catalyst	0*	0.0000079*	0.0000359*
Oxydizing:No Catalyst-Nitrogen:No Catalyst	0.0004154*	0.2854879	0.1181765
Reducing:No Catalyst-Nitrogen:No Catalyst	0.0000139*	0.0000031*	0.0697326
Ethylene:RRM-Nitrogen:No Catalyst	0.0000003*	0.0000001*	0.0015914*
Nitrogen:RRM-Nitrogen:No Catalyst	0*	0.0001088*	0.0000142*
Oxydizing:RRM-Nitrogen:No Catalyst	0.0000092*	0*	0.0625874
Reducing:RRM-Nitrogen:No Catalyst	0*	0.0000001*	0.0000231*
Reducing:No Catalyst-Oxydizing:No Catalyst	0.2679906	0.0000605*	0.9999998
Ethylene:RRM-Oxydizing:No Catalyst	0.0004562*	0.0000005*	0.2859558
Nitrogen:RRM-Oxydizing:No Catalyst	0.0000007*	0.0050993*	0.0009286*
Oxydizing:RRM-Oxydizing:No Catalyst	0.1524685	0.0000001*	0.9999986
Reducing:RRM-Oxydizing:No Catalyst	0.0000007*	0.0000009*	0.0017582*
Ethylene:RRM-Reducing:No Catalyst	0.0313434*	0.0102067*	0.4379153
Nitrogen:RRM-Reducing:No Catalyst	0.0000108*	0.1427658	0.0015084*
Oxydizing:RRM-Reducing:No Catalyst	0.9999991	0.0002515*	1
Reducing:RRM-Reducing:No Catalyst	0.00001*	0.0393367*	0.0029032*
Nitrogen:RRM-Ethylene:RRM	0.0021498*	0.0001039*	0.0657894
Oxydizing:RRM-Ethylene:RRM	0.0586635	0.3755437	0.4733693
Reducing:RRM-Ethylene:RRM	0.0019192*	0.998438	0.1311516
Oxydizing:RRM-Nitrogen:RRM	0.0000164*	0.000006*	0.0016662*
Reducing:RRM-Nitrogen:RRM	1	0.0003074*	0.9999967
Reducing:RRM-Oxydizing:RRM	0.0000151*	0.1132069	0.0032172*

*Statistical difference ($p<0.05$)

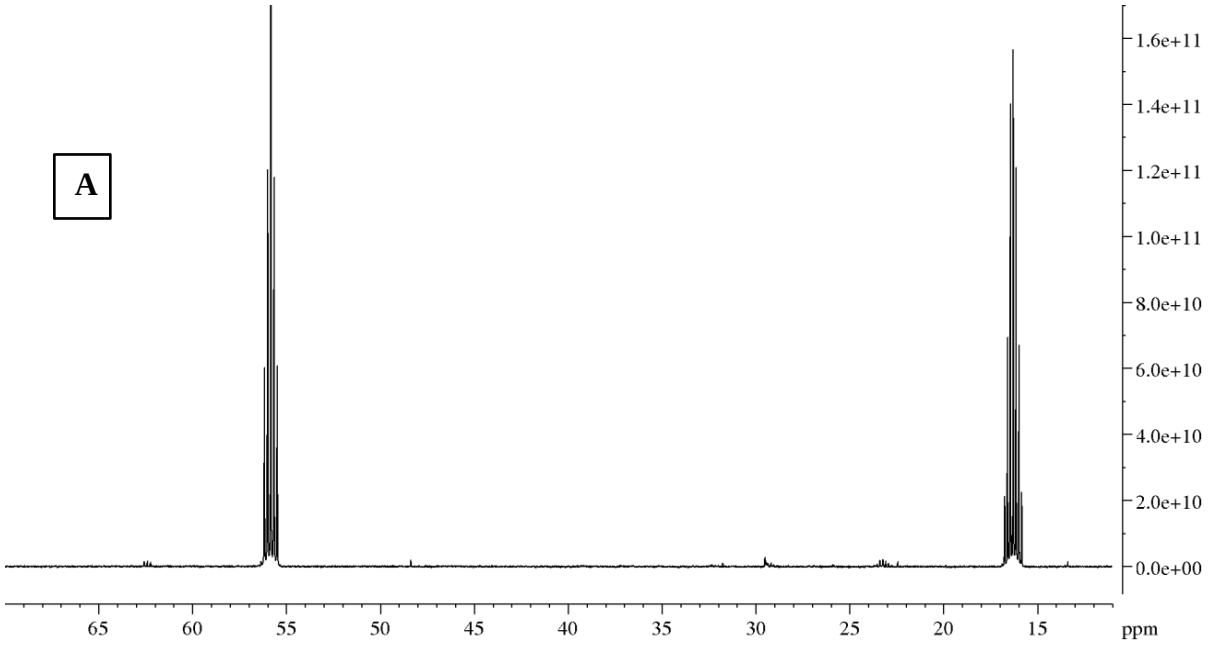
A
1.6e+11
1.4e+11
1.2e+11
1.0e+11
8.0e+10
6.0e+10
4.0e+10
2.0e+10
0.0e+00
65
60
55
50
45
40
35
30
25
20
15
ppm

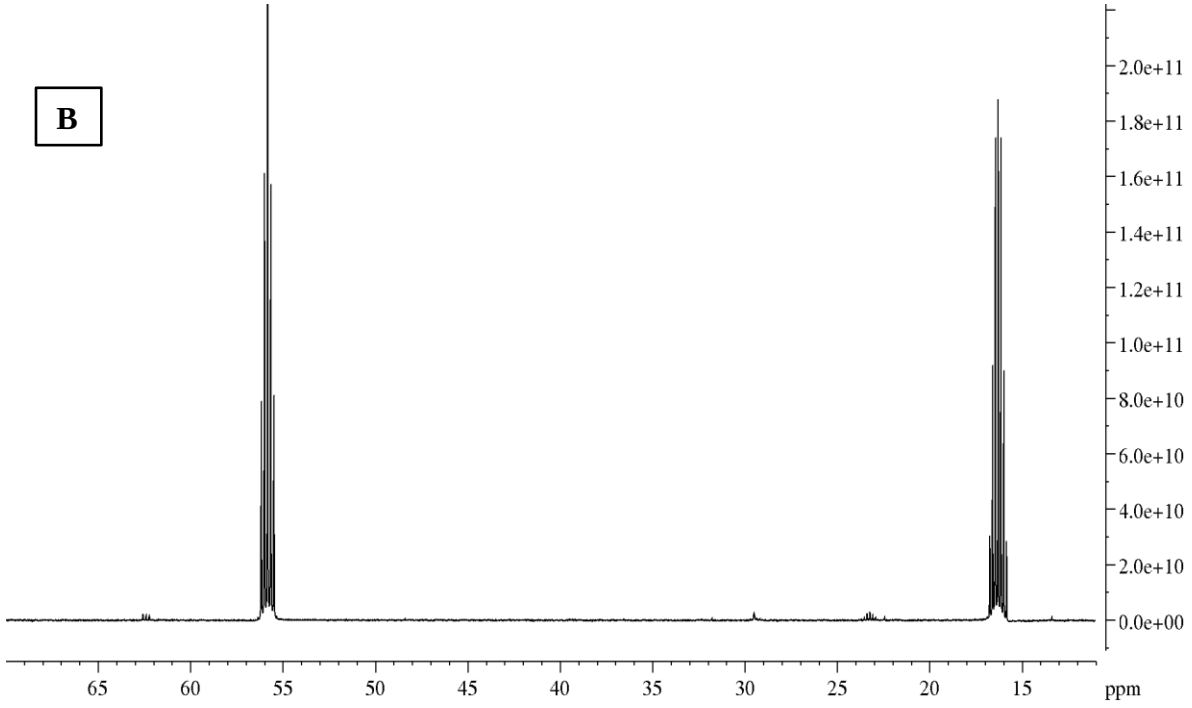
B
2.0e+11
1.8e+11
1.6e+11
1.4e+11
1.2e+11
1.0e+11
8.0e+10
6.0e+10
4.0e+10
2.0e+10
0.0e+00
65
60
55
50
45
40
35
30
25
20
15
ppm

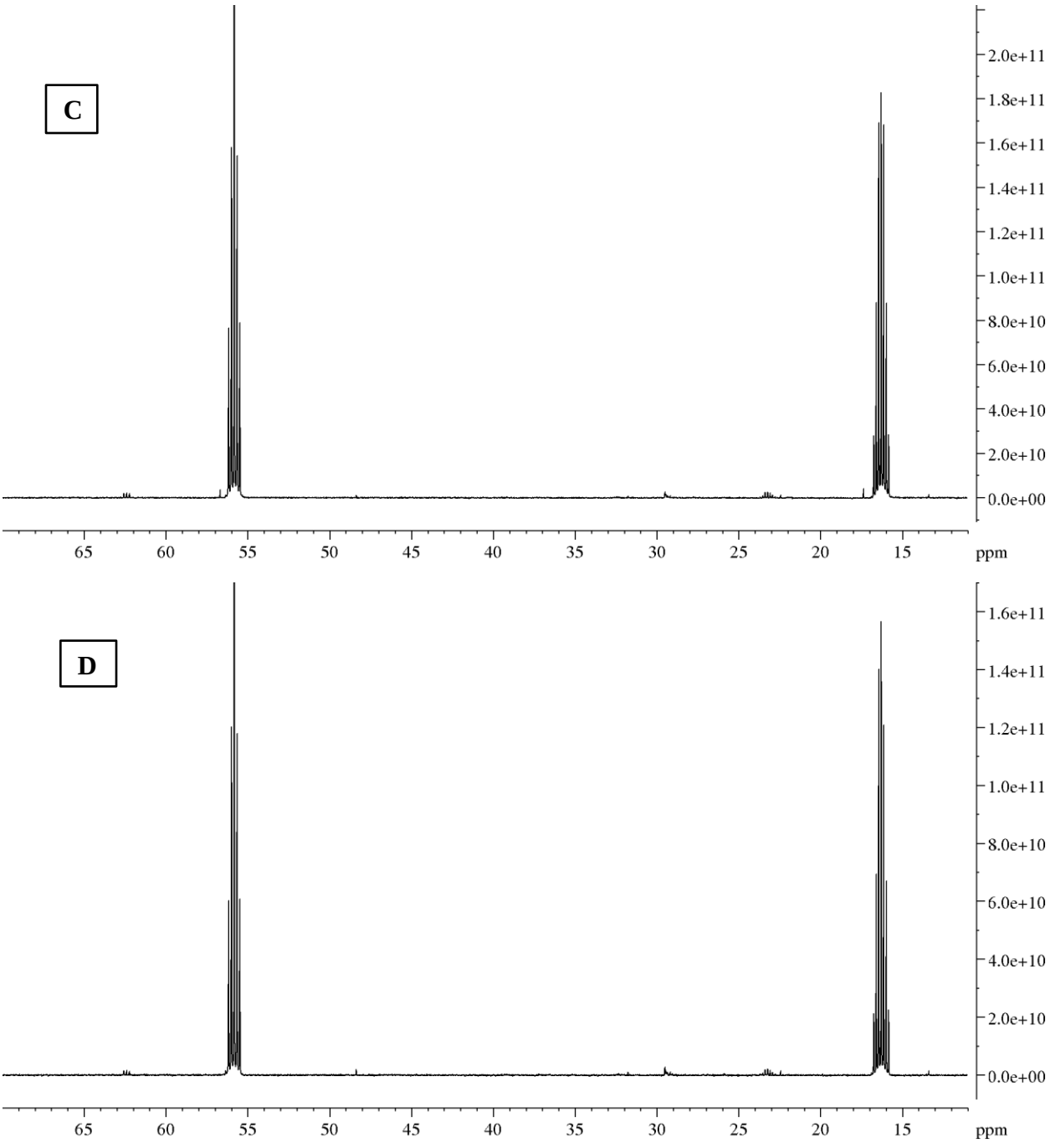

Figure B1: ^{13}C NMR spectra of Ni/RM catalyst derived *Tetraselmis* biocrudes: A-Nitrogen, B-Ethylene, C-Reducing and D-Oxidizing reaction environments

Table B5: Functional group distribution in biocrudes from ^{13}C NMR spectral integration

		Peak area($x10^{10}$) based on ^{13}C analysis[1]		
		Saturated Aliphatic Groups (0-28 ppm)	Unsaturated Aliphatic Groups (28-55 ppm)	Alcohols, ethers, phenolic methoxys, anhydrosugars (55-95 ppm)
Nitrogen	No Catalyst	4.9	4.2	2.3
	RRM	6.8	6.7	3.7
	Ni/RM	5.8	4.4	3.5
Ethylene	No Catalyst	3.4	3.8	3.0
	RRM	5.4	5.5	3.5
	Ni/RM	6.6	3.8	3.4
Reducing	No Catalyst	3.5	2.3	3.4
	RRM	3.3	1.3	3.7
	Ni/RM	4.4	4.5	3.4
Oxidative	No Catalyst	4.3	5.2	2.4
	RRM	4.6	4.9	2.6
	Ni/RM	4.1	4.3	2.4

[1]absolute integral

Appendix

C

Supporting Materials for Chapter 4

Depolymerization of household plastic waste via catalytic hydrothermal liquefaction

Table C1: Recipe of plastic mixture PM

Resin Identification Code	Plastic Type	Mixing Ratio (wt.%)
1	PET	42
2	HDPE	20
3	PVC[a]	0
4	LDPE	20
5	PP	4
6	PS	14
7	Other[b]	0
	Total	100

[a]Polyvinyl Chloride

[b]Other = polycarbonate, acrylic,nylon,bioplastic, composite etc.

[a,b] Due to high probability of corrosion and simplicity, the plastic component of PVC (resin code 3) and other(resin code 7) from original plastic recipe were excluded from this work.

Table C2: Reaction temperature and time of Plastic HTL experiments

	Plastic Type	Temperature [a] (°C)	Reaction time [b] (hour)	Pressure [a] (psi)
Non-Catalytic	PET	442	2	2247
	HDPE	408	2	2181
	LDPE	425	2	2327
	PP	450	1.5	2313
	PS	426	2.5	2053
	PM	429	2	2157
Catalytic	PET	430	2	2147
	HDPE	415	2	2100
	LDPE	426	2	2377
	PP	450	2	2385
	PS	450	3.5	2151
	PM	436	2	2196

[a] highest value obtained in 7-hour long experiment

[b] Reaction time at highest temperature

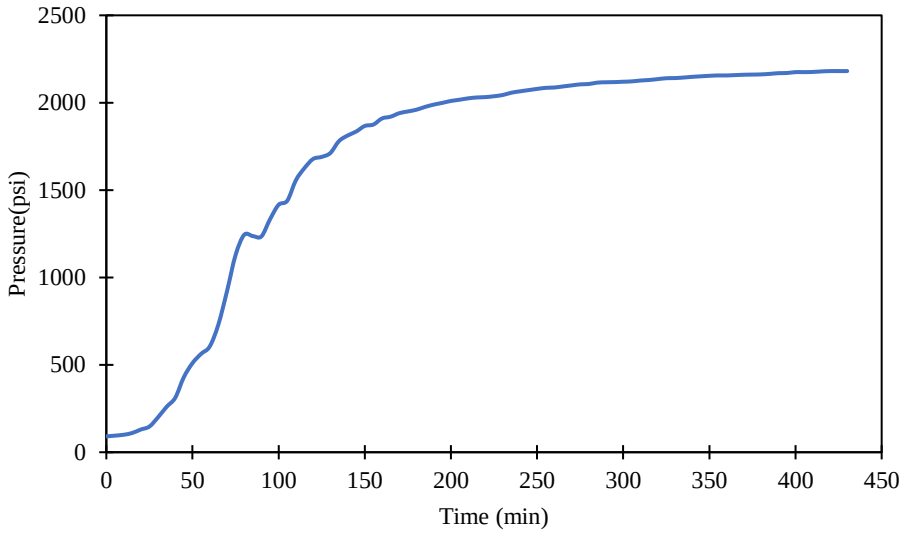

Figure C1:Typical Pressure Profile of plastic depolymerization in 7 hour long experiment

Table C3: ICP analysis of RRM500 catalyst

Metals	Catalyst (ppm)
Al	70102.7
B	193.7
Ca	24391.6
Cd	10.0
Co	7.5
Cr	253.4
Cu	15.4
Fe	435473.0
K	247.2
Mg	2201.6
Mn	2.5
Mo	13.7
Na	32176.4
Ni	19.2
P	165.1
Pb	62.1
S	620.6
Si	24.7
Zn	25.9

Table C4: Physisorption data of the catalysts

Specific Surface area (m^2/g)	Average Pore Size nm	Total Pore Volume (cc/g)
21.92	6.15	0.07

Table C5: ICP analysis of Plastic Feedstock

Metal (ppm)	PET	HDPE	LDPE	PP	PS
Al	<1.00	<1.00	108.9	43.58	256
B	1.06	1.38	3.85	0.55	1.69
Ca	137.5	97.8	91228	111.3	338.5
Cd	<0.50	<0.50	0.94	<0.50	<0.50
Co	53.21	1.84	1.57	1.13	0.84
Cr	<1.00	0.76	5.68	<1.00	<1.00
Cu	<0.50	<0.50	<0.50	<0.50	3.7
Fe	13.13	<1.00	192.5	12.77	56.74
K	<2.50	<2.50	<2.50	<2.50	113.89
Mg	39.9	32	2973	474.1	69.5
Mn	<2.50	<2.50	8.71	<2.50	<5.00
Mo	<0.50	1.13	<0.50	<0.50	<0.50
Na	<5.00	<5.00	107.52	<5.00	231.2
Ni	<0.50	<0.50	5.72	<0.50	3.4
P	30.48	12.7	51.82	29.81	41.24
Pb	<1.00	<1.00	<1.00	<1.00	<1.00
S	8.68	9.5	605.8	<2.50	90.68
Si	194	477	716	4352	376
Zn	<0.50	<0.50	47.23	<0.50	111.9

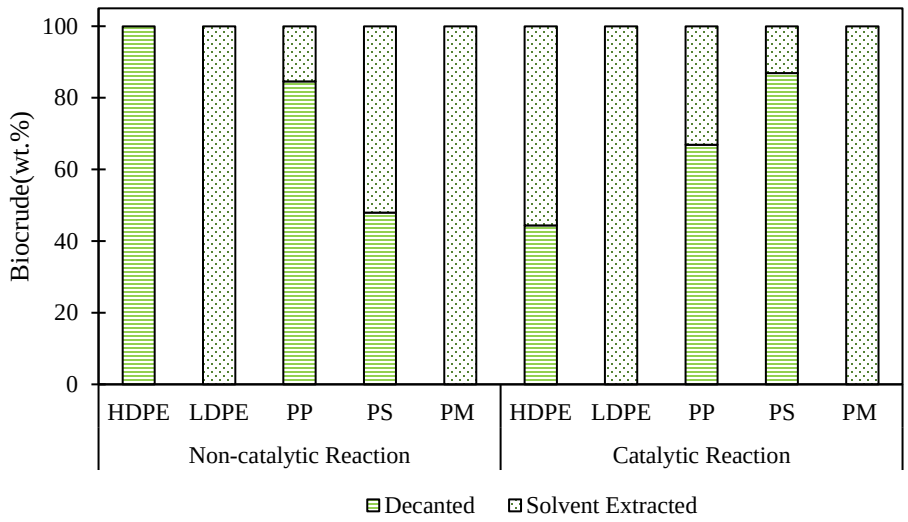

Figure C2: Biocrude composition on basis of extraction method

Table C6: Heavy metals in plastic HTL biocrudes

		ppm						
		Co	Cr	Cu	Fe	Mn	Ni	Zn
Non-Catalytic	HDPE	16	8	3	270	3	1	3
	LDPE	7	1	3	91	3	1	9
	PP	6	1	3	41	3	1	3
	PS	6	1	3	14	3	1	3
	PM	20	1	3	206	3	2	6
Catalytic	HDPE	28	1	3	465	3	1	3
	LDPE	12	1	3	91	3	1	8
	PP	31	1	3	160	3	1	3
	PS	21	1	3	65	3	1	3
	PM	18	1	3	164	3	1	3

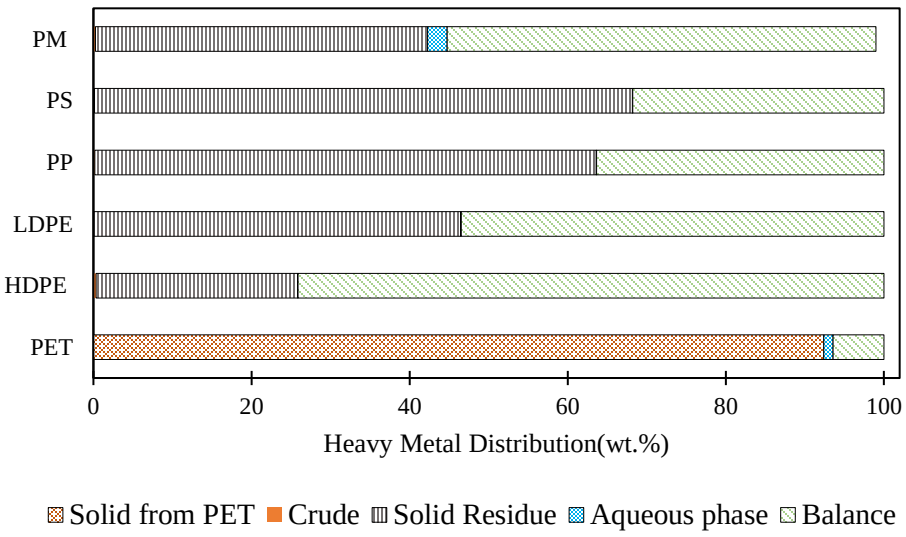

Figure C3: Heavy metal distribution in catalytic plastic oil.

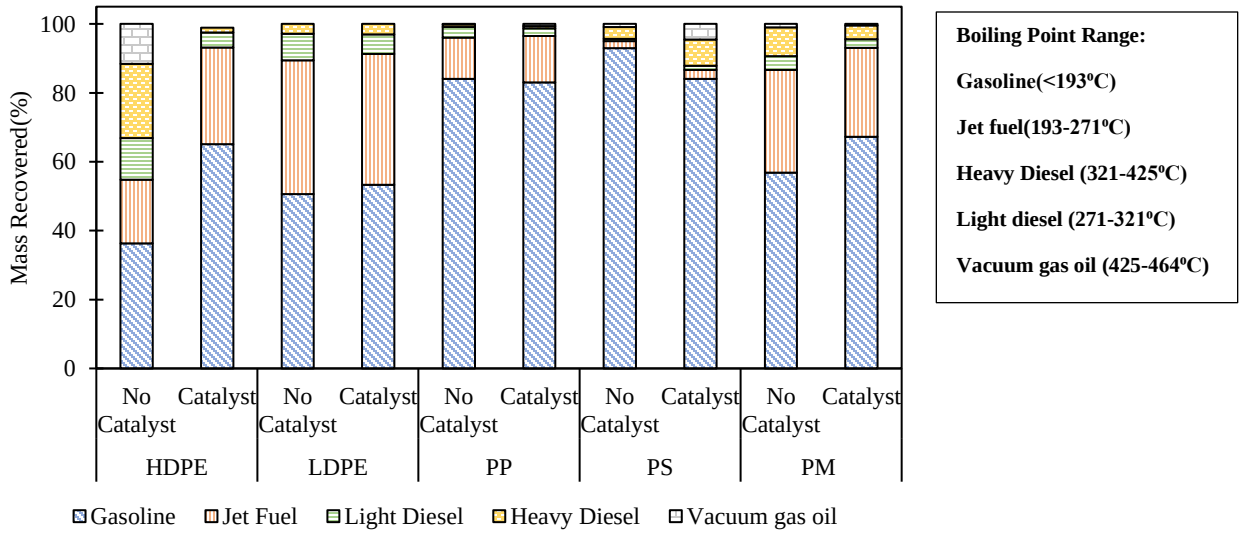

Figure C4: Simulated distillation of biocrudes from plastic HTL

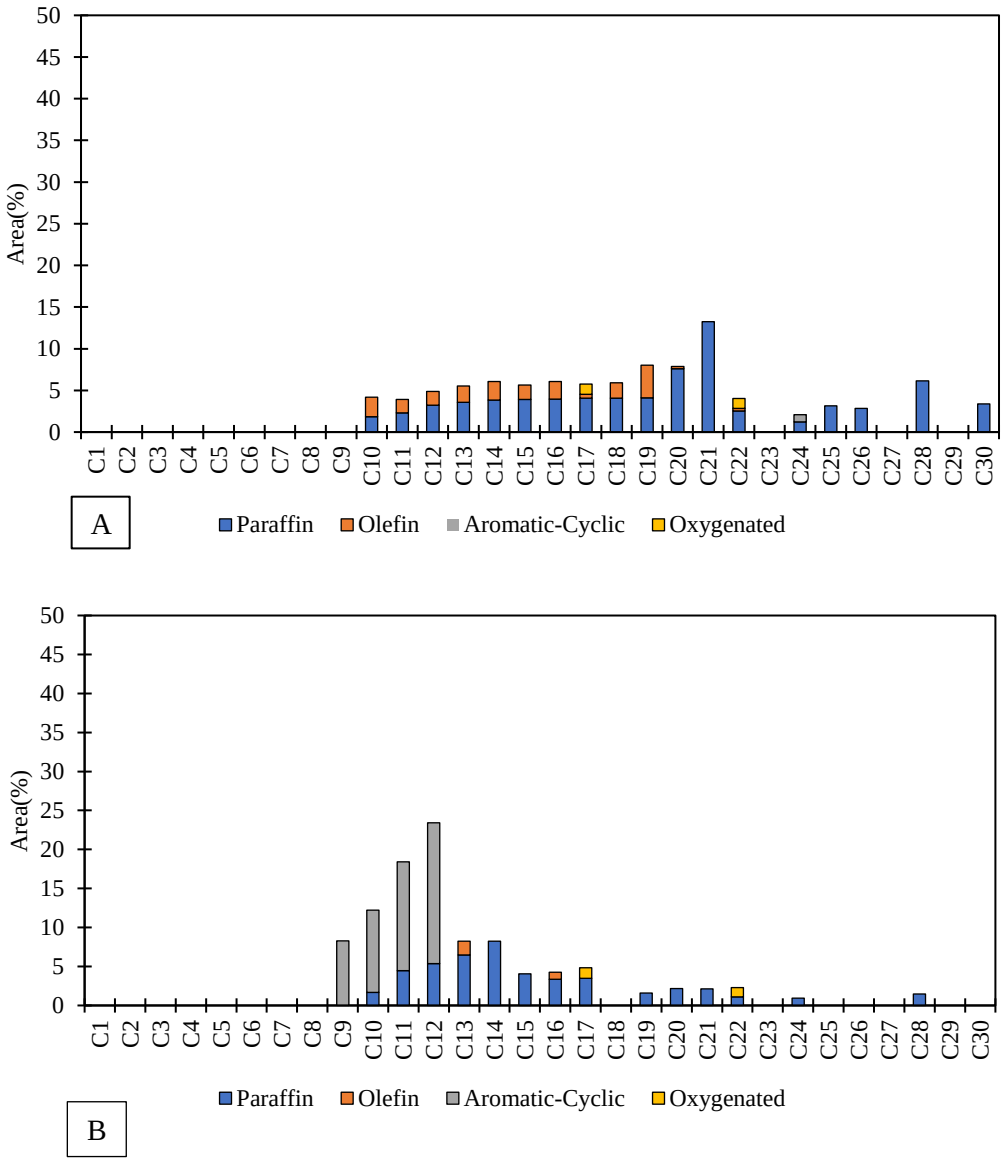

Figure C5: GC-MS detected compounds distribution by carbon number in HDPE crude oil : A- Non-Catalytic, B- Catalytic

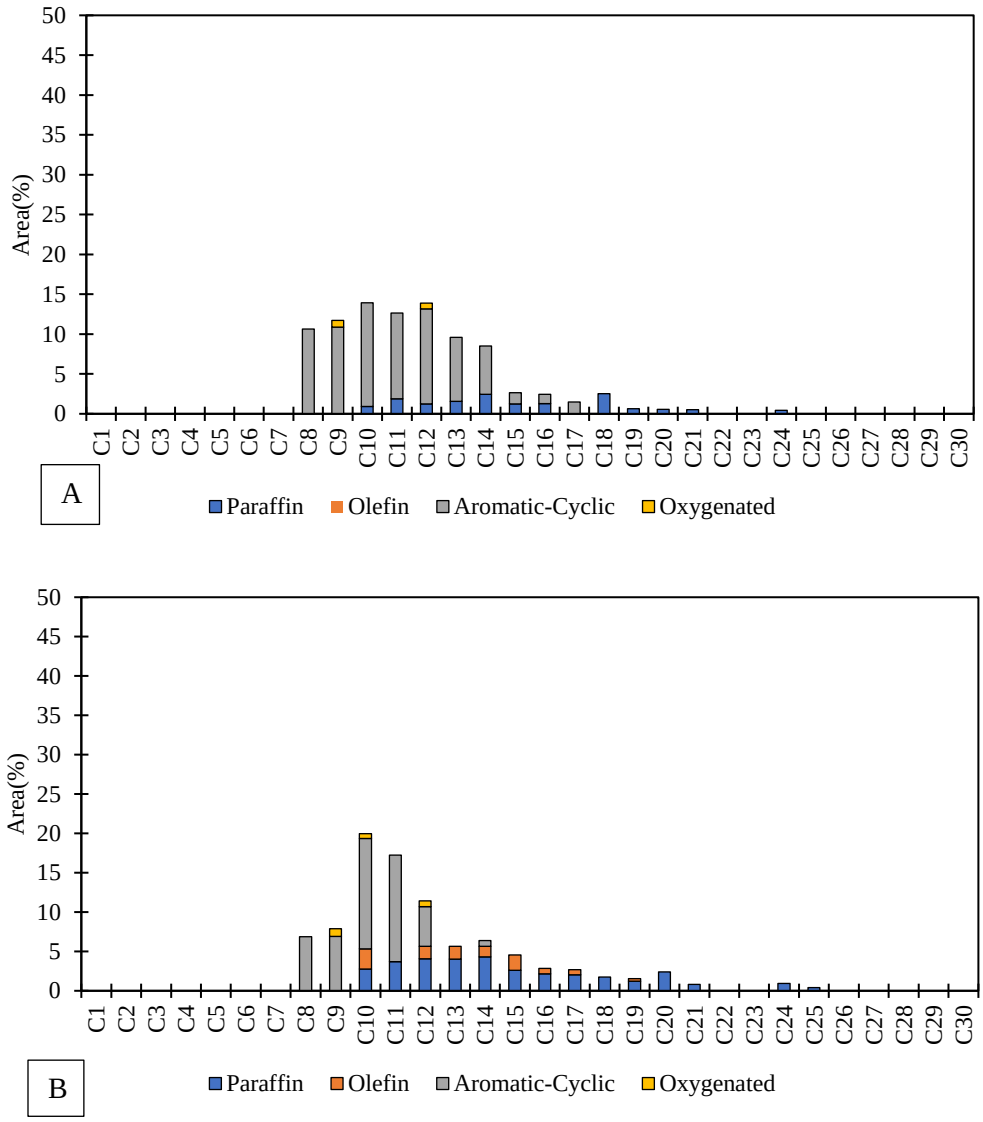

Figure C6: GC-MS detected compounds distribution by carbon number in LDPE crude oil : A- Non-Catalytic, B- Catalytic

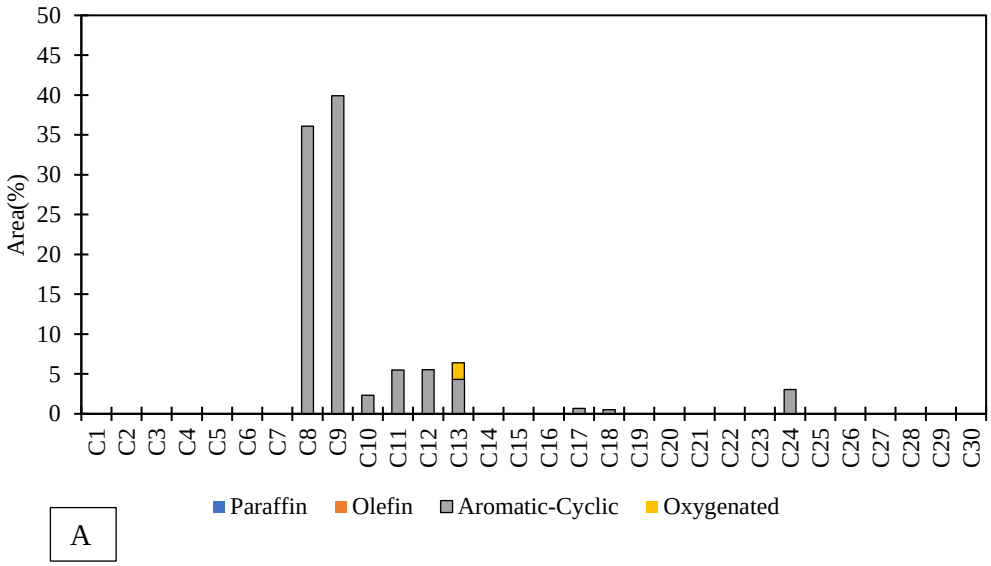

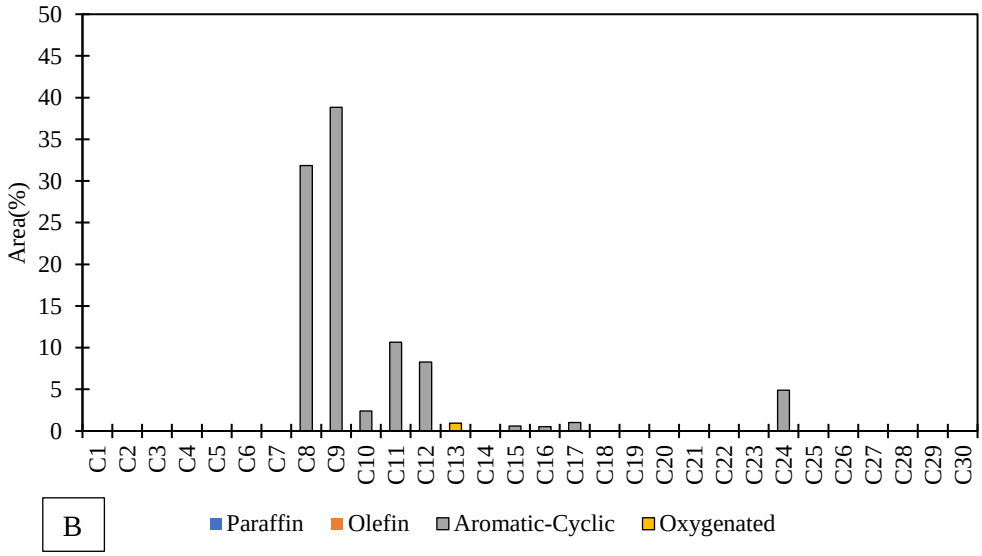

Figure C7: GC-MS detected compounds distribution by carbon number in PP crude oil : A- Non-Catalytic, B- Catalytic

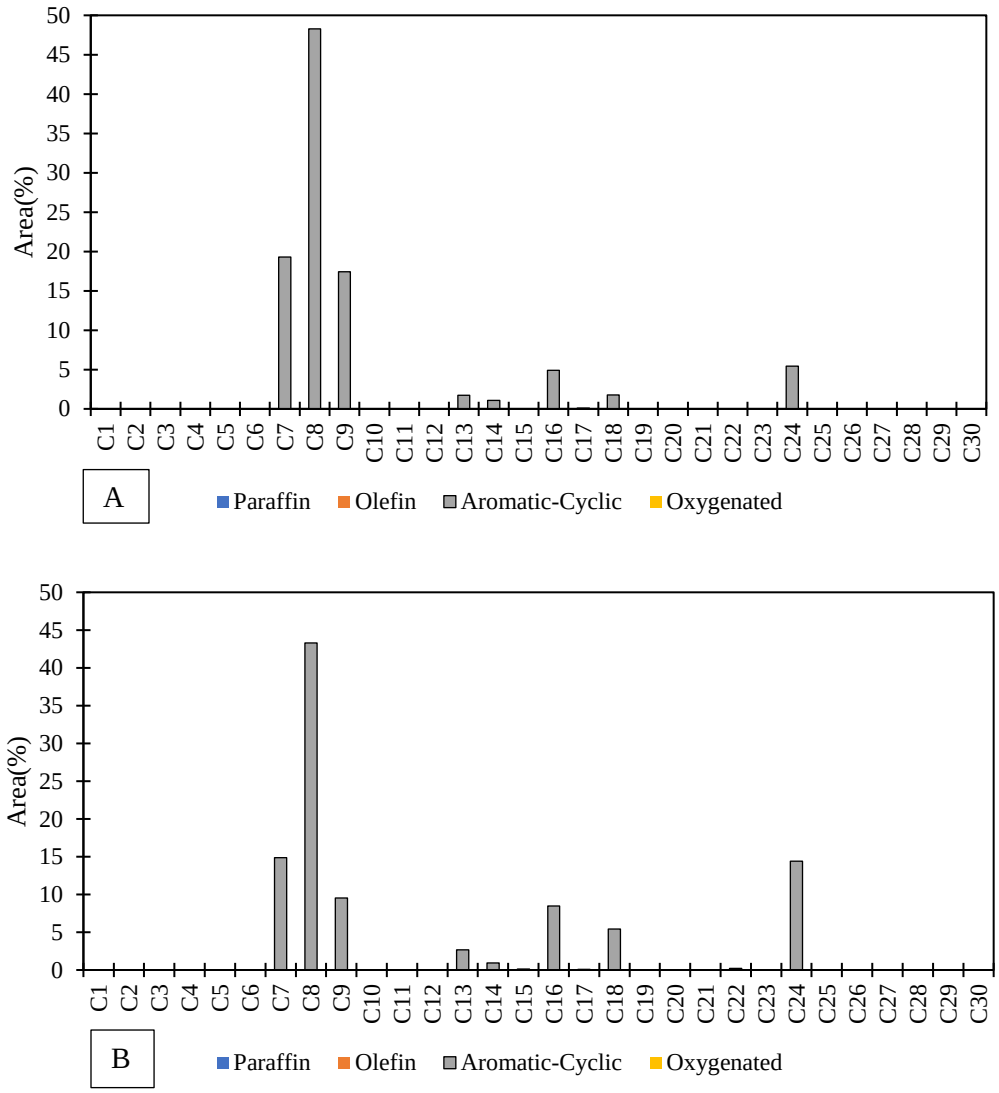

Figure C8: GC-MS detected compounds distribution by carbon number in PS crude oil : A- Non-Catalytic, B- Catalytic

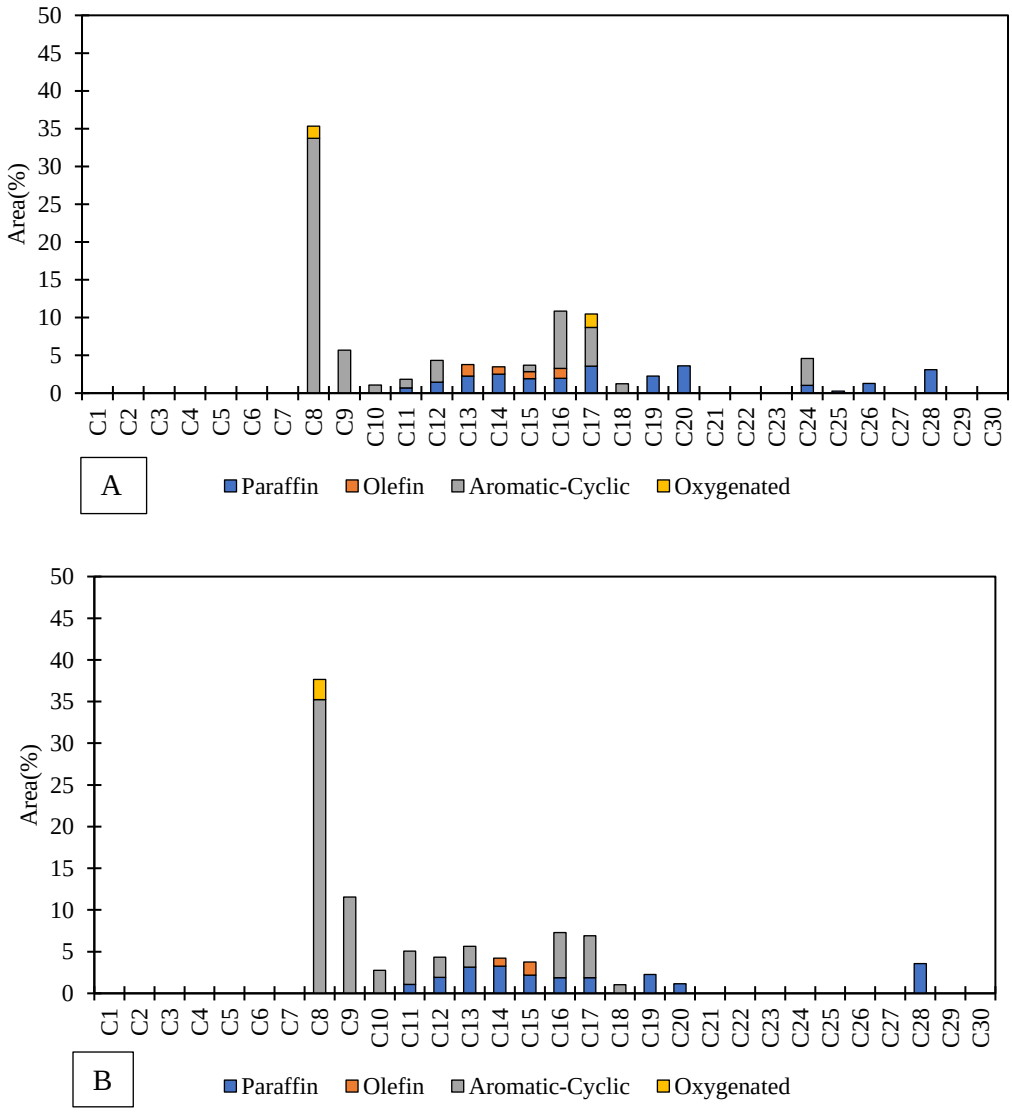

Figure C9: GC-MS detected compounds distribution by carbon number in plastic mixture (PM) crude oil : A- Non-Catalytic, B- Catalytic

Table C7: Semi quantification of GC-MS detectable compounds from non-catalytic HDPE HTL crude

Chemical Formula	Paraffin	Area
C10H22	Decane	1.8
C11H24	Undecane	2.3
C12H26	Dodecane	2.2
C13H28	Tridecane	2.6
C14H30	Tetradecane	2.8
C15H32	Pentadecane	3.9
$C_{16}H_{34}$	Hexadecane	4.0
C17H36	Heptadecane	4.1
C30H62	Triacontane	3.4
C21H44	Heneicosane	2.7
C22H44	Heptadecane	2.6
C30H62	Triacontane	3.4
C28H58	Tetracosane	1.6
C28H58	Tetracosane	2.0
C21H44	Heneicosane	3.9
C20H42	Eicosane	3.6
C18H38	Octadecane	4.1
C19H40	Nonadecane	4.1
C20H42	Eicosane	4.0
C21H44	Heneicosane	3.9
C25H52	Pentacosane	3.1
C26H54	Hexacosane	2.8
C21H44	Heneicosane	2.7
C28H58	Octacosane	2.6
C24H50	Tetracosane	1.2
	Total	75.4
Chemical Formula	Olefin	Area
C10H20	1-Decene	2.3
C11H22	1-Undecene	1.6
C12H24	1-Dodecene	1.7
C13H26	1-Tridecene	1.6
C13H26	4-Nonene, 5-butyl-	0.3
C14H28	2-Tetradecene, (E)-	1.9
C14H28	3-Tetradecene, (Z)-	0.3
C15H30	1-Pentadecene	1.7
C16H32	1-Hexadecene	1.6
C16H32	7-Hexadecene, (Z)-	0.5
C17H34	3-Heptadecene, (Z)-	0.4
C18H36	1-Octadecene	1.4
C18H36	5-Octadecene, (E)-	0.4
C19H38	Z-5-Nonadecene	1.3
C19H38	Z-5-Nonadecene	0.5
C20H40	5-Eicosene, (E)-	0.3
C19H38	1-Nonadecene	1.0
C19H38	Z-5-Nonadecene	1.1
C22H44	1-Docosene	0.3
	Total	20.4
Chemical Formula	Aromatic-Cyclic	Area
C24H48	Cyclotetracosane	0.9
Chemical Formula	Oxygenates	Area
C22H44O2	1-Heneicosyl formate	0.8
C22H44O2	1-Heneicosyl formate	0.4
C17H32O	E-15-Heptadecenal	1.3
	Total	2.4

Table C8: Semi quantification of GC-MS detectable compounds from catalytic HTL crude from HDPE

Chemical Formula	Paraffin	Area
C10H22	Decane	1.6
C11H24	Undecane	4.2
C12H26	Dodecane	5.0
C13H28	Tridecane	6.1
C14H30	Tetradecane	7.7
C15H32	Pentadecane	3.8
$C_{16}H_{34}$	Hexadecane	3.1
C17H36	Heptadecane	3.3
C19H40	Benzene, [1-(2,4-cyclopentadien-1-ylidene)ethyl]-	2.5
C20H42	Anthracene, 9,10-dihydro-	1.8
C20H42	Heneicosane	1.2
C21H44	Nonadecane	2.0
C22H46	Eicosane	1.0
C24H50	Tetracosane	0.9
C28H58	Docosane	1.4
	Total	45.5
Chemical Formula	Olefin	Area
C13H26	1-Tridecene	1.7
C16H32	1-Hexadecene	0.8
	Total	2.5
Chemical Formula	Aromatic-Cyclic	Area
C9H10	Benzene, 1,3,5-trimethyl-	1.8
C9H12	Benzene, 1,3,5-trimethyl-	1.8
C9H12	Undecane	4.2
C10H8	1H-Indene, 2,3-dihydro-4-methyl-	1.6
C10H10	Cyclododecane	1.4
C10H10	1H-Indene, 2,3-dihydro-4-methyl-	1.6
C10H12	1H-Indene, 2,3-dihydro-4-methyl-	1.6
C10H12	2-Methylindene	1.9
C10H12	2-Methylindene	1.7
C11H10	Naphthalene	2.7
C11H10	Naphthalene, 1,2-dihydro-3-methyl-	2.5
C11H12	Naphthalene, 1,2-dihydro-3-methyl-	2.5
C11H12	1H-Indene, 1,3-dimethyl-	3.0
C11H14	Naphthalene, 1,2-dihydro-3-methyl-	2.5
C12H10	(1-Methylpenta-1,3-dienyl)benzene	2.6
C12H12	Pentadecane	2.8
C12H12	(1-Methylpenta-1,3-dienyl)benzene	1.6
C12H12	1,2,3-Trimethylindene	1.3
C12H12	Naphthalene, 1-ethyl-	2.1
C12H14	Naphthalene, 2,7-dimethyl-	1.8
C12H14	Naphthalene, 1,6-dimethyl-	1.5
C12H24	1,2,3-Trimethylindene	1.3
	Total	49.7
Chemical Formula	Oxygenates	Area
C22H44O2	1-Heneicosyl formate	0.4
C17H32O	E-15-Heptadecenal	1.3
	Total	2.4

Table C9: Semi quantification of GC-MS detectable compounds from non- catalytic HTL crude from LDPE

Chemical Formula	Paraffin	Area
$C_{10}H_{22}$	Decane	0.9
C11H24	Undecane	1.9
C12H26	Dodecane	1.3
C13H28	Tridecane	1.6
C14H30	Tetradecane	2.5
C15H32	Pentadecane	1.2
$C_{16}H_{34}$	Hexadecane	1.3
C18H38	Octadecane	1.6
C19H40	Nonadecane	1.6
C20H42	Eicosane	0.5
C21H44	Heneicosane	0.5
C18H38	Octadecane	1.4
C24H50	Tetracosane	0.4
$C_{16}H_{34}$	Hexadecane	0.5
C18H38	Octacosane	0.5
	Total	17.8
Chemical Formula	Aromatic-Cyclic	Area
C8H10	Ethylbenzene	1.4
C8H10	p-Xylene	7.1
C8H10	Benzene, 1,3-dimethyl-	2.2
C9H12	Benzene, 1-ethyl-2-methyl-	3.5
C9H12	Benzene, 1,3,5-trimethyl-	1.2
C9H12	Benzene, 1-ethyl-2-methyl-	1.0
C9H12	Benzene, 1,3,5-trimethyl-	2.6
C10H14	Benzene, 1-methyl-4-propyl-	1.1
C9H10	Indane	2.6
C10H14	Benzene, 1-methyl-2-(1-methylethyl)-	1.5
C10H15	Benzene, 1-methyl-2-(1-methylethyl)-	0.8
C10H12	Benzene, (2-methyl-2-propenyl)-	1.6
C11H14	1H-Indene, 2,3-dihydro-1,3-dimethyl-	0.4
C10H12	1H-Indene, 2,3-dihydro-4-methyl-	1.8
C10H13	1H-Indene, 2,3-dihydro-4-methyl-	1.8
C10H10	1,4-Dihydronaphthalene	1.8
C10H10	Tetracyclo[5.3.0.0<2,6>.0<3,10>]deca-4,8-diene	1.6
C11H14	1H-Indene, 2,3-dihydro-1,6-dimethyl-	1.4
C11H12	1H-Indene, 2,3-dimethyl-	0.4
C10H8	Naphthalene	2.6
C11H14	2,3,4,5,6,7-Hexahydro-1H-cyclopenta[a]pentalene	0.7
C11H14	1H-Indene, 2,3-dihydro-4,7-dimethyl-	0.8
C11H12	1H-Indene, 1,3-dimethyl-	2.0
C11H13	1H-Indene, 1,3-dimethyl-	2.4
C11H14	1H-Indene, 2,3-dihydro-4,6-dimethyl-	0.5
C12H14	1,2,3-Trimethylindene	0.6

C11H10	Naphthalene, 1-methyl-	3.3
C11H10	Naphthalene, 2-methyl-	2.6
C12H14	1,2,3-Trimethylindene	1.4
C12H14	1,2,3-Trimethylindene	0.8
C13H16	Naphthalene, 1,2-dihydro-1,4,6-trimethyl-	0.3
C12H10	Naphthalene, 2-ethenyl-	2.1
C12H12	Naphthalene, 1,5-dimethyl-	0.5
C12H12	Naphthalene, 1,3-dimethyl-	0.2
C12H12	Naphthalene, 2,6-dimethyl-	0.6
C13H16	Naphthalene, 1,2-dihydro-3,5,8-trimethyl-	0.5
C12H12	Naphthalene, 2,3-dimethyl-	0.7
C12H12	Naphthalene, 2,3-dimethyl-	0.6
C12H12	Naphthalene, 2,3-dimethyl-	0.5
C13H12	1,1'-Biphenyl, 4-methyl-	0.4
C13H14	Naphthalene, 2-(1-methylethyl)-	0.9
C13H14	Naphthalene, 1,4,5-trimethyl-	0.4
C12H10	Acenaphthene	0.9
C13H14	Naphthalene, 1,4,6-trimethyl-	0.4
C13H14	Naphthalene, 1,6,7-trimethyl-	1.5
C13H14	Naphthalene, 2,3,6-trimethyl-	0.6
C13H14	Azulene, 4,6,8-trimethyl-	0.6
C13H14	Naphthalene, 1,4,5-trimethyl-	0.7
C13H10	Fluorene	1.1
C14H12	9H-Fluorene, 9-methyl-	1.7
C13H12	1-Isopropenylnaphthalene	0.6
C14H12	9H-Fluorene, 2-methyl-	0.5
C14H12	Anthracene, 9,10-dihydro-	1.0
C14H12	9H-Fluorene, 2-methyl-	0.9
C14H12	4a,9a-Methano-9H-fluorene	0.3
C14H14	4,4'-Dimethylbiphenyl	0.4
C14H10	Phenanthrene	0.7
C14H10	Phenanthrene, 9,10-dihydro-1-methyl-	0.5
C15H12	Phenanthrene, 2-methyl-	0.4
C15H12	Phenanthrene, 1-methyl-	0.4
C15H12	Phenanthrene, 2-methyl-	0.6
C16H10	Pyrene	1.2
C17H12	Pyrene, 1-methyl-	0.4
C17H12	Pyrene, 2-methyl-	0.5
C17H12	Pyrene, 1-methyl-	0.5
	Total	77.3
Chemical Formula	Oxygenates	Area
C9H10O	Benzenepropanal	1.8
C12H16O	1-Naphthalenemethanol, 1,2,3,4-tetrahydro-8-methyl-	1.7
	Total	3.6

Table C10: Semi quantification of GC-MS detectable compounds from catalytic HTL crude from LDPE

Chemical Formula	Paraffin	Area
$C_{10}H_{22}$	Decane	2.8
C11H24	Undecane	3.7
C12H26	Dodecane	4.0
C13H28	Tridecane	4.0
C14H30	Tetradecane	4.3
C15H32	Pentadecane	2.6
C16H34	Hexadecane	2.1
C17H36	Heptadecane	2.0
C18H38	Octadecane	1.7
C19H40	Nonadecane	1.2
C20H42	Eicosane	0.9
C21H44	Heneicosane	0.8
C20H42	Eicosane	0.9
C20H42	Eicosane	0.6
C24H50	Tetracosane	0.5
C25H52	Pentacosane	0.4
C24H50	Tetracosane	0.4
	Total	33.1
Chemical Formula	Olefin	Area
C10H20	1-Decene	2.5
C12H24	1-Dodecene	1.6
C13H26	1-Tridecene	1.7
C14H28	1-Tetradecene	1.4
C15H30	1-Pentadecene	1.9
C16H32	1-Hexadecene	0.7
C17H34	1-Heptadecene	0.6
C19H38	1-Nonadecene	0.3
	Total	10.8
Chemical Formula	Aromatic-Cyclic	Area
C8H10	Ethylbenzene	1.1
C8H10	p-Xylene	3.9
C8H10	p-Xylene	1.8
C9H12	Benzene, 1-ethyl-3-methyl-	3.3
C9H12	Benzene, 1-ethyl-2-methyl-	1.2
C19H12	Benzene, 1,2,3-trimethyl-	2.4
C12H24	Cyclopropane, nonyl-	2.1
C10H14	Benzene, 1-methyl-2-propyl-	1.1
C9H10	Benzene, cyclopropyl-	2.4
C10H14	Benzene, 1-methyl-3-(1-methylethyl)-	1.9
C10H14	Benzene, 2-ethyl-1,3-dimethyl-	1.0
C10H12	Benzene, 1-ethenyl-3-ethyl-	1.6
C11H14	1H-Indene, 2,3-dihydro-1,3-dimethyl-	0.8
C10H12	1H-Indene, 2,3-dihydro-4-methyl-	1.4
C10H12	Benzene, 2-ethenyl-1,4-dimethyl-	1.8
C10H10	1,4-Dihydronaphthalene	1.8
C10H10	1H-Indene, 1-methyl-	1.3
C11H14	1H-Indene, 2,3-dihydro-1,6-dimethyl-	1.6
C11H12	1H-Indene, 1,3-dimethyl-	0.8
C10H8	Naphthalene	2.2
C11H14	2-Ethyl-2,3-dihydro-1H-indene	0.7
C11H14	1H-Indene, 2,3-dihydro-4,7-dimethyl-	0.6
C11H12	1H-Indene, 1,3-dimethyl-	1.7
C11H12	1H-Indene, 1,3-dimethyl-	1.1

C11H12	1H-Indene, 1,3-dimethyl-	0.9
C12H14	Benzene, 1,4-bis(1-methylethenyl)-	0.6
C11H10	Naphthalene, 2-methyl-	1.3
C11H10	Naphthalene, 1-methyl-	1.0
C12H14	1,2,3-Trimethylindene	0.9
C12H12	Naphthalene, 1-ethyl-	0.8
C12H12	Naphthalene, 1,7-dimethyl-	1.0
C12H12	Naphthalene, 1,4-dimethyl-	0.9
C12H12	Naphthalene, 1,3-dimethyl-	0.4
C12H12	Naphthalene, 1,5-dimethyl-	0.6
C12H10	Acenaphthene	0.5
C14H12	Anthracene, 9,10-dihydro-	0.7
	Total	48.3
Chemical Formula	Oxygenates	Area
C10H12O	4-Methylphenyl acetone	0.6
C12H16O	1-Naphthalenemethanol, 1,2,3,4-tetrahydro-8-methyl-	0.7
C9H10O	Benzenepropanal	1.0
	Total	2.3

Table C11: Semi quantification of GC-MS detectable compounds from non-catalytic PP HTL crude

Chemical Formula	Aromatic-Cyclics	Area
C8H10	Ethylbenzene	2.5
C8H10	o-Xylene	17.8
C8H10	p-Xylene	9.9
C8H10	Benzene, 1,3-dimethyl-	3.9
C9H12	Benzene, 1,2,3-trimethyl-	34.5
C9H18	Cyclohexane, 1,2,4-trimethyl-, (1.alpha.,2.beta.,4.beta.)-	3.4
C11H10	Naphthalene, 1-methyl-	2.3
C13H14	Naphthalene, 1,4,5-trimethyl-	0.5
C11H14	Benzene, (3-methyl-2-butenyl)-	3.2
C12H12	Naphthalene, 2,6-dimethyl-	5.5
C11H14	1H-Indene, 2,3-dihydro-1,2-dimethyl-	2.2
C13H14	Naphthalene, 1,4,6-trimethyl-	2.8
C13H18	Naphthalene, 1,2,3,4-tetrahydro-1,5,7-trimethyl-	1.0
C17H16	6,7,8,9-Benzo[b]fluorene	0.7
C18H14	o-Terphenyl	0.5
C24H18	1,1':2',1''-Terphenyl, 4'-phenyl-	3.0
C10H14	Benzene, 1,2-diethyl-	0.2
C10H14	Benzene, 2-ethyl-1,4-dimethyl-	2.1
	Total	96.0
	Oxygenates	Area
C13H10O	[1,1'-Biphenyl]-4-carboxaldehyde	2.1

Table C12: Semi quantification of GC-MS detectable compounds from catalytic PP HTL crude oil

Chemical Formula	Aromatic-Cyclic	Area
C8H10	Ethylbenzene	1.6
C8H10	p-Xylene	28.0
C8H10	o-Xylene	1.0
C8H10	Benzene, 1,3-dimethyl-	2.3
C9H12	Benzene, 1,2,3-trimethyl-	23.4
C9H12	Naphthalene, 1,4,5-trimethyl-	6.1
C9H12	Benzene, 1-ethyl-3-methyl-	3.0
C9H18	Cyclohexane, 1,2,4-trimethyl-, (1.alpha.,2.beta.,4.beta.)-	2.4
C10H12	1-Phenyl-1-butene	1.7
C10H14	Benzene, 1,2-diethyl-	0.7
C11H10	Naphthalene, 1-methyl-	4.6
C11H14	Benzene, 2-ethenyl-1,3,5-trimethyl-	3.0
C11H14	.alpha.,.beta.,.beta.-Trimethylstyrene	0.6
C11H14	Benzene, (3-methyl-2-butenyl)-	3.4
C12H12	Naphthalene, 2,6-dimethyl-	8.3
C15H14	9H-Fluorene, 2,3-dimethyl-	0.6
C16H14	Phenanthrene, 2,5-dimethyl-	0.5
C17H12	Fluoranthene, 2-methyl-	0.2
C17H12	Pyrene, 1-methyl-	0.8
C24H18	1,1':2',1"-Terphenyl, 4'-phenyl-	4.9
	Total	97.1
	Oxygenates	Area
C13H10O	[1,1'-Biphenyl]-4-carboxaldehyde	2

Table C13: Semi quantification of GC-MS detectable compounds from non-catalytic PS HTL crude oil

Chemical Formula	Aromatic-Cyclic	Area
C7H8	Toluene	19.3
C8H10	Ethylbenzene	48.4
C13H12	1,1'-Biphenyl, 2-methyl-	0.2
C13H12	Diphenylmethane	1.0
C14H14	Benzene, 1,1'-ethylidenebis-	0.9
C14H14	Benzene, 1,1'-(1,2-ethanediyl)bis-	0.2
C16H12	Anthracene, 9-ethenyl-	1.5
C16H12	2-Phenylnaphthalene	0.4
C16H12	Naphthalene, 2-phenyl-	0.3
C16H12	1H-Indene, 1-(phenylmethylene)-	0.1
C17H14	Anthracene, 9-(2-propenyl)-	0.1
C18H14	m-Terphenyl	2.2
C24H18	1,1':2',1"-Terphenyl, 4'-phenyl-	5.3
C9H12	Benzene, (1-methylethyl)-	17.4
	Total	97.3

Table C14: Semi quantification of GC-MS detectable compounds from catalytic PS HTL crude

Chemical Formula	Aromatic-Cyclic	Area
C7H8	Toluene	14.8
C8H10	Ethylbenzene	43.1
C9H12	Benzene, 1,2,3-trimethyl-	8.6
C13H12	1,1'-Biphenyl, 2-methyl-	1.0
C13H12	Diphenylmethane	0.6
C14H10	Anthracene	0.1
C14H14	Benzene, 1,1'-ethylidenebis-	0.8
C15H12	1H-Indene, 2-phenyl-	0.1
C16H12	Anthracene, 9-ethenyl-	1.9
C16H12	Naphthalene, 2-phenyl-	3.8
C16H12	2-Phenylnaphthalene	0.5
C16H12	1H-Indene, 1-(phenylmethylene)-	0.3
C17H12	Pyrene, 1-methyl-	0.1
C18H14	m-Terphenyl	5.4
C24H18	1,1':2',1"-Terphenyl, 4'-phenyl-	13.8
C24H18	1,1':2',1":3",1'"-Quaterphenyl	0.6
C9H12	Benzene, (1-methylethyl)-	0.9
C22H16	1H-Indene, 1-(diphenylmethylene)-	0.2
	Total	96.7

Table C15: Semi quantification of GC-MS detectable compounds from non-catalytic HTL crude from Plastic mixture(PM)

Chemical Formula	Paraffin	Area
C11H24	Undecane	0.7
C12H26	Dodecane	1.4
C13H28	Tridecane	2.3
C14H30	Tetradecane	2.5
C15H32	Pentadecane	1.9
C16H34	Hexadecane	2.0
C17H36	Heptadecane	1.8
C19H40	Nonadecane	1.3
C20H42	Eicosane	1.0
C21H44	Heneicosane	1.9
C17H36	Heptadecane	1.8
C20H42	Eicosane	1.6
C25H52	Pentacosane	0.3
C26H54	Hexacosane	1.3
C24H50	Tetracosane	1.0
C28H58	Octacosane	1.1
C28H58	Octadecane	2.0
	Total	25.9
Chemical Formula	Olefin	Area
C13H26	1-Tridecene	1.5
C14H28	2-Tetradecene, (E)-	1.0
C15H30	1-Pentadecene	0.9
C16H32	1-Hexadecene	1.3
	Total	4.7
Chemical Formula	Aromatics	Area
C8H10	Ethylbenzene	33.7
C9H12	Benzene, (1-methylethyl)-	5.7
C10H8	Naphthalene	1.1
C11H10	Naphthalene, 2-methyl-	1.1
C12H10	Biphenyl	2.9
C15H16	Benzene, 1,1'-(1,3-propanediyl)bis-	0.9
C16H12	Anthracene, 9-ethenyl-	3.1
C16H14	3-Methyl-1-phenyl-1H-indene	1.0
C16H12	2-Phenylnaphthalene	3.5
C17H14	Anthracene, 9-(2-propenyl)-	1.3
C17H14	Naphthalene, 2-(phenylmethyl)-	3.8
C18H14	m-Terphenyl	1.3
C24H18	1,1':2',1"-Terphenyl, 4'-phenyl-	3.6
	Total	62.9
	Oxygenates	Area
C8H8O	Acetophenone	1.6
C17H32O	E-15-Heptadecenal	1.0
C17H32O	E-15-Heptadecenal	0.8
	Total	3.4

Table C16: Semi quantification of GC-MS detectable compounds from catalytic HTL crude from Plastic mixture(PM)

Chemical Formula	Paraffin	Area
C11H24	Undecane	1.1
C12H26	Dodecane	1.9
C13H28	Tridecane	3.1
C14H30	Tetradecane	3.2
C15H32	Pentadecane	2.2
C16H34	Hexadecane	1.9
C17H36	Heptadecane	1.9
C28H58	Octadecane	1.8
C19H40	Nonadecane	1.2
C20H42	Eicosane	1.1
C19H40	Nonadecane	1.0
C28H58	Octadecane	1.8
	Total	22.3
Chemical Formula	Olefin	Area
C14H28	1-Tetradecene	1.0
C15H30	1-Pentadecene	1.6
	Total	2.5
Chemical Formula	Aromatic-Cyclic	Area
C8H10	Ethylbenzene	35.2
C9H12	Benzene, (1-methylethyl)-	8.2
C9H12	Benzene, propyl-	3.4
C10H8	Naphthalene	2.8
C11H10	Naphthalene, 1-methyl-	1.6
C11H10	Naphthalene, 2-methyl-	2.4
C12H10	Biphenyl	2.4
C13H12	Diphenylmethane	1.4
C13H12	1,1'-Biphenyl, 3-methyl-	1.1
C16H12	2-Phenylnaphthalene	3.2
C17H14	7b-Phenyl-2a,7b-dihydro-3H-cyclobuta[a]indene	0.8
C17H14	1H-Cyclopenta[l]phenanthrene, 2,3-dihydro-	4.2
C18H14	m-Terphenyl	1.0
C16H12	Anthracene, 9-ethenyl-	2.2
	Total	69.9
Chemical Formula	Oxygenates	Area
C8H8O	Acetophenone	2.4

Appendix

D

Supporting Materials for Chapter 5

Hydrothermal Liquefaction of Southern Yellow pine

Table D1: Pine feedstocks characterization

Proximate Analysis(wt.%)	
Moisture	7.3±0.0
Volatile	83.8±3.6
Ash	0.5±0.1
Fixed Carbon[a]	8.3±3.5
Elemental Analysis [a](wt.%)	
C	50.0±0.7
H	6.1±0.2
N	0
S	0.1±0.0
Ash	0.5±0.1
O[a]	43.3±1.0
Biochemical Composition(wt.%)	
Hemicellulose	10.3
Cellulose	42.1
Lignin	24.7

a by difference

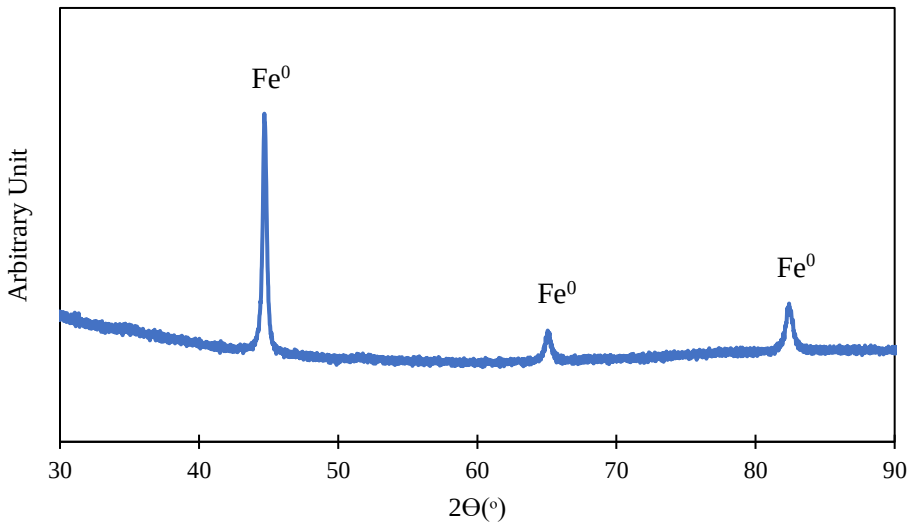

Figure D1: XRD pattern of iron particle.

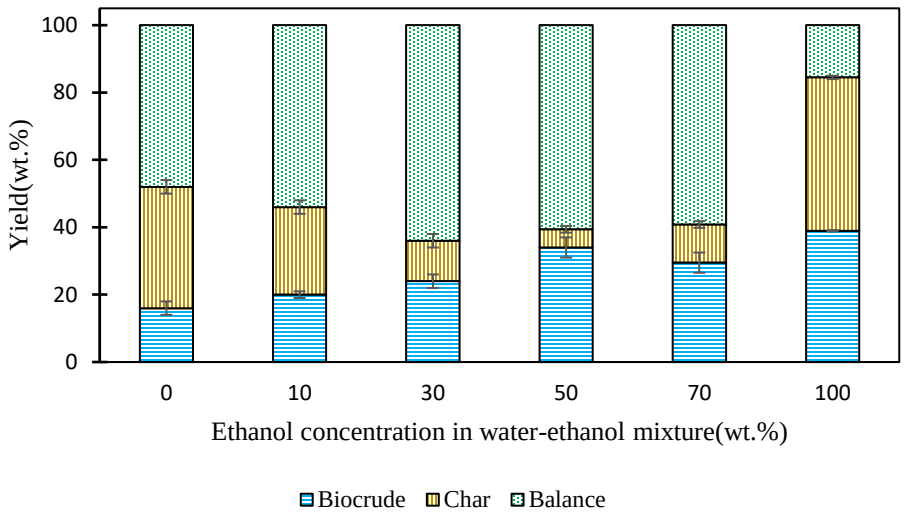

Figure D2: Pine yield distribution with increasing ethanol in water-ethanol solvent

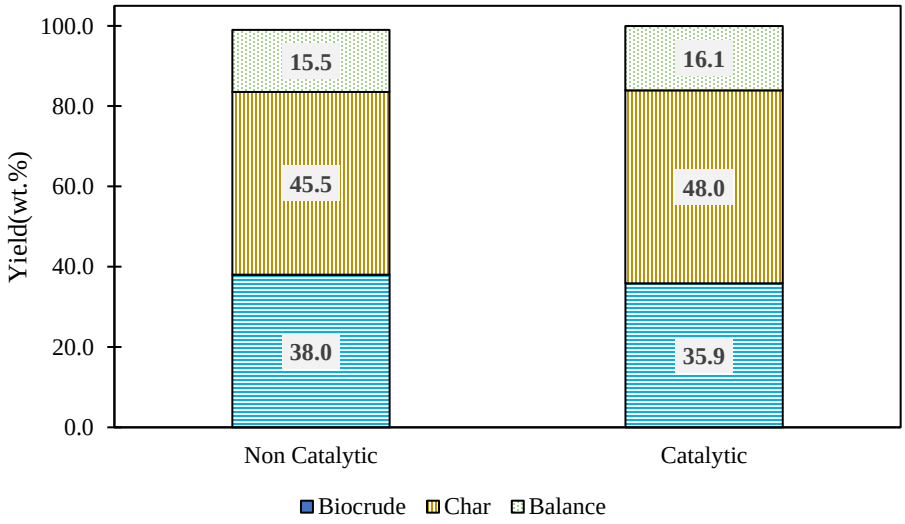

Figure D3: HTL product distribution in pure ethanol

Table D2: Physicochemical properties of pine HTL at 300°C

	Ethanol conc. (wt.%)	Elemental Composition (wt.%) C	H	Ash	O[a]	HHV (MJ/Kg)	TAN (mgKOH/g)
Non-catalytic	0	66.0±0.0	6.0±0.1	0.5±0.2	27.5±0.3	27.2±0.1	45.3±2.2
	10	65.7±0.1	6.0±0.0	0.4±0.2	27.2±0.3	28.0±0.1	40.2±2.2
	30	63.8±0.3	6.7±0.0	0.5±0.2	29.0±0.5	27.2±0.2	32.9±1.0
	50	55.8±1.2	6.9±0.1	0.2±0.1	37.1±1.4	23.8±0.7	30.4±1.4
	70	58.0±1.0	6.2±0.1	0.2±0.0	35.6±1.1	23.8±0.6	12.5±0.6
	100	65.6±0.4	6.9±0.1	0.2±0.1	27.3±0.6	28.2±0.3	12.0±0.7
Catalytic	0	67.0±3.0	6.4±0.7	0.7±0.2	25.9±3.9	28.2±2.3	32.2±1.7
	50	67.7±0.3	6.1±0.2	0.8±0.3	25.4±0.2	28.2±0.4	6.6±0.5
	100	65.7±0.1	6.9±0.1	0.2±0.1	27.2±0.3	28.2±0.2	10.1±1.0

[a] by difference

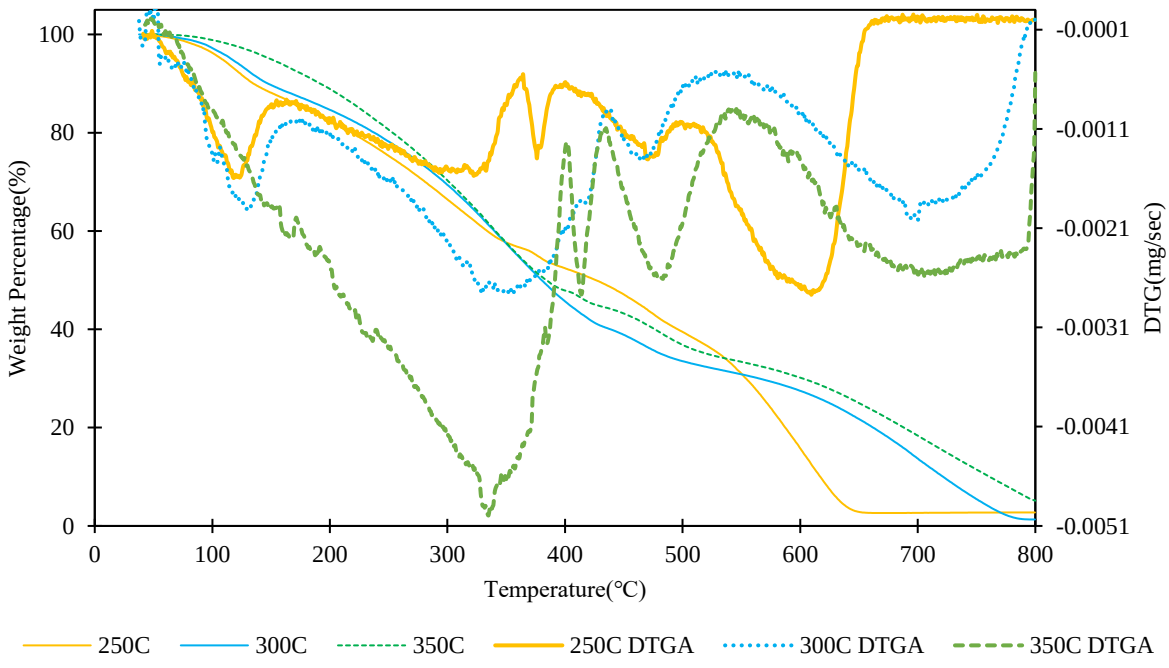

Figure D4: Comparison between pine biocrude thermograms from different temperature

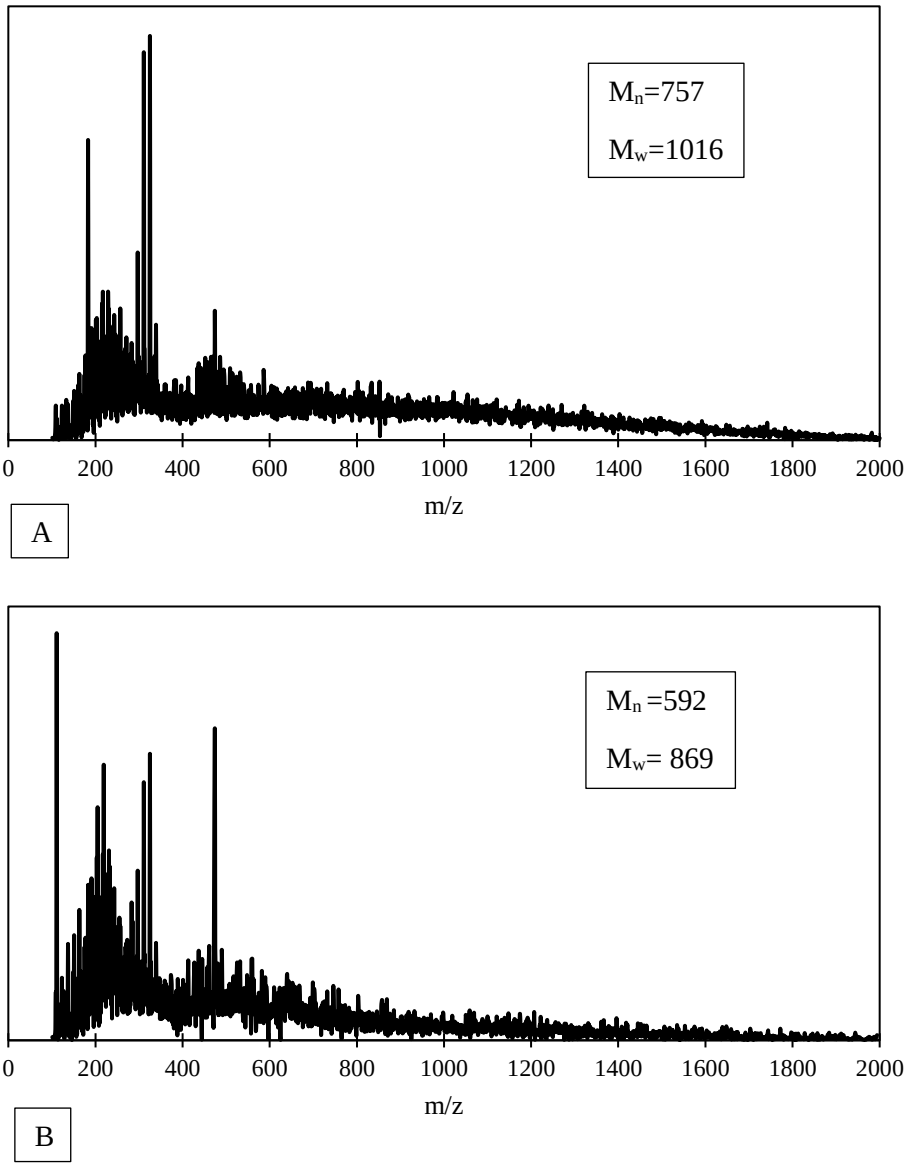

Figure D5: Negative ion ESI-MS characterization of pine oil from pure ethanol medium at 300℃: A- Non-Catalytic, B- Catalytic

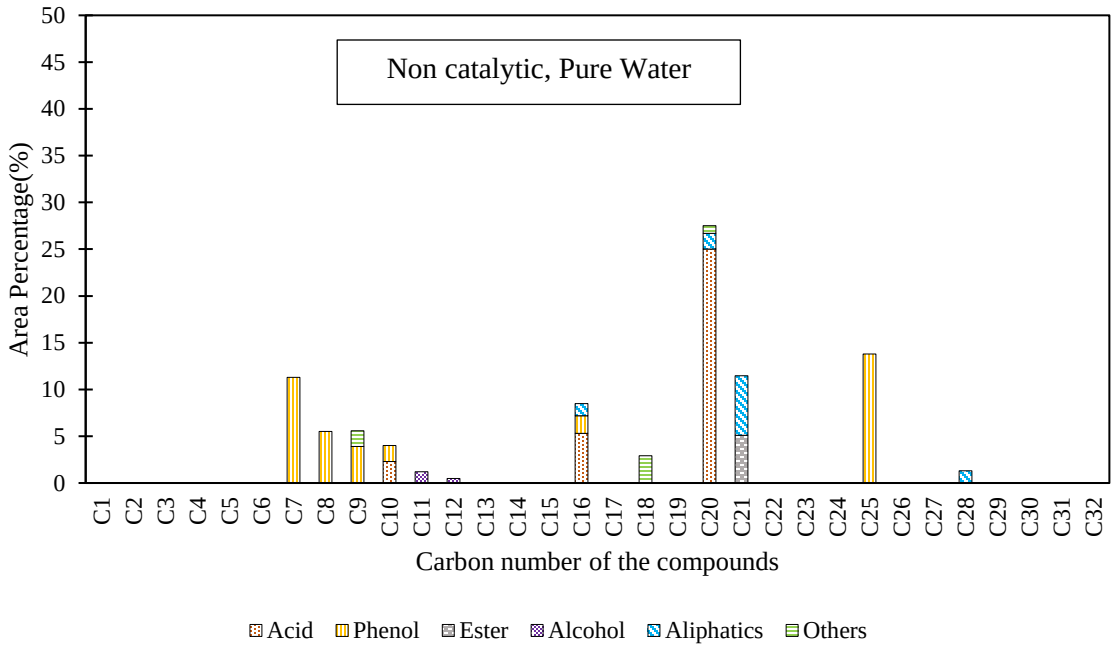
Non catalytic, Pure Water
Area Percentage(%)
Carbon number of the compounds
Acid
Phenol
Ester
Alcohol
Aliphatics
Others

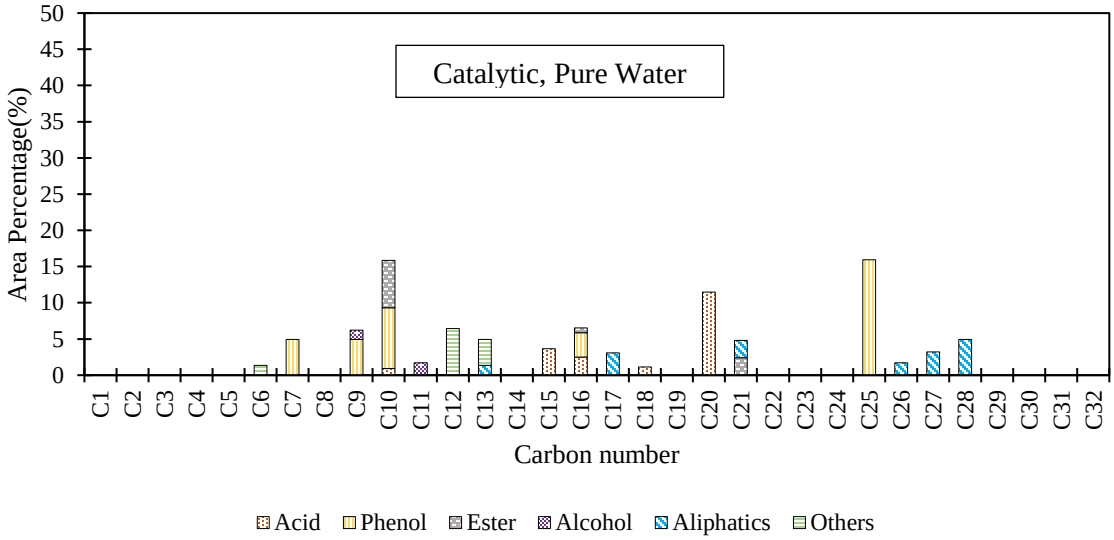
Catalytic, Pure Water
Area Percentage(%)
Carbon number
Acid
Phenol
Ester
Alcohol
Aliphatics
Others

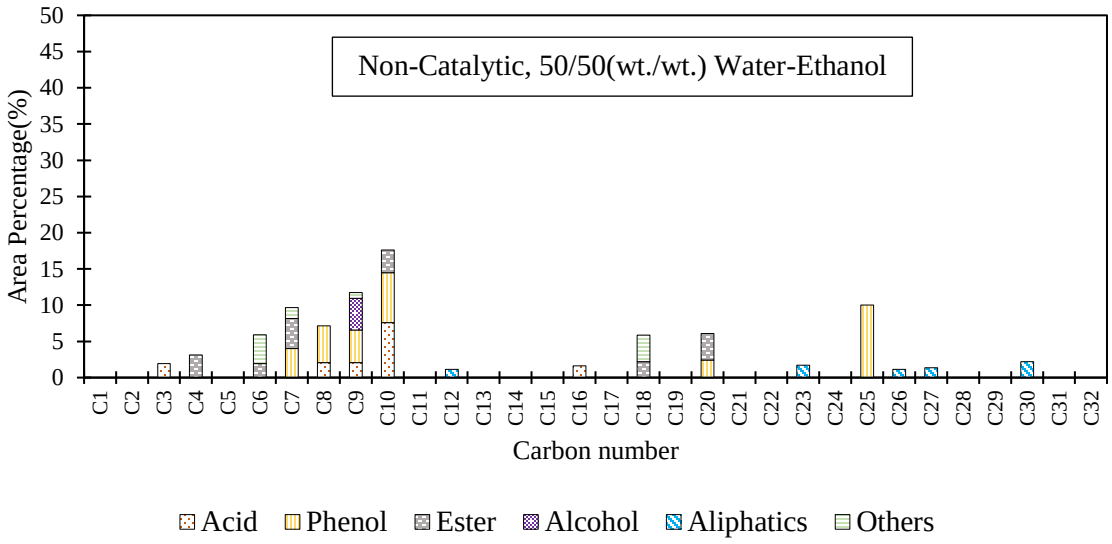
Non-Catalytic, 50/50(wt./wt.) Water-Ethanol
Area Percentage(%)
Carbon number
Acid
Phenol
Ester
Alcohol
Aliphatics
Others

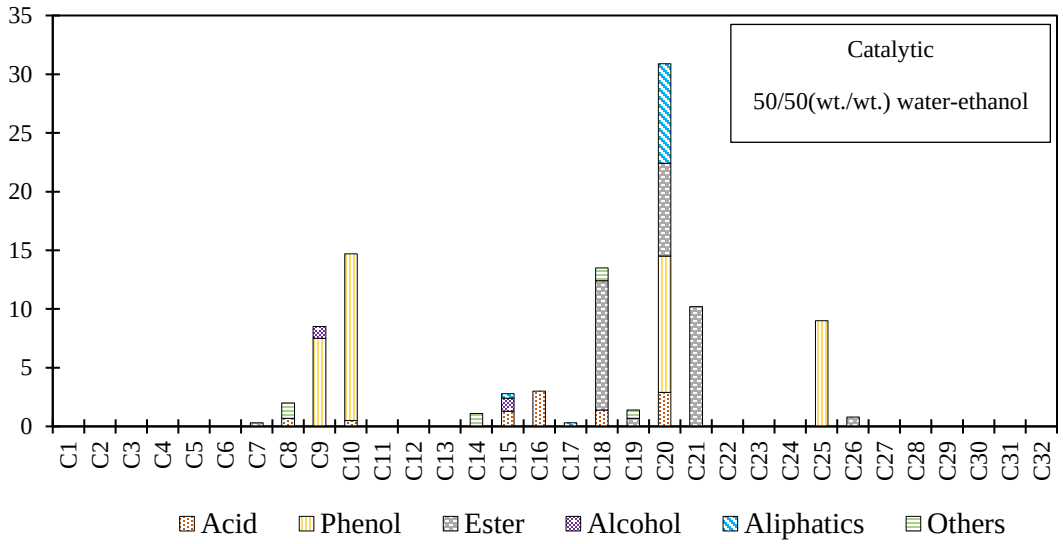
Catalytic
50/50(wt./wt.) water-ethanol
Acid
Phenol
Ester
Alcohol
Aliphatics
Others

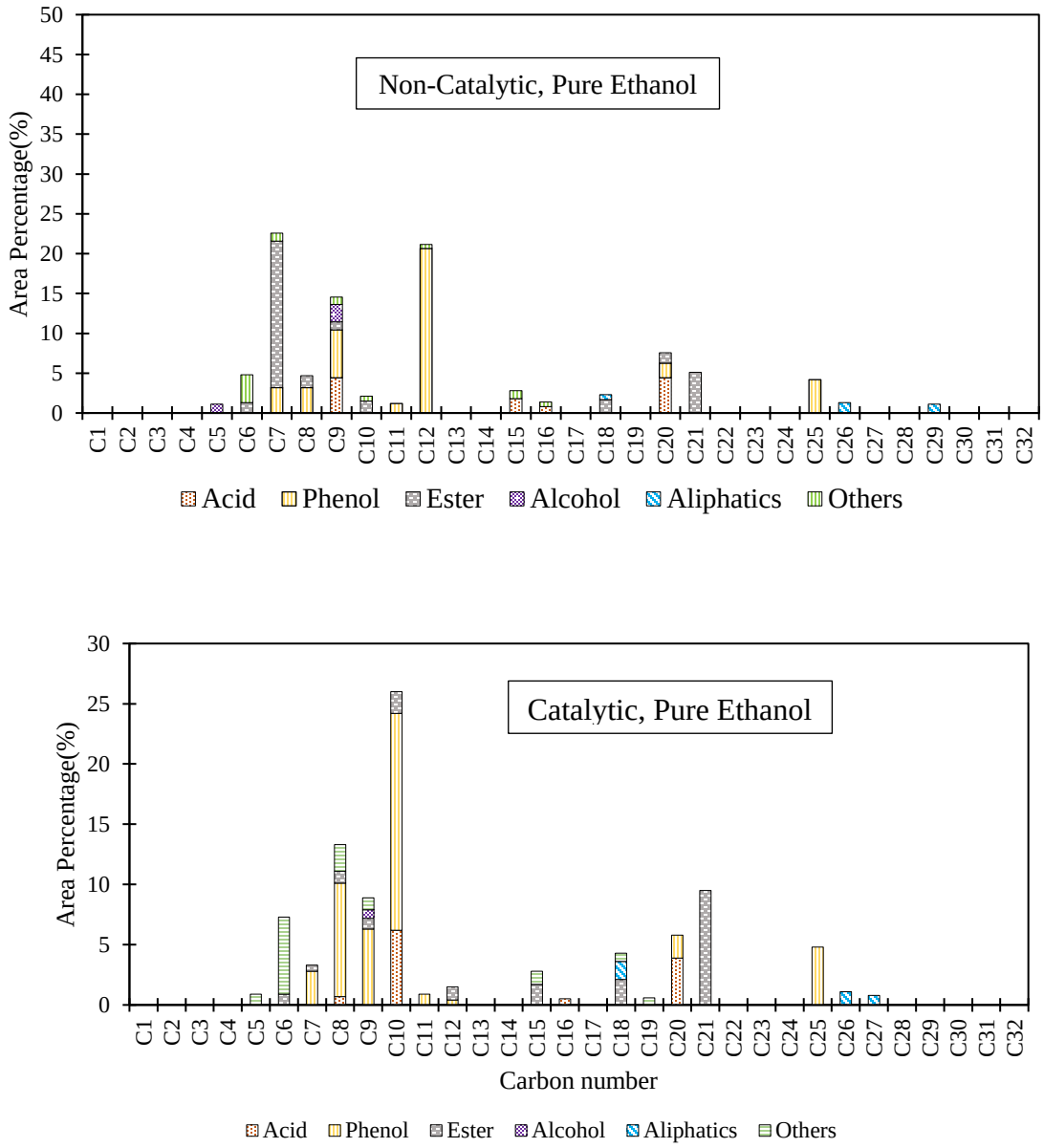

Figure D6: Compound group distribution by carbon number in pine biocrudes derived from 300℃

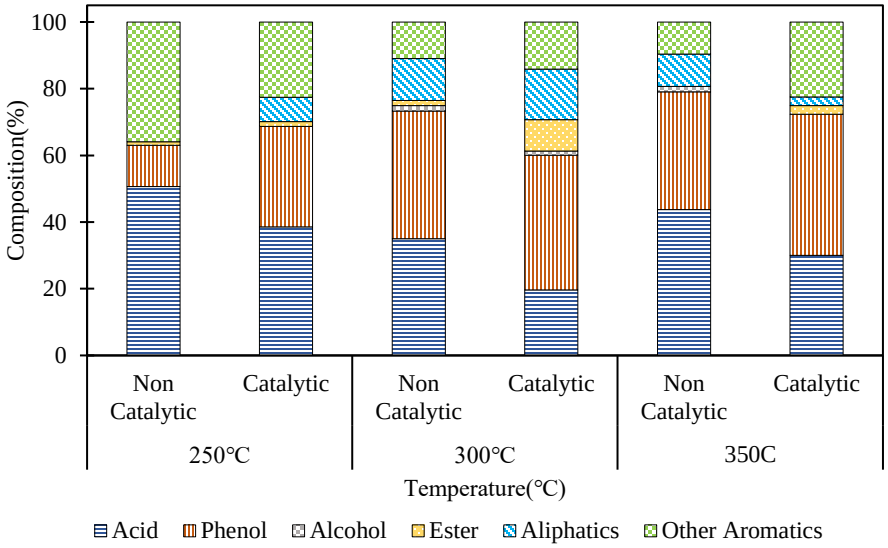

Figure D7: The GC-MS analysis of pine wood derived biocrudes from pure water

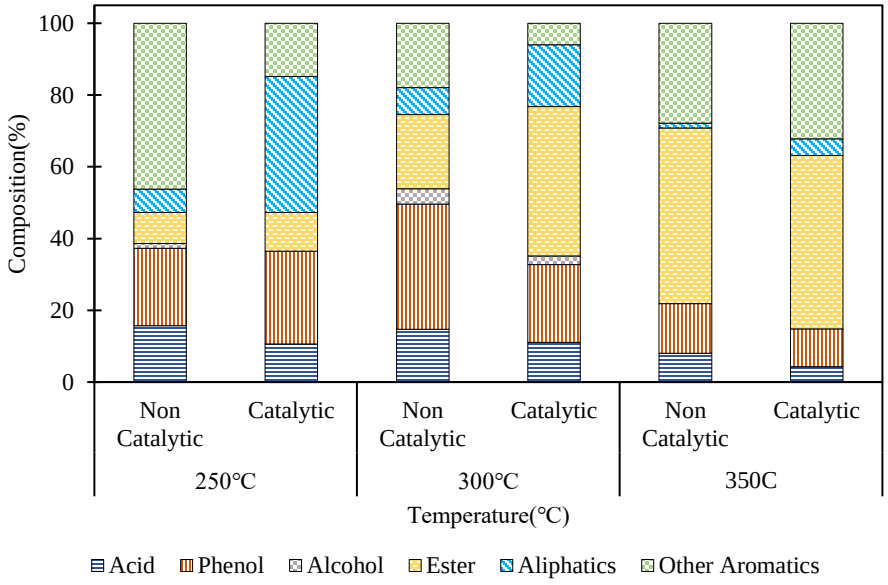

Figure D8: The chemical composition of pine HTL biocrudes of 50/50(wt./wt.) water ethanol mixture

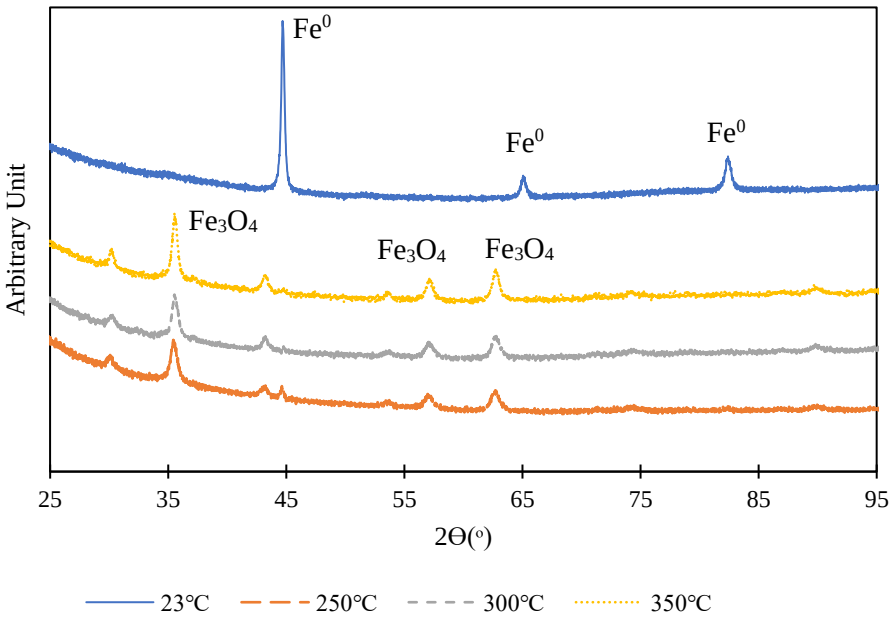

Figure D9: Comparison of iron powder XRD patterns before HTL conversion (room temperature:23℃) and after HTL reaction (at 250℃,300℃ and 350℃)